

# **Blue Light Photoreceptors**

—

## **From Mechanism to Application**

**Inaugural Dissertation**

zur

Erlangung des Doktorgrades  
der Mathematisch-Naturwissenschaftlichen Fakultät  
der Heinrich-Heine-Universität Düsseldorf

von

**M.Sc. Sarah Raffelberg**

aus Duisburg / Nordrhein-Westfalen

Mai 2013



Die vorliegende Arbeit entstand in der Zeit von Oktober 2009 bis Januar 2013 am Max-Planck-Institut für Chemische Energiekonversion, ehemals Max-Planck-Institut für Bioanorganische Chemie, in Mülheim an der Ruhr unter der Anleitung von Herrn Prof. Dr. Wolfgang Gärtner.

(Performed during the time-period from October 2009 until January 2013 under the supervision of Prof. Dr. Wolfgang Gärtner at the Max-Planck-Institute for Chemical Energy Conversion, formerly Max-Planck-Institute for Bioinorganic Chemistry.)

Gedruckt mit der Genehmigung der  
Mathematisch-Naturwissenschaftlichen Fakultät der  
Heinrich-Heine-Universität Düsseldorf

Referent (first referee):

Prof. Dr. Wolfgang Gärtner

Korreferent (second referee):

Prof. Dr. Karl-Erich Jaeger

Tag der mündlichen Prüfung (date of oral examination):

21.06.2013

*“The roots of education are bitter, but the fruit is sweet.”*

Aristotle

## Acknowledgement

Foremost, my sincere gratitude to Prof. Dr. Wolfgang Gärtner for his constant and invaluable support during my Ph.D. studies and for providing me with this challenging and highly up-to-date topic, introducing me into the fascinating world of photoreceptors. His honest attention, trust and patience motivated me to go on through all the three years, keeping my spirits up. With enthusiasm and his detailed knowledge, he sparked my interest in new details and new perceptions. His guidance helped me in all the time of research and writing of this thesis, especially his critical reading of thesis and papers.

I would particularly like to express my thanks to Prof. Dr. Karl-Erich Jaeger for agreeing to be the second evaluator of my thesis.

Dr. Aba Losi, University of Parma, Italy, is at the top of my list of very important colleagues of my Ph.D. work. Being full of power, she pushed me with motivating discussions, great ideas and a fruitful cooperation. I had the privilege to work in her lab during two stays in Parma, getting to know the method of Laser Induced Opto Acoustical Spectroscopy (LIOAS).

Furthermore, I would like to thank Dr. Francesca Cella for providing me the opportunity to visit her lab at the Italian Institute of Technology in Genova, Italy, and introducing me into the complex world of advanced physical microscopy techniques.

Thanks to Prof. Dr. Georg Nagel for having me in his lab at the University of Würzburg, Germany and teaching me oocytes experiments.

I wish to thank all my colleagues and staff at the Max-Planck-Institute for Chemical Energy Conversion for their support, encouragement, suggestions and guidance.

First, my gratitude to Dr. rer nat Zhen Cao, who guided me during my first months in the lab and always took care that I would not lose the track.

A “Thank you” to Mr. Dennis Naumann, who provided me with good lab support and a productive team work during the last year. I could not have a better laboratory assistant.

My gratitude to Mr. Leslie Currel and Mr. Norbert Dickmann for their technical support and great help with laser flash photolysis measurements and Maldi-TOF mass spectrometry, as well as to Mrs. Gülümse Koc-Weier for instilling me into fluorescence lifetime measurements.

My lab mates have a big contribute to the inspiring, cheery working atmosphere with many laughs and cakes, especially Mr. Dr. Sebastian Gandor, Mr. M.Sc. Alexander Gutt, Ms. Dipl.-Biol. Jana Riethausen and Mr. M.Sc. Julian Simon.

Herewith, I would like to thank the Max-Planck Organisation, the graduate school “Biostruct” at the University of Düsseldorf and the DAAD (Vigoni program) for the financial support of my work.

Last but not least, to the persons I love:

To my family I am indebted for their love and support throughout the years at university and during my Ph.D. study. I am absolutely thankful to my parents for allowing me to choose my path and to let me follow my dreams while keeping me grounded.

To the man by my side: your encouragement, emotional support and your endless patience were a great backup. You saw all the ups and downs; you shared my happiness, you dried my tears and you kicked my ass whenever needed. Thank you!

## Summary

Light sensing photoreceptors connect the environment and a living organism by transforming the outer stimulus light into a physiological signal. They are important to sense and to react to light, sensing spectral quality, intensity, direction and its periodicity. Several kinds of photoreceptors are known, classified into different photoreceptor families. One of these families, the family of so-called light, oxygen, voltage (LOV) domain proteins, was originated by the identification of the blue light sensitive flavin-binding plant phototropins (phot) in 1997. Five years later, a bacterial phot-like LOV domain-containing protein was discovered. Since then, scientific information on photoreceptors is continuously growing.

This thesis is focused to move forward from fundamental knowledge on photoreceptor function to the development of applications, here mainly addressing the blue light-sensing photoreceptors YtvA and mPAC. With this thesis the available knowledge about bacterial LOV proteins was extended with respect to i) mechanism of YtvA's photochemistry, ii) structure of YtvA full-length protein, iii) application of blue light photoreceptors in the field of nanoscopy and optogenetics, iv) introducing a novel adenylyl cyclase by characterization of the novel blue light protein mPAC.

### i) Mechanism of photochemistry:

The main part of this thesis deals with the topic of how residues within or nearby the chromophore binding pocket influence the photochemistry of a blue light sensitive LOV protein like YtvA from *Bacillus subtilis*. This work aims to investigate selected amino acids forming a hydrogen bonding network within the chromophore pocket and to identify some hot spots, residues in close vicinity to the cofactor that play an important role in kinetics. Therefore, site directed mutagenesis was performed to generate different mutants of YtvA. In total, 19 mutants of YtvA, located at the Positions T30, N37, R63, Q66, N94, N104 and Q123, were compared to the wild type protein by means of steady-state and time-resolved absorption and fluorescence spectroscopy, laser flash photolysis, fluorescence anisotropy and laser induced optoacoustic spectroscopy (LIOAS).

Using these comprehensive data sets, the role of the hydrogen bonds to the chromophore positions C(2)=O, N(3)H, C(4)=O and N(5) could be identified. The amino acids N94 and Q123 seems to have the greatest impact in the hydrogen

boning network, mutation into an alanine (N94A) or asparagine (Q123N) strongly decreases the energetics and recovery time in both cases. Position T30 could be identified as a tuner position, surprisingly altering the wild type LOV2-like spectrum of YtvA into a LOV1-like one.

#### ii) Structure of full-length YtvA:

The elucidation of protein structures plays a major role in understanding photoreceptors and provides the basis for investigations of about intra- and interprotein arrangements and conformational changes of the protein upon light activation. Despite the remarkable research activity in the field of the blue light sensitive YtvA since 2002, no X-ray-, NMR- or EPR-based structural information of the full-length protein is available. In the last decade, several suggestions were made about YtvAs full-length structure based on investigations of isolated, truncated LOV domain constructs. For the first time now, a full-length structure-prediction of YtvA based on ENDOR EPR spectroscopy is presented within this thesis. MTSSL-spin labelled, mutated variants of the wild type protein were generated and investigated by ENDOR EPR, followed by intensive calculations of the protein structure based on distances data and relaxation times. The study revealed a conformation consisting of two homo-dimers connected by two coiled helices and is in high agreement with the most recent published literature.

#### iii) Application:

Only during the last few years, photoreceptors have made their way from mechanism to application, i.e., from being the main target of fundamental research to a novel, but still small part in advanced biotechnological and biomedical applications.

Physical applications like fluorescence tagging (using photoreceptors as the counterparts to the various GFP derivatives) and nanoscopy are at this time one of the most hopeful applications. Nanoscopy is based on random activation of single molecules resulting in a high resolution picture of a cell. This thesis presents for the first time the application of the blue light receptor YtvA in nanoscopy. With the high resolution microscopy the detection of single YtvA molecules in a living cell could be demonstrated. Moreover, an advanced set-up obtained the proof-of-principle of a phenomenon called photoswitch in *in vitro* experiments. With selected light qualities in the UV and near-UV wavelengths the excited protein can be converted back into



its ground state within ps, thus reducing the recovery time of YtvA by several magnitudes and identifies the LOV domains to an outstanding, favorable group of photoreceptors, offering many various ways for advanced applications in nanoscopy and optogenetics.

iv) mPAC:

A novel, LOV domain mediated photoactivated adenylyl cyclase (PAC) of the cyanobacterium *Microcoleus chthonoplastes* was identified, cloned, expressed and purified from *Escherichia coli* as heterologous host. According to the organism *M. chthonoplastes* and the other already identified PAC proteins, euPAC, bPAC, and nPAC this cyclase was designated mPAC. In contrast to formerly reported adenylyl cyclases that are regulated through a blue light-sensing BLUF domain this novel proteins carries a LOV domain. It consists of a PAS-LOV-cyclase domain architecture, 483 residues and 54.2 kDa in size. Testing the photochemical behaviour by absorption and fluorescence spectroscopy, a very fast photocycle with a recovery time of 16 sec at 20 °C could be observed. Cyclase activity was investigated by activity assays *in vitro* and following *in vivo*, e.g., with *Xenopus* oocytes and the amoeba *Dictyostelium*.

These data, in combination with the above discussed tested proof-of-principle of a LOV photoswitch, identify mPAC as a very suitable tool to enlarge the optogenetic toolkit.

## Zusammenfassung

Lichtsensitive Photorezeptoren stellen eine Verbindung zwischen einem Organismus und seiner Umwelt dar, indem sie einen äußeren Lichtreiz in ein physiologisches Signal umwandeln. Dabei detektieren die Photorezeptoren nicht nur das Licht, sondern erfassen auch dessen Wellenlänge, Intensität, Richtung und Periodizität. Bis heute sind verschiedene Arten von Photorezeptoren bekannt, die in unterschiedliche Photorezeptorfamilien klassifiziert werden können. Eine dieser Familien, die Familie der sogenannten Licht-, Sauerstoff- und Spannungssensitiven Domänen Proteine (light, oxygen and voltage; LOV), entstammt der Familie der Blaulicht-sensitiven, Flavin-bindenden Pflanzenphototropinen (phot), die 1997 identifiziert wurden. Fünf Jahre später wurde das erste bakterielle Phototropin-ähnliche LOV Protein entdeckt. Seitdem steigt die Anzahl an wissenschaftlichen Informationen über Photorezeptoren kontinuierlich.

Diese Thesis beinhaltet die Weiterentwicklung vom grundlegenden Wissen über Photorezeptoren hin zu der Entwicklung von Anwendungsmöglichkeiten, im Fokus stehen dabei die Blaulicht-sensitiven Photorezeptoren YtvA und mPAC. Die Arbeiten zu dieser Thesis erweitern das Wissen über bakterielle LOV Proteine bezüglich i) des photochemischen Mechanismus von YtvA, ii) der Struktur des Volllängenproteins YtvA, iii) der Anwendung von Blaulichtphotorezeptoren in dem Bereich der Nanoskopie und Optogenetik, sowie iv) der Einführung einer neuartigen Adenylzyklase durch die Charakterisierung des neuen Blaulichtproteins mPAC.

### i) Der photochemische Mechanismus:

Der Hauptteil dieser Thesis geht der Frage nach, wie Aminosäurenreste innerhalb der Chromophorbindetasche oder in ihrer direkten Nähe die Photochemie eines Blaulicht-sensitiven Proteins wie YtvA aus *Bacillus subtilis* beeinflussen kann. Ziel dieser Arbeit ist die Untersuchung von ausgewählten Aminosäuren, die ein Wasserstoffbrückenbindungsnetzwerk innerhalb der Chromophorbindetasche bilden, sowie die Identifizierung von so genannten „Hot Spots“, Aminosäuren in der direkten Nähe zum Cofaktor, die einen entscheidenden Einfluss auf die Kinetik ausüben. Dazu wurde gezielte Punktmutagenese durchgeführt, um verschiedene Mutanten von YtvA zu generieren. Insgesamt wurden 19 Mutanten, an den Positionen T30, N37, R63, Q66, N94, N104 und Q123, mit dem Wildtypprotein mit Hilfe von Steady-

state und Zeitaufgelöster Absorptions- und Fluoreszenzspektroskopie, Laserblitzlichtphotolyse, Fluoreszenzanisotropie und Laser induzierte optoakustische Spektroskopie (LIOAS) verglichen.

Auf Grund dieser umfassenden Datensätze konnte die Rolle der Wasserstoffbrückenbindungen zu den Positionen C(2)=O, N(3)H, C(4)=O und N(5) des Chromophors identifiziert werden. Die Aminosäuren N94 und Q123 scheinen dabei den größten Einfluss auf das Wasserstoffbrückenbindungsnetzwerk auszuüben, ihre mutierten Varianten N94A und Q123N vermindern sehr stark die Energetik und Rückkehrzeiten der Mutanten. Für die Position T30 konnte gezeigt werden, dass sie überraschenderweise das LOV2-Spektrum des YtvA Wildtyp-Proteins in ein LOV1-Spektrum verändert.

#### ii) Struktur des Volllängenproteins YtvA:

Die Aufklärung von Proteinstrukturen spielt eine wichtige Rolle für das Verständnis von Photorezeptoren und bildet die Grundlage für Untersuchungen von Intra- und Interproteinanordnungen und den Konformationsänderungen die einem Protein bei Lichtaktivierung widerfahren. Trotz der bemerkenswerten Forschungsaktivität im Bereich des Blaulicht-sensitiven YtvAs seit 2002, gibt es noch keine Röntgen-, NMR- oder EPR-basierten Strukturinformationen des Volllängenproteins. In den vergangenen zehn Jahren wurden verschiedene Vorschläge über die Volllängenstruktur gemacht, alle basierten auf Untersuchungen von isolierten, verkürzten LOV-Domänen-Konstrukten. Im Rahmen dieser Arbeit wird nun zum ersten Mal eine Volllängen-Strukturvorhersage für YtvA basierend auf ENDOR EPR Spektroskopie vorgestellt. MTSSL-Spin-markierte und mutierte Varianten des Proteins wurden generiert und mittels ENDOR EPR untersucht, gefolgt von intensiven Berechnungen der Struktur anhand der Abstandsdaten und Relaxationszeiten. Die Studie ergab eine Anordnung aus zwei Homodimeren, die durch je eine gewundene Helix verbunden sind. Die Konformation ist in hoher Übereinstimmung mit der neusten veröffentlichten Literatur.

#### iii) Anwendung:

Erst in den letzten Jahren wandelte sich die Photorezeptorforschung vom Mechanismus zur Anwendung. Die Photorezeptoren wurden vom Hauptziel der Grundlagenforschung zu einem neuen, aber immer noch kleinen Teil in der

fortgeschrittenen biotechnologischen und biomedizinischen Anwendung. Physikalische Anwendungen wie Fluoreszenzmarkierung, bei der Photorezeptoren als Alternative zu den zahlreichen GFP Derivaten genutzt werden, und Nanoskopie sind zurzeit die vielversprechendsten Anwendungsmöglichkeiten. Nanoskopie basiert auf der zufälligen Aktivierung von einzelnen Molekülen und ermöglicht somit ein hochauflösendes Bild einer Zelle. Diese Thesis präsentiert zum ersten Mal die Anwendung des Blaulichtrezeptors YtvA in der Nanoskopie. Mit der Hochauflösungsmikroskopie konnte die Detektion von einzelnen YtvA Molekülen in einer lebenden Zelle demonstriert werden. Desweiteren konnte ein erweiterter Versuchsaufbau das Phänomen des Photoswitches in *in vitro* Experimenten beweisen. Durch selektive Lichtqualitäten im UV und UV-nahen Wellenlängenbereich kann das angeregte Protein innerhalb von wenigen Pikosekunden in seinen Grundzustand zurückkonvertiert werden, wodurch die Rückkehrzeit von YtvA um ein Vielfaches reduziert werden kann. Dieser Effekt identifiziert die LOV Proteine als eine außergewöhnliche und vorteilhafte Photorezeptorgruppe, die viele verschiedene Möglichkeiten der fortgeschrittenen Anwendung in Nanoskopie und Optogenetik bietet.

#### iv) mPAC:

Eine neuartige, LOV Domänen regulierte, photoaktivierbare Adenylylzyklase (photoactivated adenylyl cyclase; PAC) aus dem Cyanobakterium *Microcoleus chthonoplastes* wurde identifiziert, in *Escherichia coli* als heterologen Wirt kloniert, exprimiert und aufgereinigt. Aufgrund des Organismus *M. chthonoplastes* und den anderen schon identifizierten PAC Proteinen, euPAC, bPAC und nPAC, wurde dieses Protein mPAC genannt. Im Gegensatz zu den schon bekannten PAC Proteinen wird das neuartige mPAC durch eine LOV Domäne reguliert. Es besteht aus einer PAS-LOV-Zyklasen-Architektur, bestehend aus 483 Aminosäuren und mit einer Gesamtgröße von 54,2 kDa. Die Untersuchungen der photochemischen Eigenschaften anhand von Absorptions- und Fluoreszenzspektroskopie zeigten einen sehr schnellen Photozyklus mit einer thermalen Rückkehrzeit von nur 16 Sekunden bei 20°C. Die Zyklasteaktivität wurde mit Aktivitätsassays *in vitro* und anschließend *in vivo*, z.B. in *Xenopus* Oozyten und in der Amöbe *Dictyostelium*, nachgewiesen. Diese Daten, in Kombination mit dem schon erwähnten und

nachgewiesenen LOV-Photoswitch-Effekt, identifizieren mPAC als ein vielversprechendes Protein um die Optogenetik voranzubringen.

## Publications and manuscripts

Parts of this work that are in advance or already published are listed up below.

**Raffelberg S**, Mansurova M, Gärtner W, Losi A. (2011): Modulation of the photocycle of a LOV domain photoreceptor by the hydrogen-bonding network. *J Am Chem Soc.* **133**:5346-5356

Losi A, Gärtner W, **Raffelberg S**, Cella Zanacchi F, Bianchini P, Diaspro A, Mandalari C, Abbruzzetti S, Viappiani C. (2013): A photochromic bacterial photoreceptor with potential for super-resolution microscopy. *Photochem Photobiol Sci.* **12**:231-235

Engelhard C, **Raffelberg S**, Tang Y, Diensthuber RP, Möglich A, Losi A, Gärtner W, Bittl R (2013): A structural model for the full-length blue light-sensing protein YtvA from *Bacillus subtilis*, based on EPR spectroscopy. *Photochem. Photobiol. Sci.* (accepted).

**Raffelberg S**, Gutt A, Gärtner W, Mandalari C, Abbruzzetti S, Viappiani C, Losi A (2013): The amino acids surrounding the flavin 7a-methyl group determine the UVA spectral features of a LOV protein. *Biol. Chem.* (accepted).

**Raffelberg S**, Wang L, Gao S, Losi A, Gärtner W, and Nagel G (2013): A LOV domain-mediated, blue light-activated Adenylyl Cyclase from the cyanobacterium *Microcoleus chthonoplastes* PCC 7420. *Biochem. J.* (accepted).

## Abbreviations

The following list contains all abbreviations repeatedly used in this thesis excluding common SI units. For DNA bases and amino acids the standard one or three letter codes were used, respectively.

aa	amino acid
AC	adenylyl cyclase
AMP	adenosine monophosphate (5'-adenylic acid)
Asphot	<i>Avena sativa</i> phototropin
ATP	adenosine 5'-triphosphate
Atphot	<i>Arabidopsis thaliana</i> phototropin
BLUF	sensor of blue-light using FAD domain
<i>B. subtilis</i>	<i>Bacillus subtilis</i> (Bs)
BV	biliverdin IX $\alpha$
cAMP	cyclic adenosine monophosphate
CBCR	cyanobacteriochrome
CCE	cryptochrome C-terminal extension
cGMP	cyclic guanosine monophosphate
CHD	cyclase homologue domain
CO	carbon monoxide
CPD	cyclobutane pyrimidine dimers
<i>C. reinhardtii</i>	<i>Chlamydomonas reinhardtii</i> (Cr)
CRY	cryptochrome
C-terminal	Carboxy-terminal
<i>D. discoideum</i>	<i>Dictyostelium discoideum</i> (Dd)
DNA	deoxyribonucleic acid
EPR	electron paramagnetic resonance
ENDOR-EPR	electron nuclear double resonance - EPR
FAD	flavin adenine dinucleotide
FbFP	FMN-binding fluorescent proteins
FDBR	ferredoxin-dependent bilin reductase
FKF1	flavin-binding kelch repeat F-Box protein
FLIM	fluorescence lifetime imaging microscopy
FMN	flavin mononucleotide (riboflavin 5'-monophosphate)

FPALM	fluorescence photoactivation localization microscopy
GAF	cGMP phosphodiesterase, adenylyl cyclase and FhIA protein
GFP	green fluorescent protein
GTP	guanosine 5'-triphosphate
HB	hydrogen bond/-ing
HK	histidine kinase (domain)
ho1	heme oxygenase 1
HPLC	high performance liquid chromatography
HTH	helix- turn- helix DNA-binding domain
LOV	light, oxygen, voltage (domain)
LOV390	LOV signaling state
LOV447	LOV dark state
LOV660	LOV excited triplet-state
LOV-HK	LOV histidine kinase
NADPH	nicotinamide adenine dinucleotide phosphate
N-cap	Amino-terminal cap
NMR	nuclear magnetic resonance
nph1	non-phototropic hypocotyls
npl1	non-phototropic hypocotyl like 1
N-terminal	Amino-terminal
<i>M. chthonoplastes</i>	<i>Microcoleus chthonoplastes (Mc)</i>
ORF	open reading frame
PAC	photoactivated adenylyl cyclase
PAS	per, arndt, sim domain
pca	p-coumaric acid chromophore
PCB	phycocyanobilin
PΦB	phytochromobilin
pcyA	phycocyanobilin : ferredoxin reductase
phot	phototropin
PHR	photolyase homologous region
PHY	phytochrome
PYP	photoactive yellow protein
RF	riboflavin
RNA	ribonucleic acid



ROS	reactive oxygen species
RR	response regulator
SCF	Skp1, Culin and F-box type
STAS	sulfate transporter anti-sigma factor antagonist (domain)
UV	ultraviolet
UVR-8	UV resistance locus 8
VIS	visible light
WC-1	white-collar-1
wt-YtvA	wild type of YtvA
YFP	yellow fluorescent protein
ZTL	ZEITLUPE

## Table of Figures

Figure 1-1: solar radiation spectrum. ....	2
Figure 1-2: Jablonski diagram. ....	3
Figure 1-3: photoreceptor families according to their absorption spectra ....	8
Figure 1-4: x-ray diffracted crystal structure of a homo-dimer of UVR-8.....	9
Figure 1-5: structure of a LOV domain ....	12
Figure 1-6: photocycle of LOV proteins ....	13
Figure 1-7: domain architecture of selected LOV domains. ....	16
Figure 1-8: chromophore pocket of YtvA ....	21
Figure 1-9: domain architecture of mPAC from <i>M. chthonoplastes</i> PCC 7420 .....	24
Figure 1-10: structure of two BLUF domains in an asymmetric unit of BlrB.....	27
Figure 1-11: intermediate generation of different bilin chromophores.....	33
Figure 6-1: HB network stabilizing the FMN chromophore in YtvA. ....	113
Figure 6-2: shifts in the transition II region of YtvA mutants.....	117
Figure 6-3: structure of C-terminally truncated LOV domain dimers from YF1 .....	121
Figure 6-4: chemical structure of MTSSL ....	122
Figure 6-5: structural model of full-length YtvA based on ENDOR-EPR data.....	123
Figure 6-6: STAS-STAS dimer of YtvA. ....	124
Figure 6-7: microcrystals of T30V and T30S. ....	124
Figure 6-8: conventional fluorescence and super-resolution imaging.....	126
Figure 6-9: principle of blinking effect ....	127
Figure 6-10: schematic photocycle of YtvA.....	128
Figure 6-11: cAMP synthesis from ATP and hydrolysis to AMP. ....	130
Figure 6-12: absorption spectra of dark state mPAC.....	132
Figure 6-13: kinetics of mPAC.....	133
Figure 6-14: comparison of mPAC residues A162 and M169 to other LOV domains .....	134
Figure 6-15: domain alignment of known PAC proteins.....	134
Figure 6-16: <i>in vitro</i> activity assay of mPAC with ATP to cAMP conversion .....	135
Figure 6-17: life cycle of <i>Dictyostelium</i> .....	138
Figure 6-18: comparison of <i>Dd</i> ACA and <i>Dd</i> null mutant with mPAC .....	139

## Table of Content

Acknowledgement .....	II
Summary .....	IV
Publications and manuscripts .....	XI
Abbreviations .....	XII
Table of Figures.....	XV
1. Introduction .....	1
1.1 Photoreceptors .....	5
1.2 UV-B light photoreceptors .....	9
1.3 Blue light photoreceptors .....	10
1.3.1 LOV proteins .....	11
1.3.1.1. Phototropins .....	14
1.3.1.2 Phot-like LOVs.....	15
1.3.1.3 ZTL/FKF1/LKP2.....	25
1.3.2 Cryptochromes.....	26
1.3.3 BLUF proteins .....	27
1.3.4 Xanthopsins .....	28
1.4 Red light photoreceptors .....	30
1.4.1 Phytochromes .....	30
1.4.2 CBCRs .....	32
1.4.3 Rhodopsins .....	34
1.5 State of the Art.....	35
1.6 Aim of this work .....	37
2. Mechanisms of the blue light photoreceptor YtvA .....	39
2.1 Modulation of the Photocycle of a LOV Domain Photoreceptor by the Hydrogen-Bonding Network .....	39
2.2 The amino acids surrounding the flavin 7a-methyl group determine the UVA spectral features of a LOV protein.....	51
3. Structure of the blue light photoreceptor YtvA.....	84
3.1 A structural model for the full-length blue light-sensing protein YtvA from <i>Bacillus subtilis</i> , based on EPR spectroscopy .....	84
4. Application of the blue light photoreceptor YtvA.....	94
4.1 A photochromic bacterial photoreceptor with potential for super-resolution microscopy .....	94

5. Characterization of the novel PAC protein mPAC .....	101
5.1 A LOV domain-mediated, blue light-activated Adenylyl Cyclase from the cyanobacterium <i>Microcoleus chthonoplastes</i> PCC 7420 .....	101
6. General Discussion .....	109
6.1 Influencing the mechanism .....	110
6.1.1 The hydrogen bonding network.....	112
6.1.2 Shifts of absorption bands.....	117
6.2 Structure of YtvA .....	119
6.3 Nanoscopy .....	125
6.4 mPAC .....	129
6.5 Conclusion and further perspectives .....	141
Curriculum vitae.....	157
References .....	142

## 1. Introduction

Light is an ever present energy source for practically all organisms with crucial influence on the evolution since the beginning of life on earth. During all times of development, specialization, and refinement of living organisms, all species had to adapt to earth's surface and atmosphere and to the given condition of sun light.

This fascinating dependence of life from light has challenged philosophers and scientists since ancient times. Many great scientists can be named here, including Galileo Galilei who wanted to confirm the measurement of the propagation speed, but did not succeed. First quantitative results, even if inaccurate, could be achieved by Ole Romer, which were improved and brought forward by Hippolyte Fizeau and Jean Foucault. Isaac Newton's theory of light as small particles disregarded any wave phenomena such as the diffraction of light. These aspects were taken into account, among other things by Christiaan Huygens, James Clark Maxwell and Thomas Young in the so-called wave theory. Still, both theories did not fit in all areas to the nature of light. Only the wave-particle duality by Albert Einstein and Max Planck covered all effects of light. Their scientific work represents the starting point for today's valid quantum physics and quantum electrodynamics.

Light is defined as electromagnetic radiation, however, in common usage only the visible light is meant; yet, this definition is a very subjective one and was made for mankind, as many animals and plants are able to detect light outside the determined limits of "visible" light. A wavelength range of about 380 nm to about 740 nm was defined as "visible", embedded between the "invisible" infrared at longer wavelengths and the "invisible" ultraviolet at shorter wavelengths. Whereas longer wavelengths (infrared irradiation) still arrives at the earth surface, the atmosphere and the ozone layer cause a filtering effect for most of the harmful UV radiation.

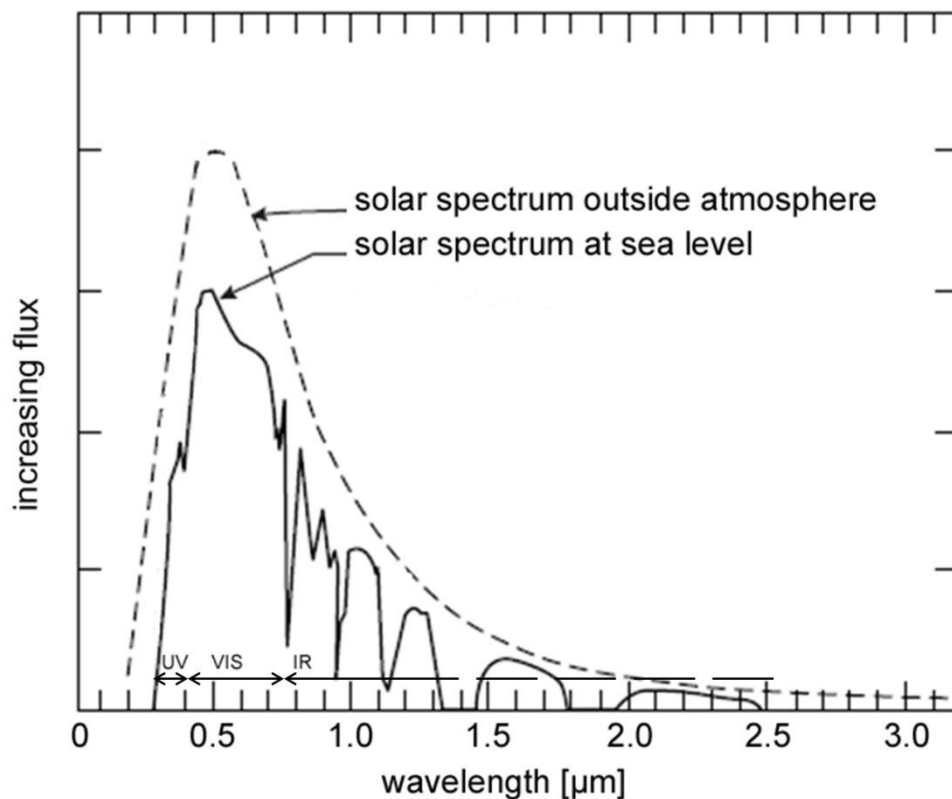


**Figure 1-1: solar radiation spectrum;** showing filter effects of the ozone layer in the UV range and absorbing effects of atmospheric water vapour and CO<sub>2</sub> in the range of infrared radiation <sup>1</sup>.

Prime characteristics of visible light are intensity, direction of propagation, frequency, spectral wavelength, and polarisation, while its speed in a vacuum, about 300 000 kilometres/second, is one of the fundamental constants of nature.

During evolution, light is always one of the most important selection factors, thus the emerging life had to adapt and also to utilize it. Light is the primary carrier of information and the key energy source on earth. These two aspects led to the development of photosensitivity in nearly every organism. Sensing light and transferring this information, however, requires a system of at least two components that are indispensable and only function in a tight, precisely determined manner: light absorbing molecules (“chromophores”) and proteins as the chromophore-tuning and biologically functional elements in living cells.

Chromophores in general are low molecular-weight organic molecules that, by absorbing a photon, transform their electronic state. A Jablonski diagram explains the possible transitions of valence electrons in the various electronic states of a molecule

upon irradiation with light and the back conversion into the ground state, causing the phenomena of fluorescence and phosphorescence <sup>2</sup>.

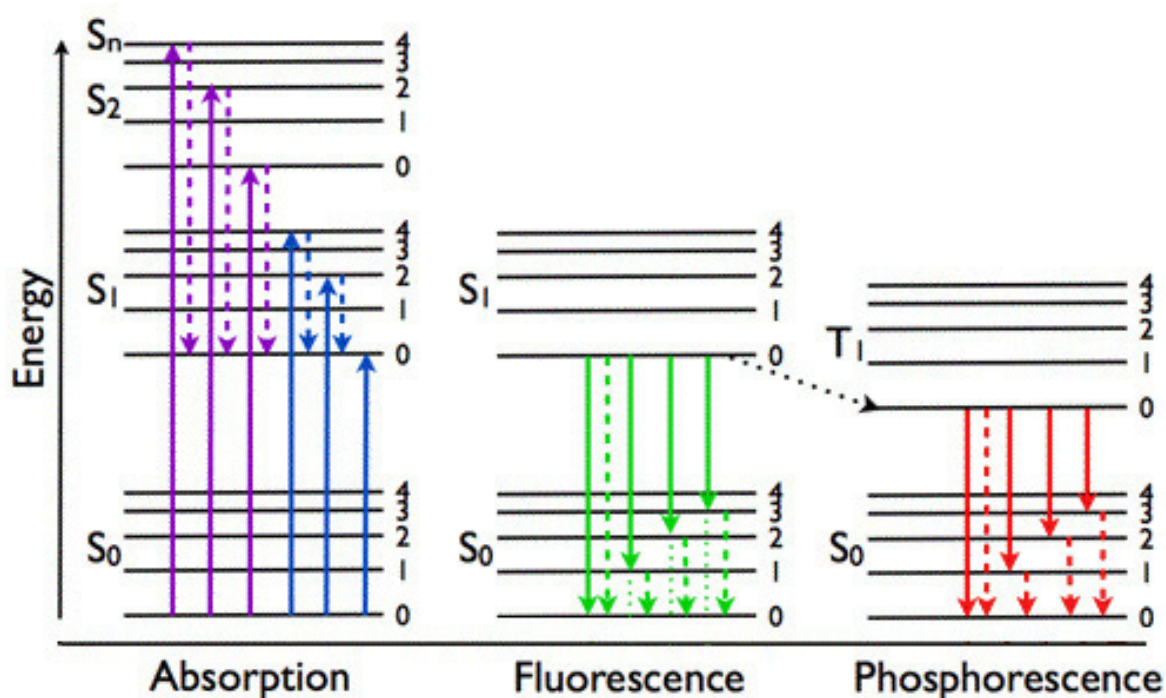


**Figure 1-2: Jablonski diagram** showing different energy states of a molecule. Radiative transitions, absorption (violet and blue) and emission (green for fluorescence; red for phosphorescence) are indicated as solid arrows. Non-radiative transitions (relaxation, internal conversion and intersystem crossing) are represented by dashed arrows <sup>3</sup>.

The state- or Jablonski diagram illustrates all processes relevant for photobiological phenomena. Initiating with photon absorption, ground stated electrons ( $S_0$ ) are promoted to an excited state ( $S_{1-n}$ ) depending on its transition probability. With few exceptions visible light populates the lowest excited state  $S_1$ . If higher energy sources are applied, also  $S_2 - S_n$  states can be reached, however, even then, the conversion to the lowest excited state level ( $S_1$ ) is the directly following, ultrafast process, usually accompanied with vibrational relaxation. The excited state surface is the starting point for all variations, by which a molecule can proceed its reaction pathway: vibrational relaxation again by direct contact to reaction partners allows dissipation of the absorbed energy, and the molecule reverts to its ground state by “internal conversion”. Fluorescence, the emission of light upon de-activation, occurs when an electron from the  $S_1$  state falls back into the ground state. According to geometric constraints that can be expressed by the so-called “Stokes shift”, the energy of the emitted photon is lower than that of the absorbed photon, i.e., the

wavelength of the fluorescent light is longer than that of the excitation light. "Intersystem crossing" describes an alternative transition pathway with a change of spin multiplicity of the excited state electron from a singlet to a triplet state. Also triplet molecules return to the ground state, however, each of the de-activation pathways is symmetry forbidden regarding electrons with parallel spins. Return to ground state can be accomplished again through reaction partner collisions, e.g., the most prominent case might be generation of singlet oxygen from a triplet state excited molecule, but also through the emission of light which then is called phosphorescence. Due to the above mentioned symmetry rules, triplet states usually exhibit a longer lifetime than singlet states.

The reactive molecules (chromophores) discussed here are incorporated in proteins. This combination makes the "photoreceptors" that are described in the following chapter.



## 1.1 Photoreceptors

The first scientific publication about light effects on leaves can be traced back to 1817, nearly 200 years ago <sup>4</sup>. For a historical consideration, it should be mentioned that studies on the light effects on plants even date back further <sup>5</sup>. Starting from these early descriptions of light-regulated phenomena, enormous efforts have been invested in the field of light-sensing organisms and biological photoreceptors. Amongst others, Julius von Sachs observed strong influence of blue light on plant growth (1864) and C. Darwin & F. Darwin (1880) described first experiments about phototropism; however, no detailed information could be provided due to the still missing molecular knowledge on plant physiology. Nevertheless, they postulated that red light does not induce phototropism <sup>6</sup>.

Apart from the basic investigations of light effects on leaves, the identification of red light sensitive phytochromes of plants dates back more than fifty years and was reported by Butler and colleagues <sup>7</sup>. Their findings were the starting point for intensive research on the level of molecular characterization of plant photoreceptors. The red light absorbing phytochromes were for a long time the only known photoreceptors, excluding rhodopsins. Meanwhile, function, mechanism and physiology had been investigated in great detail, however some aspects are still far from been completely clarified. All phytochrome research was performed on these photoreceptors extracted and studied in plants, until 1997, when the first phytochrome was found in prokaryotes <sup>8</sup>.

The effects of blue light on plants had been recognized more than 100 years ago <sup>9</sup>, but the molecular identification of the first blue light photoreceptor was made in 1993 when the “cryptic” cryptochrome cry1 was discovered in *Arabidopsis thaliana* <sup>10</sup>. Just four years later the family of phototropin proteins responsible for phototropism was described. Since then a great developmental leap in photoreceptor research has been seen. Blue light sensing using FAD (BLUF) proteins were found in eukaryotes, probably the most prominent one being the photoactivated adenylyl cyclase (PAC) from *Euglena gracilis*.

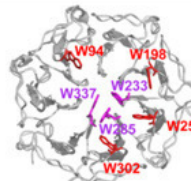
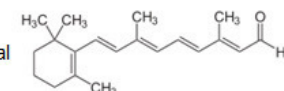
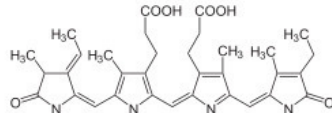
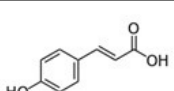
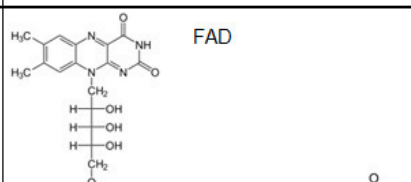
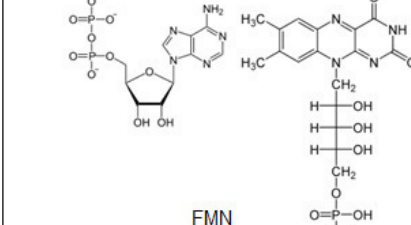
At the beginning of the new millennium the first prokaryotic blue light receptor was found by Losi and co-workers in the bacterium *Bacillus subtilis*<sup>11</sup>; since then genomic mining has revealed a lot more photoreceptors in nearly all kingdoms of life<sup>12</sup>.

Speaking of photoreceptors in general means speaking of two different kinds of proteins based on their biological use of light. Both groups consist of important proteins, helping organism to sense light, to react on radiation and/or to utilize photons.

The first group of proteins uses light as an energy source, e.g., photosynthetic reaction centres that occur in chloroplasts (plants) or within the plasma membrane (photosynthetic bacteria). The captured light energy of a photon is transformed into ATP and NADPH, followed by carbon fixation when carbon dioxide is converted into carbohydrates.

The second type of proteins is photo-sensitive, meaning they use light as an environmental signal or as an information source. Nevertheless, also this group of light-absorbing proteins is also called photoreceptors in relevant literature. These light-sensing photoreceptors form a huge group of proteins that were adapted during evolution to nearly all wavelengths of the light spectrum. Based on the chemical structure of deployed chromophores, the photochemistry of these photoreceptors varies and leads to a classification into eight distinct families: rhodopsins, phytochromes, xanthopsins, BLUF proteins, cryptochromes, UVR-8 and the LOV families, phototropins and ZTL/ADO/FKF1. An overview is given in table 1-1, where the eight families of photoreceptors, as known so far, are listed.

**Table 1-1: photoreceptor families with their typical photochemistry and chromophores.** An example of chromophore including its structure is given. Structure of UVR-8 is from <sup>13</sup>.

Photoreceptor family	Photochemistry	Chromophore	Example
UVR-8	not clearly resolved	triad tryptophan core	
Rhodopsins	trans ↔ cis	retinals	all-trans-retinal 
Pytochromes incl. CBCRs		tetrapyrroles	PCB 
Xanthopsins		trans-p-coumaric acid	trans-p-coumaric acid 
Cryptochromes	e <sup>-</sup> transfer	flavin derivatives	FAD 
BLUF proteins	e <sup>-</sup> transfer and rearrangement of hydrogen bonding network		
LOV proteins: phototropins, ZTL/FKF1/LKP2	adduct formation via FMN-cys(C4a)		

As can be seen in table 1-1, the eight photoreceptor families share similarities in either their chromophore or their photochemistry, with the only exception being the UV-B detecting UVR-8.

Rhodopsins, phytochromes and xanthopsins follow the same reaction mechanism of a *cis-trans* double bond photoisomerization, although, they employ different classes of chromophores; the situation is just opposite with almost all blue light sensitive proteins. They host the same group of chromophores (flavin derivatives), but perform different kinds of photochemistry, like electron transfer, hydrogen bond rearrangement or chemical bond formation. Although photoreceptors are adapted to the whole spectrum of light (fig. 1-3), they can be roughly divided by

phenomenological aspects into two groups: proteins that use light qualities from the blue wavelength range and proteins that work with red light. Exceptions are non-classical phytochromes, like CBCRs, and rhodopsins, which cover the whole range of the light spectrum and UVB receptors.

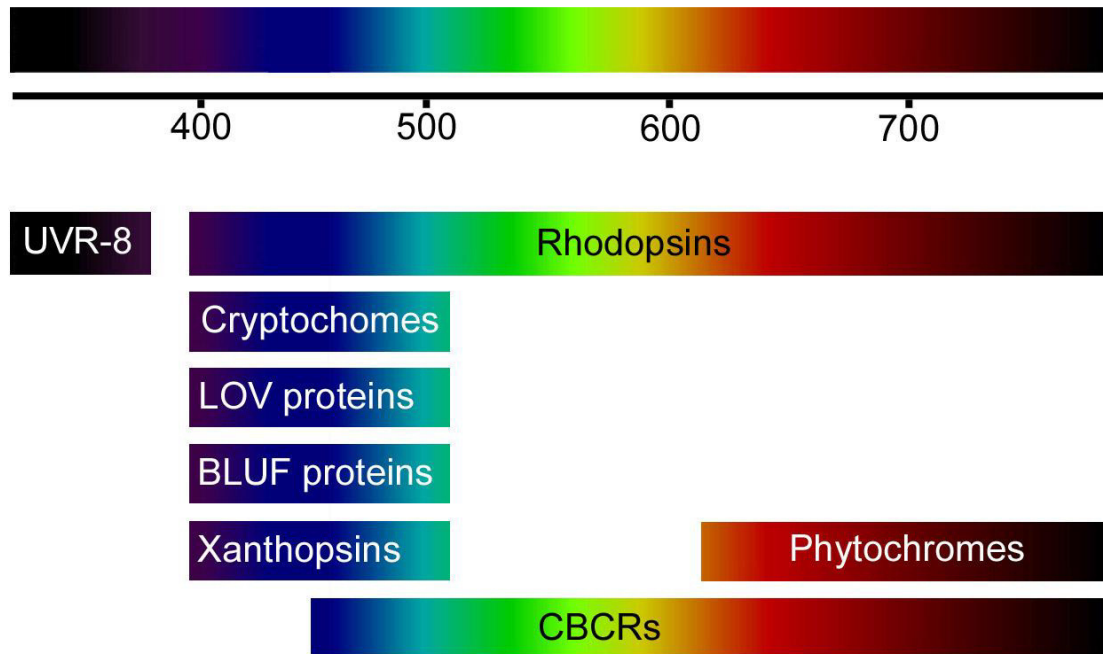


**Figure 1-3: photoreceptor families according to their absorption spectra.**

Photoreceptors perceive information from a large part of the light spectrum.

In the following, these groups of UV-B, blue and red light photoreceptors are described in greater detail. The family of LOV proteins contains the photoreceptors YtvA and mPAC which are the main aspects of this work.

## 1.2 UV-B light photoreceptors

UV radiation is defined as the ultraviolet spectrum of wavelengths in the range of 100 to 400 nm, it can be divided into the three sub-ranges UV-C, UV-B and UV-A. The ozone layer protects the earth from most of the biologically harmful UV radiation, though still UV-A and UV-B light reach the earth's surface. While humans just can see light between 380 nm to 780 nm, plants can also detect light from the UV range, especially UV-B. Plants are dependent on light and on position, they cannot move away from harmful UV-B light. They therefore have to protect themselves from these light qualities and utilize UV receptors.

In 2002 Kliebenstein et al. identified and characterized UVR8 (UV resistance locus 8), a crucial component of the UV-B response of plants<sup>14</sup>. Besides being a photoreceptor not acting in the range of visible light, another feature of UVR-8 makes it an exceptional protein: Up to now, it is the only photoreceptor that bears no exogenous chromophore. Christie and colleagues proposed that the high amount of tryptophans within the amino acid sequence of the photoreceptors plays a critical role in photosensing<sup>15</sup>. Recent publications identified the tryptophan triad W233, W285 and W337 as a major player in the photochemistry of UVR-8<sup>16, 17</sup>.

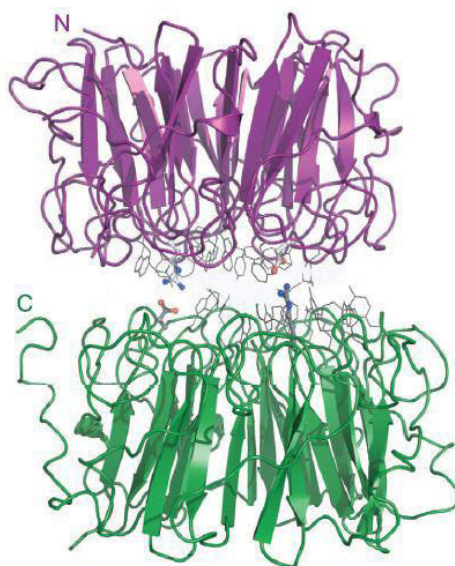


**Figure 1-4: x-ray diffracted crystal structure of a homo-dimer of UVR-8<sup>15</sup>**

UVR-8 appears in its dark state as a dimer (fig. 1-4), but upon excitation by light it converts into a monomeric protein that interacts with other proteins, like COP1. This photoreceptor is localized in the cytoplasm of a plant cell and its x-ray diffracted crystal structure of the dimer showed two seven-bladed  $\beta$ -propeller monomers that are packed face-to-face onto each other. The dimeric interface is built up by aromatic loops whose residue side chains point to the dimeric interface. Here one can find a relatively high concentration of the above mentioned tryptophans, maybe responsible for photosensitivity. Moreover, a bunch of double and single hydrogen bonded salt bridges can be found within this structure <sup>15, 18</sup>.

### 1.3 Blue light photoreceptors

The wavelength region between 320 and 500 nm (sensed as blue light) deserves special attention. These relatively short wavelengths have the highest inherent energy in the region between 420 nm and 500 nm, and this light quality penetrates deepest of all spectral ranges into a clear water column <sup>19</sup>.

In addition, there is another aspect to keep in mind: blue light is the absorbance range especially for many photosensitizing compounds like porphyrins, free flavins etc. via their strong Soret band absorption, which converts these molecules in high efficiency into their triplet state. These molecules, upon light absorption, cause formation of singlet oxygen and other reactive oxygen species (ROS). Singlet oxygen is harmful for its high reactivity and can cause immense damages for, e.g., DNA and RNA and eventually may lead to cell death <sup>20</sup>.

Blue light triggers also a great number of physiological responses, including DNA-repair enzymes, photosynthesis, phototropism, stomatal opening <sup>21</sup>, chloroplast photoaccumulation / photoavoidance <sup>22</sup>, stress response (YtvA), cyclase activity (EuPAC, bPAC) <sup>23, 24</sup> and many more.

These tasks are taken over by a total of five families of the blue light-sensitive receptors that are present in plants as well as in bacteria. These five protein families

are: cryptochromes, xanthopsins, BLUF proteins, phototropins and ZTL/FKF1/LKP2 (see table 1-1). The latter two subgroups can also be included into the group of LOV proteins. All these blue light receptor families carry a flavin as a chromophore, except for the xanthopsins which incorporates a p-coumaric acid chromophore. Although cryptochromes, BLUF proteins and LOV proteins contain the same group of chromophore, they undergo different types of photochemistry. In the following, each blue light receptor family is presented briefly, adding some greater detail to the proteins studied in this work.

### 1.3.1 LOV proteins

Two blue light photoreceptor families, phototropins, including phot-like LOV domain proteins and ZTL/FKF1/LKP2 proteins, can be summarized as the group of light, oxygen, voltage (LOV) proteins, that use flavin derivatives as a chromophore. LOV domains constitute a subfamily of the PER-ARNT-SIM (PAS) domain superfamily; the acronym PAS originates from *Drosophila* period (PER), vertebrate aryl hydrocarbon receptor nuclear translocator (ARNT), and *Drosophila* single-minded (SIM) <sup>25</sup>. PAS proteins are proven to be sensory proteins and can be found in combination with many different regulatory modules in multidomain proteins <sup>25</sup>.

The typical structure of a PAS domain consists of a five-stranded antiparallel  $\beta$ -sheet surrounded by three helical segments <sup>26, 27</sup>. Several types of sensory PAS domains have been described that differ in the bound cofactors, as 4-hydroxycinnamic acid in xanthopsins, FAD in *E. coli* aerotaxis sensors, iron protoporphyrin IX in FixL from *Rhizobium*, and FMN in phototropins <sup>22</sup>.

Genomic research still reveals new and unknown LOV domains <sup>28</sup>. Screening is usually initiated by the conserved amino acid motif GRNCRFLQ, then followed by more sophisticated inspection for essential amino acids or secondary structure elements. Approximately, over 10% of all bacteria carry at least one gene encoding such a sensory domain <sup>29</sup>. Designing a phylogenetic tree based on LOV sequences clearly identifies two distinct classes of LOV domains <sup>12</sup>. On the one hand, LOV



sequences from proteobacteria, cyanobacteria, actinobacteria, firmicutes and chloroflexi cluster together; this group contains mainly proteins very much akin the phot-like LOV proteins. This subgroup also holds eukaryotic sequences from the family of plant ZTL/FKF1/LKP2. The other subgroup holds mainly eukaryotic sequences from plants (phototropins and neochromes), algae (aureochromes) and fungi (WC-1). In addition, bacterial LOVs from alphaproteobacteria can be found here. Most of the sequences originate from cyanobacteria and alphaproteobacteria, leading to the assumption that they might be the origin for plant photoreceptors <sup>12</sup>.

LOV proteins are composed of one (phot-like LOV proteins) or two (phototropins) LOV domains coupled via a short helical linker  $J\alpha$  to an effector domain. The typical structure of a LOV domain consists accordingly to the PAS structure of five antiparallel  $\beta$ -strands ( $A\beta$ ,  $B\beta$ ,  $G\beta$ ,  $H\beta$ ,  $I\beta$ ) and two  $\alpha$ -helices with a C-terminal attached linker helix, called  $J\alpha$  (fig 1-5). This structure forms a chromophore-binding pocket, that holds non-covalently a flavin derivate as a cofactor <sup>22, 30</sup>.

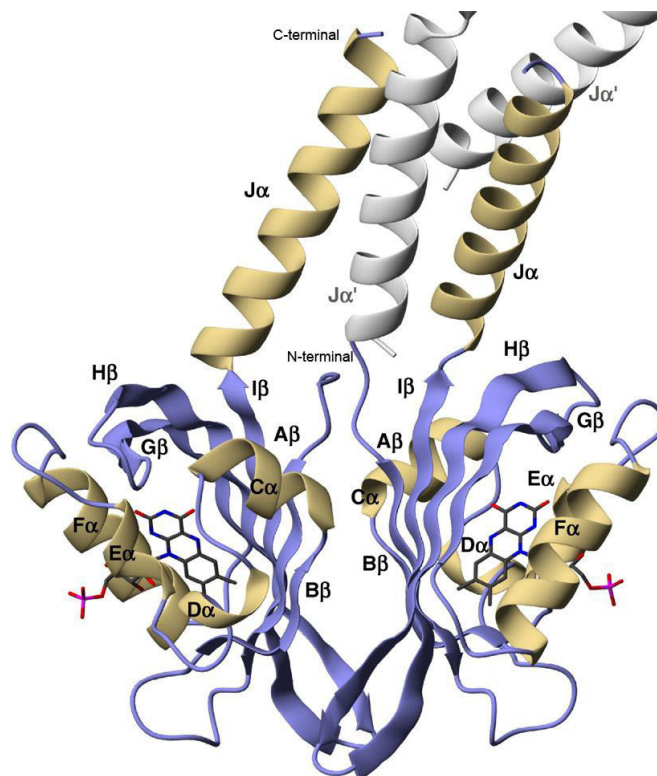


**Figure 1-5: structure of a LOV domain;** here the LOV domain of YtvA from *B.subtilis* in its dark state head-to-head dimer conformation <sup>31</sup>.

Upon blue light illumination, it could be demonstrated that the  $J\alpha$  in some plant LOV proteins undocks from the  $\beta$ -scaffold and partly changes its conformation in order to



transmit a signal from the LOV core to the effector domain <sup>32</sup>. However, this effect could not be detected in prokaryotic LOV proteins <sup>33</sup>. Starting from the first LOV protein, *Atphot1*, for which a serine / threonine kinase was identified as signalling domain, many other effector domains were identified, like histidine kinases <sup>34, 35, 36, 37</sup>, phosphodiesterases <sup>38</sup>, STAS domains <sup>39</sup>, helix-turn-helix proteins <sup>40</sup> and GGDEF-EAL proteins <sup>41</sup>.

The photocycle of LOV proteins is a conserved paradigm (fig. 1-6). Upon blue light exposure the chromophore is covalently bound via a thio-ether, formed from a conserved cysteine residue (e.g. C62, YtvA counting) to position C(4a) of the flavin molecule. Recovery in the dark depends on the biophysical properties of the protein and varies from seconds to hours at room temperature <sup>29</sup>. Some LOV domains have lost the thermal recovery reaction entirely and remain in the photoadduct state. The photocycle and the signalling process can be blocked by mutation of the conserved cysteine within the LOV motif GRNCRFLQ into an alanine or serine, implying that the covalent bond is needed for the photochemical reactivity of the protein <sup>42</sup>. Cysteine mutations render the protein photochemical inactive and keep it in a constitutively active fluorescent state. This fact is important for the employment of LOV domains as *in vivo* fluorescent reporters <sup>43, 44</sup>.

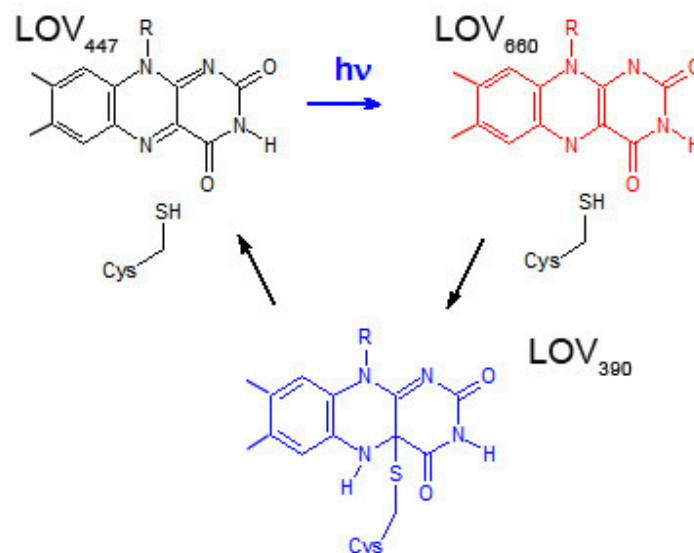


**Figure 1-6: photocycle of LOV proteins.** Dark state LOV<sub>447</sub> transforms via triplet and radical state into LOV<sub>390</sub>.

### 1.3.1.1. Phototropins

Phototropins are blue light receptors in plants, named after their induced effect of phototropism. Phototropism was one of the first investigated light-dependent plant response discovered back in 1880 by Darwin and his son <sup>6</sup>.

It was a long and challenging way to identify and express the responsible protein for phototropism, but in 1997 Huala and coworkers made the first important step by cloning *nph1* (non-phototropic hypocotyls) from *Arabidopsis thaliana* <sup>45</sup>. One year later, it was demonstrated that NPH1 is a photosensitive serine/threonine kinase binding FMN as a cofactor, so the protein was renamed as phot1 <sup>46</sup>. Later, NPL1 (non-phototropic hypocotyl like 1) was found, named phot2 accordingly to phot1. The two photos show a considerably homology but perform different functions <sup>42</sup>.

Besides phototropism <sup>47</sup> both isoforms, phot 1 and phot2, have been proven to regulate a wide bunch of blue light sensitive responses in plants like light-induced chloroplast movement <sup>48</sup>, leaf expansion and movement <sup>49</sup>, and stomatal opening <sup>50</sup>. Each isoform has its very own responses, as phot1 regulates transcript stability and rapid inhibition of hypocotyls growth, and phot2 is responsible for chloroplast avoidance, respectively. Phot1 is constitutively expressed under low light intensities, whereas phot2 is only expressed under high light intensities mediated by the red/far-red sensitive phytochrome photoreceptor phyA <sup>42</sup>.

Phots consist of two N-terminal LOV domains and a C-terminal canonical serine/threonine kinase coupled by the short linker helix J $\alpha$  <sup>51</sup>. In the world of blue light photoreceptors, phot1 have an outstanding role, as they are the only receptors with two LOV domains in a tandem arrangement, LOV1 and LOV2, both binding FMN as a cofactor <sup>52</sup>. The two LOV domains exhibit a sequence similarity of about 40 % to each other <sup>45</sup>. The task of LOV1 has been proven for receptor dimerization upon blue light illumination <sup>53, 54, 55</sup>, whereas LOV2 has the role of a kinase activator <sup>56, 57</sup>. LOV2 senses blue light, undergoes autophosphorylation and transmits the signal to the C-terminal J $\alpha$  helix, which in the dark state is bound to the  $\beta$ -scaffold of LOV2. Upon receiving a signal from LOV2 the helix undocks and thereby activates the serine/threonine kinase.

Both LOV domains of phototropins show the typical LOV domain features making them members of the superfamily of PAS domains. Thus, they undergo normal LOV photochemistry as described in chapter 1.3.1.

### **1.3.1.2 Phot-like LOVs**

A subfamily of the phototropins is the phototropin-like (phot-like) LOV domains. As described before, phototropins are proteins possessing two LOV domains and a serine/threonine kinase at the C-terminus that can be found in plants. However, the highly conserved amino acid sequence GXNCRFLQ encoding a LOV domain can be found in all kingdoms of life, except animals. This large number of LOV domains includes the group of phot-like LOV proteins. Initially, Huala and coworkers<sup>45</sup> proposed in 1997 the existence of LOV domains also in the prokaryotic world.

Major differences between phot-like LOVs and phototropins are for example that phot-like LOV occur in plants and bacteria and the presence of only one LOV domain in phot-like LOVs instead of two LOV domains like in phototropins. The group of fused effector domains is very diverse (fig. 1-7) and responsible for many different physiological responses within the organism.

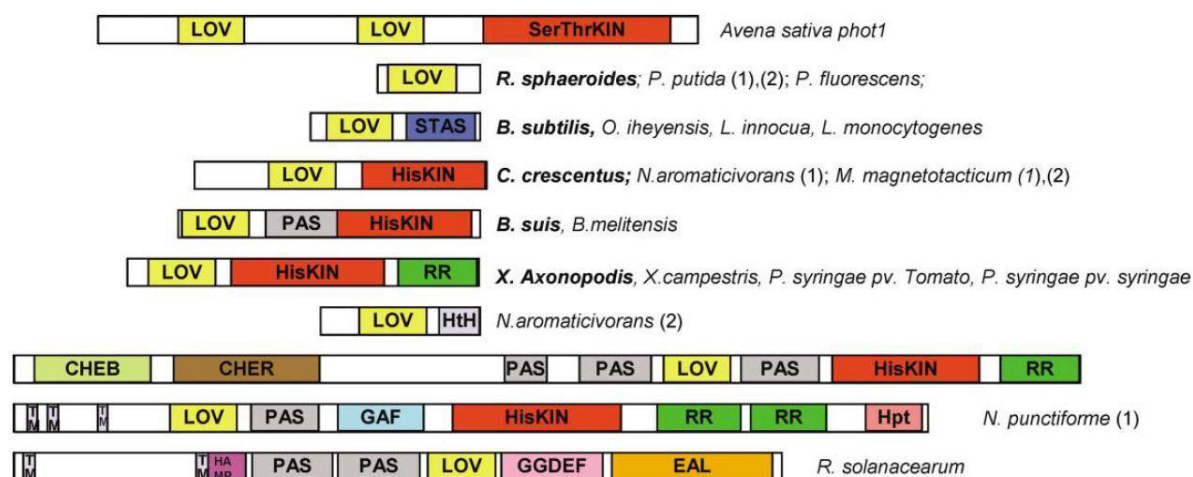


**Figure 1-7: domain architecture of selected LOV domains.** TM: transmembrane helices; STAS: Sulfate transporter/anti-sigma factor antagonist domain; HisKIN: histidine kinase; RR: response regulator, receiver domain; HTH: HelixTurnHelix transcriptional regulator domain; Hpt = Histidine phosphotransfer domain; CheB: CheB methylesterase domain; CheR: CheR ethyltransferase domain; GGDEF, EAL = domains named after their conserved aa motifs, found in diguanylate cyclases and phosphodiesterases; HAMP = domain found in Histidine kinases, Adenylyl cyclases, Methyl binding proteins, Phosphatases <sup>58</sup>.

About one half of bacterial LOV domains are fused to histidine kinases <sup>33</sup>. In some cases, the histidine kinase domain is fused to a response regulator (RR), e.g., the LOV-HK proteins from *Pseudomonas syringae* or *Brucella abortus* <sup>36</sup>. LOV proteins with a histidine kinase having been proven to contain an enzymatically active effector domain that is very versatile further research like light-regulated enzyme activities in optogenetics <sup>59</sup>.

A second, large group of phot-like LOV proteins is equipped with diguanylate cyclases (GGDEF) and phosphodiesterases (EAL) that play an important role in controlling the cellular level of cyclic-di-GMP, a second messenger regulating diverse responses within bacteria. A prototype for this group is the protein SL1 from *Synechococcus* sp. PCC 7942 <sup>38</sup>.

Furthermore, another famous and well known phot-like LOV protein is YtvA from *Bacillus subtilis* <sup>11</sup>. This blue light photoreceptor is composed of a LOV and a STAS domain. As it is one of the proteins which have been intensively investigated in this work, the properties of YtvA are discussed later in greater detail.

In addition, a new type of LOV domain-regulated enzyme activity is presented in this thesis: a naturally occurring protein from the cyanobacterium *Microcoleus*

*chthonoplastes* PCC 7420, composed of a PAS-, a LOV-, and an AMP cyclase domain. This is the first LOV domain fused to an AMP cyclase, offering the opportunity to regulate second messengers in bacterial cells not only by histidine kinases.

### The phot-like photoreceptor YtvA

After the scientific community had worked for nearly one decade on plant phototropins, in 2002 the first bacterial phot-like blue light photoreceptor was discovered by Losi and colleagues <sup>11</sup>. Genomic alignments had shown a strong homology between the already known plant phototropins and YtvA, a small two domain receptor in *Bacillus subtilis*.

*B. subtilis* is a non-photosynthetic, rod shaped bacterium, living mainly in soil; it can be found in nearly all habitats on earth <sup>11</sup>. Due to its ability to form endospores it can protect itself from extreme environmental conditions that often prevail in the upper layers of the ground. In other *Bacillus*, like *Bacillus licheniformis*, a light activation of sporulation had been proven <sup>60</sup>.

The protein itself consists of an N-terminal truncated PAS (1 – 24 aa) in front of a light sensing LOV domain (25 – 126 aa), a 20 aa long linker region, the so-called J $\alpha$ , and a signalling, C-terminal STAS domain (148 – 258 aa). The LOV domain in YtvA is responsible for light detecting and signal transduction, and is built following the common blueprint as a five-stranded antiparallel beta-sheet and four helices in the order of A $\beta$ B $\beta$ C $\alpha$ D $\alpha$ E $\alpha$ F $\alpha$ G $\beta$ H $\beta$ I <sup>61</sup>. These secondary structure elements can be assigned to the following amino acid positions (table 1-2).

**Table 1-2: secondary structure elements of the LOV domain of YtvA.**

name	secondary structure element	residues
A $\beta$	strand	26 - 30
B $\beta$	strand	39 - 42
C $\alpha$	helix	44 - 50
D $\alpha$	helix	54 - 56
E $\alpha$	helix	62 - 65
F $\alpha$	helix	72 - 83
G $\beta$	strand	88 - 95
H $\beta$	strand	101 - 113
I $\beta$	strand	116 - 125
J $\alpha$	linker	127 - 145

The LOV domain forms a chromophore binding pocket mainly with the  $\beta$ -sheet residues and the helices E $\alpha$  and F $\alpha$ , holding a flavin mononucleotide (FMN) molecule as a chromophore. The main stabilization forces to keep the chromophore fixed in the protein are hydrogen bonds. The stabilization of the ribityl chain of FMN is accomplished via hydrogen bonds from N61 and Q66 and two water molecules. For a stable fixation of the isoalloxazine ring, a complex network of hydrogen bonds was identified including the residues Q66, N94, N104 and Q123. Moreover, the amino acids V28, T30, F46, L65, I78, L82, L106 and I108 assist the hydrogen bond network by hydrophobic contacts. Another strategy to keep the chromophore in place is the formation of salt bridges (electrostatic interactions) with the terminal phosphate group of the organic compound (residues R63 and R79). These interactions seem to stabilize the complete protein during photocycle <sup>31</sup>.

The connection between the LOV domain and the STAS domain as an effector domain is realized by a helical linker of 18 amino acids in length, the so-called J $\alpha$ . This helix, appearing C-terminal of the LOV domain, is connected only by a short loop to the light sensing domain <sup>58</sup>. Sequence alignments identified some homology to the J $\alpha$  of phot1-LOV2 from *Avena* <sup>11, 51</sup>, however, the polarity of J $\alpha$  of YtvA is higher than in other LOV domains. Though different LOV domains have nearly the same fold, the orientation of the linker is not the same. Measurements of YtvA-LOV crystals had shown that the linker points outwards and seems to be important for

inter- and intraprotein signaling<sup>31</sup>. No evidence could be found for an unfolding of J $\alpha$  implied by illumination<sup>62</sup>, as proposed for the plant phot-LOV2<sup>51</sup>, but a generation of a scissor-like turning of a monomer is assumed, driven by rotation movements between J $\alpha$  helices<sup>28</sup>. Another suggestion has been made by Avila Perez and colleagues (2009) proposing that the J $\alpha$  may form a coiled-coil structure<sup>63, 64</sup>.

The C-terminal sulfate transporter and anti-sigma factor antagonist (STAS) is the effector domain of YtvA. The ability of this domain to bind GTP was investigated intensively, first results proposed a GTP-binding as the function of YtvA<sup>39, 62, 65</sup>, accordingly, it hosts a typical DxxG motif in its conserved D $\beta$  – E $\alpha$  loop<sup>66</sup>. However, recent publications had shown that YtvA probably does not bind GTP<sup>67, 68</sup>. The secondary structure of the STAS domain consists of four strands forming a central parallel  $\beta$ -sheet connected by three helices on the one side and a poorly conserved, distorted carboxy-terminal helix on the other side<sup>66, 63</sup>.

The photochemistry of YtvA consists of three steps (figure 1-6) and shows the typical LOV behaviour. Upon illumination with blue light (~ 450 nm) the protein converts from the dark adapted ground state into a red-shifted FMN triplet state (after intermediate formation of an excited singlet state) within ps. With the decay of this triplet a reversible formation of the so-called blue-shifted, non-fluorescent FMN-Cys photoadduct (also called LOV<sub>390</sub>) is generated within 2  $\mu$ s. The quantum yield for this process has been determined for YtvA as 0.49<sup>11</sup>. This light state of the protein is the biologically active form, i.e., the signalling state. The thermally driven recovery back to the dark state protein requires up to three hours at 20°C in the dark. YtvA has one of the slowest back-converting LOV domains within the LOV domain family, offering complete steady-state accumulation of the light state of YtvA<sup>61, 69, 70</sup>.

An alternative way to return into the ground state is its photoconversion by illumination with near UV (356 nm) or violet light (405 nm), as, in particular at 400 nm, the absorbance of the photoadduct is higher than that of the parent state. While illuminating a light state YtvA solution with one of these light qualities, some molecules are converted back to the dark state, albeit with a moderate quantum yield of 0.05. Evidence for this effect was reported quite some time ago, but it remained nearly unnoticed<sup>71</sup>. Following, detailed studies were performed on this observation



and are part of this thesis, since its potential for high resolution microscopy was assumed <sup>69</sup>. The rate-limiting step for the thermal dark recovery seems to be a proton-transfer reaction from N(5) to the protein, evidenced by the finding that the addition of imidazole accelerates this reaction <sup>72</sup>.

Physiologically, it is assumed that YtvA is part of a protein complex responsible for the general stress response in *B. subtilis*, the so-called stressosome, by interaction with the alternative transcription factor  $\sigma^B$  <sup>73</sup>. Environmental, growth-limiting stress signals activate the complex, preventing future stresses to the cell by building up resistances <sup>74</sup>. There are three major stress factors to which cells are exposed: energy stress, environmental stress and low temperatures. The important mechanism in the activation of the stressosome is the phosphorylation of serine / threonine residues to guide the stress signal towards the target protein  $\sigma^B$ . This takes the STAS domain into account, as STAS domains carry one conserved serine or two conserved threonine residues as phosphorylation sites. The YtvA-STAS domain, a member of the RsbR family, holds charged glutamine residues instead of the two threonines, most likely to mimick the phosphorylation state of other RsbR proteins. After light activation of the LOV domain, a cascade of four paralog proteins starts by phosphorylation of these proteins, releasing and activating  $\sigma^B$ . The involvement of YtvA in this cascade of reactions has been demonstrated by Gaidenko et al. who could show that overexpression of YtvA leads to a higher  $\sigma^B$  activity only upon blue light irradiation; this effect could not be observed in the dark <sup>74</sup>. Most recent investigations of YtvA inside the stressosome revealed that YtvA only plays a role the stressosome if RsbRA is present inside the complex <sup>75</sup>.

An important impact factor on the photocycle, beside the photophysical and photochemical properties of the bound FMN chromophore, is the microenvironment surrounding the FMN (fig. 1-8) <sup>52, 76</sup>. Its stability in the protein is dependent on residues within the chromophore binding pocket that form interactions with the organic compound such as hydrogen bonds and also provide spatial constraints due to their side chains; these aspects will be outlined in detail in the following.



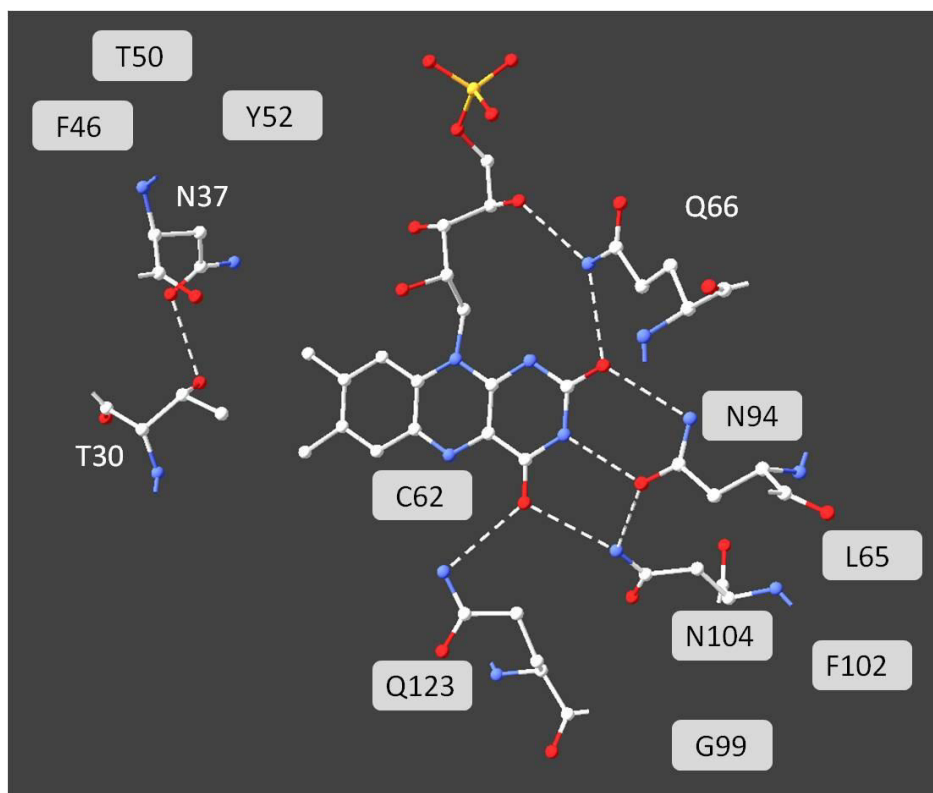


**Figure 1-8: chromophore pocket of YtvA;** showing the ten superconserved LOV residues (highlighted in blue) and the HB network stabilizing the FMN cofactor

Factors that influence the FMN binding cavity are expected to affect the photochemical characteristic of LOV-like kinetics, energetics, and efficiency of the photocycle steps<sup>77, 61</sup>. For a general understanding of the photocycle and for further development in future applications, it is essential to get a more detailed knowledge of the inner protein microenvironment and to identify such “hot spots”<sup>78</sup>. There are two different possibilities to investigate the impact of residues onto the photocycle: first, site-directed mutagenesis within or nearby the chromophore binding pocket or second, identifying naturally occurring amino acid exchanges by sequence alignment and potentially aligning these exchanges to photochemical or physiological properties of these LOV domains<sup>77</sup>. Besides the ten super-conserved residues in YtvA, F46, T50, Y52, C62, L65, N94, G99, F102, N104 and Q123 (fig. 1-8), there are also other amino acids around the isoalloxazine moiety playing a crucial role in chromophore – protein interactions.

Parts of this work focus on the residues with a possible effect on the photocycle like the hydrogen bonding network in YtvA including the positions Q66<sup>78</sup>, N94, N104 and Q123<sup>61</sup>. Previous investigations had already demonstrated that the conserved

glutamine (Q123 in YtvA) rotates its side chain by 180° during the photocycle and therefore modifies the hydrogen bonding network, and potentially represents the gate through which the signal is transferred to the STAS domain <sup>31</sup>. Selectively mutated Q123 variants still undergo a photocycle but at a significantly decreased level or even do not show any functionality in the stress response <sup>63</sup>.

In 2011 Zoltowski et al. discovered EL222 from *Erythrobacter litoralis* that undergoes a modified photocycle, but shows no changes in native protein conformation and signalling mechanisms compared to other LOV domains. In EL222, an alanine is found in the canonical LOV motif instead of a glutamine (A79 in GRNCRFLA instead GRNCRFLQ); in fact, insertion of a common glutamine renders the photoadduct very stable <sup>77</sup>.

The most important residue connecting the chromophore to the protein is the functionally essential cysteine (C62), involved in the formation of a FMN-cysteine C (4a)-thiol adduct after illumination <sup>61</sup>. Avila Perez and colleagues have shown that mutation of C62 into a serine leads to a loss of  $\sigma^B$ -activated response. Residue E56 stabilizes the wild type through the formation of a salt bridge to position K97 and slows down the recovery rate of the dark state, as was demonstrated upon mutagenizing this position into a glutamine and thereby disrupting the salt bridge <sup>63</sup>.

Full-length YtvA exists in solution in three different dimerization states, dimeric, elongated monomeric and spherical monomeric. The LOV domain of YtvA had been demonstrated as an elongated dimer, only hindered by a coupled C-terminal domain. This effect led Buttani et al. to the assumption that the LOV core uses mostly the same residues for homodimerization and for interdomain interactions <sup>36</sup>. In following experiments, the amino acids E105 and D109 were identified to stabilize the dimeric YtvA-LOV construct by forming intermolecular contact <sup>63</sup>. The hydrophobic amino acids involved in dimerization are V25, V27, I29, Y41, M111, I113, Y118, V120 and I122. Crystal structure analysis had revealed that the dimeric YtvA-LOV construct adopts a head-to-head dimerization <sup>31</sup>. Also the STAS domain appears in dimeric state. It has been demonstrated that dimeric proteins, such as the STAS domain dimers, including YtvA, are typical for the structure of the stressosome <sup>63</sup>.

Ongoing, intense research in the field of blue light photoreceptors has revealed a number of protein structures<sup>22, 79, 54</sup>. Nevertheless, structural data on full-length photoreceptor proteins are still limited especially in the case of YtvA. Only LOV-constructs of YtvA could be crystallized and analyzed so far<sup>31, 80</sup>. The availability of a structural model for the full-length protein would be of great importance to understand the function of YtvA, and would provide a reliable basis for a deeper understanding of conformational changes during photocycle. A somewhat different approach for elucidating the full-length structure was chosen in this thesis, as site-selective EPR probes were introduced into YtvA, allowing the distance determination of two or three interacting EPR spin labels<sup>81</sup>.

## The phot-like photoreceptor mPAC

Up to now, only cyclases are known that are coupled to a BLUF domain to sense blue light. This field of BLUF cyclases has brought optogenetics a big step forward as it offers a very good spatial control of cAMP production *in vivo*.

Now, this work presents a completely new kind of blue light sensitive cyclase, a photoactivated adenylyl cyclase fused to a LOV domain which occurs naturally in the cyanobacterium *Microcoleus chthonoplastes* PCC 7420. Accordingly, this protein was named mPAC. *Microcoleus chthonoplastes* is a cosmopolitan, gram-negative, benthic marine cyanobacterium that belongs to the order oscillatoriales and plays a major role in building intertidal and hypersalinic microbial mats by forming out filaments<sup>82</sup>. Moreover, it is able to move on semi-solid and solid surfaces, and the organism tolerates a broad range of saline conditions.

Genome screening of the organism *M. chthonoplastes* PCC 7420, employing the conserved LOV motif GRNCRFLQ yielded first hints for a gene encoding a protein characteristic for a blue light driven adenylyl cyclase function. Bioinformatics research revealed a protein that consists of an N-terminal PAS domain (127 aa), a photoreceptive LOV domain (residues 157 - 260) and a C-terminal adenylyl cyclase (182 aa); in total the protein is 483 aa in size with a molecular mass of 54.2 kDa (fig. 1-9).



**Figure 1-9: domain architecture of mPAC from *M. chthonoplastes* PCC 7420.** Small numbers indicated the beginning and end residue of a domain.

The high sequence homology of mPAC to other LOV domains calls for a typical LOV photochemistry. First photochemical characterisation of mPAC had to prove whether the LOV domain is an active, blue light-sensitive domain and if its photocycle indeed is comparable to those of other LOV domains. The even more important question would be to demonstrate the physiological activity of the light-driven AMP cyclase. Positive results of an enzymatically active cyclase fused to a favourable LOV domain would be a great benefit in the field of versatile tools in optogenetics. The chapter 5

of this work presents the first photochemical and physiological characterisation of mPAC, both *in vivo* and *in vitro*.

### 1.3.1.3 ZTL/FKF1/LKP2

The family of ZTL/FKF1/LKP2 as a subgroup of the generic LOV domains consists of three protein types, ZEITLUPE (ZTL), Flavin-binding Kelch repeat F-box protein (FKF1) and LOV Kelch Protein (LKP2), all three sharing a high sequence homology to each other and to canonical LOV domains <sup>83</sup>. These protein types were first identified in *Arabidopsis thaliana*, a facultative long-day plant with a day length-dependent flowering <sup>84</sup>. Flowering, as well as leaf movement, photosynthesis and hypocotyls elongation are physiological plant responses regulated by the circadian clock. This is a complex gene network influencing the expression of about one-third of proteins in *A. thaliana* as a response, amongst others, to light intensity and duration <sup>85</sup>.

Members of the ZTL/FKF1/LKP2 family have been well studied on the level of molecular and biochemical functions <sup>86</sup>. They consist of an N-terminal LOV domain, an F-box and a C-terminal six kelch repeat domain, all three domains are highly conserved among the family members <sup>84</sup>. The LOV domain is similar to the phot LOV domains, in structure and in binding FMN as a cofactor <sup>83</sup>. The F-box motif is a ubiquitous part of Skp1, Culin and F-box (SCF)-type ubiquitin E3 ligase, forming the SCF complex in *Arabidopsis* that is responsible for targeting protein substrates for degradation <sup>83, 87, 88</sup>. The six kelch motif builds a  $\beta$ -propeller structure, assumed for protein-protein interactions and thereby supporting the F-box by supplying specific proteins for degradation. It has been shown by Imaizumi et al. (2003) that the expressed LOV domain reveals the same absorption spectra <sup>89</sup>, in dark and in light, like phototropin LOV domains, however, with one very remarkable difference. Members of the ZTL family do not show any dark recovery of its LOV domain or recover very slowly within several days, suggesting that they control non-reversible or very slow light responses <sup>88</sup> like induction of flowering <sup>90</sup>.

### 1.3.2 Cryptochromes

Although effects of blue light on plants were studied for more than a hundred years, the first gene for a blue light photoreceptor was identified not until 1993 by Ahmad and Cashmore<sup>10</sup>. As the photosensor appeared “cryptic” it was simply named cryptochrome (cry), the very first cryptochrome from *Arabidopsis thaliana* was called cry1.

The family of cry consists of flavoproteins that use two chromophores, a flavin adenine dinucleotide (FAD) and a flavin antenna/pterin<sup>91, 92</sup>. They show a great similarity to photolyases, a group of enzymes responsible for DNA repair<sup>92</sup>, e.g., the cyclobutane pyrimidine dimers (CPD). Despite the structural similarity, it has been proposed that cryptochromes do not have the capability to repair CPDs. Interestingly, however, the subgroup of cry-DASH builds a bridge between cry and photolyases, by being cryptochromes that are able to split CPD but have up to now no clear prove of light sensitivity<sup>93</sup>. Cry, photolyases and cry-DASH form a very large photoreceptor family due to their high sequence homology. Cry proteins hold an approximately 500 amino acid long, N-terminal photolyase homologous region (PHR) core and a cryptochrome C-terminal extension (CCE) that can differ in length and sequence, and apparently is involved in their signalling function<sup>94</sup>. The PHR core domain consists of an  $\alpha/\beta$  subdomain at the N-terminus. The  $\beta$ -scaffold consists of five parallel  $\beta$ -strands, whereas at the C-terminus of this subdomain is a 4 $\alpha$  helical structure that binds non-covalently the FAD<sup>94</sup>.

As the chromophore FAD is a two electron carrier, it can have three different redox states in the protein, oxidized, semi-reduced and fully reduced. The oxidized redox state of FAD absorbs mostly in the blue light region, so it is assumed that this redox state constitutes the ground state of the protein. Exposure to blue light results in a reduction of the FAD during the photocycle of the protein, and only the semi- or fully reduced FAD is able to initiate DNA repair.

Up to now, crys were found in prokaryotes, archaea, and eukaryotes<sup>95</sup>. The photosensory crys have different functions in plants and animals. In plants they control growth and development<sup>95</sup>, in some animals they are suggested to fulfil an

additional function, i.e., to act as light-dependent magnetoreceptors, e.g., in insects and migratory birds <sup>96</sup>. In plants as well as in animals, they also regulate the circadian clock <sup>94</sup>.

### 1.3.3 BLUF proteins

The photosensory family of blue light using FAD (BLUF) domain proteins is the scientifically “youngest” family in the field of blue light photoreceptors. Besides LOV proteins and cryptochromes this is the third family using a flavin derivative as a chromophore. After an intensive genomic research Gomelsky and Klug declared in 2002 the BLUF proteins as a new type of photosensory proteins <sup>97</sup>. BLUF domains are small modular proteins, quite similar in size, approximately 100 – 110 residues, and composition to the LOV proteins <sup>98, 70</sup>. The basic structure follows a very compact  $\alpha/\beta$  fold (fig. 1-10), consisting of a five-stranded  $\beta$ -sheet mixed with 3 parallel  $\alpha$ -helices, arranged like  $\beta 1\alpha 1\beta 2\beta 3\alpha 2\beta 4\beta 5$  <sup>70</sup>. On the opposite side of the  $\beta$ -sheet a helix-turn-helix motif is located <sup>99</sup>.

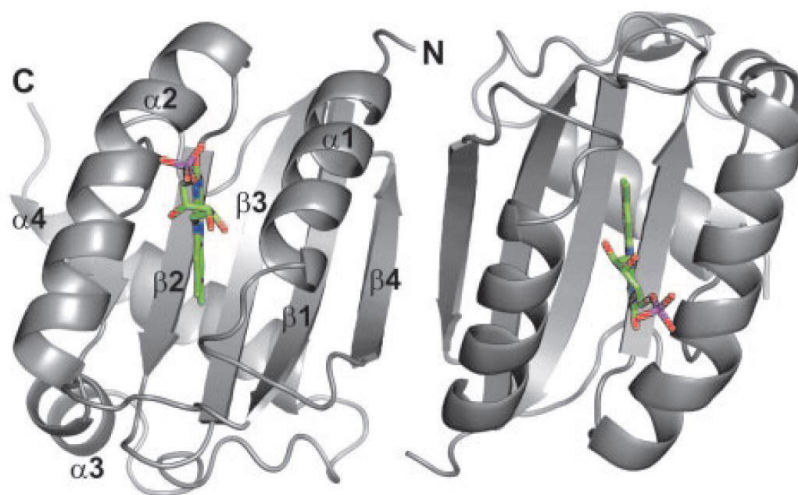


**Figure 1-10: structure of two BLUF domains in an asymmetric unit of BlrB.** Flavin chromophores are presented in green <sup>99</sup>.



The BLUF proteins use an FAD chromophore that is held within the  $\alpha/\beta$  fold. The isoalloxazine ring of FAD binds tightly, but non-covalently to both  $\alpha$  helices and is surrounded and stabilized by the  $\beta$ -sheets that form, with their side chains, a chromophore binding pocket<sup>99, 70</sup>. BLUF domains carry one FAD chromophore per protein moiety<sup>97</sup>, that is non-covalently bound similarly as FMN in LOV proteins<sup>100</sup>.

Upon blue light exposure a small, but distinct shift of the FAD absorption spectrum towards longer wavelengths is observed which upon switching off the light immediately - within seconds - reverts to the parent state in the dark. Within this photocycle, a transient light-induced electron transfer reduces FAD to  $\text{FAD}^{\bullet-}$ , then  $\text{FADH}^{\bullet}$  is formed by an  $\text{H}^+$  transfer. The signalling state,  $\text{BLUF}_{\text{red}}$ , is formed within 1 ns, the photocycle including the red shift can differ slightly and the recovery of BLUF domains can range from seconds to minutes<sup>101</sup>. Ultrafast studies of this photocycle revealed a radical anion as a reaction intermediate<sup>102</sup>, further intermediates or reaction steps are still under debate.

Today, two types of BLUFs are known: short, single proteins and complex, multidomain proteins, all found in different classes of bacteria and lower eukarya. The short proteins, up to about 170 amino acids, cover most of the BLUF proteins. They consist of the BLUF core and a short C-terminus, usually dissimilar to any known motif. It is assumed that these short BLUFs are assumed to take part in protein-protein interactions<sup>97</sup>. Well studied prototypes for the group of complex BLUF proteins are for example AppA from *Rhodobacter sphaeroides*<sup>103</sup>, EuPAC from the protist *Euglena gracilis*<sup>104, 105, 23</sup>, BlaC<sup>106</sup> or bPAC from *Beggiatoa*<sup>24</sup>. Though first steps to unravel the mystery of BLUF paradigm have already been performed, the detailed reactions upon illumination and their biological roles are still not known.

### 1.3.4 Xanthopsins

The photoreceptor family of xanthopsins has its origin in the photoactive yellow protein (PYP) from *Halorhodospira halophila*, identified in 1985<sup>107</sup>. *H. halophila* PYP is characteristic for the group of xanthopsins; it is a 14 kDa small, stable protein consisting of 125 amino acids. This short sequence is folded into a typical PAS



domain  $\alpha/\beta$  secondary structure with a central six-stranded antiparallel  $\beta$ -sheet arrangement surrounded by five  $\alpha$ -helices<sup>108</sup>. The PYP protein can structurally be divided into four parts, an N-terminal  $\alpha$ -helical cap, a PAS core, a helical linker, and an anti-parallel  $\beta$ -scaffold<sup>109</sup> in full accordance to the PAS proteins.

PAS domains are often located in multidomain proteins acting as sensors for numerous stimuli<sup>108</sup>. Even PYP could be found in large photoactive multidomain proteins, like Ppr that has a PYP fused to a bacteriophytochrome and a histidine kinase in *Rhodospirillum centenum*<sup>110</sup>. However, PYPs can also act as a single domain photoactive receptor.

To sense blue light, PYPs ( $\lambda_{\text{max}} = 446 \text{ nm}$ ) contain a p-coumaric acid chromophore (pca) that is, in dark state, deprotonated in its *trans* configuration. The main chemical process upon blue light excitation is a *trans* – *cis* isomerization of the chromophore followed by conformational changes within the protein that lead to the formation of the signalling state. Due to the three major photochemical processes, i.e., isomerization, protonation change and the recovery, the photochemistry is the same like in sensory rhodopsins although the two protein families differ in protein and chromophore structure<sup>111</sup>.

In recent years, genome mining has added ca. 140 PYP-related proteins to the family of xanthopsins. Sequencing research has revealed 35 named bacterial species. In addition, in metagenome screening more than 100 defined species were found that potentially carry a PYP. While the first PYPs were all found in proteobacteria (still hosting the most PYP species), now also species from bacteriodes and spirochaetes were identified. PYPs have been found in purple photosynthetic bacteria as well as in aerobic anoxygenic phototrophes, in non-phototrophic aerobes and in strict anaerobe bacteria<sup>112</sup>. Based on homology, insertions, deletions and conserved amino acids the xanthopsins can be divided into seven structural subgroups<sup>112</sup>. Within each subgroup the homology is quite high and it is assumed that PYPs from one particular subgroup have similar functional roles like, e.g., phototaxis regulation, DNA repair, polyketide synthases, osmotic regulation and cell buoyancy.

## 1.4 Red light photoreceptors

Most of the red light photoreceptors, like traditional phytochromes, can adopt two spectroscopic states, both absorbing within the range of 600 nm to 750 nm.

In the following, the traditional phytochromes are presented with a closer look at cyanobacteriochromes (CBCRs), a new subfamily with fascinating properties. Nowadays, these CBCRs extend the traditional group of red light photoreceptors in a broader sense as they exist in two or sometimes more states <sup>113, 114</sup>; at least with one state absorbing red or far red light, the other one(s) can peak in other spectral regions like orange, green or even blue light. The last part of this chapter describes very briefly the rhodopsins. Rhodopsins cover practically all wavelengths of visible light and have therefore an outstanding position in the photoreceptors; however, their properties are not relevant for this thesis.

### 1.4.1 Phytochromes

Red and far red light qualities are detected by phytochromes (phy), a very well-known and expanding family of photoreceptors <sup>115</sup>. Since the 1950th phytochromes are of high scientific interest and for a long time they were the only known photoreceptors besides visual rhodopsins. In 1982, the first full length phy was isolated from *Avena sativa* <sup>116</sup>, shortly followed by the identification of its gene and amino acid sequence <sup>117</sup>. Fifteen years later, Hughes and co-workers identified and characterized the first prokaryotic phy in the cyanobacterium *Synechocystis* <sup>8</sup>, and since then these proteins have been found in several organisms like cyanobacteria, nonoxygenic photosynthetic bacteria, nonphotosynthetic bacteria, diatoms and fungi <sup>115, 118, 119</sup>. Today, the large family of phytochromes can be divided into five sub-families: plant phytochromes, bacteriophytochromes, cyanobacterial phytochromes, fungal phytochromes, and phytochrome-like sequences <sup>120</sup>.

The family of phy contains three different covalently bound chromophores, all based on open-chain tetrapyrroles, also referred to as bilins. They include phycocyanobilin

(PCB) in cyanobacteria, phytochromobilin (PΦB) in plants, and biliverdin IX $\alpha$  (BV) in most other bacterial phys and fungi, all detecting red and far red light. BV can be further metabolized either to yield PCB by a ferredoxin-dependent bilin reductase (FDBR) or by a two–electron transferring bilin reductase / phytochromobilin synthase to generate PΦB.

All subfamilies of phytochromes, except of cyanobacteriochromes, are built of an N-terminal photo-sensitive module, which is a fusion of a PAS, a GAF (cGMP phosphodiesterase, adenylyl cyclase and FhlA protein) and a phytochrome-specific PHY domain. The C-terminus carries the regulatory part of the protein; the majority of phys hold a histidine kinase or a histidine kinase-related domain, sometimes in combination with additional PAS domains or response regulators (RR). In plants, it is assumed that they hold a C-terminal serine/threonine kinase instead of a histidine kinase. Moreover, a so called “Quail module” can be found between the sensory and effector parts of plant phytochromes <sup>121, 122</sup>. In 2005 the first three-dimensional structure of Bph1 of *Deinococcus radiodurans* was published, however, this construct comprised only the PAS and the GAF domain <sup>123</sup>. Although the chromophore pocket was not complete due to the missing PHY domain, important conclusions could be obtained from this first, initial structure. The PAS and GAF domain are interloped together, holding the chromophore that is in a periplanar ZZZssa configuration. This result of x-ray crystallography made a big step in revealing the structural features of phytochromes <sup>123, 124</sup>. A structure for the complete sensory module of Cph1 from *Synechocystis* 6803 including PAS-GAF-PHY in its Pr state was published in 2008 <sup>125</sup>.

Phytochromes are involved in several different physiological processes, depending on their sub-family. Plant phys are for example responsible for mediating seed germination, growth inhibition, leaf development, induction of flowering, and phototropism; in addition, they are important for the regulation of the circadian clock <sup>126</sup>. Regarding their physiological role, prokaryotic phytochromes are not that well investigated like their plant orthologs. Known physiological tasks are, e.g., regulation of the organism’s light response and again the entrainment of the circadian clock, phototaxis and the chromatic adaption <sup>127, 128, 129</sup>.

### 1.4.2 CBCRs

The cyanobacteriochromes (CBCRs) comprise a special group of phys that should be mentioned here. They are photochromic biliproteins from cyanobacteria with principally the same light induced chromophore reactions as classical phytochromes, but also showing a greater variation of the classical photochemical properties. Different to “classical” phytochromes, CBCRs cover a much broader spectral range, extending from the near-ultraviolet into the near infrared wavelengths<sup>130, 113</sup>.

Astonishingly, these light-sensing qualities of CBCRs depend on bearing one or more GAF and PAS domains instead of the light sensing module PAS-GAF-PHY of canonical phytochromes<sup>129, 120</sup>. Not all of the GAF domains of the oligo-GAF CBCR are assumed to be photoactive<sup>131</sup>.

Similarities to phys can be found in the homologous chromophore-binding GAF domain within the light sensing module, in bilin based chromophores and in their two, in some cases even more, reversible light switchable states<sup>132</sup>. Although the mentioned GAF domain is homologous, it is grouped into a distinct family regarding sequence alignments<sup>129</sup>. CBCRs use PCB as chromophore (fig. 1-11), but in addition, in some of these proteins, the PCB chromophore experiences a chemical modification such that phycoviolobilin (PVB) is formed after incorporation into the protein, and in other cases 10-thio-phycocyanorubin (TPcR) and 10-thio-phycoviolorubin (TPvR) are formed in some states of their photochemical process which are generated from PCB or PVB by an additional nucleophilic reaction of a second cysteine to the C10 position of the bilin chromophore<sup>113</sup>.

Until the last years, working with bilinproteins was quite laborious. For *in vitro* measurements phytochromes could be loaded to 100 % with chromophore in additional working steps, however, *in vivo* applications were limited. To circumvent the problem of assembly the overexpressed apoproteins, CBCR proteins are for most applications co-expressed with genes coding for chromophore biosynthesis, ho1 (heme oxygenase) and pcyA (phycocyanobilin : ferredoxin reductase), to generate holo-CBCRs<sup>129, 132</sup> *in vivo*.

The photochemistry of all CBCRs includes photoisomerization between the 15Z and 15E photostates at the C15 methine bridge of their bilin chromophores with an attended rotation of the bilin D-ring (fig. 1-11) <sup>113, 133</sup>.

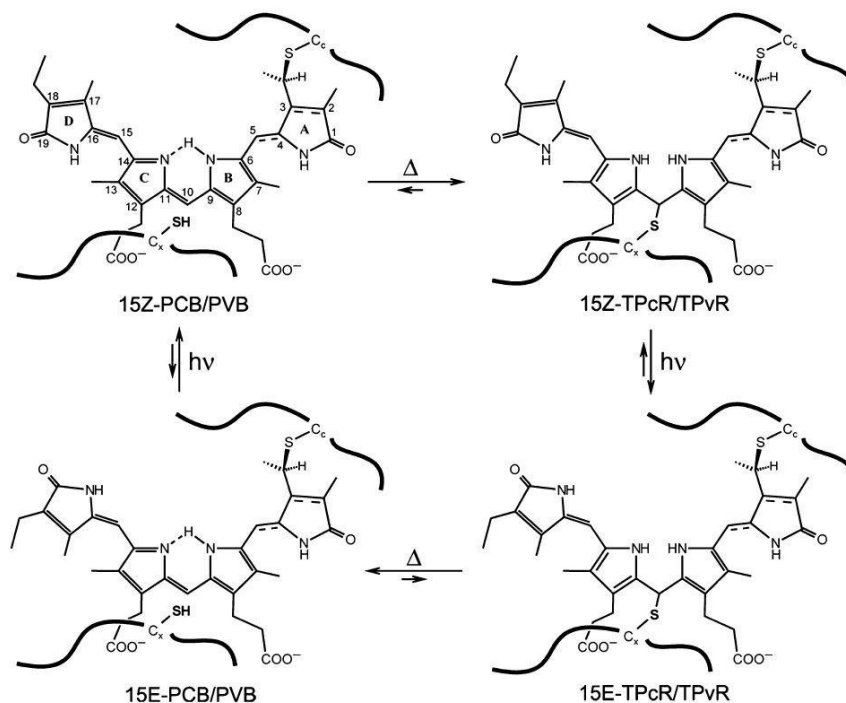


**Figure 1-11: intermediate generation of different bilin chromophores in CBCRs** <sup>132</sup>.

As mentioned above, CBCRs cover the whole spectra of visible light and therefore they undergo different conversions that are wavelength and chromophore dependent. Up to now, five subfamilies of CBCRs could be identified, dependent on their photochemistry and spectral absorbing regions: (i) they can undergo red/far red photochromism with a switch of dark state 15Z into 15E, just akin phytochromes; (ii) green/red interconvertible proteins; (iii) proteins with a red/green conversion due to a blue shifted 15E conversion into 15Z; (iv) blue shifted red/orange photocromism <sup>131</sup>; (v) CBCRs which 15Z states peaks in the blue region or in the near UV <sup>134</sup>.

As CBCRs were just discovered recently, not much is known about their physiological roles. PixJ1 of *Synechocystis* sp. PCC 6803 regulates the positive phototaxis <sup>135</sup>. The cyanobacteria *Synechocystis* sp. PCC 6803 and *Nostoc* sp. PCC 7120 are the currently best studied hosts for CBCRs. The latter one holds more than 50 ORFs that may code for putative CBCRs with at least one GAF domain. Some of these genes

were already characterized <sup>132, 136</sup>, but there are still many oligo-GAF proteins undiscovered.

### 1.4.3 Rhodopsins

The structurally most characteristic element of rhodopsins is their arrangement into seven transmembrane helices.

Sequence-based studies revealed two types of opsins: type I contains microbial, and type II covers animal ones <sup>137</sup>. Microbial rhodopsins occur in archaea, fungi, eubacteria and algae and function as light-driven proton and chloride pumps, light-gated cation or anion channels and photoreceptors <sup>138, 137</sup>. Type II rhodopsins are found in animals and are photoreceptive proteins in visual cells of invertebrates and vertebrates <sup>138</sup>. These two types of rhodopsins can be further divided into different sub-groups according to their physiological function: bacteriorhodopsins and halorhodopsins are light-driven energy pumps, whereas sensory rhodopsins I and sensory rhodopsins II have visual, light-sensing functions.

The above-mentioned heptahelical structure is best seen in these “visual” rhodopsins which also show three extended extracellular loops and three cytoplasmic loops involved in signal transduction by interaction with the visual G-protein transducing <sup>139</sup>.

Common to both classes of rhodopsins is their covalently bound chromophore, a retinal (vitamin-A aldehyde) covalently attached via a protonated Schiff base to a lysine residue in the seventh helix. Whereas type I rhodopsins carry the *all-trans* isomer, the animal rhodopsins bind the *11-cis* isomer. The wide spectral variation of rhodopsins is generated by the protonated state of the chromophore which is stabilized and modulated by counter ions (aspartates, glutamates, or even chloride ions), and the interaction with polar amino acids of the binding site. Upon light exposure the chromophore isomerizes and the protein undergoes structural changes, sometimes including chromophore deprotonation, which then leads to their physiological function.

## 1.5 State of the Art

The previous chapter has outlined the importance of light and its impact on evolution covering the history of photoreceptors and light sensing proteins. As these proteins are ubiquitous in all habitats on earth and perform physiological functions, the field of photoreceptors is still of high interest for the scientific community. Since the first identification of photosensitive proteins, the collected information about photoreceptors is exponentially growing. Many scientific groups all over the world, organized in different communities focused on photobiology and photochemistry, push on the knowledge about photosensitive proteins. Up to now, many details are known about photoreceptors, especially about the molecular mechanisms of the typical photocycles in the photoreceptor families. For some of them, physiological functions could be identified, but even the most “popular” photosensitive proteins are not completely understood yet. Many open questions about the detailed mechanisms of the photocycle, signal transduction or protein-protein interactions are far from being resolved. What are the photocycle intermediates? Which residues play an important role within the photochemistry? How can a signal be transduced from the sensor domain toward an effector domain? What kind of physiological responses are mediated by photoreceptors?

For many more questions of this type, one may find suggestions and partial information in the literature but none of these questions are answered completely in our days. Moreover, studying photoreceptors can also be a big help in understanding dynamic alterations in general protein structure based on their function. Van der Horst and Hellingwerf gave three reasons to study photoreceptors, first, they offer very high time-resolved data about dynamical alteration in their structure after laser illumination, and second, they undergo large conformational transitions during signalling state formation. Third, for the time scale, relevant to resolve structural transitions, the changing colour of the proteins can be a good indicator<sup>100</sup>.

Many photoreceptors have been discovered so far in all kingdoms of life, bacteria, archaea and eukaryotes. It is estimated that in the bacterial world about 25% of the organisms carry a conserved sequence for photosensitive proteins. Screening for the conserved LOV motif within the bacteria results in more than 10% of all bacteria



containing such a motif in their sequence<sup>33</sup>. New sequencing projects combined with further genomic screening will reveal many more photoreceptors in new organisms that have so far not been reported to be light sensing, with possibly new photochemical mechanisms and/ or new physiological roles.

Both, a detailed knowledge about the photoreceptors' mechanisms and the identification of new candidates point to the development of new, fascinating application methods based on photosensitive proteins. Now, we are only at the onset of such possibilities arising from photoreceptors in system biology and other fields of applications. To focus light sensing proteins for applications means coevally that a better if not complete understanding of the mechanisms is necessary to design the best techniques.

The two types of applications developed so far are on the one hand physical applications like nanoscopy and on the other hand medical applications like light-gated cation channels. These latter ones are mostly driven from the applications of channelrhodopsins. Physical applications use the light sensing domains of known photoreceptors fused to proteins for, e.g., high resolution microscopy, so-called nanoscopy. This technique might answer questions about the location of proteins within a cell. Also, one might ask, whether proteins accumulate, maybe under special conditions like stress? "Medical" applications can be used in the fields of systems biology and neurobiology. All mechanisms within a cell underlie precise spatial and temporal control, mainly mediated by second messengers like cAMP or cGMP or cations like sodium and potassium. Applications like optogenetics aim to offer inducible control over cellular processes<sup>140, 24</sup> like activation of signal cascades and transcription.

Only with an excellent understanding of how the photochemistry works and which residues play important roles in holding the chromophore and affecting the kinetics and fluorescent characteristic, these receptors can be improved and tuned for further applications.



## 1.6 Aim of this work

The information about photoreceptors is growing since several decades. Many important steps could be made and many small details were revealed, both pushing forward the knowledge about light sensitive systems and offering the basic principle for endless possibilities in the field of applications.

This thesis is focused on the transition from basic knowledge of photoreceptors to the development of applications. Questions addressed were, how can a photocycle be tuned to undergo specific, distinct light switching reactions? Are the photoreceptors, used in this work, good fluorescent markers? What kind of new photoreceptors and mechanisms are out there, leading to the next step in photoreceptor knowledge?

All these questions were addressed to extend our knowledge about bacterial and archaea photochemistry. The results are presented within the next chapters, which consist of publications already published or under review process, and unpublished data, still in progress for publication.

The principles of biological photochemistry and structural aspects are dealt with in **chapter two** of this present work. The well-characterized blue light photoreceptor YtvA was used as a model system. As this protein has been studied already for several years, many features and properties are well characterized so that the impact of the selected details can be analyzed in great detail. The first publication “Modulation of the Photocycle of a LOV Domain Photoreceptor by the Hydrogen-Bonding Network” deals with the hydrogen bonding network in YtvA’s chromophore binding pocket investigating the impact of these interactions on kinetics and energetics of the photocycle. The second paper in this chapter “The amino acids surrounding the flavin 7a-methyl group determine the UVA spectral features of a LOV protein” shows that a typical LOV2-like bacterial LOV domain (of YtvA) can be turned into a LOV domain with a LOV1-like behaviour via just one single point mutation. Investigations like this one aim to turn and improve photoreceptors to make them adequate tools with special features for applications like optogenetics or nanoscopy. Another aspect besides the photophysical one in understanding a protein is certainly the protein structure of the protein, shown in **chapter three**. Some structures of LOV

domain constructs have been investigated but how exactly the full-length LOV-STAS construct of YtvA is arranged is still speculative. Accordingly, this third publication provides the shape of the full-length YtvA protein received with the help of spin labelled residues by EPR spectroscopy.

YtvA wild type carries three cysteines, an amino acid whose side chains react selectively with the spin label compound. Inserted cysteines of four mutants were labelled with a nitric oxide spin label for EPR measurements to determine a full-length protein structure as well as the oligomeric protein state.

**Chapter four** addresses the topic of photoreceptors for applications. To show the highly promising potential of YtvA as a candidate for physical applications, the protein was investigated with nanoscopy, attempting to obtain high resolution images of its fluorescence. Essential for this application was the demonstration of back irradiation of YtvA with UV/near UV light (356 and 405 nm). This effect converts YtvA into a light-switchable protein as the basis for high resolution (<30 nm) fluorescence microscopy.

**Chapter five** demonstrates that genomic mining and database research yield new, fascinating photoreceptors. Introduction and characterization of the blue light sensitive protein mPAC is described in publication number 5.1, showing a small, very fast-cycling cyanobacterial photoreceptor coupled to a physiological active AMP cyclase. As functionally characterized in frog oocytes, this protein may offer new possibilities in controlling second messenger levels *in vivo*. The second manuscript in this chapter enters the field of red light photoreceptors, presenting a first broad spectroscopic and partly unpublished characterization of the 2699 GAF1 and GAF3 from *Nostoc* and 1393 GAF 3 domain from *Syneccocystis*.

The last chapter, **chapter six**, discusses the work and the conclusions of this thesis and summarizes and outlines the important results.

## **2. Mechanisms of the blue light photoreceptor YtvA**

### **2.1 Modulation of the Photocycle of a LOV Domain Photoreceptor by the Hydrogen-Bonding Network**

Journal of American Chemical Society, 9.9, 1. author

Sample generation and preparation: 100 %

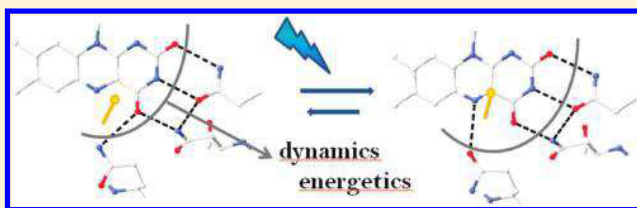
Measurements: 40 %

# Modulation of the Photocycle of a LOV Domain Photoreceptor by the Hydrogen-Bonding Network

Sarah Raffelberg,<sup>†</sup> Madina Mansurova,<sup>†</sup> Wolfgang Gärtner,<sup>†</sup> and Aba Losi<sup>\*,†,§</sup><sup>†</sup>Max-Planck-Institute for Bioinorganic Chemistry, Stiftstrasse 34-36, 45470 Mülheim, Germany<sup>§</sup>Department of Physics, University of Parma, viale G.P. Usberti 7/A, 43100 Parma, Italy

S Supporting Information

**ABSTRACT:** An extended hydrogen-bonding (HB) network stabilizes the isoalloxazine ring of the flavin mononucleotide (FMN) chromophore within the photosensing LOV domain of blue-light protein receptors, via interactions between the C(2)=O, N(3)H, C(4)=O, and N(5) groups and conserved glutamine and asparagine residues. In this work we studied the influence of the HB network on the efficiency, kinetics, and energetics of a LOV protein photocycle, involving the reversible formation of a FMN–cysteine covalent adduct. The following results were found for mutations of the conserved amino acids N94, N104, and Q123 in the *Bacillus subtilis* LOV protein YtvA: (i) Increased (N104D, N94D) or strongly reduced (N94A) rate of adduct formation; this latter mutation extends the lifetime of the flavin triplet state, i.e., adduct formation, more than 60-fold, from 2  $\mu$ s for the wild-type (WT) protein to 129  $\mu$ s. (ii) Acceleration of the overall photocycle for N94S, N94A, and Q123N, with recovery lifetimes 20, 45, and 85 times faster than for YtvA-WT, respectively. (iii) Slight modifications of FMN spectral features, correlated with the polarization of low-energy transitions. (iv) Strongly reduced (N94S) or suppressed (Q123N) structural volume changes accompanying adduct formation, as determined by optoacoustic spectroscopy. (v) Minor effects on the quantum yield, with the exception of a considerable reduction for Q123N, i.e., 0.22 vs 0.49 for YtvA-WT. The data stress the importance of the HB network in modulating the photocycle of LOV domains, while at the same time establishing a link with functional responses.



## INTRODUCTION

The photocycle of LOV (light, oxygen, voltage) protein domains is chiefly dictated by the photophysical and photochemical properties of the bound flavin mononucleotide (FMN) chromophore<sup>1</sup> but also influenced by the surrounding microenvironment.<sup>2,3</sup> Weak interactions, such as hydrogen-bonding (HB), and spatial constraints imposed by the side chains of amino acids forming the FMN binding cavity are expected to affect the kinetics, the energetics, and the efficiency of the different steps of the photocycle. In this respect the hydrogen bonds formed around the polar groups of the FMN isoalloxazine could be of primary importance, besides being a major determinant in chromophore stabilization and the first protein–chromophore interface undergoing conformational changes upon light activation.<sup>4–8</sup>

LOV domains are small photosensing protein modules of ca. 100 amino acids forming a quite compact and structurally conserved  $\alpha/\beta$  core flanked by variable N- and C-terminal helical regions.<sup>9–11</sup> They host FMN as a non-covalently bound chromophore and absorb maximally around 450 nm (resting or dark-adapted state, referred to as LOV<sub>447</sub>), and they constitute a subclass of the PAS (PerArntSim) superfamily.<sup>12</sup> According to a recently proposed nomenclature,<sup>13</sup> we assign the following secondary structure elements to the LOV core (from the N-terminal part):  $\alpha\beta\beta\beta\text{C}\alpha\text{D}\alpha\text{E}\alpha\text{F}\alpha\text{G}\beta\text{H}\beta\text{I}$ . LOV domains are the

photochemically active moiety of LOV proteins, a class of blue-light (BL) photoreceptors comprising, among others, plant phototropins (phot),<sup>9</sup> the fungal protein VIVID,<sup>14</sup> and a growing number of prokaryotic photoresponsive proteins.<sup>11,15–21</sup> The photochemistry of LOV domains, first elucidated for phot and afterward for a variety of bacterial and fungal proteins, involves the formation of a FMN–cysteine C(4a)–thiol adduct, significantly blue-shifted with respect to the dark state and non-fluorescent (referred to as LOV<sub>390</sub>), generated via the short microsecond decay of the FMN triplet state.<sup>1,22,23</sup> In LOV<sub>390</sub>, a covalent bond is formed between the carbon atom at position 4a and the thiol group of a conserved cysteine localized in the D $\alpha$ –E $\alpha$  loop (Figure 1 provides structural views of the chromophore and its protein surroundings for both the parent state and the photo-adduct; amino acid numbering herein refers to YtvA from *Bacillus subtilis*). LOV<sub>390</sub> reverts in the dark to the unphotolyzed state (LOV<sub>447</sub>) on a time scale ranging from a few seconds to many hours at room temperature.<sup>1,24–27</sup> Importantly, the recovery is accelerated by imidazole, suggesting a base-catalyzed reaction.<sup>28,29</sup> Furthermore, pH,<sup>23,29</sup> deuterium effects,<sup>22,30</sup> and structural studies indicate that a proton-transfer reaction from N(5) is the rate-limiting step for the dark recovery reaction.

Received: November 12, 2010

Published: March 16, 2011

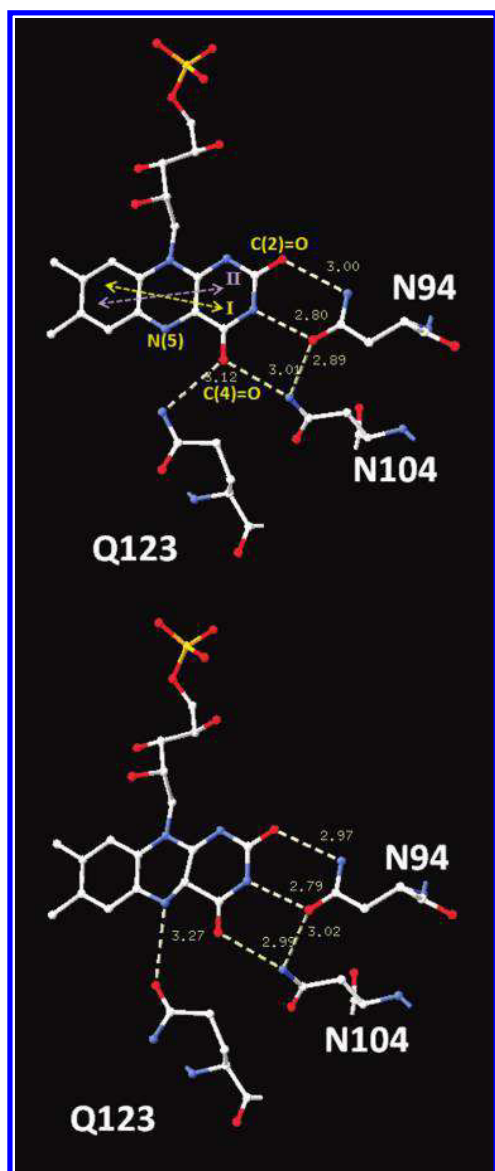


**Figure 1.** Hydrogen-bonding network of YtvA-LOV investigated in this work, in the (top) dark-adapted and (bottom) light-activated (photoadduct) states (PDB coordinates from 2pr5 and 2pr6). For the dark state we show the calculated polarization directions of the low-energy electronic transitions: I, blue-light range,  $\lambda_{\text{max}} \sim 450$  nm; II, UVA range,  $\lambda_{\text{max}} \sim 350$  nm (modified from ref 41, but see also ref 42 for an experimental determination). The atoms of FMN involved in the HB network studied here are shown in yellow.

Nevertheless, despite this well-established photocycle, the details for both  $\text{LOV}_{390}$  formation from the triplet state and its reversion are still a matter of debate,<sup>31–33</sup> as is the molecular basis of the dramatically different photocycle kinetics in different proteins. In this respect, understanding how the microenvironment surrounding the chromophore influences the photocycle, i.e., the effects of protein–chromophore interactions, is of crucial importance. Furthermore, modulation of the photocycle might turn out to be a very important aspect for BL photoreceptor-based optogenetic applications, by tuning the kinetics and yielding the requirements of the particular cell system and/or metabolic process of interest.<sup>34–37</sup>

Recently, a series of mutations have been designed to alter steric restrictions in the vicinity of the  $8\alpha$ -methyl group at the xylene side of FMN in *Avena sativa* phot1-LOV2 domain of phototropin 1 (Asphot1-LOV2) and studied by means of proton ENDOR and optical spectroscopy.<sup>3</sup> Asn 425, localized within the  $A\beta$ – $B\beta$  loop, appears to have a significant influence on the recovery lifetime of the adduct, which decreased from 48 s in the wild-type (WT) protein to 7.5 s in Asphot1-LOV2-N425C. Interaction between Asn425 and the  $8\alpha$ -methyl group appears to force the isoalloxazine ring into a precise conformation, thus stabilizing the cysteinyl–C(4a) adduct. Another important residue influencing the kinetics of the photocycle that stabilize the photoadduct through steric effects is Ile427 (I39 in YtvA) on strand  $B\beta$  of Asphot1-LOV2.<sup>2</sup> Nevertheless, in that case the 2-fold slower formation and 10-fold faster decay of the photoadduct by removing the  $\delta$ -carbon of the isoleucine chain (I427V mutation) are not due to direct interaction of Ile427 with FMN but rely on van der Waals contact between a  $\text{CH}_2$  group and the nearby sulfur of the reactive cysteine. The corresponding substitution I403V has been recently used to achieve a very fast photocycle in *Arabidopsis thaliana* (At) phot1-LOV2, in order to productively allow Fourier transform infrared (FTIR) step-scan measurements of chromophore and protein dynamics during formation of the photoadduct.<sup>32</sup> Further, mutations of residues interacting with the ribityl chain of FMN have been shown to affect the recovery reaction<sup>38,39</sup> by as much as 2 orders of magnitude.<sup>27</sup> Recently, a double mutation of YtvA, I39V/F46H, was demonstrated to accelerate 75-fold the recovery reaction, although the two residues are not directly interacting with the chromophore.<sup>34</sup> In particular, F46 undergoes a light-induced flipping, suggesting that this region of the protein is particularly flexible.<sup>7,34</sup>

An alternative approach has been recently reported by Mansurova et al., who exchanged the native chromophore with sterically modified flavins as chromophores via a chromophore exchange protocol.<sup>40</sup> Also in those experiments, the tight interactions between the chromophore and the protein were documented as a change of this interplay that significantly alters the thermal recovery kinetics.<sup>40</sup>

Here we focus instead on the HB network between the N(5), C(4)=O, N(3)H, and C(2)=O positions of the isoalloxazine moiety of FMN and an ensemble of conserved polar, uncharged amino acids (Figure 1). The hydrogen bonds at these positions of the chromophore undergo changes after blue-light absorption, as was recently documented in detail by means of advanced infrared spectroscopy techniques.<sup>8,31,32,43</sup> In particular, hydrogen bonds at C(2)=O and C(4)=O are weakened upon formation of the adduct, to somewhat different extents in different LOV systems.<sup>8,44–46</sup> In YtvA, the *B. subtilis* LOV protein investigated here, the three involved amino acids are Asn94, Asn104, and Gln123 (Figure 1; in the following we will refer to the amino acid coding of YtvA from *B. subtilis*).

Our study was prompted by formerly reported observations that hydrogen bonds affect not only the UV–vis absorption spectrum of riboflavin but also its photoreactivity.<sup>47,48</sup> In particular, H-bonding at N(1), C(2)=O, N(3)H, and C(4)=O was shown to increase the rate of hydrogen abstraction from a donor substrate, thus facilitating flavin reduction, when the riboflavin derivative was converted to its triplet state.<sup>48</sup> A theoretical investigation, based on quantum mechanics/molecular mechanics (QM/MM) methods applied to lumiflavin, has contributed to our knowledge of the influence that the HB network



exerts on the low-lying excited state of the flavin cofactor, indicating that the protein microenvironment enables participation of the ( $n\pi^*$ ) states in the decay processes of the lowest ( $\pi\pi^*$ ) excited singlet state (transition I in Figure 1), i.e., by enhancing singlet–triplet spin–orbit coupling.<sup>49</sup> Mutations of the three conserved polar residues that chiefly contribute to the HB network within the FMN binding pocket are thus expected to affect the photocycle kinetics, efficiency, and/or energetics. Indeed, it was shown recently that mutation of Q513 in Asphot1-LOV2 (Q123 in YtvA) can strongly affect the recovery reaction kinetics.<sup>50</sup> Furthermore, N94, N104, and Q123 belong to the  $\beta$ -scaffold of the LOV core (strands G $\beta$ , H $\beta$ , and I $\beta$ , respectively), participating in light-to-signal transmission, probably with the intervention of helical regions flanking the LOV core.<sup>7,10,32,39,51,52</sup> In particular, the conserved glutamine on strand I $\beta$  (here Q123) was recently identified as a potential switch to convey light-triggered conformational changes from the chromophore cavity to the LOV domain surface, e.g., Q575 in Atphot1-LOV2,<sup>53</sup> Q513 in Asphot1-LOV2,<sup>50</sup> Q182 in the fungal protein VIVID,<sup>51</sup> and Q1029 in *Adiantum capillus veneris* Aphy3-LOV2.<sup>43</sup> The mechanism underlying the conformational change effects resides in the fact that formation of the thioether bond in the adduct reduces the flavin ring and protonates N(S).<sup>31</sup> In order to maintain HB with N(S)H, this requires that the lateral chain of Q123 must flip in the lit state, as suggested by the structural data of several LOV domains.<sup>4,5,7,10,51</sup> Time-resolved FTIR spectroscopy has demonstrated that the Gln flipping, with loss of HB, is completed within a few microseconds, concomitant with formation of the adduct.<sup>32</sup> This flipping is then reversed, with recovery of the dark state and breakage of the covalent FMN–Cys bond. A link between this glutamine-based conformational switch and *in vivo* effects is indicated by the lack of light activation of the stress factor  $\sigma^B$  with the mutated YtvA-Q123N in *B. subtilis*.<sup>54</sup> Furthermore, it has been reported that the mutation Q575L (on LOV2) attenuates light-induced self-phosphorylation in Atphot1.<sup>55</sup> However, similar functional investigations have not been carried out for the positions (in YtvA) Asn94 and Asn104.

In this work we have investigated a series of mutations at Q123, N94, and N104 with the aim of characterizing the kinetics, efficiency, and energetics of the photocycle of YtvA proteins with an altered HB network around FMN, by means of steady-state spectroscopy, nanosecond flash photolysis, and time-resolved calorimetry. The aim of our investigation was twofold: first to assess the direct influence of the H-bonding situation of the chromophore on the photochemical and thermally driven steps, and second to understand the link between chromophore–protein interactions and signal propagations from the LOV core to domain/protein partners in the signal transduction chain. The outcome of our investigation will also be discussed in the frame of recently published experimental data on the mechanism of adduct formation and decay, and of possible extensions of the designed mutations for biotechnology applications.

## MATERIALS AND METHODS

**Mutagenesis, Protein Expression, and Purification.** A total of seven new mutations were generated: Q123N, N94S, N94D, N94A, N104S, N104D, and N104A. Mutagenesis was performed by the QuikChange method (QuikChange II XL, Stratagene). The primer design was performed with PrimerX<sup>56</sup> using the option

“DNA-based”. The primer sequences suggested by this program were again inspected individually, before primers were ordered for mutagenesis (see Supporting Information for the primer sequences). For all mutagenesis experiments, the obtained PCR products were treated with the restriction enzyme *DpnI* (New England BioLabs). *DpnI* is specific for methylated and hemimethylated DNA (targeting sequence: 5'-Gm<sup>6</sup>ATC-3') and is used to digest the parental DNA template in the PCR products. A 0.5  $\mu$ L portion of *DpnI* (20 000 U/mL) was added to each PCR product, and the digestion reaction was carried out at 37 °C for 30 min. In all cases, mutations were confirmed by sequencing.

Expression in *E. coli* (BL21) (Stratagene, Amsterdam, The Netherlands) yielded His-tagged, mutated proteins, using IPTG (BioMol, Hamburg, Germany) induction and employing the pET28a plasmid (Novagen-Merck, Darmstadt, Germany), as described.<sup>57</sup> The proteins were purified by affinity chromatography on a Talon resin (Qiagen, Hilden, Germany) and finally concentrated in sodium phosphate buffer 10 mM, NaCl 10 mM, pH = 8.

**Steady-State and Transient Optical Spectroscopy.** Absorbance spectra were recorded with a Jasco 7850 UV/vis spectrophotometer. Steady-state fluorescence measurements were carried out with a Perkin-Elmer LS50 luminescence spectrometer. The output signal was divided by the fraction of absorbed energy ( $1 - 10^{-A}$ , where  $A$  is the absorbance at the excitation wavelength) in order to obtain a signal that is proportional to the quantum yield.

Transient absorbance changes after nanosecond laser flash excitation were recorded using an LFP111 detection system (Luzchem, Ontario, Canada). For excitation, a Nd:YAG-driven tunable OPO laser was used (Nd:YAG, Innolas, Garching, Germany; OPO, GWU Lasertechnik, Erfstadt, Germany). The single-shot experiments were performed in the linear laser-energy dependence region of the transient absorbance changes with  $\lambda_{\text{exc}} = 450$  nm. All measurements were done at 20 °C using 1 cm light-path quartz cuvettes. The data were handled and analyzed using Origin Professional version 5.0 (Microcal Software, Inc., Northampton, MA).

Arrhenius and Eyring plots for the dark recovery reaction of the photoadduct were built by recording the recovery of FMN fluorescence ( $\lambda_{\text{ex}} = 303$  nm,  $\lambda_{\text{em}} = 500$  nm). The kinetics traces were fitted with a mono- or bi-exponential function, furnishing the recovery lifetime ( $\tau_{\text{rec}}$ ) as a function of temperature, in the range of the protein stability (11–25 °C). Excitation was at 303 nm, in order to minimize secondary photochemistry leading to the formation of the photoproduct during recording of the traces.<sup>39</sup>

**Laser-Induced Optoacoustic Spectroscopy (LIOAS).** For the LIOAS experiments, excitation at 450 nm was achieved by pumping the frequency-tripled pulse of a Nd:YAG laser (SL 456G, 6-ns pulse duration, 355 nm, Spectron Laser System, Rugby, Great Britain) into a  $\beta$ -barium borate optical parametric oscillator (OPO-C-355, bandwidth 420–515 nm, GWU Lasertechnik, Erfstadt, Germany) as previously described.<sup>58,59</sup> The FLASH 100 cuvette holder (Quantum Northwest Inc., Spokane, WA) was temperature-controlled to  $\pm 0.02$  °C. The signal was detected by a V103-RM ultrasonic transducer and fed into a 5662 preamplifier (Panametrics Inc., Waltham, MA). The pulse fluence was varied with a neutral density filter and measured with a pyroelectric energy meter (RJP735 head connected to an RJ7620 meter from Laser Precision Corp.). The beam was shaped by a  $1 \times 12$  mm slit, allowing a time resolution of  $\sim 60$  ns by using deconvolution techniques.<sup>60</sup> The experiments were performed in the linear regime of amplitude versus laser fluence, and the total incident energy normally used was  $\sim 40$   $\mu$ J/pulse (corresponding to  $15 \times 10^{-11}$  einstein for 450 nm excitation, photon energy 265.8 kJ/mol). The sample concentration was about 15  $\mu$ M, giving  $1.8 \times 10^{-9}$  mol in the excitation volume  $V_0 = 0.12$  mL. These conditions correspond to a ratio of 0.08 photon per protein molecule. New coccine (Fluka, Neu-Ulm, Germany) was used as calorimetric

reference.<sup>61</sup> The time evolution of the pressure wave was assumed to be a sum of monoexponential functions. The deconvolution analysis yielded the fractional amplitudes ( $\varphi_i$ ) and the lifetimes ( $\tau_i$ ) of the transients (Sound Analysis 3000, Quantum Northwest Inc.). The time window was between 20 ns and 5  $\mu$ s. At a given temperature and for each resolved  $i$ th step, the fractional amplitude  $\varphi_i$  is the sum of the fraction of absorbed energy released as heat ( $\alpha_i$ ) and the structural volume change per absorbed einstein ( $\Delta V_i$ ), according to eq 1:<sup>62,63</sup>

$$\varphi_i = \alpha_i + \frac{\Delta V_i c_p \rho}{E_\lambda \beta} \quad (1)$$

where  $E_\lambda$  is the molar excitation energy,  $\beta = (\partial V / \partial T)_p \Delta V$  is the volume expansion coefficient,  $c_p$  is the heat capacity at constant pressure, and  $\rho$  is the mass density of the solvent. In this work we used the so-called “two temperature” method in order to separate  $\alpha_i$  from  $\Delta V_i$ .<sup>64</sup> The sample waveform was acquired at a temperature for which heat transport is zero,  $T_{\beta=0} = 3.2$  °C, and at a slightly higher temperature,  $T_{\beta>0} = 10$  °C. At  $T_{\beta=0}$ , the LIOAS signal is only due to  $\Delta V_i$ . The reference for deconvolution was recorded at  $T_{\beta>0}$ , and eqs 2a and 2b were then used to derive  $\alpha_i$  and  $\Delta V_i$ :

$$\Phi_i \Delta V_i = \varphi_i|_{T_{\beta=0}} \times E_\lambda \frac{\beta}{c_p \rho} \Big|_{T_{\beta>0}} \quad (2a)$$

$$\alpha_i = \varphi_i|_{T_{\beta>0}} - \varphi_i|_{T_{\beta=0}} \quad (2b)$$

**Photophysical Parameters and LIOAS Data Handling.** The LIOAS signals for YtvA-WT and the mutated proteins were best fitted (with some exceptions, *vide infra*) by a two-exponential decay function as previously described.<sup>57,59</sup> The unresolved step ( $\tau_1 < 20$  ns) is assigned to the fast reactions resulting in the formation of the flavin triplet state (subscript T; this step is not time-resolved by LIOAS). The microsecond process ( $\tau_2 = 2$   $\mu$ s for YtvA-WT) corresponds to the triplet decay with formation of the photoadduct (subscript 390, according to the approximate absorption maximum). Energy balance considerations and the results of deconvolution directly provide the products  $\Phi_T E_T$  and  $\Phi_{390} E_{390}$  (eqs 3a and 3b), referring to the quantum yield of formation for the triplet state and adduct, respectively, multiplied by the energy level of the two transient species:<sup>65</sup>

$$\Phi_T \frac{E_T}{E_\lambda} = 1 - \alpha_1 - \Phi_F \frac{E_F}{E_\lambda} \quad (3a)$$

$$\alpha_2 = \Phi_T \frac{E_T}{E_\lambda} - \Phi_{390} \frac{E_{390}}{E_\lambda} \quad (3b)$$

where  $E_F$  is the average energy for the fluorescence emission (232 kJ/mol), and  $E_\lambda$  (265.8 kJ/mol) is the photonic energy corresponding to  $\lambda_{\text{ex}} = 450$  nm excitation wavelength. In this work we used  $E_T \approx 200$  kJ/mol, as previously measured<sup>38,57,66</sup> to obtain  $\Phi_T$ , and we estimated the energy content of the adduct after the independent determination of  $\Phi_{390}$  (*vide infra*).<sup>65</sup>

The molecular volume changes that the system suffers upon formation of the flavin triplet state and of the photoadduct (with respect to the unphotolyzed state) are calculated with eqs 4a and 4b:

$$\Delta V_T = \frac{\Delta V_1}{\Phi_T} \quad (4a)$$

$$\Delta V_{390} = \Delta V_T + \frac{\Delta V_2}{\Phi_{390}} \quad (4b)$$

The fluorescence quantum yield,  $\Phi_F$  of the bound flavin for the mutated proteins was measured at 20 °C, by comparison with YtvA-WT

( $\Phi_F = 0.22$ ) and FMN ( $\Phi_F = 0.26$ ), employing steady-state spectroscopy.<sup>57,59,67</sup> The value of  $\Phi_{390}$  was estimated by recording the bleaching of the unphotolyzed state on the microsecond time scale, at 450 and 475 nm, after laser excitation at 450 nm, employing the laser flash photolysis instrumentation, and by comparison with YtvA-WT ( $\Phi_{390} = 0.49$ ),<sup>57</sup> assuming that the absorption coefficient of the mutated proteins remains unaltered.

## RESULTS

**Spectral Features and Light–Dark Difference Spectra.** All the mutated proteins exhibit absorption spectra similar to that of YtvA-WT. The three major bands (blue, UVA, and UVB regions, transitions I, II, and III, respectively) undergo large light-induced changes upon formation of the photoadduct, well described by the light–dark (L-D) difference spectra, with a defined pattern of maxima and minima (Figure 2, Table 1).

The largest effects on the absorption spectra are produced by the Asn/Asp exchange at positions 94 and 104, and by the Q123N mutation (Figure 2 and Table 1). Replacing asparagine 104 with aspartate has an effect only on transition I (Figure 2a), inducing a blue-shift. In contrast, in YtvA-N94D a small blue-shift of transition I is accompanied by a larger red-shift of the UVA transition II (Figure 2b), accordingly polarized in the direction of C(2)=O and N(3)H. This UVA transition is in fact the most sensitive to the polarity and HB ability of the solvent<sup>47,48,68</sup> and shows the greatest variation among various LOV domains.<sup>46,69</sup> Interestingly, YtvA-Q123N shows a 3 nm blue-shift of the lowest energy transition with respect to YtvA-WT, whereas its fluorescence spectrum is virtually unaffected (Figure 3). A similar feature was recently described for mutations of glutamate 46 in the photoactive yellow protein and was predicted to arise from a broadening of the excited-state energy surface, although in our case the effects are very small.<sup>70</sup>

**Photochemical Events: Triplet Decay and Formation of the Photoadduct.** The most notable features of the micro-second time-resolved transient absorbance measurements (flash photolysis) are summarized in Table 2: (i) the faster formation of the adduct/decay of triplet state observed for YtvA-N94D, YtvA-N104D, and, to a lesser extent, also for YtvA-Q123N; (ii) the remarkable slowing down of the triplet decay/photoproduct formation in YtvA-N94A (Figure 4); and (iii) the smaller  $\Phi_{390}$  for YtvA-Q123N (about half that for YtvA-WT).

The data curves could be readily interpolated by means of a mono-exponential decay (Table 2), with the exception of YtvA-N104A, for which the curve was better described by a bi-exponential decay (i.e., the  $\chi^2$  improved more than 10% with respect to a mono-exponential fitting).

**Photocalorimetric (LIOAS) Experiments: Triplet Formation and Decay, Energetics, and Structural Changes.** LIOAS experiments have been previously performed with YtvA-WT<sup>57,59</sup> and other LOV proteins.<sup>38</sup> Given the time scale and time resolution of LIOAS, the production of FMN triplet state and its decay into the adduct are readily recorded, but the former process cannot be time-resolved ( $\tau_1 < 20$  ns), and we see only the result of the sub-nanosecond reactions leading to triplet formation. The formation of the adduct can instead be followed in real time, provided that it occurs with a lifetime  $\tau_2 \leq 5$   $\mu$ s (Table 3).

The majority of the mutated proteins behave similarly to YtvA-WT, with some notable exceptions: (i) YtvA-Q123N does not show any structural volume change upon formation of the adduct, i.e.,  $\Delta V_2 = 0$ , although the heat released in this step is

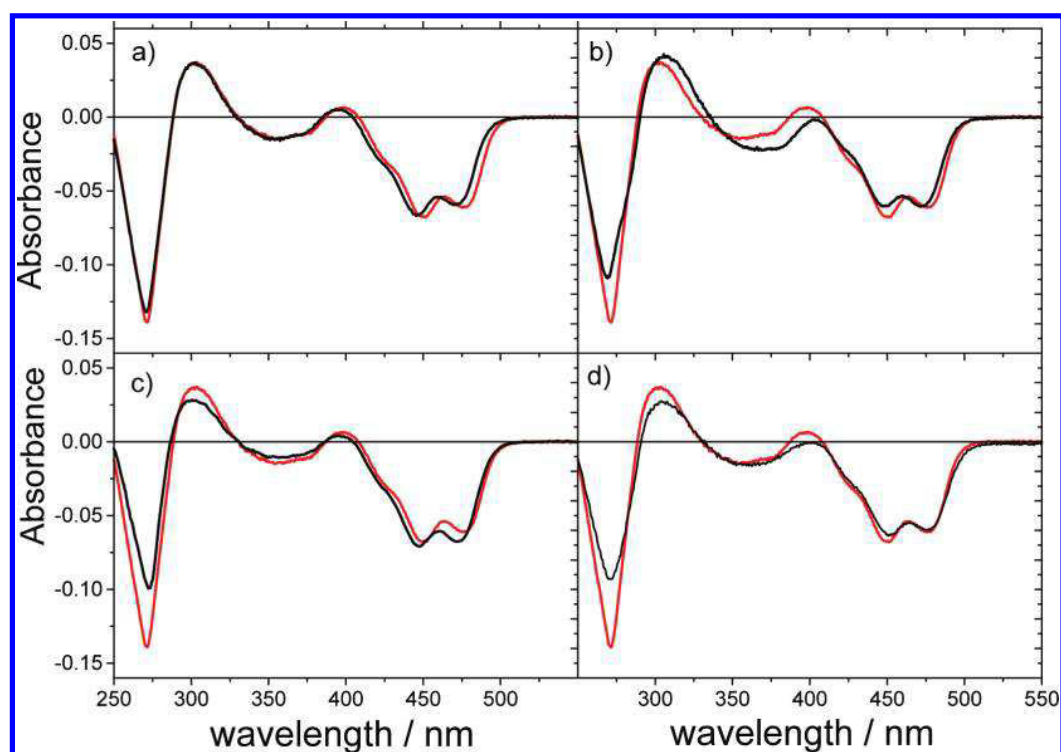


**Figure 2.** Light–dark difference absorption spectra for selected mutated YtvA proteins (black lines), compared to YtvA-WT (red line): (a) YtvA-N104D, (b) YtvA-N94D, (c) YtvA-Q123N, and (d) YtvA-N104S. See Table 1 for the maxima–minima patterns of all studied proteins.

**Table 1. Absorption Light–Dark (L-D) Maxima and Minima and Fluorescence Parameters of YtvA Proteins**

	L-D min/nm (parent state bleaching) <sup>a</sup>	L-D max/nm (photoadduct) <sup>a</sup>	fluorescence max/nm	$\Phi_F$
YtvA-WT	272/354;374/450;477	398;302	497	0.22
YtvA-N94D	269/364;380/448;473	404;306	497	0.15
YtvA-N94A	271/355/449;477	386;306	501	0.25
YtvA-N94S	271/354;370/452;477	402;303	501	0.14
YtvA-N104D	272/335;361/446;472	396;302	494	0.22
YtvA-N104A	272/348/449;475	396;304	497	0.20
YtvA-N104S	271/354;374/451;477	398;302	501	0.20
YtvA-Q123N	273/350;373/447;473	396;300	496	0.27

<sup>a</sup>Transitions in the UVB, UVA, and blue light spectral regions are separated by “/”; shoulders and vibrational bands in the same spectral region are separated by “;”.

well detectable with the correct time constant (Table 3 and Figure 5); (ii)  $\Delta V_2$  is strongly reduced in YtvA-N94S; and (iii) the formation of the adduct cannot be detected for YtvA-N94A, in agreement with the long lifetime of the triplet state (see Table 2).

The deconvolution of LIOAS waveforms thus provides the fraction of heat released ( $\alpha_i$ ) in each step and the lifetime of the triplet states; i.e.,  $\tau_2$  in Table 3 should be the same as  $\tau_T$  as recorded from transient absorption experiments (Table 2), provided that spectrally silent transitions do not occur on the same time scale. By performing temperature-dependent experiments, it is also possible to obtain the structural volume changes ( $\Delta V_i$ , per mole of absorbed photons) that accompany each step (Table 3; eqs 2a, 2b, 3a, and 3b).

Equation 3a allows us to determine the triplet formation quantum yield,  $\Phi_T$ , which is very similar among all the proteins

investigated (Table 4), with the exception of YtvA-N104S, which has a higher value,  $\Phi_T = 0.79$ , underscored by the small fraction of released heat in the short nanosecond step ( $\alpha_1$  in Table 3).

The evaluation of  $E_{390}$  as the energy content of the photoadduct is negatively affected by the large errors associated in some cases with both  $\Phi_{390}$  as determined by flash photolysis (Table 2) and the quantity  $E_{390}\Phi_{390}$ , independently determined by LIOAS. In at least two cases, YtvA-N104S and YtvA-Q123N, the energy stored in the signaling state appears larger with respect to YtvA-WT, i.e., close to the triplet energy level,  $E_T \approx$  ca. 200 kJ/mol.<sup>38,57,66</sup>

The total contraction,  $\Delta V_{390}$ , that the system suffers upon light activation (Table 4) is strongly reduced in YtvA-Q123N and YtvA-N94S. This is due to the fact that the volume change associated with the formation of the photoadduct is zero or close to zero, respectively, whereas the structural changes associated



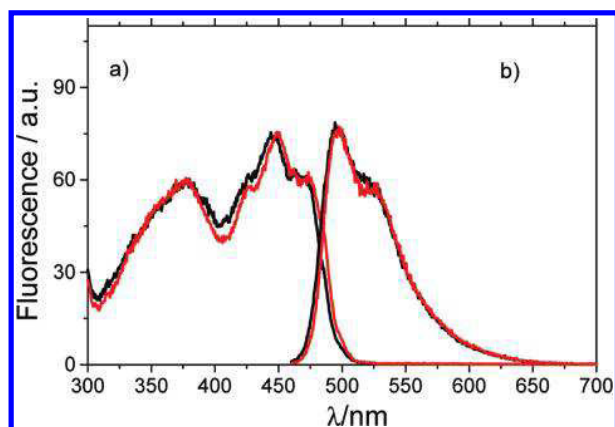


**Figure 3.** (a) Excitation ( $\lambda_{\text{em}} = 500$  nm) and (b) emission ( $\lambda_{\text{ex}} = 450$  nm) fluorescence spectra for YtvA-Q123N (black) and YtvA-WT (red). Note that the 3 nm blue-shift in the excitation spectrum (identical to that observed in absorbance) is not accompanied by a concomitant shift in the emission profile.

**Table 2. Triplet Lifetimes and Photocycle Quantum Yields**

	$\tau_T$	$\Phi_{390}^a$
YtvA-WT	$2.00 \pm 0.20$	$0.49 \pm 0.04$
YtvA-N94D	$1.34 \pm 0.14$	$0.22 \pm 0.09^b$
YtvA-N94A	$129 \pm 10$	$0.46 \pm 0.05$
YtvA-N94S	$2.05 \pm 0.14$	$0.51 \pm 0.16$
YtvA-N104D	$1.27 \pm 0.12$	$0.47 \pm 0.30$
YtvA-N104A	$2.50 \pm 0.70$ (93%)	
	$9.96 \pm 1.57$ (7%)	$0.35 \pm 0.11$
YtvA-N104S	$3.0 \pm 0.2$	$0.4 \pm 0.06$
YtvA-Q123N	$1.6 \pm 0.14$	$0.22 \pm 0.03$

<sup>a</sup>The errors derive from two independent measurements (three for YtvA-N104D). <sup>b</sup>This value is probably underestimated due to partial chromophore detachment from the protein.

with triplet formation are poorly affected by the mutations. This latter parameter is solely strongly reduced in YtvA-N104A, for which also the value of  $\Phi_T$  is slightly smaller. Thus, together with N104S, N104A is the only substitution, among those investigated, that affects triplet formation.

**Temperature Dependence of the Recovery Kinetics.** As for the recovery lifetimes,  $\tau_{\text{rec}}$ , all mutations affect to some extent the kinetics as measured at 20 °C and/or the activation energy or the pre-exponential factor as derived from Arrhenius or Eyring plots (eqs 5a and 5b, respectively), where  $k_B$  and  $R$  are the Boltzmann and gas constants, respectively, and  $h$  is the Planck's constant.<sup>71</sup>

$$\ln \frac{1}{\tau_{\text{rec}}} = \ln A - \frac{E_a}{R} \frac{1}{T} \quad (5a)$$

$$\ln \frac{1}{\tau_{\text{rec}} T} = \ln \frac{k_B}{h} + \frac{\Delta S^\ddagger}{R} - \frac{\Delta H^\ddagger}{R} \frac{1}{T} \quad (5b)$$

Major changes are observed for (i) Q123N, with a dramatic fastening of the photocycle, correlated to a lowering of  $E_a$ , i.e., of  $\Delta H^\ddagger$  (activation enthalpy change), and furthermore the decay is clearly bi-exponential for this protein (the weighted average value is reported in Table 5), and for (ii) N94A and N94S, with a significant acceleration of the photocycle, but in this case it is

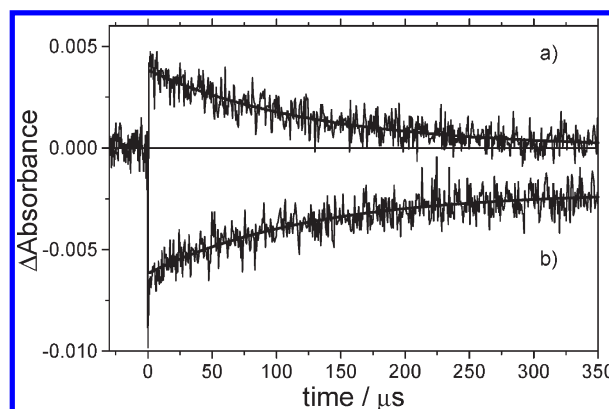


**Figure 4.** (a) Triplet decay (detection at 650 nm) and (b) photo-product formation (detection at 450 nm, corresponding to the bleaching of the parent state) for YtvA-N94A. The curves derived from a mono-exponential fitting decay function of the flash photolysis signals (excitation at 450 nm) are overlaid with the experimental traces. The two processes are synchronous, with recovered lifetimes  $\tau_T$  of 129 and 126  $\mu\text{s}$ , respectively; these kinetics are more than 60 times slower than for YtvA-WT, for which  $\tau_T = 2$   $\mu\text{s}$  (see Table 2).

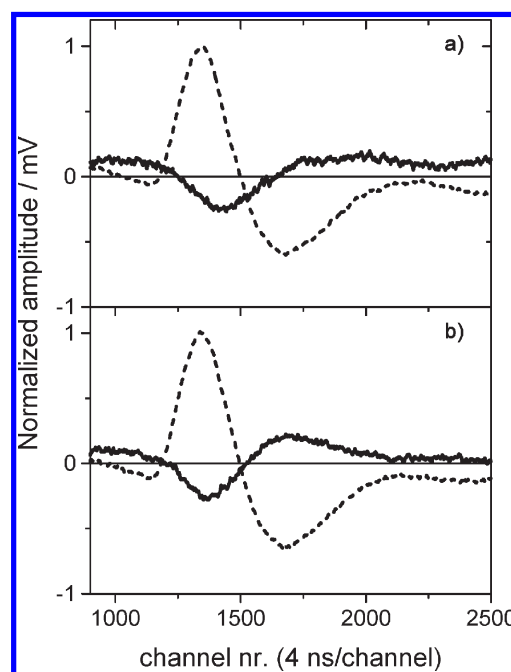


**Figure 5.** LIOAS signals (solid lines) for (a) YtvA-N104D and (b) YtvA-Q123N, showing light-induced structural changes ( $\Delta V_i$ ) as detected at  $T_{\beta=0} = 3.2$  °C. The reference curves (dotted lines), with normalized maximal amplitude = 1, are recorded at  $T_{\beta>0} = 10$  °C. Notice that the  $\Delta V_i$  pattern extends to a longer time scale in YtvA-N104D (which behaves similarly to YtvA-WT<sup>59</sup>); i.e., it bears contributions both from triplet formation ( $\Delta V_1$ ,  $\tau_1 < 20$  ns) and from triplet decay/adduct formation ( $\Delta V_2$ ,  $\tau_2 \approx 1.3$   $\mu\text{s}$ ). The second volume change component is absent in YtvA-Q123N, although the adduct is formed on the same time scale as YtvA-WT (see Tables 3 and 4 for the detailed results of deconvolution).

correlated to an increase of the Arrhenius pre-exponential factor, i.e., an increase of  $\Delta S^\ddagger$  (activation entropy change). In N94D the increase in  $\Delta S^\ddagger$  more than compensates for the concomitant increase in  $\Delta H^\ddagger$ , thus resulting in a faster photocycle at 20 °C,

Table 3. Parameters Derived from Deconvolution of LIOAS Signals

	$\alpha_1$ ( $\tau_1 < 20$ ns)	$\alpha_2$	$\tau_2/\mu\text{s}$	$\Delta V_1/\text{mL einstein}^{-1}$	$\Delta V_2/\text{mL einstein}^{-1}$
YtvA-WT <sup>a</sup>	0.30 ± 0.03	0.23 ± 0.04	1.90 ± 0.21	−0.44 ± 0.05	−5.8 ± 0.2
YtvA-N94D	0.38 ± 0.01	0.16 ± 0.03	1.2 ± 0.30	−0.66 ± 0.03	−2.36 ± 0.22
YtvA-N94A	0.29 ± 0.02		>5	−0.50 ± 0.01	
YtvA-N94S	0.41 ± 0.02	0.16 ± 0.05	1.96 ± 0.22	−0.93 ± 0.08	−0.6 ± 0.3
YtvA-N104D	0.26 ± 0.03	0.32 ± 0.05	1.36 ± 0.2	−0.75 ± 0.18	−3.2 ± 0.2
YtvA-N104A	0.41 ± 0.03	0.14 ± 0.03	1.95 ± 0.60	−0.05 ± 0.03	−3.5 ± 0.2
YtvA-N104S	0.18 ± 0.03	0.28 ± 0.07	2.47 ± 0.79	−0.84 ± 0.17	−4.11 ± 0.26
YtvA-Q123N	0.31 ± 0.02	0.20 ± 0.01	1.16 ± 0.10	−1.70 ± 0.08	

<sup>a</sup> From ref 59. The errors are from two independent signals and four deconvolutions.

Table 4. Triplet Yield, Energy Storage, and Structural Changes in Mutated YtvA Proteins

	$\Phi_T^a$	$E_{390}\Phi_{390}/\text{kJ mol}^{-1b}$	$E_{390}/\text{kJ mol}^{-1c}$	$\Delta V_{660}/\text{mL mol}^{-1d}$	$\Delta V_{390}/\text{mL mol}^{-1e}$
YtvA-WT	0.62 ± 0.03	67 ± 9	137 ± 19	−0.70 ± 0.07	−12.60 ± 0.80
YtvA-N94D	0.59 ± 0.01	76 ± 10	ND <sup>f</sup>	−1.10 ± 0.05	ND <sup>f</sup>
YtvA-N94A	0.56 ± 0.02			−0.89 ± 0.03	
YtvA-N94S	0.56 ± 0.03	69 ± 15	131 ± 40	−1.66 ± 0.15	−2.90 ± 0.60
YtvA-N104D	0.64 ± 0.04	43 ± 18	133 ± 107	−1.18 ± 0.25	−11.10 ± 5.90
YtvA-N104A	0.47 ± 0.04	57 ± 9	175 ± 56	−0.11 ± 0.05	−10.80 ± 2.70
YtvA-N104S	0.79 ± 0.03	84 ± 18	213 ± 49	−1.06 ± 0.19	−11.50 ± 1.30
YtvA-Q123N	0.50 ± 0.03	48 ± 4	224 ± 30	−3.40 ± 0.20	−3.40 ± 0.20

<sup>a</sup> Equation 3a. <sup>b</sup> Equation 3b. <sup>c</sup> Using  $\Phi_{390}$  values and the associated errors from Table 2. <sup>d</sup> Equation 4a, using  $\Phi_T$  from this table and  $\Delta V_1$  from Table 3, with associated errors. <sup>e</sup> Equation 4b, using  $\Phi_{390}$  from Table 2 and  $\Delta V_2$  from Table 3, with associated errors. <sup>f</sup> ND = not determined. The underestimation of  $\Phi_{390}$  in Table 2, due to protein instability, would give for  $E_{390}$  a value of 345 kJ/mol; this value is larger than the excitation photon energy of 265.8 kJ/mol.

Table 5. Recovery Kinetics (20 °C) and Arrhenius and Eyring Parameters

	$\tau_{\text{rec},20}/\text{s}$	$A/\text{s}^{-1}$	$E_a/\text{kJ mol}^{-1}$	$\Delta H^\ddagger/\text{kJ mol}^{-1}$	$\Delta S^\ddagger/\text{kJ mol}^{-1} \text{K}^{-1}$
YtvA-WT	6240	$6.9 \times 10^{14}$	104	101	+0.031
YtvA-N94D	1250	$3.4 \times 10^{23}$	151	148	+0.20
YtvA-N94A	140	$4.9 \times 10^{18}$	117	115	+0.10
YtvA-N94S	300	$7.2 \times 10^{15}$	103	100	+0.05
YtvA-N104D	6890	$4.9 \times 10^{16}$	115	112	+0.066
YtvA-N104A	2250	$4.0 \times 10^8$	67	65	−0.09
YtvA-N104S	1120	$9.2 \times 10^{10}$	78	76	−0.043
YtvA-Q123N	72	$5.0 \times 10^9$	65	62	−0.067

albeit not so dramatic as in N94A and N94S. Mutations of N104 (see Figure 1 for the HB network centered on this residue) result in less profound effects on the overall kinetics of the photocycle, but they still considerably lower the activation energy (N/A and N/S changes).

## DISCUSSION

**Switching Glutamine on Strand Iβ and N(5) of the Flavin Ring.** The strong acceleration of the photocycle in YtvA-Q123N, which recovers with a  $\tau_{\text{rec}}$  about 85 times faster than YtvA-WT (at 20 °C), parallels the 1.8 times acceleration observed for the corresponding Q513N mutation in Asphot1-LOV2,<sup>50</sup> although for YtvA the effect is significantly more pronounced. We can therefore safely state that this substitution destabilizes the covalent adduct. This is reflected in the high energy content of

the photoadduct for YtvA-Q123N (Table 4) and in the lowering of the activation energy for the recovery reaction (Table 5, Figure 6), accounting for the fast photocycle at room temperature. The decay of the adduct, clearly bi-exponential in this mutated protein, also points to a conformational heterogeneity in the light-activated state. Interestingly, Alexandre and co-workers detected a mixed one-/two-HB arrangement at C(4)=O in the dark state of Asphot-LOV2, indicative of a conformational flexibility in this protein region.<sup>8</sup> The asparagine substitution could enhance this flexibility, which becomes clearly evident in the double-exponential decay. This mutation also affects the forward photochemistry, although to a minor extent, by accelerating the triplet decay and lowering the quantum yield of the photocycle (Table 2). These latter effects, together with the subtle shifts observed in absorption and fluorescence, point to a limited but well detectable role of the direct HB partner of N(5)

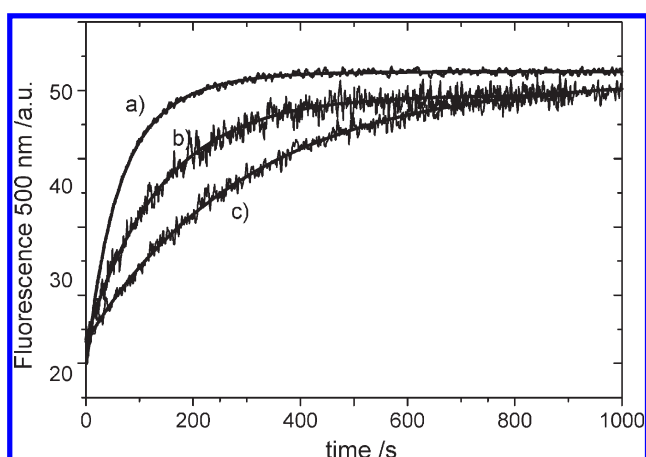


**Figure 6.** Recovery kinetics of fast-cycling mutated YtvA proteins at 20 °C, monitored via the growing fluorescence of FMN at 500 nm (excitation at 303 nm). Interpolated lines, as obtained by exponential fitting, are superimposed on the experimental curves. (a) YtvA-Q123N (showing biexponential kinetics),  $\tau_{\text{rec1}} = 44$  s (51%) and  $\tau_{\text{rec2}} = 102$  s (49%); (b) YtvA-N94A,  $\tau_{\text{rec}} = 140$  s; (c) YtvA-N94S,  $\tau_{\text{rec}} = 300$  s (Table S).

in the light state in determining the efficiency of the photochemical step in LOV domains. In addition, the much more substantial role that this residue plays in the later steps of the photocycle and during the molecular events underlying signal propagation has to be kept in mind. In Asphot1-LOV2, the molecular event crucial for activation of the C-terminal kinase domain is the light-triggered unfolding of the J $\alpha$  helical linker, otherwise organized underneath the LOV2  $\beta$ -scaffold in the dark state.<sup>13,72</sup> In these investigations, LOV2-Q513N is conformationally locked in a pseudo-lit state, i.e., the linker is not helical in the dark, whereas Q513L is locked in a pseudo-dark state, i.e., there is no light-triggered unfolding of the linker.<sup>50</sup> These observations are fully compatible with the general proposed role for this conserved glutamine to act as a conformational switch in LOV domains.<sup>32,51,53</sup> This suggestion is well supported by our results that reveal the lack of structural changes in Q123N during the formation of the adduct (Tables 3 and 4). Only in few cases has the link between reduced or suppressed conformational changes and functional effects been established, e.g., in Atphot1, where the Q575L mutation on LOV2 diminishes light-driven conformational changes<sup>53</sup> and attenuates light-induced self-phosphorylation.<sup>55</sup> Most important for our work is the finding of the physiological effect for this YtvA mutation (Q123N), which suppresses the light-dependent upregulation of the alternative transcription factor  $\sigma^B$ ,<sup>54</sup> thus complementing our photophysical data.

**Hydrogen-Bond Network Builder Asparagines N94 and N104: Tuning the Photocycle.** Besides their obvious role in stabilizing the polar part of the isoalloxazine ring via the formation of hydrogen bonds to C(2)=O, N(3)H, and C(4)=O within the protein cavity, the two conserved asparagines seem to play a major role in determining the kinetics of the photocycle, including the formation of the adduct, by building an optimal HB network. Mutation of these polar residues into aspartates in principle is not innocent, in that we most probably introduce a negative charge within the protein cavity that requires a rearrangement of the HB network shown in Figure 1. We note that N94D induces a red-shift in the UVA absorption band, a

phenomenon that, for free flavins, has been correlated with the presence of proton-donating solvents.<sup>47</sup> The red-shift of transition II, observed only for N94D and not for N104D, confirms that the transition dipole is oriented toward C(2)=O, as previously proposed (see Figure 2 for the transition dipole orientation of this band).<sup>41,42</sup> The data could indicate that the aspartate in position 94 is protonated or shares its proton such that the hydroxy group interacts with C(2)=O as a donor in the HB. However, we note that a similar red-shift of the UVA band is observed for Asphot1-LOV2 with respect to LOV1,<sup>69</sup> for which NMR analysis has suggested a weaker HB to C(2)=O.<sup>45</sup>

Transition I undergoes a slight blue-shift for both mutations, larger for N104D (4 nm) than for N94D (2 nm). This could be well explained by a geometric effect such that the HB formed by the lateral chain of aspartic acid with the C(4)=O/N(3)H groups on FMN is extended in length or even is lost. Yet, residue N94 might also be partly involved in these effects in supporting the ring geometry to be re-adjusted to the introduced carboxylate moiety (N104D). A slight hypsochromic shift is observed for this band in LOV2 with respect to LOV1,<sup>69</sup> for which HB at C(4)=O and C(2)=O is stronger.<sup>45</sup> Furthermore, Asphot1-LOV2 exists in an equilibrium of singly and doubly H-bonded C(4)=O conformers in the dark state, in which the stronger (double-bonded) HB induces a red-shift of this band.<sup>8</sup> Therefore, we can suggest that, in YtvA-Q123N, YtvA-N104D, and, to a lesser extent, YtvA-N94D, the HB at C(4)=O is weaker than in YtvA-WT, and this feature induces a moderate acceleration of triplet decay/adduct formation. Nevertheless, the effects of aspartic acid might be due instead to the presence of a negative charge within the cavity, due to the low  $pK_a$  (ca. 4) of the lateral chain in this residue. Due to instability of the protein at low pH, we were not able to determine the  $pK_a$  of D94 and D104, but we note that, as for the energy of the electronic transitions, the introduction of aspartic acid in position 94 or 104 is more perturbing than introducing residues such as serine or alanine that conceivably suppress local HB with the chromophore (Table 1). The latter mutations have instead a more pronounced effect on the photochemical reactions, ranging from an increase of triplet quantum yield in YtvA-N104S to a slowing-down of triplet decay into the adduct, which becomes dramatic in YtvA-N94A. In the latter mutant, photoadduct formation is 65-fold slower than for YtvA-WT (see Table 2), counteracted by a 44-fold faster recovery kinetics. This large effect on the forward kinetics is not accompanied by a concomitant decrease of the photocycle quantum yield, indicating that possible competitive processes, e.g., quenching from molecular oxygen, have a negligible yield.

**Recovery Reaction and the Link between Chromophore–Protein Interactions and Signal Propagation.** From Table S, the increase in the rate of the recovery reaction due to the substitution of the “flipping” glutamine Q123<sup>7</sup> appears to be related to a more favorable activation enthalpy, i.e., a value lower than for YtvA-WT. Concomitantly, the LIOAS data indicate a high energy level for the photoadduct in YtvA-Q123N, which might be responsible for lowering the energy barrier for the recovery reaction. These results, together with the lack of structural changes concomitant with this step (Tables 3 and 4), suggest that the light-induced flipping does not occur in this mutated protein and that this missing “switch” could be responsible for the observed *in vivo* effects, where YtvA-Q123N does not show any light-induced activity.<sup>54</sup> A similar effect on the activation parameters is observed for N104A/S mutations that conceivably

disrupt the HB network centered on C(4)=O, thus also influencing the effect of Q123 (Figure 1). We note that N104 is adjacent to E105, a residue functionally essential for inter-domain signal transmission in YtvA<sup>52</sup> and for its *in vivo* light-induced effects.<sup>54</sup> Therefore, this chromophore region, with its HB partner amino acids, could represent the link between light activation, photocycle duration, and signal propagation from the FMN binding pocket to the surface of the LOV core, thereby confirming and extending the proposed key role of the “switching glutamine”.<sup>50,51,53</sup>

In contrast, suppression of the extended HB network centered at N94 (N94S and N94A) and involving C(2)=O/N(3)H still results in an accelerated photocycle at 20 °C, but in this case the activation parameters point to a more favorable entropic term that is larger than for YtvA-WT. This indicates that the rearrangement of this HB network is one of the rate-limiting steps on the way back to the dark state, besides being a major determinant for triplet formation and decay (*vide supra*). We are instead not aware of any link between the protein region containing N94, localized on strand G $\beta$ , and signal propagation. Strand G $\beta$  residues are not part of the LOV–LOV interface in the crystal structure<sup>7</sup> and in the structural model<sup>52</sup> of YtvA–LOV. One putative mechanism could rely on the adjacent conserved salt bridge formed by E56 (on D $\alpha$ ) and K97 (G $\beta$ –H $\beta$  loop), linked to the inner FMN cavity via a conserved arrangement of several amino acids.<sup>73</sup> Molecular dynamics (MD) simulations have suggested that light-induced strengthening of the E–K salt bridge is a characteristic of LOV1 which thereby becomes less mobile in the light state.<sup>74</sup> In LOV2, instead, the E–K salt bridge should be stable in both dark and light states, with conformational changes occurring mainly within the H $\beta$ –I $\beta$  loop and the adjacent regions of the central  $\beta$ -sheet that becomes more mobile.<sup>74</sup> Freddolino et al. have suggested that these changes are initiated in LOV1 by the asparagines corresponding to N104 in YtvA, thus solely indirectly involving N94, whereas LOV2 activation should be mediated by Q123.<sup>74</sup> Accordingly, mutation of the E–K in LOV2 does not affect light-driven self-phosphorylation of phot1.<sup>55</sup> There is, however, up to now no experimental evidence in favor of the MD simulations of the activation mechanism of LOV1, given that we still are missing a readout response for LOV1 functional activity. In any case, these two proposed different activation mechanisms between LOV1 and LOV2 should both be triggered by modifications of the HB around FMN.

**Relevance for the Mechanism of Adduct Formation and Decay.** High-resolution FTIR techniques have recently provided evidence that the triplet state of FMN bound to LOV domains is unprotonated,<sup>31,32</sup> thus disfavoring a previously proposed ionic mechanism.<sup>75</sup> According to the latter, the increase in pK<sub>a</sub> of N(5) in the triplet state should trigger its protonation, leaving a single HN(5)–C(4a) bond that can be easily attacked by the thiolate of the cysteine.<sup>75</sup> The radical pair mechanism predicts the formation of a triplet-state FMN $\dot{\text{H}}^{\bullet}$ –H<sub>2</sub>CS $\dot{\text{C}}^{\bullet}$  biradical, where a rapid triplet–singlet conversion is induced by the sulfur atom, followed by radical-pair recombination between H<sub>2</sub>CS $\dot{\text{C}}^{\bullet}$  and the unpaired electron on C(4a).<sup>76,77</sup> Recently it was suggested that the first FMN radical species formed might be the negatively charged semiquinone FMN $\dot{\text{C}}^{\bullet-}$ .<sup>33</sup> During the revision of this manuscript, the first direct evidence of an intermediate species between the triplet state and the adduct, by means of nanosecond flash photolysis with CCD camera detection and a special flow cell design, was reported.<sup>78</sup> The new transient species is

spectrally similar to a neutral flavin radical, and it is suggested to decay fast into the adduct.<sup>78</sup>

The time resolution and the molecular details provided by the techniques employed in this work are certainly not suitable to detect the putative radical intermediates, but we can observe that the introduction of probably negatively charged aspartates in the cavity has no dramatic effect on the dynamics and energetics of adduct formation (Tables 2 and 4). This would probably be the case if transiently charged species (e.g., in the ionic mechanism) were present. Our data seem thus to agree with the occurrence of a neutral flavin radical.<sup>78</sup> The extremely slow decay of the flavin triplet in N94A suggests that polarity/polarizability effects must be operating during formation of the adduct, indeed pointing to a strong electronic rearrangement, which is not in contrast with the radical-pair hypothesis. High-resolution FTIR techniques applied to this mutated protein could provide useful information on the mechanism of adduct formation.

Modulation of the photocycle by altering the HB network at the flavin ring complements previous data suggesting that the microenvironment around N(5) is a major determinant for the dark recovery reaction, in particular suggested by pH effects, base catalysis, and mutations at position Q123.<sup>28,29,50</sup> Other mutations are able to affect the photocycle kinetics by altering steric restrictions or the HB network that stabilizes the ribityl chain.<sup>2,3,27,29,34,38,50</sup> To our knowledge, we have here, for the first time, highlighted the role played by the asparagine residues directly H-bonded to C(4)=O and C(2)=O, namely at polar sites on the isoalloxazine ring that determine chromophore spectral properties and photoreactivity.

**Hydrogen-Bond Network as a Tool To Modulate the Photocycle: Relevance for Optogenetics Applications.** BL receptors of the LOV and BLUF families are increasingly employed as photofunctional proteins in the growing field of optogenetics, a research field prompted by the possibility of regulating cellular machinery with optimal spatial and temporal control.<sup>11,12,34,35,37,79,82</sup> The lifetime of the photoactivated state is of primary importance, in that it determines the duration of the cellular response of interest and has to be tuned to meet the particular metabolic characteristics of a given cell.<sup>37</sup> Mutations of amino acids in the vicinity of the flavin chromophore, such as those we have presented here, can be readily exploited to achieve a given photocycle kinetics. The only condition required is the intactness of the light-to-signal transduction, namely the fact that the protein must remain functionally active, a condition that might not be met in certain instances, e.g., upon mutation of the flipping glutamine (*vide supra*).

**Hydrogen-Bond Network as a Possible Redox Potential Regulator?** While this article was under review, novel data on the midpoint potential of FAD bound to a BLUF domain were reported, suggesting that the HB network around the flavin chromophore might modulate both the absorption maximum and the midpoint potential of BL photoreceptors.<sup>83</sup> Those authors determined the values of both parameters for WT and mutated BLUF domains of the protein AppA (referred to as AppA<sub>1–125</sub>), and for two LOV proteins. The values are as follows (absorption maximum/midpoint potential): AppA<sub>1–125</sub>, 448 nm/–255 mV; AppA<sub>1–125</sub>Q63N, 446 nm/–260 mV; AppA<sub>1–125</sub>Y21F, 444 nm/–260 mV; AppA<sub>1–125</sub>W104A, 444 nm/–260 mV; AppA<sub>1–125</sub>Q63H, 441 nm/–230 mV; AppA<sub>1–125</sub>Y21FW104F, 442 nm/–217 mV; YtvA, 449 nm/–308 mV; Asphot1-LOV2, 448 nm/–307 mV.<sup>83</sup> The correlation between absorption maxima and midpoint potential is rather



vague and certainly needs to be better substantiated within the LOV series, in view of a potential integration of light and redox signals within the cell. Such integration has been shown to be possible for the LOV kinase (LOVK) from *C. crescentus*, for which the midpoint potential of  $-258$  mV has been determined, a value very similar to AppA, and in the same range as the proposed redox potential of a bacterial cell ( $-260$  to  $-280$  mV).<sup>84</sup> The absorption maximum of LOVK lies indeed at  $446$  nm, as for AppA.<sup>83,84</sup> Interestingly, the midpoint potential changes to  $-303$  mV if the LOV core alone of LOVK (aa 1–138) is investigated; this truncation does not alter the absorption maximum, indicating that structural aspects seem also to be important in determining the midpoint potential.<sup>84</sup>

This subject is certainly intriguing, and some of the mutated YtvA proteins discussed here, in particular those able to shift the absorption maximum, are good candidates to test the possible interrelation between transition energy and redox potential in LOV proteins.

## CONCLUSIONS

Modifications of the conserved HB network that stabilizes the isoalloxazine ring within a LOV domain, affects the photocycle kinetics, both for formation and decay of the signaling state. A major contribution is provided by the glutamine residue interacting with N(S) in the light-activated state, a position that becomes protonated, thus causing a flipping of the amino acid side chain and being identified as a major event during signal transmission to the LOV domain surface. A second key element is the extended HB network centered on N94: suppression of the network by the Asn/Ala mutation dramatically slows down the photochemical reaction and accelerates the decay of the photoadduct. The intactness of the HB network thus appears to be essential for the optimization of the photocycle, most probably by tuning it to the velocity and efficiency of signal-transduction events and, ultimately, of functional and *in vivo* responses.

## ASSOCIATED CONTENT

**S Supporting Information.** Details of primer design and sequences used in this work for site-directed mutagenesis. This material is available free of charge via the Internet at <http://pubs.acs.org>.

## AUTHOR INFORMATION

### Corresponding Author

[aba.losi@fis.unipr.it](mailto:aba.losi@fis.unipr.it)

## ACKNOWLEDGMENT

This work has been partially supported by the Deutsche Forschungsgemeinschaft (FOR526). We thank Sarah Klassen for her valuable help in the laboratory. The LIOAS equipment and the laser system employed in this work were kindly donated by the Max-Planck-Institute for Bioinorganic Chemistry (Muelhim and der Ruhr, Germany) to the University of Parma.

## REFERENCES

- (1) Losi, A. *Photochem. Photobiol.* **2007**, *83*, 1283–1300.
- (2) Christie, J. M.; Corchnoy, S. B.; Swartz, T. E.; Hokenson, M.; Han, I. S.; Briggs, W. R.; Bogomolni, R. A. *Biochemistry* **2007**, *46*, 9310–9319.

- (3) Brosi, R.; Illarionov, B.; Mathes, T.; Fischer, M.; Joshi, M.; Bacher, A.; Hegemann, P.; Bittl, R.; Weber, S.; Schleicher, E. *J. Am. Chem. Soc.* **2010**, *132*, 8935–8944.
- (4) Crosson, S.; Moffat, K. *Plant Cell* **2002**, *14*, 1067–1075.
- (5) Fedorov, R.; Schlichting, I.; Hartmann, E.; Domratcheva, T.; Fuhrmann, M.; Hegemann, P. *Biophys. J.* **2003**, *84*, 2492–2501.
- (6) Iwata, T.; Nozaki, D.; Tokutomi, S.; Kagawa, T.; Wada, M.; Kandori, H. *Biochemistry* **2003**, *42*, 8183–8191.
- (7) Möglich, A.; Moffat, K. *J. Mol. Biol.* **2007**, *373*, 112–126.
- (8) Alexandre, M. T. A.; van Grondelle, R.; Hellingwerf, K. J.; Kennis, J. T. M. *Biophys. J.* **2009**, *97*, 238–247.
- (9) Christie, J. M. *Annu. Rev. Plant Biol.* **2007**, *58*, 21–45.
- (10) Halavaty, A. S.; Moffat, K. *Biochemistry* **2007**, *46*, 14001–14009.
- (11) Möglich, A.; Yang, X. J.; Ayers, R. A.; Moffat, K. *Annu. Rev. Plant Phys.* **2010**, 21–47.
- (12) Möglich, A.; Ayers, R. A.; Moffat, K. *Structure* **2009**, *17*, 1282–1294.
- (13) Harper, S. M.; Neil, L. C.; Gardner, K. H. *Science* **2003**, *301*, 1541–1544.
- (14) Schwerdtfeger, C.; Linden, H. *EMBO J.* **2003**, *22*, 4846–4855.
- (15) Briggs, W. R.; Tseng, T. S.; Cho, H. Y.; Swartz, T. E.; Sullivan, S.; Bogomolni, R. A.; Kaiserli, E.; Christie, J. M. *J. Integr. Plant Biol.* **2007**, *49*, 4–10.
- (16) Losi, A.; Gärtner, W. *Photochem. Photobiol. Sci.* **2008**, *7*, 1168–1178.
- (17) Krauss, U.; Minh, B. Q.; Losi, A.; Gärtner, W.; Eggert, T.; von Haeseler, A.; Jaeger, K.-E. *J. Bacteriol.* **2009**, *191*, 7234–7242.
- (18) Pathak, G.; Ehrenreich, A.; Losi, A.; Streit, W. R.; Gärtner, W. *Environ. Microbiol.* **2009**, *11*, 2388–2399.
- (19) Swartz, T. E.; Corchnoy, S. B.; Christie, J. M.; Lewis, J. W.; Szundi, I.; Briggs, W. R.; Bogomolni, R. A. *J. Biol. Chem.* **2001**, *276*, 36493–36500.
- (20) Purcell, E. B.; Siegal-Gaskins, D.; Rawling, D. C.; Fiebig, A.; Crosson, S. *Proc. Natl. Acad. Sci. U.S.A.* **2007**, *104*, 18241–18246.
- (21) Idnurm, A.; Crosson, S. *PLoS Pathogens* **2009**, *5*, e1000470.
- (22) Swartz, T. E.; Corchnoy, S. B.; Christie, J. M.; Lewis, J. W.; Szundi, I.; Briggs, W. R.; Bogomolni, R. A. *J. Biol. Chem.* **2001**, *276*, 36493–36500.
- (23) Kottke, T.; Heberle, J.; Hehn, D.; Dick, B.; Hegemann, P. *Biophys. J.* **2003**, *84*, 1192–1201.
- (24) Kasahara, M.; Swartz, T. E.; Olney, M. A.; Onodera, A.; Mochizuki, N.; Fukuzawa, H.; Asamizu, E.; Tabata, S.; Kanegae, H.; Takano, M.; Christie, J. M.; Nagatani, A.; Briggs, W. R. *Plant Physiol.* **2002**, *129*, 762–773.
- (25) Nakasako, M.; Matsuoka, D.; Zikihara, K.; Tokutomi, S. *FEBS Lett.* **2005**, *579*, 1067–1071.
- (26) Kikuchi, S.; Unno, M.; Zikihara, K.; Tokutomi, S.; Yamauchi, S. *J. Phys. Chem. B* **2009**, *113*, 2913–2921.
- (27) Jentzsch, K.; Wirtz, A.; Circolone, F.; Drepper, T.; Losi, A.; Gärtner, W.; Jaeger, K.-E.; Krauss, U. *Biochemistry* **2009**, *48*, 10321–10333.
- (28) Alexandre, M. T. A.; Arents, J. C.; van Grondelle, R.; Hellingwerf, K. J.; Kennis, J. T. M. *Biochemistry* **2007**, *46*, 3129–3137.
- (29) Zoltowski, B. D.; Vaccaro, B.; Crane, B. R. *Nat. Chem. Biol.* **2009**, *5*, 827–834.
- (30) Corchnoy, S. B.; Swartz, T. E.; Lewis, J. W.; Szundi, I.; Briggs, W. R.; Bogomolni, R. A. *J. Biol. Chem.* **2003**, *278*, 724–731.
- (31) Alexandre, M. T. A.; Domratcheva, T.; Bonetti, C.; van Wilderen, L. J. G. W.; van Grondelle, R.; Groot, M. L.; Hellingwerf, K. J.; Kennis, J. T. M. *Biophys. J.* **2009**, *97*, 227–237.
- (32) Pfeifer, A.; Majerus, T.; Zikihara, K.; Matsuoka, D.; Tokutomi, S.; Heberle, J.; Kottke, T. *Biophys. J.* **2009**, *96*, 1462–1470.
- (33) Lanzl, K.; Sanden-Flohe, M. V.; Kutta, R. J.; Dick, B. *Phys. Chem. Chem. Phys.* **2010**, *12*, 6594–6604.
- (34) Möglich, A.; Moffat, K. *Photochem. Photobiol. Sci.* **2010**, *9*, 1286–1300.
- (35) Zoltowski, B. D.; Gardner, K. H. *Biochemistry* **2011**, *50*, 4–16.
- (36) Ryu, M. H.; Moskvina, O. V.; Silberg-Liberles, J.; Gomelsky, M. *J. Biol. Chem.* **2010**, *285*, 41501–41508.

- (37) Stierl, M.; Stumpf, P.; Udvari, D.; Gueta, R.; Hagedorn, R.; Losi, A.; Gärtner, W.; Peterleit, L.; Efetova, M.; Schwarzel, M.; Oertner, T. G.; Nagel, G.; Hegemann, P. *J. Biol. Chem.* **2011**, *286*, 1181–1188.
- (38) Losi, A.; Kottke, T.; Hegemann, P. *Biophys. J.* **2004**, *86*, 1051–1060.
- (39) Tang, Y.; Cao, Z.; Livoti, E.; Krauss, U.; Jaeger, K.-E.; Gärtner, W.; Losi, A. *Photochem. Photobiol. Sci.* **2010**, *9*, 47–56.
- (40) Mansurova, M.; Scheercousse, P.; Simon, J.; Kluth, M.; Gärtner, W. *ChemBioChem* **2011**, *12*, 641–646.
- (41) Climent, T.; Gonzalez-Luque, R.; Merchan, M.; Serrano-Andres, L. *J. Phys. Chem. A* **2006**, *110*, 13584–13590.
- (42) Johansson, L. B.; Davidsson, A.; Lindblom, G.; Naqvi, K. R. *Biochemistry* **1979**, *18*, 4249–4253.
- (43) Nozaki, D.; Iwata, T.; Ishikawa, T.; Todo, T.; Tokutomi, S.; Kandori, H. *Biochemistry* **2004**, *43*, 8373–8379.
- (44) Iwata, T.; Nozaki, D.; Sato, Y.; Sato, K.; Nishina, Y.; Shiga, K.; Tokutomi, S.; Kandori, H. *Biochemistry* **2006**, *45*, 15384–15391.
- (45) Eisenreich, W.; Joshi, M.; Illarionov, B.; Richter, G.; Römisch-Margl, W.; Müller, F.; Bacher, A.; Fischer, M. *FEBS J.* **2007**, *274*, 5876–5890.
- (46) Alexandre, M. T. A.; Purcell, E. B.; van Grondelle, R.; Robert, B.; Kennis, J. T. M.; Crosson, S. *Biochemistry* **2010**, *49*, 4752–4759.
- (47) Kotaki, A.; Naoi, M.; Yagi, K. *J. Biochem.* **1970**, *68*, 287–292.
- (48) Yagi, K.; Ohishi, N.; Nishimoto, K.; Choi, J. D.; Song, P. S. *Biochemistry* **1980**, *19*, 1553–1557.
- (49) Salzmann, S.; Silva-Junior, M. R.; Thiel, W.; Marian, C. M. *J. Phys. Chem. B* **2009**, *113*, 15610–15618.
- (50) Nash, A. I.; Ko, W. H.; Harper, S. M.; Gardner, K. H. *Biochemistry* **2008**, *47*, 13842–13849.
- (51) Zoltowski, B. D.; Schwerdtfeger, C.; Widom, J.; Loros, J. J.; Bilwes, A. M.; Dunlap, J. C.; Crane, B. R. *Science* **2007**, *316*, 1054–1057.
- (52) Buttani, V.; Losi, A.; Eggert, T.; Krauss, U.; Jaeger, K.-E.; Cao, Z.; Gärtner, W. *Photochem. Photobiol. Sci.* **2007**, *6*, 41–49.
- (53) Yamamoto, A.; Iwata, T.; Sato, Y.; Matsuoka, D.; Tokutomi, S.; Kandori, H. *Biophys. J.* **2009**, *96*, 2771–2778.
- (54) Avila-Perez, M.; Vreede, J.; Tang, Y.; Bende, O.; Losi, A.; Gärtner, W.; Hellingwerf, K. *J. Biol. Chem.* **2009**, *284*, 24958–24964.
- (55) Jones, M. A.; Feeney, K. A.; Kelly, S. M.; Christie, J. M. *J. Biol. Chem.* **2007**, *282*, 6405–6414.
- (56) Lapid, C. *PrimerX*, Automated design of mutagenic primers for site-directed mutagenesis; 2003; <http://www.bioinformatics.org/primerx/>.
- (57) Losi, A.; Polverini, E.; Quest, B.; Gärtner, W. *Biophys. J.* **2002**, *82*, 2627–2634.
- (58) Losi, A.; Wegener, A. A.; Engelhard, M.; Gärtner, W.; Braslavsky, S. E. *Biophys. J.* **2000**, *78*, 2581–2589.
- (59) Losi, A.; Quest, B.; Gärtner, W. *Photochem. Photobiol. Sci.* **2003**, *2*, 759–766.
- (60) Rudzki, J. E.; Goodman, J. L.; Peters, K. S. *J. Am. Chem. Soc.* **1985**, *107*, 7849–7854.
- (61) Abbruzzetti, S.; Viappiani, C.; Murgida, D. H.; Erra-Balsells, R.; Bilmes, G. M. *Chem. Phys. Lett.* **1999**, *304*, 167–172.
- (62) Braslavsky, S. E.; Heibel, G. E. *Chem. Rev.* **1992**, *92*, 1381–1410.
- (63) Rudzki-Small, J.; Libertini, L. J.; Small, E. W. *Biophys. Chem.* **1992**, *41*, 29–48.
- (64) Malkin, S.; Churio, M. S.; Shochat, S.; Braslavsky, S. E. *J. Photochem. Photobiol. B: Biol.* **1994**, *23*, 79–85.
- (65) Losi, A.; Braslavsky, S. E. *Phys. Chem. Chem. Phys.* **2003**, *5*, 2739–2750.
- (66) Gauden, M.; Crosson, S.; van Stokkum, I. H. M.; van Grondelle, R.; Moffat, K.; Kennis, J. T. M. In *Femtosecond Laser Applications in Biology*; Avrilleir, S.; Tualle, J. M., Eds.; SPIE: Bellingham, WA, 2004; pp 97–104.
- (67) Van den Berg, P. W.; Widengren, J.; Hink, M. A.; Rigler, R.; Visser, A. G. *Spectrochim. Acta A* **2001**, *57*, 2135–2144.
- (68) Zirak, P.; Penzkofer, A.; Mathes, T.; Hegemann, P. *Chem. Phys.* **2009**, *358*, 111–122.
- (69) Salomon, M.; Christie, J. M.; Knieb, E.; Lempert, U.; Briggs, W. R. *Biochemistry* **2000**, *39*, 9401–9410.
- (70) Philip, A. F.; Nome, R. A.; Papadantonakis, G. A.; Scherer, N. F.; Hoff, W. D. *Proc. Natl. Acad. Sci. U.S.A.* **2010**, *107*, 5821–5826.
- (71) Winzor, D. J.; Jackson, C. M. *J. Mol. Recognit.* **2006**, *19*, 389–407.
- (72) Harper, S. M.; Christie, J. M.; Gardner, K. H. *Biochemistry* **2004**, *43*, 16184–16192.
- (73) Crosson, S.; Rajagopal, S.; Moffat, K. *Biochemistry* **2003**, *42*, 2–10.
- (74) Freddolino, P. L.; Dittich, M.; Schulten, K. *Biophys. J.* **2006**, *91*, 3630–3639.
- (75) Corchnoy, S. B.; Swartz, T. E.; Szundi, I.; Lewis, J. W.; Briggs, W. R.; Bogomolni, R. A. *Biophys. J.* **2003**, *84*, 398A.
- (76) Schleicher, E.; Kowalczyk, R. M.; Kay, C. W. M.; Hegemann, P.; Bacher, A.; Fischer, M.; Bittl, R.; Richter, G.; Weber, S. *J. Am. Chem. Soc.* **2004**, *126*, 11067–11076.
- (77) Bonetti, C.; Stierl, M.; Mathes, T.; van Stokkum, I. H. M.; Mullen, K. M.; Cohen-Stuart, T. A.; van Grondelle, R.; Hegemann, P.; Kennis, J. T. M. *Biochemistry* **2009**, *48*, 11458–11469.
- (78) Bauer, C.; Rabl, C. R.; Heberle, J.; Kottke, T. *Photochem. Photobiol.* **2011**No. DOI: 10.1111/j.1751-1097.2011.00901.x.
- (79) Nagahama, T.; Suzuki, T.; Yoshikawa, S.; Iseki, M. *Neurosci. Res.* **2007**, *59*, 81–88.
- (80) Strickland, D.; Moffat, K.; Sosnick, T. R. *Proc. Natl. Acad. Sci. U.S.A.* **2008**, *105*, 10709–10714.
- (81) Wu, Y. I.; Frey, D.; Lungu, O. I.; Jaehrig, A.; Schlichting, I.; Kuhlman, B.; Hahn, K. M. *Nature* **2009**, *461*, 104–108.
- (82) Möglich, A.; Ayers, R. A.; Moffat, K. *J. Mol. Biol.* **2009**, *385*, 1433–1444.
- (83) Arents, J. C.; Perez, M. A.; Hendriks, J.; Hellingwerf, K. J. *FEBS Lett.* **2011**, *585*, 167–172.
- (84) Purcell, E. B.; McDonald, C. A.; Palfey, B. A.; Crosson, S. *Biochemistry* **2010**, *49*, 6761–6770.

## **2.2 The amino acids surrounding the flavin 7a-methyl group determine the UVA spectral features of a LOV protein**

Accepted. Biol. Chem., 4.7, 1. author

Sample generation and preparation: 100 %

Measurements: 80 %

**Research Article**

**The amino acids surrounding the flavin 7a-methyl group determine the UVA spectral features of a LOV protein**

Sarah Raffelberg<sup>1</sup>, Alexander Gutt<sup>1</sup>, Wolfgang Gärtner<sup>1</sup>, Carmen Mandalari<sup>2</sup>, Stefania Abbruzzetti<sup>2</sup>, Cristiano Viappiani<sup>2</sup> and Aba Losi<sup>2,\*</sup>

<sup>1</sup>Max Planck Institute for Chemical Energy Conversion, Stiftstrasse 34-36, D-45470 Mülheim, Germany

<sup>2</sup>Department of Physics and Earth Sciences, University of Parma, Viale G.P. Usberti 7/A, I-43124, Parma, Italy

\*Corresponding author

e-mail: aba.losi@fis.unipr.it



## Abstract

Flavin-binding LOV domains (LOV, light, oxygen, voltage) are UVA/Blue-light sensing protein units that form upon light induction a reversible FMN-cysteine adduct. In their dark-adapted state LOV domains exhibit the typical spectral features of fully oxidized riboflavin derivatives. A survey on the absorption spectra of various LOV domains revealed that the UVA spectral range is the most variable region (whereas the absorption band at 450 nm is virtually unchanged), showing essentially two distinct patterns found in plant phototropin LOV1 and LOV2 domains respectively. In this work we have identified a residue directly interacting with the isoalloxazine methyl group at C(7a), as the major UVA spectral tuner. In YtvA from *Bacillus subtilis* this amino acid is threonine 30 and its mutation into apolar residues converts the LOV2-like spectrum of native YtvA into a LOV1-like pattern. Mutation T30A also accelerates the photocycle ca. 4-fold. Together with control mutations at different positions, our results experimentally confirm the previously calculated direction of the transition dipole moment for the UVA  $\pi\pi^*$  state and identify the mechanisms for tuning the spectral properties of LOV domains.

**Keywords:** photobiophysics, photochemistry, UVA/blue-light sensing, spectral tuning, mutagenesis

## Introduction

Plant phototropins (phot) were the first photoreceptor proteins in which the blue light-sensing, flavin-binding LOV domains (LOV, light, oxygen, voltage) were identified as sensor modules (Briggs et al. 1999). Following their initial finding in *Arabidopsis thaliana* (At) and in several other plants, Losi et al identified in 2002 the bacterial ortholog to phot LOV domains in the protein YtvA from the soil bacterium *Bacillus subtilis* (Bs) (Losi et al. 2002). YtvA consists of a LOV domain fused to a STAS (Sulphate Transporters AntiSigma-factor antagonist) domain. It has been identified as a regulatory component of the Bs stressosome (Gaidenko et al. 2006; Avila-Perez et al. 2006). Due to its significantly smaller size (compared to plant phot) YtvA has been established as a model system for studying blue-light sensing/signaling in bacteria.

LOV domains constitute a subgroup of the PAS (Per-Arnt-Sim) superfamily (Möglich et al. 2009). The capability to sense UVA and blue-light is given by their chromophore, a non-covalently bound flavin mononucleotide (FMN) (Losi et al. 2012). Excitation of the FMN molecule causes its conversion to the triplet state. During triplet decay a covalent bond is formed between the position 4a of FMN and a close-by located cysteine residue (C62 in case of YtvA), probably via a radical intermediate (Bauer et al. 2011). The newly formed covalent C4a-S bond, defining the so-called adduct or signaling state, decays thermally to the unphotolyzed state with a lifetime between some seconds to several hours, at room temperature, depending on the specific protein studied (Losi et al. 2011). Besides thermal recovery, there is evidence for photochromicity in LOV domains, whereby the lit state can be photoexcited, yielding the dark state in a rapid reaction, yet with a very moderate quantum yield ( $\Phi = 0.05$ ) (Kennis et al. 2004; Losi et al. 2013).

Although ongoing research yields more and more information about the photochemistry of blue-light sensitive photoreceptors, still a number of unanswered questions remains, mostly addressing the absorption properties and the thermal recovery kinetics of the signalling state. In recent years the role of specific amino acids during adduct formation and decay has been increasingly investigated, and site directed mutagenesis has identified “hot spots” in the protein that induce strong changes in the photochemical processes of LOV proteins, and also significantly influence the thermal stability of the photo-generated signaling state. Several factors have been identified that strongly affect the photocycle dynamics (Losi et al. 2011),

most notably the hydrogen bonding (HB) network accomplished by highly conserved polar residues (N94-N104-Q123, YtvA) (Raffelberg et al. 2011), a steric trigger (N425, Asphot1-LOV2, As = *Avena sativa*) (Brosi et al. 2010), and a conserved residue, which is not a direct interaction partner in the binding pocket (F434, Asphot1-LOV2) (Song et al. 2011). (Figure 1)

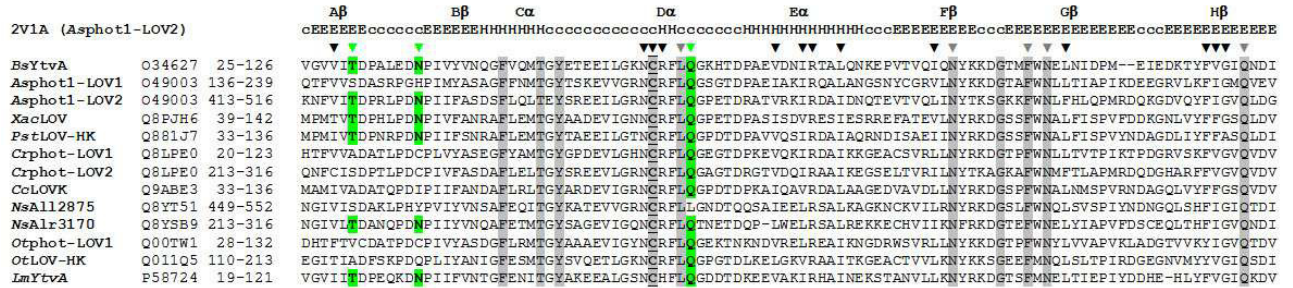


**Figure 1:** sequence alignment of YtvA-LOV with selected, photochemically active LOV domains. The three amino acids mutated in this work (T30, N37 and Q66) are highlighted in green. Secondary structures elements, with the most common nomenclature, are indicated above for Asphot1-LOV2 (PDB code 2V1A): E = strands, H = helices, c = unordered, loops, turns. Triangles indicate residues interacting with the chromophore (within 4 Å distance); the substrate cysteine involved in LOV-type photochemistry is underlined. The ten superconserved amino acids (Mandalari et al. 2013) in photoactive LOV domains are highlighted in gray. Species abbreviations: Bs = *Bacillus subtilis*; As = *Avena sativa*; Xac = *Xanthomonas axonopodis* pv. citri; Pst = *Pseudomonas syringae* pv. tomato; Cr = *Chlamydomonas reinhardtii*; Cc = *Caulobacter crescentus*; Ns = *Nostoc* sp. PCC 7120; Ot = *Ostreococcus tauri*; Lm = *Listeria monocytogenes*.

Only very few studies have addressed the UVA spectral region of LOV-based photoreceptors, although there are evidences that illumination with this spectral light quality results in a lower quantum yield of photoadduct formation ( $\Phi_{DL}$ , DL =dark-light conversion),(Islam et al. 2003; Losi et al. 2004; Penzkofer et al. 2005) compared to the excitation in the blue-light region. Furthermore, both calculations and experimental data, indicate that the major  $\pi\pi^*$  transition of flavins in the UVA range ( $S_0 \rightarrow S_5$ ), should have a larger solvent dependence than the  $\pi\pi^*$  in the blue-light range ( $S_0 \rightarrow S_1$ ), specifically related to solvent proticity and HB formation (Salzmann et al. 2008). The characterization of these spectral parameters becomes more important, as nanoscopy applications based on the photochromicity of LOV domains may require an optimized tuning of the spectral properties (Losi et al. 2013). In the

following, we refer to the composite transitions in the two spectral regions as I (blue) and II (UVA) (Figure 2).

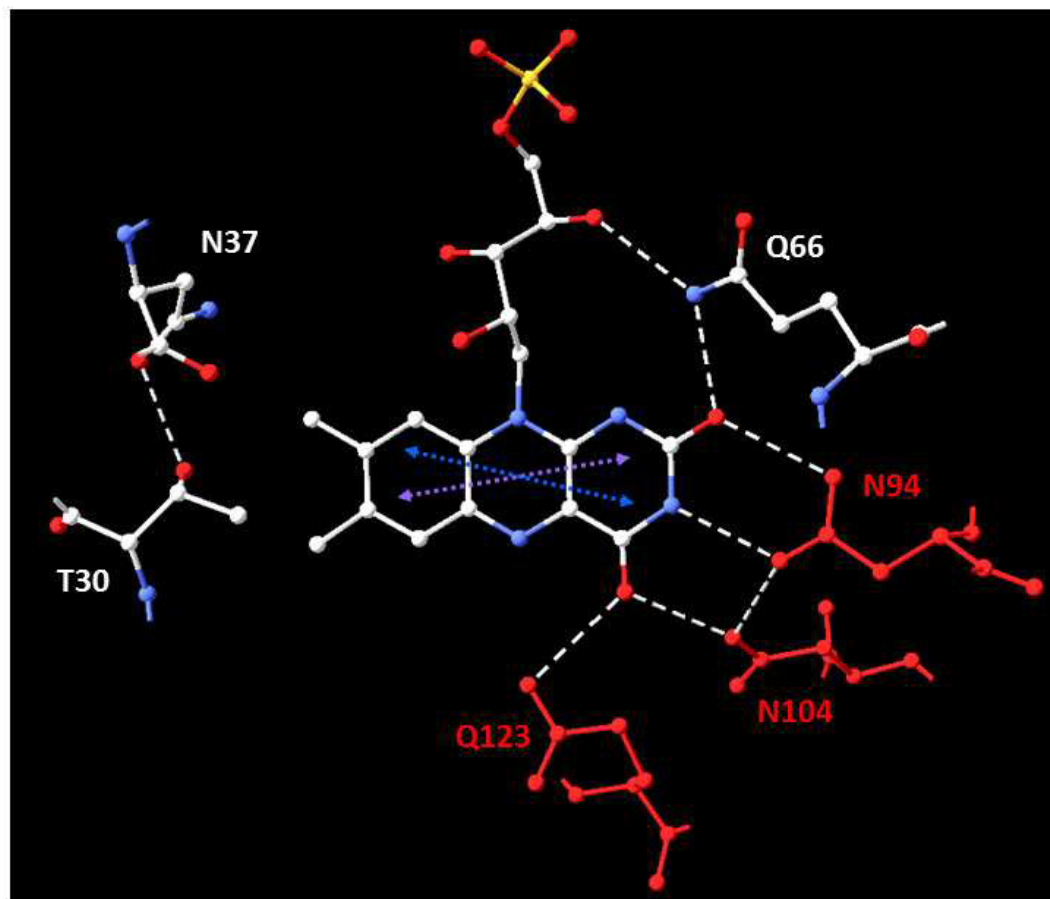


**Figure 2:** graphics of the binding cavity in YtvA-LOV (dark adapted state, PDB accession number 2pr5), showing the three residues modified in this work (T30, N37 and Q66) in white; in red, the three polar amino acids form a HB network around the polar part of the isoalloxazine ring in YtvA-LOV that were the subject of a previous investigation (Raffelberg et al. 2011). The calculated polarization directions of the low-energy  $\pi\pi^*$  transitions are also shown (Climent et al. 2006), blue, I with  $\lambda_{\max}$  at ca. 450 nm; violet, II with  $\lambda_{\max}$  at ca. 350-375 nm.

In LOV proteins the spectral position of transition I is very similar in the different systems for which photochemistry has been demonstrated, whereas this is not the case for transition II. The available literature data identify two major groups of LOV domains: proteins showing an Asphot1-LOV2 or YtvA-like UVA pattern, with one resolved maximum at ca. 375 nm, and those having an Asphot1-LOV1-like pattern,

with an overall blue-shift of transition II and two resolved peaks at ca. 350 and 370 nm (Salomon et al. 2000; Losi et al. 2002). Apparently, evolution of LOV domains has generated two subfamilies that can clearly be distinguished by their transition II properties. It is not clear, up to now, which residues determine the appearance of one or the other UVA pattern. Upon close inspection of amino acid sequences of LOV domains with known photochemistry, two partially conserved residues, part of the chromophore binding pocket, appear as major candidates as UVA tuning residues: T30 and N37 (YtvA numbering, see Figures 1 and 2), interacting with the isoalloxazine methyl groups at C(7a) and C(8a), respectively. Position N37 is equivalent to the already investigated N425 in Asphot1-LOV2 (Brosi et al. 2010). These authors demonstrated the importance of asparagine at position 425 by generating two variants (N425S and N425C) for investigations using ENDOR EPR. N425S showed an increased rotational freedom of the methyl group at C(8a) and N425C altered the dihedral angle between the isoalloxazine (benzol[*g*]pteridine-2,4(3H,10H)-dione) ring system and the C(8a)-methyl group by about 10°. This mutation also reduced the lifetime for the thermal recovery reaction ( $\tau_{\text{rec}} = 7.5$ ) ca. 7-fold compared to wild-type (WT) Asphot1-LOV2 ( $\tau_{\text{rec}} = 45.8$  s) (Brosi et al. 2010).

In *Neurospora crassa* Vivid (NcVVD), an extended LOV domain binding flavin adenine dinucleotide (FAD), C76 and T83 corresponds to YtvA T30 and N37, respectively. (Schwerdtfeger et al. 2003) Together with the phosphodiester side chain of FAD these two amino acids have been proposed to line a solvent accessible channel to the isoalloxazine ring (Zoltowski et al. 2007). Furthermore, the reactive cysteine is oriented with the sulfhydryl group toward C76 in one of the two conformations, supposed to be the less reactive one (Zoltowski et al. 2009). Mutations at C76 and T83 (C76A/V, T83V) have some effect on NcVVD  $\tau_{\text{rec}}$ , but they have not been further inspected. To our knowledge there are no other investigations addressing the role of residues corresponding to YtvA T30 in LOV domains.

In this work we identify the effects of mutations at T30 and N37 positions on spectral properties, dynamics and yield of the photocycle of YtvA. Following a previous article, in which we examined the role of conserved polar residues forming an extended HB network (Raffelberg et al. 2011), we added mutations at position Q66 (a residue

conserved in most LOV domains), where the glutamine is part of the HB network and H-bonded to the flavin ribityl chain (Fig. 2).

For the two positions T30 and N37, mutations were designed according to already existing variations identified in other LOV domains (compared to the consensus sequence, Figure 1). The following changes were introduced: T30 was mutated into alanine, serine, and valine, and N37 was converted into alanine, cysteine, and valine, respectively. The replacement of threonine and asparagine by alanine introduces a small, apolar amino acid and in case of valine a slightly more bulky but still apolar side chain; on the other hand, insertion of the polar, but less bulky residues serine and cysteine should yield a less compact chromophore pocket, suggesting to affect FMN spectral features and photochemistry. Mutations were also introduced at position Q66, to test its effects on spectral features and on the photocycle. Four mutations were designed for this position, introducing proline, leucine, histidine and lysine. All variants of YtvA were investigated by steady state and transient absorption and fluorescence spectroscopies, fluorescence microscopy and Laser Induced Optoacoustic Spectroscopy (LIOAS).

We demonstrate that T30 is, in YtvA, a major spectral-tuning residue for the UVA region whereas N37 has a negligible role. However, both residues have an impact on the photocycle dynamics. Our results are discussed with respect to photophysical and photochemical features and spectral tunability for biotechnological applications.



## Results

### *Spectral parameters and fluorescence lifetimes*

Following the identification of two amino acids that are potentially UVA-absorbance regulators by above presented sequence alignment of LOV domains, positions 30 (threonine) and 37 (asparagine, nomenclature following YtvA) were mutated. Whereas none of the mutations performed had a significant effect on transition I ( $\lambda_{\text{max}} = 448/475 \text{ nm}$ ), remarkable shifts in spectral properties are observed in the UVA range. Interestingly, the most significant changes are caused by T30 substitution with an apolar residue (A, V), whereas negligible effects are observed for mutations of N37 (Table 1, Figure 3). This is also confirmed by the observation that the double mutation T30V/N37C produces spectral features virtually identical to T30V (Table 1). YtvA-WT exhibits a UVA maximum at 375 nm with a shoulder at ca. 359 nm, whereas in T30A/V the band is blue-shifted and resolved in two distinct peaks ( $\lambda_{\text{max}} = 354/370 \text{ nm}$ , Table 1).

**Table 1:** Spectral parameters and fluorescence anisotropy (*A*)

	<sup>a</sup> Dark state		<sup>b</sup> <i>F</i> <sub>max</sub> /nm	<sup>c</sup> $\Phi_F$		<sup>d</sup> $\tau_{F1/2}$ /ns (fraction 1/2)	<sup>e</sup> <i>A</i>	
	Abs. maxima/nm			$\lambda_{ex}$ / nm			$\lambda_{ex}$ /nm	
	UVA	Blue		355	450	405 nm	355	450
FMN <sub>aq</sub>	372	445/472	526	0.25	0.25	4.7/-- (1/--)	< 0.01	0.01
YtvA-WT	359 <sub>s</sub> /375	448/475	497	0.16	0.22	4.6 /2.1 (0.33/0.67)	0.25	0.33
N37C	359 <sub>s</sub> / 375	448/475	498	0.20	0.22	4.8/2.1 (0.89/0.11)	0.23	0.30
N37F	358 <sub>s</sub> / 374	448/475	496	0.20	0.26	4.8/2.7 (0.47/0.53)	0.22	0.30
N37V	359 <sub>s</sub> / 375	448/475	496	0.20	0.26	5.1/2.1 (0.73/0.27)	0.23	0.31
T30A	354/ 370	448/475	496	0.22	0.25	4.8/2.1 (0.85/0.15)	0.20	0.30
T30S	358 <sub>s</sub> /373	448/475	497	0.28	0.27	4.4/2.2 (0.74/0.26)	0.24	0.31
T30V	354/371	448/475	497	0.18	0.18	4.9/2.6 (0.72/0.28)	0.21	0.31
T30V/N37C	354/372	448/475	497	0.17	0.16	5.0/2.2 (0.66/0.34)	0.26	0.32
Q66H	358 <sub>s</sub> / 374	448/475	496	0.08	0.11	4.6/1.3 (0.60/0.40)	0.28	0.34
Q66K	358 <sub>s</sub> / 374	450/476	499	0.21	0.27	4.6/2.7 (0.75/0.25)	0.22	0.32
R63K	359 <sub>s</sub> /375	448/475	497	0.20	0.22	4.9/2.5 (0.55/0.45)	0.23	0.31

<sup>a</sup>: shoulders (suffix "s") /vibrational bands in the same transition are separated by a slash; <sup>b</sup>: fluorescence maximum; <sup>c</sup>: fluorescence quantum yield; <sup>d</sup>: fluorescence lifetime with violet light-induced photoequilibrium; in parenthesis, the fractions associated to each component; <sup>e</sup>: *A* = fluorescence anisotropy.



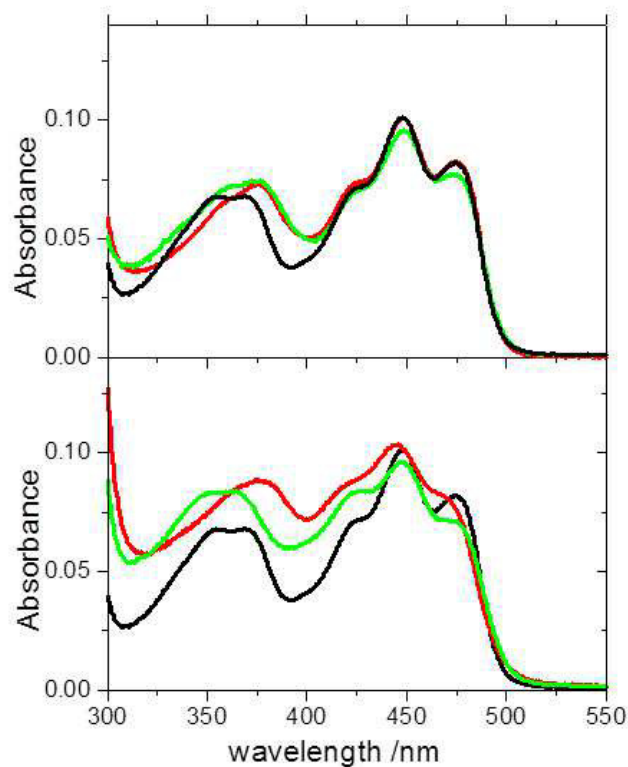


**Figure 3:** absorption spectra of YtvA proteins in the dark-adapted state: **a)** T30A (black line), WT (red) and N37C (green); **b)** T30A (black line), N104A (red) and N94A (green)

A similar blue-shift of the UVA transition was formerly reported for N94A (Fig. 3) (Raffelberg et al. 2011). Interestingly, N94 is interacting with position 3 of the isoalloxazin, and is, as T30, directly in line with the transition dipole moment. Including two other positions into this investigation, Q66 and R63, we find that the blue-light transition and the fluorescence maxima are solely and minimally affected by Q66K. Fluorescence anisotropy, reflecting the rigidity of the flavin binding cavity, appears virtually unaffected by all mutations. Interestingly, Q66H has a much lower value of  $\Phi_F$  and a faster fluorescence lifetime, indicating a mechanism of dynamic quenching: this is possibly due to electron transfer from histidine to the flavin excited state (Penzkofer et al. 2007). Q66L and Q66P showed a very low chromophore loading and were not further investigated.

Measurements of fluorescence lifetimes with the confocal microscope-based methodology gave a single value,  $\tau_F = 4.7 \div 4.9$  ns, under blue-light illumination and two

values under photoequilibrium conditions with violet illumination:  $\tau_{F1}=4.6\div5.1$  ns and  $\tau_{F2}=1.3\div2.7$  ns (Table 1). The longer lifetime  $\tau_{F1}$  corresponds to a non-photoconvertible fraction, possibly a small amount of free FMN, given the identical fluorescence lifetime, whereas  $\tau_{F2}$  originates from the small percentage of protein molecules driven back to the fluorescent state by violet light (Losi et al. 2013). The shorter lifetime,  $\tau_{F2}$ , should therefore correspond to the fluorescence lifetime of bound FMN, although we cannot exclude it is bound to the protein in a non specific manner/alternative conformation (Figure 4).

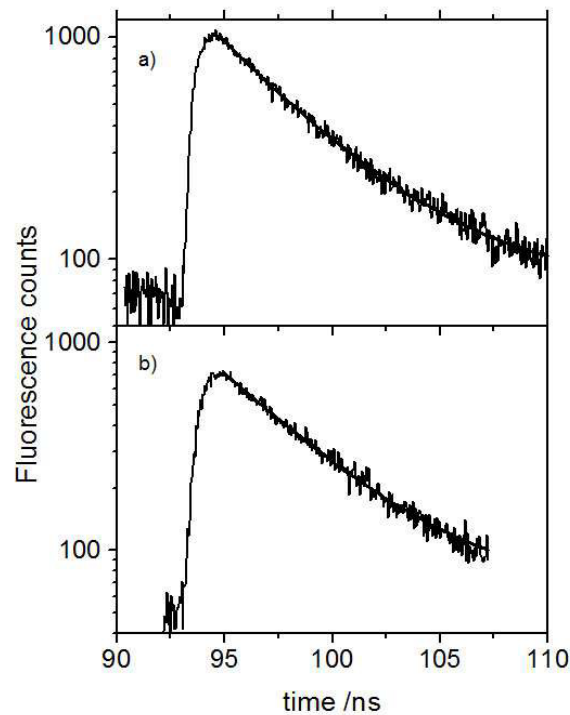


**Figure 4:** fluorescence decay of T30A under: **a)** violet illumination (405 nm), photoequilibrium condition; the best fitting is with a double exponential function (superimposed to the experimental curve), giving  $\tau_{F1}= 4.8$  ns and  $\tau_{F2} = 2.1$  ns; **b)** blue-light illumination (475 nm), giving a single  $\tau_{F1}=4.6$  (Table 1).

This method appears thus to be, for slow-cycling LOV proteins, more reliable than conventional single photon counting, in that the conventional method requires long measuring times and a larger amount of absorbed photons, thus forming considerable amounts of photoadduct and inducing loss of fluorescence intensity and

two-exponential fittings of fluorescence decays as possibly being artifacts (Losi et al. 2002; Losi et al. 2003b).

Nevertheless, we cannot exclude that the long-lived component measured in this work corresponds to a non-photoconvertible fraction of FMN bound to the protein.

### ***Photocycle dynamics and efficiency***

All investigated mutated proteins formed a triplet state and a photoadduct with yields comparable to, or even higher than YtvA-WT (Table 2). The only exception again is Q66H, with a lower quantum yield ( $\Phi_{DL}$ ) possibly due to quenching of the flavin triplet state by the introduced, nearby histidine via electron transfer (Tsentalovich et al. 2002). Interestingly, mutations at T30 tend to shorten the triplet lifetime,  $\tau_T$ , probably reflecting the fact that at the triplet state level the protein microenvironment has started to respond to the modified electronic structure of the chromophore.

Both mutations of Q66 considerably increase  $\tau_T$ , in line with previous data that have suggested a role of the extended HB network in modulating the dynamics of the photocycle (Raffelberg et al. 2011).

**Table 2:** Triplet state properties and adduct formation efficiency

	<sup>a</sup> $\Phi_T$	<sup>b</sup> $\tau_T$ / $\mu$ s	<sup>c</sup> $\Phi_{DL}$ ill. range =		<sup>d</sup> $\Phi_{LD}$ LED405	
			UVA	Blue	Photoeq.	Kin. mod.
YtvA-WT	0.46	1.8	0.32	0.49	0.049(Losi et al. 2013)	0.050(Losi et al. 2013)
N37C	0.62	2.0	0.30	0.52	--	--
N37F	0.60	3.1	0.34	0.28	0.060	0.047
N37V	0.54	2.3	0.36	0.58	0.100	0.044
T30A	0.63	1.5	0.33	0.28	0.038	0.040
T30S	0.45	0.8	0.28	0.40	0.046	0.040
T30V	0.69	1.3	0.25	0.61	0.057	0.030
T30V/N37C	0.63	1.3	0.26	0.51	--	--
Q66H	0.59	4.2	0.12	0.20	0.050	0.030
Q66K	0.77	6.3	0.28	0.40	0.027	0.025
R63K	0.51	2.2	0.23	0.40	0.080	0.100

<sup>a</sup>: triplet quantum yield as determined by LIOAS (eq. 3a), based on the energy level of the triplet state as 200 kJ/mol;  $\lambda_{ex}$  = 355 nm; <sup>b</sup>:triplet lifetime, flash photolysis,  $\lambda_{ex}$  = 355 nm; <sup>c</sup>:as determined from the time-course of fluorescence bleaching induced by LED356 and LED465; YtvA-WT was used as reference, with  $\Phi_{DL}$  = 0.32 (Losi et al. 2013) and 0.49 (Losi et al. 2002) for UVA and blue-light illumination, from independent LIOAS and flash photolysis measurements. <sup>d</sup>: as determined from the photoequilibrium absorption spectra and from the kinetic model applied to rates fluorescence recovery as a function of LED405 power. In the latter case the average fitting error is 25%.

LIOAS and fluorescence measurements indicate that UVA and violet light are able to induce a photoequilibrium in all cases investigated, as was previously demonstrated with YtvA-WT (Losi et al. 2013). All mutated proteins exhibit photochromism, as underscored by the possibility to determine fluorescence lifetimes of bound FMN under photoequilibrium conditions (figure 4 and table 1). In LIOAS experiments this is readily visualized by recording a small volume expansion ( $< 1$  ml/einstein, data not shown), occurring in less than 20 ns (eq. 1), upon UVA excitation of the adduct at  $T_{\beta=0}$  (eq. 2a, see Materila and Methods). Adduct formation corresponds instead to a volume contraction, considerably larger (between 3 and 6 ml/einstein), in agreement with the low yield of  $\Phi_{LD}$  determined for YtvA-WT (Losi et al. 2013).

By means of absorption and fluorescence spectroscopy it is possible to directly visualize the UVA/Violet-inducible photoequilibrium and to estimate the value of  $\Phi_{LD}$  as previously demonstrated with YtvA-WT. This is done either by establishing a photoequilibrium and applying eq. 4, or by following the kinetics of fluorescence recovery under violet light with different LED power and applying the kinetic model (eq. 5) (see. Materials and Methods). In some cases (N37C and T30V/N37C), the signal-to-noise ratio was not sufficient to allow the determination of  $\Phi_{LD}$ , but in general the protein variants investigated did not show a large deviation from YtvA-WT (Table 2). An example of fluorescence recovery curves and kinetic fitting is given in figure 5.

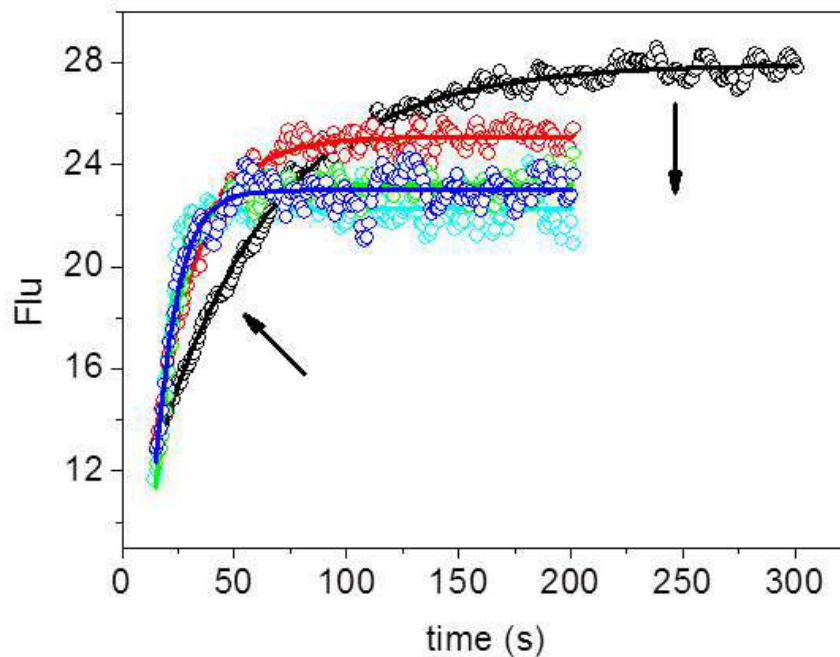


**Figure 5.** Fluorescence emission recovery of YtvA-T30S under violet illumination with LED405 (the arrows indicate increasing LED power, between 0.05 mW and 0.8 mW). Light adapted protein solutions were prepared by 5 min irradiation with LED465.  $T = 20\text{ }^{\circ}\text{C}$ ;  $\lambda_{\text{ex}} = 330\text{ nm}$ ,  $\lambda_{\text{em}} = 500\text{ nm}$ .

### ***Kinetics of the thermal dark-recovery reaction***

The lifetime  $\tau_{\text{rec}}$  for the completion of the photocycle (thermal recovery to the dark-adapted state with breakage of the covalent FMN-Cys bond) is in some cases considerably faster than in YtvA-WT, at  $20^{\circ}\text{C}$  (Table 3), e.g., for N37F/V, T30A/S, Q66H. Also other mutations have previously shown such a feature, e.g. R63K, N94A/S or Q123N (Table 3) (Tang et al. 2010; Raffelberg et al. 2011).

**Table 3:** Recovery kinetics, (20°C), and Arrhenius and Eyring parameters.

	$\tau_{\text{rec},20^\circ/\text{s}}$	$A/\text{s}^{-1}$	$E_a/\text{kJ mol}^{-1}$	$\Delta H^\#/\text{kJ mol}^{-1}$	$\Delta S^\#/\text{kJ mol}^{-1}\text{K}^{-1}$
YtvA-WT	<b>6240</b>	<b><math>6.9 \times 10^{14}</math></b>	<b>104</b>	<b>101</b>	<b>+0.031</b>
N37C	3300	$5.7 \times 10^7$	63	60	-0.10
N37F	1470	$6.5 \times 10^{12}$	90	87	-0.008
N37V	930	$1.15 \times 10^{11}$	49	76	-0.033
T30A	1690	$2.6 \times 10^{11}$	82	80	-0.034
T30S	1625	$8.4 \times 10^8$	68	65	-0.082
T30V	4280	$4.9 \times 10^9$	75	72	-0.067
T30V/N37C	5260	$2.2 \times 10^7$	62	60	-0.110
Q66H	1650	$1.2 \times 10^{12}$	86	83	-0.022
Q66K	2510	$3.6 \times 10^{14}$	95	92	+0.006
R63K	485	$6.9 \times 10^9$	70	68	-0.065
N94D	1250	$3.4 \times 10^{23}$	151	148	+0.20
YtvA-N94A	140	$4.9 \times 10^{18}$	117	115	+0.10
YtvA-N94S	300	$7.2 \times 10^{15}$	103	100	+0.05
YtvA-N104D	6890	$4.9 \times 10^{16}$	115	112	+0.066
YtvA-N104A	2250	$4.0 \times 10^8$	67	65	-0.09
YtvA-N104S	1120	$9.2 \times 10^{10}$	78	76	-0.043
YtvA-Q123N	72	$5.0 \times 10^9$	65	62	-0.067

The temperature dependence of the recovery reaction demonstrates nevertheless that a faster photocycle may be related to a more favorable (larger) activation entropy or to a more favorable (smaller) activation enthalpy (Table 3, Figure 6). Although the phenomenon is complex, the relation between the activation entropy and enthalpy is linear, revealing a compensation, most probably related to the network of weak interactions within the cavity (Losi et al. 2001).

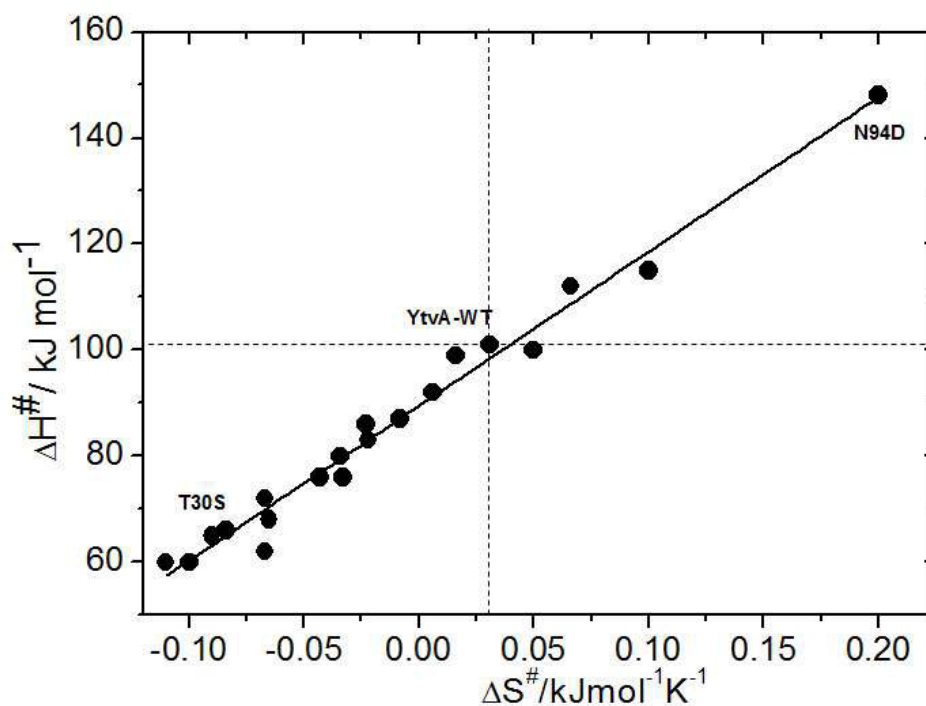


**Figure 6:** activation enthalpy-entropy correlation in the recovery reaction of YtvA-WT and mutated YtvA proteins. The mutations T30S and N94D give comparably short  $\tau_{\text{rec}}$  with respect to YtvA-WT (see table 4) but for T30S this appears to be linked to a more favorable (lower)  $\Delta H^\ddagger$ , whereas for N94D the faster kinetics is related to a larger  $\Delta S^\ddagger$ .



## Discussion

We here identify T30 as a major determinant for the spectral features of the LOV protein YtvA in the UVA range. Its substitution with an apolar residue, such as alanine, converts a typical *Asphot1*-LOV2-like spectrum into a LOV1-like spectrum. N37, although important for the duration of the photocycle as previously reported for the equivalent N425 position in *Asphot1*-LOV2 (Brosi et al. 2010), does not seem to be involved in spectral tuning.

The UVA  $\pi\pi^*$  transition has, according to computational studies, a larger dipole moment than the blue-light  $\pi\pi^*$  one (Climent et al. 2006; Salzmann et al. 2008). In a simplified view, the energy stabilization or destabilization of the ground and excited states in polar solvents, and thus the position of the absorption maxima, is connected to their dipole moments and to the polarization that they induce in their microenvironment. Both calculations and experimental data show that the  $\pi\pi^*$   $S_0 \rightarrow S_5$  transition in the UVA range should have a larger solvent dependence than the  $\pi\pi^*$   $S_0 \rightarrow S_1$  in the blue-light range, specifically related to solvent proticity and HB formation (Salzmann et al. 2008). This is exemplified for FMN which shows a large red-shift from 359 to 373 nm when dissolved in methanol or water, respectively, whereas the maximum position of the lowest energy transition is virtually unaffected (supplementary material, Fig. S1). A solvatochromic analysis of FMN reveals that the energy of the UVA transition is negatively correlated with the HB-donor ability of the solvent and positively correlated with the HB-acceptor/electron pair donor ability of the solvent; transition I in the blue-light range shows solely a weaker negative correlation with the HB-donor ability of the solvent (supplementary material, Fig. S2, Table S2). The quite large blue shift in the UVA range, induced in YtvA by T30A and N94A substitutions, is in line with the solvatochromic analysis of FMN (i.e. blue shift in the UVA range with decreased HB-donor ability of the microenvironment) and with the proposed polarization directions for transition II (Johansson et al. 1979; Climent et al. 2006). The advantage of a mutation at T30 over N94 for tuning the spectral properties of YvA (or other LOV domains), is the larger stability of the proteins in the former case, comparable to YtvA-WT; N94 is instead important for chromophore stabilization and is, accordingly, part of a pool of 10 superconserved amino acids within the LOV series (Fig. 1).

A survey of literature data confirms that, in the majority of cases, LOV proteins having a threonine at the position corresponding to T30 in YtvA, exhibit indeed the same UVA pattern, with a maximum at ca. 375 nm (Salomon et al. 2000) (Swartz et al. 2001) (Onodera et al. 2002; Christie et al. 1999) (Losi et al. 2002) (Swartz et al. 2007; Narikawa et al. 2006); (Hendrischk et al. 2009) (Djouani-Tahri et al. 2011), whereas a serine, an alanine or a valine in that position results in a phot-LOV1 pattern with a double 350-370 nm peak (Salomon et al. 2000; Kottke et al. 2003; Islam et al. 2003; Holzer et al. 2004; Kasahara et al. 2002; Iwata et al. 2005; Purcell et al. 2010; Swartz et al. 2007; Nash et al. 2011; Jentzsch et al. 2009; Krauss et al. 2005; Narikawa et al. 2006; Cao et al. 2010).

There is at least one exception of this observation, namely, the recently published LOV protein from *Listeria monocytogenes* that has a threonine in position 30, but still exhibits a 350-370 nm UVA pattern {Chan, 2013 24692 /id}. An attempt to assess for this protein the possible role of His57 (corresponding to Arg63 in YtvA, adjacent to the reactive Cys62) in determining the shape of the UVA band, has failed given that the H57R mutation resulted in a purified protein devoided of chromophore {Chan, 2013 24692 /id}. Furthermore, some bacterial LOV-kinases, with Thr in position 30, are further red-shifted with respect to YtvA (ca. 380 nm), albeit retaining the same YtvA-like UVA pattern of a single maximum with an additional, unresolved shoulder. (Swartz et al. 2007; Cao et al. 2008) These data allow suggesting the existence of further, still unidentified tuning residues.

In NcVVD the reactive C108 shows two conformers in the dark state, denominated *conf1* and *conf2*. In *conf1* (90%) C108 is directly above the C4a that forms the photoadduct, whereas in *conf2* (10%) the sulfhydryl group of C108 is in close proximity (3.4 Å) to C76 (corresponding to YtvA T30) (Zoltowski et al. 2007). A similar situation is observed for YtvA-LOV domain, for which the ratio *conf1*: *conf2* = 70:30, and for other LOV domains (Fedorov et al. 2003; Sato et al. 2007). *Conf1* is thought to form the adduct more efficiently, while stabilization of *conf2* leads, at least in mutated NcVVD proteins, to a faster  $\tau_{\text{rec}}$ . (Zoltowski et al. 2009) However, there are not sufficiently enough structural data to confirm that this holds for every LOV protein, but it is tempting to suggest that mutations at T30 in YtvA could alter the *conf1*: *conf2* equilibrium concomitant with the shift in the UVA transition, thus accounting for a

faster  $\tau_{\text{rec}}$  and, possibly for the formerly reported different photoreactivity of phot-LOV1 vs. LOV2 (Losi 2007).

The ability to tune spectrally LOV domains might be important for advanced biotechnological applications with such proteins (Losi et al. 2012; Walter et al. 2012), with special emphasis on spectral separation between the dark-adapted state and the adduct, an important aspect to maximize photochromicity (Losi et al. 2013). Interestingly, for mutations investigated in this work, the absorption maximum of the adduct is barely affected, also in the case of T30A (supplementary material, fig. S3). Nevertheless, mutations at T30 apparently do not affect the value of  $\Phi_{\text{LD}}$  that is solely increased for R63K, suggesting that localized structural factors might be involved in the process. Surely, for further studies on the photochromism of LOV domains, a wider range of proteins should be employed in order to identify criteria for optimization of  $\Phi_{\text{LD}}$ .

## Materials and methods

### *Mutagenesis, protein expression and purification*

A total of ten new single mutations and one double mutant of YtvA were generated: T30A, T30S, T30V, N37C, N37F, N37V, Q66H, Q66K, Q66P, Q66L and the double mutant T30V/N37C. A previously partially characterized mutated YtvA protein, R63K (Tang et al. 2010), was here further inspected. All variants of YtvA carry an N-terminal His<sub>6</sub> tag.

The mutations were induced by site-directed PCR using the QuikChange method (QuikChange II XL, Stratagene), as recently described (Raffelberg et al. 2011). Primers for PCR (see supplementary material, Table S1), were designed by the “DNA-based” option of PrimerX (Copyright © 2003 by Carlo Lapid). PCR products were treated with the restriction enzyme DpnI (New England BioLabs) that especially digests methylated and hemimethylated parental DNA. Sequencing revealed that all mutations were successfully introduced.

After transformation and expression in *E. coli* BL21 cells (induction by 0.4 mM isopropyl- $\beta$ -D-thiogalactopyranoside), the His-tagged proteins were purified via affinity chromatography (Ni-IMAC column, 4°C) with gradient elution (10 to 200 mM

imidazole); after removal of imidazole, the samples were stored in sodium-phosphate buffer (10 mM NaCl, 10 mM NaPi, pH 8.0).

### *Steady state and transient spectroscopy*

Absorbance spectra were recorded with a Jasco 7850 UV/Vis spectrophotometer. Steady-state fluorescence measurements were carried out with a Perkin-Elmer LS50 luminescence spectrometer.

The fluorescence quantum yield,  $\Phi_F$ , of the bound flavin for the mutated proteins was measured at 20°C, using FMN as standard ( $\Phi_F = 0.26$ ) (van den Berg et al. 2001).

Laser flash photolysis apparatus for transient absorbance detection was described previously. (Losi et al. 2013) Photoexcitation was carried out with the third harmonic (355 nm) of a Q-switched Nd:YAG laser (Surelite II-10, Continuum, Santa Clara, CA). The 633 nm line of a He-Ne laser (NEC Corp., 10 mW) was used as probe source for transient absorption signals. The transmitted intensity of the cw beam was monitored by a preamplified (Avtech AV149) avalanche silicon photodiode (Hamamatsu, S2382). A 0.25-m monochromator (H25, Jobin Yvon) was placed before the photodiode in order to remove scattering light from the pump laser. The voltage signal was digitized by a digital sampling oscilloscope (LeCroy 9370, 1GHz, 1GS/s). The sample was changed after each flash. The data were handled and analyzed using Origin Professional version 8.5 (Microcal Software, Inc., Northampton, MA, USA).

Arrhenius and Eyring plots for the dark recovery reaction of the photoadduct were built by recording the recovery of FMN fluorescence ( $\lambda_{ex} = 330$  nm,  $\lambda_{em} = 500$  nm). The kinetics traces were fitted with a mono- or biexponential function, furnishing the recovery lifetime ( $\tau_{rec}$ ) as a function of temperature, in the range of the protein stability (11-25°C). Excitation was at 330 nm, in order to minimize secondary photochemistry leading to the formation of the photoproduct during recording of the traces (Raffelberg et al. 2011).

Some experiments were performed with the aid of LEDs with emission peaks at 356 nm (LED356), 405 nm (LED405), and 465 nm (LED465) and FWHM of  $\sim 25$  nm (Roithner Lasertechnik GmbH, Vienna, Austria), as previously described (Losi et al. 2013). LED465 and LED405 were used for complete dark to light conversion and to

establish photoequilibrium, respectively. LED356 and LED465 were also employed to determine the quantum yield of adduct formation upon UVA and blue-light excitation (*vide infra*).

Fluorescence lifetimes were measured using a Microtime 200 from Picoquant, based on an inverted confocal microscope (Olympus IX70) and equipped with two SPADs (single photon avalanche diodes). Switch-off of mutants' dark state was achieved by a 475 nm picosecond diode laser, also used as excitation for fluorescence emission. From lit state, mutants were switched on by a 405 nm picosecond diode laser, which also served as excitation for fluorescence emission. Fluorescence emission was split with a 50/50 splitter between the two detection channels and collected through matched bandpass filters (AHF, SMD Emitter HQ 520/40). The concentration of all mutants was 100 nM. SymPhoTime software (PicoQuant) was used for data handling and analysis. Data accumulation time was 2 minutes for all samples.

#### *Laser Induced Optoacoustic Spectroscopy (LIOAS)*

For the LIOAS experiments, samples were excited using the frequency-tripled pulse of a Nd:YAG laser (SL 456G, 6-ns pulse duration, 355 nm, Spectron Laser System, Rugby, Great Britain). The cuvette holder FLASH 100 (Quantum Northwest, Spokane, WA, USA) was temperature controlled to  $\pm 0.02$  °C. The signal was detected by a V103-RM ultrasonic transducer and fed into a 5662 preamplifier (Panametrics Inc., Waltham, MA, USA). The pulse fluence was varied with a neutral density filter and measured with a pyroelectric energy meter (RJP735 head connected to a meter RJ7620 from Laser Precision Corp.). The beam was shaped by a  $1 \times 12$  mm slit, allowing a time resolution of  $\sim 60$  ns by using deconvolution techniques (Rudzki et al. 1985). The experiments were performed in the linear regime of amplitude versus laser fluence, normally  $\sim 20$   $\mu\text{J/pulse}$  (corresponding to  $30 \times 10^{-11}$  Einstein for 355 nm excitation, photon energy 337 kJ/mol). The sample concentration was about 15  $\mu\text{M}$ , giving  $1.8 \times 10^{-9}$  mol in the excitation volume  $V_0 = 0.12$  mL. These conditions correspond to a ratio of ca. 0.17 photons per protein molecule. New coccine (FLUKA, Neu-Ulm, Germany) was used as calorimetric reference (Abbruzzetti et al. 1999). The time evolution of the pressure wave was assumed to be a sum of monoexponential functions, as previously described (Raffelberg et al. 2011). The deconvolution analysis yielded the fractional amplitudes

( $\varphi_i$ ) and the lifetimes ( $\tau_i$ ) of the transients (Sound Analysis 3000, Quantum Northwest Inc., Spokane, WA). The time window was between 20 ns and 5  $\mu$ s. At a given temperature and for each resolved  $i$ -th step the fractional amplitude  $\varphi_i$  is the sum of the fraction of absorbed energy released as heat ( $\alpha_i$ ) and the structural volume change *per* absorbed Einstein ( $\Delta V_i$ ), according to eqn. (1) (Rudzki-Small et al. 1992):

$$\varphi_i = \alpha_i + \frac{\Delta V_i}{E_\lambda} \frac{c_p \rho}{\beta} \quad (1)$$

$E_\lambda$  is the molar excitation energy,  $\beta = (\partial V / \partial T)_p \Delta V$  is the volume expansion coefficient,  $c_p$  is the heat capacity at constant pressure, and  $\rho$  is the mass density of the solvent. In this work we used the so-called “two temperature” (TT) method in order to separate  $\alpha_i$  from  $\Delta V_i$  (Malkin et al. 1994). The sample waveform was acquired at a temperature for which heat transport is zero,  $T_{\beta=0} = 3.2^\circ\text{C}$  and at a slightly higher temperature  $T_{\beta>0} = 10^\circ\text{C}$ . At  $T_{\beta=0}$  the LIOAS signal is only due to  $\Delta V_i$ . The reference for deconvolution was recorded at  $T_{\beta>0}$ , and eqn. (2a) and (2b) were then used to derive  $\alpha_i$  and  $\Delta V_i$ :

$$\Phi_i \Delta V_i = \varphi_i \Big|_{T_{\beta=0}} \times E_\lambda \frac{\beta}{c_p \rho} \Big|_{T_{\beta>0}} \quad (2a)$$

$$\alpha_i = \varphi_i \Big|_{T_{\beta>0}} - \varphi_i \Big|_{T_{\beta=0}} \quad (2b)$$

The LIOAS signals of YtvA-WT and some of the mutants were best fitted by a two exponential decay function as previously described (Raffelberg et al. 2011). The unresolved step ( $\tau_1 < 20$  ns) is assigned to the formation of the flavin triplet state (subscript T). The short microsecond process ( $\tau_2 = 2$   $\mu$ s for YtvA-WT) corresponds to the triplet decay into the adduct (subscript DL). Energy balance considerations and the results of deconvolution directly provide the products  $\Phi_T E_T$  and  $\Phi_{DL} E_{DL}$  (eqn. 3a and 3b), referring to the quantum yield of formation for the triplet state and adduct, respectively, multiplied by the energy level of the two transient species: (Losi et al. 2003a)

$$\Phi_T \frac{E_T}{E_\lambda} = 1 - \alpha_1 - \Phi_F \frac{E_F}{E_\lambda} \quad (3a)$$

$$\alpha_2 = \Phi_T \frac{E_T}{E_\lambda} - \Phi_{DL} \frac{E_{DL}}{E_\lambda} \quad (3b)$$

where  $E_F$  is the average energy for the fluorescence emission (232 kJ/mol), and  $E_\lambda = 337$  kJ/mol is the photonic energy corresponding to  $\lambda_{ex} = 355$  nm excitation wavelength.

For detecting LIOAS signals originating from the dark-adapted state, we averaged 10 shots, stirring the sample to avoid appreciable accumulation of photoadduct. At the end of the experiments less than 5% of the sample was photoconverted, as proven by recording absorption spectra. For LIOAS signal from the light-adapted state, LED465 was placed on top of the cuvette, averaging then 100 shots.

#### *Quantum yield of triplet ( $\Phi_T$ ) and adduct ( $\Phi_{DL}$ ) formation*

The value of  $\Phi_T$  is readily calculated by means of eqn. 3a, given that the energy level of  $E_T =$  ca. 200 kJ/mol, as previously determined, (Losi et al. 2002; Gauden et al. 2004) and triplet state formation is always accessible to LIOAS. The determination of  $\Phi_{DL}$  is more critical, because in the case of long-lived transients, amplitudes and lifetimes are often correlated or not accessible to LIOAS. On the other hand, the necessity of single shot measurements in flash photolysis (due to the long photocycle) and the small signal amplitude for several mutated proteins give rise to a large error in the determination of  $\Phi_{DL}$  (Raffelberg et al. 2011). We thus determined the values of  $\Phi_{DL}$  by following the time course of fluorescence bleaching upon illumination of the cuvette from the top with LED356 and LED465, by comparison with the well-established values of 0.32 (this work and (Losi et al. 2013)) and 0.49 for YtvA-WT (Losi et al. 2002). In order to minimize photoconversion during fluorescence measurements samples were excited at 330 nm.

#### *Photoequilibrium and yield of photoinduced light-to-dark conversion ( $\Phi_{LD}$ )*

The methodology has been previously described (Losi et al. 2013). Briefly, two methods have been applied.



*i.* We define  $SO(YtvAD)$  and  $SO(YtvAL)$  as the spectral overlaps between the LED emission and the absorption spectra of the specified YtvAL and YtvAD variants. The value of  $\Phi_{LD}$  can thus be calculated under photostationary conditions (eq.4) , under the assumption that the thermal (dark) relaxation of YtvAL to YtvAD is much slower than the light-induced reactions at high photon density:

$$\Phi_{LD} = \frac{SO(YtvAD)[YtvAD]_{eq}}{SO(YtvAL)[YtvAL]_{eq}} \Phi_{DL} \quad (4)$$

where  $[YtvAL]_{eq}$  and  $[YtvAD]_{eq}$  are the concentrations of the two molecular species under photostationary conditions. These concentrations are determined from the absorption spectrum of the mixture, which can be described as linear combination of the pure YtvAL and YtvAD spectra under LED405 illumination.

*ii.* Reverse reaction yields were estimated also by following the kinetics of establishment of the photoequilibrium under steady state illumination. In these experiments, we monitored fluorescence emission at 500 nm under 330 nm excitation. Starting from an YtvAL solution, LED405 was switched on and the recovery of the fluorescence emission was followed. Saturation curves measured at different LED powers were analyzed using numerical solution of the rate equation (eq. 5). For details see supporting information of ref. (Losi et al. 2013).

$$\frac{d[YtvAD]}{dt} = \frac{P}{V} \ln 10 (-A_D \Phi_{DL} + A_L \Phi_{LD}) + k_{LD} ([YtvA_{tot}] - [YtvAD]) \quad (5)$$

where  $P$  is the light power,  $V$  is the illuminated volume,  $A_D$  and  $A_L$  are the absorbances at the excitation wavelength (405 nm) of YtvAD and YtvAL, respectively,  $k_{LD}$  is the rate constant for the reverse dark reaction and the concentration of YtvAD can be calculated with the knowledge that this is the only fluorescent state of the protein.

## **Acknowledgements**

S.R. is a recipient of a Ph.D. student grant from the "Biostruct" program of the Heinrich-Heine-University Düsseldorf. This work has been partially supported by the Vigoni programme (to A.L. and W.G.) and the University of Parma (fellowship to C.M.). We thank Francesca Pennacchietti for the solvatochromic data on FMN reported within the supplementary material.

## References

- Abbruzzetti S., Viappiani C., Murgida D. H., Erra-Balsells R., and Bilmes G. M. (1999). Non-toxic, water-soluble photocalorimetric reference compounds for UV and visible excitation. *Chem Phys.Lett.* 304, 167-172.
- Avila-Perez M., Hellingwerf K. J., and Kort R. (2006). Blue light activates the sigmaB-dependent stress response of *Bacillus subtilis* via YtvA. *J.Bacteriol.* 188, 6411-6414.
- Bauer C., Rabl C. R., Heberle J., and Kottke T. (2011). Indication for a Radical Intermediate Preceding the Signaling State in the LOV Domain Photocycle. *Photochem.Photobiol.* 87, 548-553.
- Briggs W. R. and Huala E. (1999). Blue-light photoreceptors in higher plants. *Ann.Rev.Cell.Develop.Biol.* 15, 33-62.
- Brosi R., Illarionov B., Mathes T., Fischer M., Joshi M., Bacher A., Hegemann P., Bittl R., Weber S., and Schleicher E. (2010). Hindered Rotation of a Cofactor Methyl Group as a Probe for Protein-Cofactor Interaction. *J.Am.Chem.Soc.* 132, 8935-8944.
- Cao Z., Livoti E., Losi A., and Gärtner W. (2010). A Blue Light-inducible Phosphodiesterase Activity in the Cyanobacterium *Synechococcus elongatus*. *Photochem.Photobiol.* 86, 606-611.
- Cao Z., Buttani V., Losi A., and Gärtner W. (2008). A blue light inducible two component signal transduction system in the plant pathogen *Pseudomonas syringae* pv. *tomato*. *Biophys.J.* 94, 897-905.
- Chan R. H., Lewis J. W., and Bogomolni R. A. (2013). Photocycle of the LOV-STAS Protein from the Pathogen *Listeria monocytogenes*. *Photochem Photobiol.* 89, 361-369
- Christie J. M., Salomon M., Nozue K., Wada M., and Briggs W. R. (1999). LOV (light, oxygen, or voltage) domains of the blue-light photoreceptor phototropin (nph1): binding sites for the chromophore flavin mononucleotide. *Proc. Natl. Acad Sci.USA* 96, 8779-8783.
- Climent T., Gonzalez-Luque R., Merchan M., and Serrano-Andres L. (2006). Theoretical Insight into the Spectroscopy and Photochemistry of Isoalloxazine, the Flavin Core Ring. *J. Phys. Chem. A* 110, 13584-13590.
- Djouani-Tahri E. B., Christie J. M., Sanchez-Ferandin S., Sanchez F., Bouget F. Y., and Corellou F. (2011). A eukaryotic LOV-histidine kinase with circadian clock function in the picoalga *Ostreococcus*. *Plant J.* 65, 578-588.

- Fedorov R., Schlichting I., Hartmann E., Domratcheva T., Fuhrmann M., and Hegemann P. (2003). Crystal structures and molecular mechanism of a light-induced signaling switch: the Phot-LOV1 domain from *Chlamydomonas reinhardtii*. *Biophys.J.* 84, 2492-2501.
- Gaidenko T. A., Kim T. J., Weigel A. L., Brody M. S., and Price C. W. (2006). The blue-light receptor YtvA acts in the environmental stress signaling pathway of *Bacillus subtilis*. *J.Bacteriol.* 188, 6387-6395.
- Gauden M., Crosson S., van Stokkum I. H. M., van Grondelle R., Moffat K. & Kennis J. T. M. 2004. Low-temperature and time-resolved spectroscopic characterization of the LOV2 domain of Avena sativa phototropin. In Avrielleir S. and Tualle J. M. eds. Femtosecond Laser Applications in Biology, pp. 97-104. SPIE Bellingham, WA5463.
- Hendrischk A. K., Moldt J., Fruhwirth S. W., and Klug G. (2009). Characterization of an Unusual LOV Domain Protein in the alpha-Proteobacterium *Rhodobacter sphaeroides*. *Photochem. Photobiol.* 85, 1254-1259.
- Holzer W., Penzkofer A., Susdorf T., Alvarez M., Islam S., and Hegemann P. (2004). Absorption and emission spectroscopic characterisation of the LOV2-domain of phot from *Chlamydomonas reinhardtii* fused to a maltose binding protein. *Chem.Phys.* 302, 105-118.
- Islam S. D. M., Penzkofer A., and Hegemann P. (2003). Quantum yield of triplet formation of riboflavin in aqueous solution and of flavin mononucleotide bound to the LOV1 domain of Phot1 from *Chlamydomonas reinhardtii*. *Chem.Phys.* 291, 97-114.
- Iwata T., Nozaki D., Tokutomi S., and Kandori H. (2005). Comparative Investigation of the LOV1 and LOV2 Domains in *Adiantum* Phytochrome3. *Biochemistry* 44, 7427-7434.
- Jentsch K., Wirtz A., Circolone F., Drepper T., Losi A., Gärtner W., Jaeger K.-E., and Krauss U. (2009). Mutual Exchange of Kinetic Properties by Extended Mutagenesis in Two Short LOV Domain Proteins from *Pseudomonas putida*. *Biochemistry* 48, 10321-10333.
- Johansson L. B., Davidsson A., Lindblom G., and Naqvi K. R. (1979). Electronic transitions in the isoalloxazine ring and orientation of flavins in model membranes studied by polarized light spectroscopy. *Biochemistry* 18, 4249-4253.
- Kasahara M., Swartz T. E., Olney M. A., Onodera A., Mochizuki N., Fukuzawa H., Asamizu E., Tabata S., Kanegae H., Takano M., Christie J. M., Nagatani A., and Briggs W. R. (2002). Photochemical properties of the flavin mononucleotide-binding domains of the phototropins from Arabidopsis, rice, and *Chlamydomonas reinhardtii*. *Plant Physiol.* 129, 762-773.

- Kennis J. T. M., van Stokkum I. H. M., Crosson S., Gauden M., Moffat K., and van Grondelle R. (2004). The LOV2 domain of phototropin: a reversible photochromic switch. *J.Am.Chem.Soc.* 126, 4512-4513.
- Kottke T., Heberle J., Dominic Hehn, Dick B., and Hegemann P. (2003). Phot-LOV1: Photocycle of a Blue-Light Receptor Domain from the Green Alga *Chlamydomonas reinhardtii*. *Biophys.J.* 84, 1192-1201.
- Krauss U., Losi A., Gärtner W., Jaeger K.-E., and Eggert T. (2005). Initial characterization of a blue-light sensing, phototropin-related protein from *Pseudomonas putida*: a paradigm for an extended LOV construct. *Phys.Chem.Chem.Phys.* 7, 2229-2236.
- Losi A. and Braslavsky S. E. (2003a). The time-resolved thermodynamics of the chromophore-protein interactions in biological photosensors. Learning from photothermal measurements. *Phys.Chem.Chem.Phys.* 5, 2739-2750.
- Losi A. and Gärtner W. (2011). Old Chromophores, New Photoactivation Paradigms, Trendy Applications: Flavins in Blue Light-Sensing Photoreceptors. *Photochem.Photobiol.* 87, 491-510.
- Losi A. and Gärtner W. (2012). The Evolution of Flavin-Binding Photoreceptors: An Ancient Chromophore Serving Trendy Blue-Light Sensors. *Annu.Rev.Plant Biol.* 63, 49-72.
- Losi A., Polverini E., Quest B., and Gärtner W. (2002). First evidence for phototropin-related blue-light receptors in prokaryotes. *Biophys.J.* 82, 2627-2634.
- Losi A., Quest B., and Gärtner W. (2003b). Listening to the blue: the time-resolved thermodynamics of the bacterial blue-light receptor YtvA and its isolated LOV domain. *Photochem.Photobiol.Sci.* 2, 759-766.
- Losi A., Wegener A. A., Engelhardt M., and Braslavsky S. E. (2001). Enthalpy-entropy compensation in a photocycle: The K to L transition in sensory rhodopsin II from *Natronobacterium pharaonis*. *J.Am.Chem.Soc.* 123, 1766-1767.
- Losi A. (2007). Flavin-based Blue-light Photosensors: a Photobiophysics Update. *Photochem.Photobiol.* 83, 1283-1300.
- Losi A., Gärtner W., Raffelberg S., Cella Zanacchi F., Bianchini P., Diaspro A., Mandalari C., Abbruzzetti S., and Viappiani C. (2013). A photochromic bacterial photoreceptor with potential for super-resolution microscopy. *Photochem.Photobiol.Sci.* 12, 231-235.
- Losi A., Kottke T., and Hegemann P. (2004). Recording of Blue Light-Induced Energy and Volume Changes within the Wild-Type and Mutated Phot-LOV1 Domain from *Chlamydomonas reinhardtii*. *Biophys.J.* 86, 1051-1060.

- Malkin S., Churio M. S., Shochat S., and Braslavsky S. E. (1994). Photochemical energy storage and volume changes in the microsecond time range in bacterial photosynthesis - a laser induced optoacoustic study. *J.Photochem.Photobiol.B: Biol.* 23, 79-85.
- Mandalari C., Losi A., and Gärtner W. (2013). Distance-tree analysis, distribution and co-presence of bilin- and flavin-binding prokaryotic photoreceptors for visible light. *Photochem.Photobiol.Sci.* in press, DOI: 10.1039/c3pp25404f.
- Möglich A., Ayers R. A., and Moffat K. (2009). Structure and Signaling Mechanism of Per-ARNT-Sim Domains. *Structure* 17, 1282-1294.
- Narikawa R., Zikihara K., Okajima K., Ochiai Y., Katayama M., Shichida Y., Tokutomi S., and Ikeuchi M. (2006). Three Putative Photosensory Light, Oxygen or Voltage (LOV) Domains with Distinct Biochemical Properties from the Filamentous Cyanobacterium *Anabaena* sp. PCC 7120. *Photochem.Photobiol.* 82, 1627-1633.
- Nash A. I., McNulty R., Shillito M. E., Swartz T. E., Bogomolni R. A., Luecke H., and Gardner K. H. (2011). Structural basis of photosensitivity in a bacterial light-oxygen-voltage/helix-turn-helix (LOV-HTH) DNA-binding protein. *Proc. Natl. Acad. Sci.USA.*
- Onodera A., Christie J. M., Kasahara M., Mochizuki N., Asamizu E., Tabata S., Fukuzawa H., Briggs W. R., and Nagatani A. (2002). Analysis of phototropin-like gene of *Chlamydomonas reinhardtii*. *Plant & Cell Physiol.* 43, S230.
- Penzkofer A., Bansal A. K., Song S. H., and Dick B. (2007). Fluorescence quenching of flavins by reductive agents. *Chem.Phys.* 336, 14-21.
- Penzkofer A., Endres L., Schiereis T., and Hegemann P. (2005). Yield of photo-adduct formation of LOV domains from *Chlamydomonas reinhardtii* by picosecond laser excitation. *Chem.Phys.* 316, 185-194.
- Purcell E. B., McDonald C. A., Palfey B. A., and Crosson S. (2010). An Analysis of the Solution Structure and Signaling Mechanism of LovK, a Sensor Histidine Kinase Integrating Light and Redox Signals. *Biochemistry* 49, 6761-6770.
- Raffelberg S., Mansurova M., Gärtner W., and Losi A. (2011). Modulation of the photocycle of a LOV domain photoreceptor by the hydrogen bonding network. *J.Am.Chem.Soc.* 133, 5346-5356.
- Rudzki J. E., Goodman J. L., and Peters K. S. (1985). Simultaneous determination of photoreaction dynamics and energetics using pulsed, time resolved photoacoustic calorimetry. *J.Am.Chem.Soc.* 107, 7849-7854.
- Rudzki-Small J., Libertini L. J., and Small E. W. (1992). Analysis of photoacoustic waveforms using the nonlinear least square method. *Biophys.Chem.* 41, 29-48.

Salomon M., Christie J. M., Knieb E., Lempert U., and Briggs W. R. (2000). Photochemical and mutational analysis of the FMN-binding domains of the plant blue light receptor phototropin. *Biochemistry* 39, 9401-9410.

Salzmann S., Tatchen J., and Marian C. M. (2008). The photophysics of flavins: What makes the difference between gas phase and aqueous solution? *J.Photochem.Photobiol.A: Chem.* 198, 221-231.

Sato Y., Nabeno M., Iwata T., Tokutomi S., Sakurai M., and Kandori H. (2007). Heterogeneous Environment of the SH Group of Cys966 near the Flavin Chromophore in the LOV2 Domain of Adiantum Neochrome1. *Biochemistry* 46, 10258-10265.

Schwerdtfeger C. and Linden H. (2003). VIVID is a flavoprotein and serves as a fungal blue light photoreceptor for photoadaptation. *EMBO J.* 22, 4846-4855.

Song S. H., Freddolino P. L., Nash A. I., Carroll E. C., Schulten K., Gardner K. H., and Larsen D. S. (2011). Modulating LOV Domain Photodynamics with a Residue Alteration outside the Chromophore Binding Site. *Biochemistry* 50, 2411-2423.

Swartz T. E., Corchnoy S. B., Christie J. M., Lewis J. W., Szundi I., Briggs W. R., and Bogomolni R. A. (2001). The photocycle of a flavin-binding domain of the blue light photoreceptor phototropin. *J.Biol.Chem.* 276, 36493-36500.

Swartz T. E., Tseng T. S., Frederickson M. A., Paris G., Commerci D. J., Rajashekara G., Kim J. G., Mudgett M. B., Splitter G. A., Ugalde R. A., Goldbaum F. A., Briggs W. R., and Bogomolni R. A. (2007). Blue-Light-Activated Histidine Kinases: Two-Component Sensors in Bacteria. *Science* 317, 1090-1093.

Tang Y., Cao Z., Livoti E., Krauss U., Jaeger K.-E., Gärtner W., and Losi A. (2010). Interdomain signalling in the blue-light sensing and GTP-binding protein YtvA: a mutagenesis study uncovering the importance of specific protein sites. *Photochem.Photobiol.Sci.* 9, 47-56.

Tsentelovich, Y. P., Lopez, J. J., Hore, P. J., and Sagdeev, R. Z. Mechanisms of reactions of flavin mononucleotide triplet with aromatic amino acids. *Spectrochim.Acta A* 58[9], 2043-2050. 2002.  
Ref Type: Abstract

van den Berg P. W., Widengren J., Hink M. A., Rigler R., and Visser A. G. (2001). Fluorescence correlation spectroscopy of flavins and flavoenzymes: photochemical and photophysical aspects. *Spectrochim.Acta A* 57, 2135-2144.

Walter J., Hausmann S., Drepper T., Puls M., Eggert T., and Dihné M. (2012). Flavin Mononucleotide-Based Fluorescent Proteins Function in Mammalian Cells without Oxygen Requirement. *Plos One* 7, e43921.



Zoltowski B. D., Schwerdtfeger C., Widom J., Loros J. J., Bilwes A. M., Dunlap J. C., and Crane B. R. (2007). Conformational switching in the fungal light sensor Vivid. *Science* 316, 1054-1057.

Zoltowski B. D., Vaccaro B., and Crane B. R. (2009). Mechanism-based tuning of a LOV domain photoreceptor. *Nat.Chem.Biol.* 5, 827-834.

### **3. Structure of the blue light photoreceptor YtvA**

#### **3.1 A structural model for the full-length blue light-sensing protein YtvA from *Bacillus subtilis*, based on EPR spectroscopy**

Accepted. Journal of Photochemical. Photobiological. Science, 2.9, 2. author

Sample generation and preparation: 100 %

Cite this: DOI: 10.1039/c3pp50128k

**A structural model for the full-length blue light-sensing protein YtvA from *Bacillus subtilis*, based on EPR spectroscopy†**Christopher Engelhard,<sup>a</sup> Sarah Raffelberg,<sup>b</sup> Yifen Tang,<sup>b</sup> Ralph P. Diensthuber,<sup>c</sup> Andreas Möglich,<sup>c</sup> Aba Losi,<sup>d</sup> Wolfgang Gärtner<sup>b</sup> and Robert Bittl<sup>\*a</sup>

A model for the full-length structure of the blue light-sensing protein YtvA from *Bacillus subtilis* has been determined by EPR spectroscopy, performed on spin labels selectively inserted at amino acid positions 54, 80, 117 and 179. Our data indicate that YtvA forms a dimer in solution and enable us, based on the known structures of the individual domains and modelling, to propose a three-dimensional model for the full length protein. Most importantly, this includes the YtvA N-terminus that has so far not been identified in any structural model. We show that our data are in agreement with the crystal structure of an engineered LOV-domain protein, YF1, that shows the N-terminus of the protein to be helical and to fold back in between the  $\beta$ -sheets of the two LOV domains, and argue for an identical arrangement in YtvA. While we could not detect any structural changes upon blue-light activation of the protein, this structural model now forms an ideal basis for identifying residues as targets for further spin labelling studies to detect potential conformational changes upon irradiation of the protein.

Received 26th April 2013,  
Accepted 9th July 2013

DOI: 10.1039/c3pp50128k

www.rsc.org/ppps

**Introduction**

In recent years, biological photoreceptors have gained remarkable scientific interest, as in many of these proteins the signalling part is an enzyme activity,<sup>1</sup> which, in connection with the light sensing domain, suggests regulation of the specific enzyme activity by light irradiation.<sup>2</sup> Among the broad variety of photoreceptors, the blue light-sensing proteins are of particular interest, as (i) their flavin chromophore is endogenous in all living organisms, and (ii) one subclass of these receptors, the LOV domain-proteins (LOV, Light, Oxygen and Voltage), shows a robust three-dimensional structure and yet a broad variety of naturally occurring signalling domains.<sup>3</sup> The first prokaryotic LOV domain protein discovered was YtvA from *Bacillus subtilis*, a photoreceptor involved in the stress response of this bacterium.<sup>4–6</sup> YtvA is a relatively small protein of only 261 amino acids and is composed of two domains, the

light-sensing LOV domain and a putative signalling STAS domain (STAS, Sulfate Transporter and Anti-Sigma antagonist), both domains being connected by a short helical linker. Despite intensive research into the structure and the function of YtvA,<sup>7–11</sup> structural information on the full-length protein is still limited.<sup>6,8,12</sup>

Detailed structural knowledge is clearly required, as information on a monomeric or dimeric state or on the domain arrangement of these receptors is essential for an understanding of their biological function. Relatively few spectroscopic techniques can be applied to proteins in solution for structural elucidation. Among these, Electron Paramagnetic Resonance (EPR) spectroscopy offers a number of advantages, as it is applicable for determining inter-protein distances over a wide range, and in addition, it provides information on the dynamics and flexibility of proteins<sup>13,14</sup> as well. For applying EPR methods, spin labels often have to be introduced into the proteins under investigation which is best accomplished *via* covalent attachment of nitrogen-oxide substituents, carrying one unpaired electron.<sup>15–17</sup> These label compounds selectively react with the side chain of cysteines and can be inserted selectively at single positions to probe, *e.g.*, the oligomeric state of a protein, or can be applied as couples, thus providing information on distances within one domain or one protein entity. For these approaches, cysteines are first removed from “unwanted” positions (by mutation into serines or alanines) and are inserted at the desired positions, always keeping in

<sup>a</sup>Freie Universität Berlin, Fachbereich Physik, Arnimallee 14, 14195 Berlin, Germany. E-mail: robert.bittl@fu-berlin.de; Fax: +49 (30) 838-56046; Tel: +49 (30) 838-56049

<sup>b</sup>Max-Planck-Institute for Chemical Energy Conversion, Stiftstr. 34-36, 45470 Mülheim, Germany

<sup>c</sup>Humboldt Universität zu Berlin, Institut für Biologie, Biophysikalische Chemie, Invalidenstr. 42, 10115 Berlin, Germany

<sup>d</sup>University of Parma, Department of Physics and Earth Sciences, Viale G.P. Usberti n. 7/A (Parco delle Scienze), 43124 Parma, Italy

†Electronic supplementary information (ESI) available. See DOI: 10.1039/c3pp50128k

mind to verify the functional integrity of the mutated proteins. We report here on the insertion of spin label compounds into several sites of the LOV and STAS domains of YtvA, providing information on the oligomeric state of this protein and also proposing a structural model for the full-length protein, as derived from intra- and intermolecular distances.

## Results

### Labelling strategy and efficiency

Labelling positions were chosen not only to determine the oligomeric state of YtvA but also to enable us to determine, based on the known crystal or homology structures for the LOV and STAS domains, the conformation of the domains within one monomer as well as the binding geometry of a potential dimer. To this end, in addition to two singly labelled mutants, several variants that were simultaneously labelled in both domains were produced. Five mutants were generated for this study, two singly labelled mutants (T117C and T179C – in all cases, the nomenclature such as T179C indicates a side chain substituted by a spin-labelled cysteine) and two doubly labelled mutants (T80C/T179C and T54C/T179C) as well as one mutant with inhibited cysteinyl-C4a-adduct formation (C62A). The positions of these sites are shown in Fig. 1. The spin label yield attached to the mutagenesis-inserted cysteine residues was determined for all five constructs and was found to be greater than 95%. Also, the extent of flavin chromophore incorporation was determined and found in all cases to be greater than 90%. A control for the photochemical properties of all mutations revealed no change caused by the mutations and the spin-labelling, including, crucially, the formation of the cysteinyl-C4a-adduct.

### cw-EPR

cw-EPR experiments on various labelled mutants were carried out at ambient temperature  $T \approx 295$  K in order to detect the mobility of the protein-bound labels and thereby investigate the immediate surroundings of the spin labels (Fig. 2).<sup>17,18</sup> Even though great care was taken to keep the sample treatment constant, a variable small amount of remaining free spin label

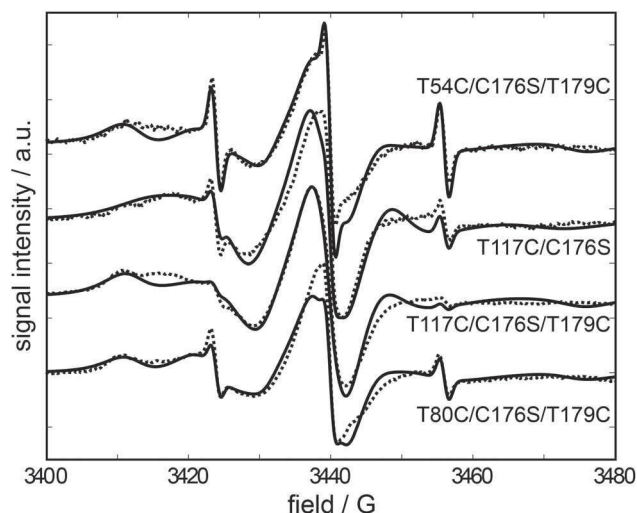


**Fig. 2** X-band cw-spectra recorded at room temperature of the investigated mutants (solid lines) with simulations (dotted lines). The differences in label mobility are clearly visible from the moving pattern of peaks between 3405 G and 3430 G.

after washing is inevitable. Since the free spin label signal is very narrow, even a small contribution of free label gives rise to a large cw-EPR signal compared to the broad signal of protein-attached label. This leads to the prominent signal triplet at 3424 G, 3440 G, and 3456 G with varying intensity between samples.

The protein-bound spin labels show complex spectra with marked differences between the individual samples in the low-field part of the spectrum between 3400 G to 3430 G, indicative of strong differences in mobility between the different labels. While the spectra of all samples show a broad background in this region, implying a distribution of label mobility, signals corresponding to dominant components could be identified by comparing the spectra of the different variants. The three mutants YtvA T80C/C176S/T179C, YtvA T54C/C176S/T179C, and YtvA T117C/C176S/T179C all yield a low field peak at 3411 G, indicative of a slowly tumbling spin label. Such behaviour is not seen for YtvA T117C/C176S. This mutant, instead, shows a clear signal at 3417 G (also present, slightly shifted to lower fields, in YtvA T117C/C176S/T179C). YtvA T80C/C176S/T179C and YtvA T54C/C176S/T179C exhibit one additional peak at 3421 G and 3425 G, respectively. Especially in the case of YtvA T54C/C176S/T179C, this signal partially merges with the signal arising from the free spin label, indicating a high degree of mobility for these labels.

The observed peak patterns allow assignment of the peak at 3411 G to the label at T179C, the signal at 3417 G to T117C and the peaks at 3421 G and 3425 G to T80C and T54C, respectively. The varying peak patterns are indicative of different mobilities of the respective labels. Using simulations performed in Easyspin<sup>19</sup> approximate rotational correlation times indicative of the mobilities were determined. As expected, the mobilities of the labels vary strongly, with the labels at T54C, T80C, and T117C being fairly mobile while the

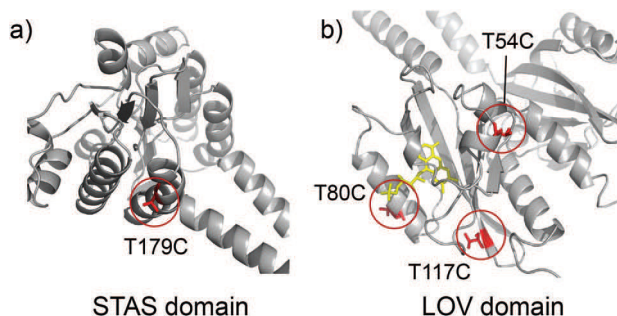


**Fig. 1** Structure of the YtvA STAS (a) and LOV (b) domains with the position of the spin-labelled sites highlighted in red. The flavin cofactor, converted into the radical form in the C62A mutant, is shown in yellow.

label at T179C is apparently almost completely immobilised by the protein backbone.

### Phase memory time measurements

To further evaluate the influence of the protein backbone on the spin labels at different positions, spin relaxation experiments at low temperatures were performed to determine the phase memory time.<sup>20</sup> For these experiments the samples were reconstituted in a fully deuterated buffer–glycerol mixture (50% v/v) in order to minimise the effects on the spin relaxation arising purely from the solvent. The spectra shown in Fig. 3 were recorded at 70 K.

All spectra show strong nuclear modulations of the intensity over time, due to coupling of the electron spin to nearby deuterium nuclei, rendering the fitting of an exponential decay to the data difficult. However, this modulation is proportional to  $1 - \sin^2(t)$ , *i.e.*, it always represents a signal loss, meaning that the fit of echo decay can be extended to the region of strong modulations by selecting only the points of maximum intensity for the fit procedure. Accordingly, an automatic peak detection algorithm was employed that yielded the

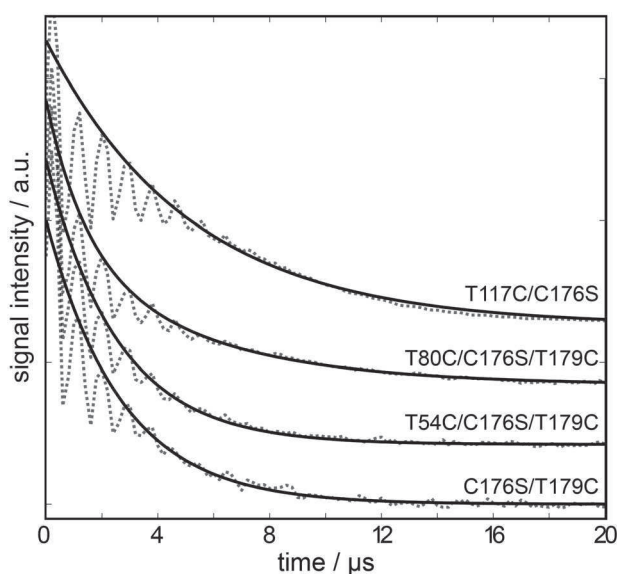


**Fig. 3** Relaxation measurements performed at 70 K (solid) with fitted exponential decays (dotted). Both YtvA T54C/C176S/T179C and YtvA C176S/T179C reveal a much faster relaxation compared to YtvA T117C/C176S. The trace for YtvA T80C/C176S/T179C required a bi-exponential fit and consists of one fast component associated with the label at T179C and one slow component with relaxation times similar to the label at T117C. The resulting relaxation times are given in Table 1.

**Table 1** Relaxation times of the investigated labels, measured at 70K

Sample	Relaxation time $T_M/\mu\text{s}$
T54C–T179C	1.27
T80C/T179C	0.69/2.53
T117C	2.59
T179C	1.34

relaxation times (Table 1). Both doubly labelled mutants, T80C/C176S/T179C and T54C/C176S/T179C, could be fitted using a double exponential; however, only for T80C/C176S/T179C two distinct components could be identified. For YtvA T117C/C176S and YtvA C176S/T179C a single exponential provided a good fit of the simulation to the data, implying that at least from the perspective of the immediate label surroundings, only one conformation of YtvA is present.

While relaxation times in protonated buffer are more or less uniform for all samples (data not shown), the  $T_M$  relaxation time in deuterated buffer varies strongly from sample to sample. Both YtvA T54C/C176S/T179C and YtvA C176S/T179C show a very fast relaxation of *ca.*  $T_M = 1.34 \mu\text{s}$ , while the relaxation of YtvA T117C/C176S is very slow ( $T_M = 2.59 \mu\text{s}$ ). Thus the spin labels attached to T54C and T179C are fast relaxing, pointing to a strong interaction with either protons in the protein backbone or the electron spin of another spin label close by. The label at T117C relaxes slowly, indicating that it is strongly exposed to the solvent and neither in close proximity to the protein backbone nor to other labels.

The *cw*-EPR data revealed that the spin label at T179C is strongly immobilised by (and thus in close proximity to) the protein backbone. This conclusion is corroborated by the short phase memory time. Since the spin label at T54C shows a similarly short phase memory time as T179C in spite of its high degree of mobility, it can neither be strongly exposed to the solvent nor immobilised by the backbone. We therefore conclude that the spin label is either located in close proximity to a second label or attached to the protein in a location that, while still allowing for a high degree of mobility, restricts the conformational space mainly to orientations on or close to the surface of the protein. Results from the simulation of the spin label bound to crystal structures support the latter conclusion (see the discussion below).

In the case of YtvA T80C/C176S/T179C, a biexponential decay is clearly visible in the time trace, indicative of significantly different  $T_M$  relaxation times for the two different labels. The biexponential fit of the data yields time constants of  $T_M = 2.53 \mu\text{s}$  and  $T_M = 0.69 \mu\text{s}$  for the slow and the fast component, respectively. The fast component has a shorter  $T_M$  than the value of  $T_M = 1.34 \mu\text{s}$  expected for the label at T179C in this mutant; however, this discrepancy is probably due to the fact that the strong nuclear modulation leaves very few significant data points in the first part of the time trace where a fast-relaxing component is most apparent. The relaxation time of the slow components places the label at T80C in a similar surrounding as the one at T117C.

### Distance measurements

Two pulsed EPR methods at cryogenic temperatures were used to determine the distances between the introduced labels: (i) field swept echo (FSE) experiments to detect short label distances below 2 nm *via* the dipolar broadening of the spectrum and (ii) 4-pulse ELDOR<sup>21</sup> to directly detect dipolar couplings for longer distances that do not result in spectral broadening.



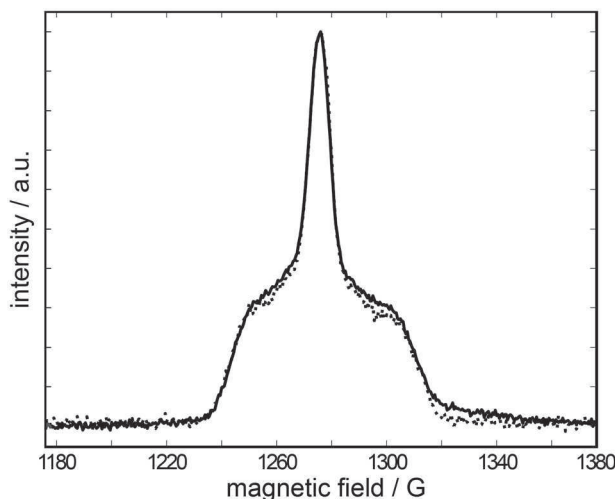


**Fig. 4** S-band FSE spectrum of YtvA T54C/C176S/T179C (solid line) and YtvA T117C/C176S (dashed line) at 80 K. The spectrum of YtvA T117C/C176S is unbroadened with respect to an isolated spin label spectrum (not shown). YtvA T54C/C176S/T179C shows slight differences when compared to T117C/C176S, but no clear dipolar broadening.

### Dipolar broadening in field swept echo spectra

FSE experiments were performed at the S-band to minimise the effects of  $g$  anisotropy. Of the investigated samples, only YtvA T54C/C176S/T179C showed a very small deviation from an isolated spin label spectrum (Fig. 4). The effect is too small to indicate significant dipolar broadening. Our data therefore strongly suggest that there are no distances  $<2$  nm present in the investigated samples.

### ELDOR measurements

To detect larger distances in the 2–8 nm range, 4-pulse ELDOR experiments at 70 K were performed (Fig. 5). For a singly labelled sample an exponential signal decay would be expected; however, in both samples, YtvA T117C/C176S and YtvA C176S/T179C, a distinct modulation with a period of  $t_{117} = 1.32 \mu\text{s}$  and  $t_{179} = 2.21 \mu\text{s}$ , respectively, was observed, proving conclusively that YtvA is not monomeric (Fig. 5a) under the measurement conditions. Modelling the data in DeerAnalysis, the time traces of both YtvA T117C/C176S and YtvA C176S/T179C result in a distinct, narrow distance distribution centred at  $d_{117} = 4.13$  nm and  $d_{179} = 4.87$  nm, respectively (Fig. 5b). The observation of a single narrow distance distribution in each of these two samples proves that YtvA is present as a dimer. The narrow distance distribution further indicates that the dimerisation is not the result of unordered or weakly ordered aggregation, but rather demonstrates the existence of a highly ordered dimerisation.

The spectra of the double mutants YtvA T80C/C176S/T179C and YtvA T54C/C176S/T179C show less pronounced modulations indicating that the distance distributions of these labels are broader compared to those of YtvA T117C/C176S and YtvA C176S/T179C. This, however, could partly be due to the dimeric nature of YtvA: since there are now four labels

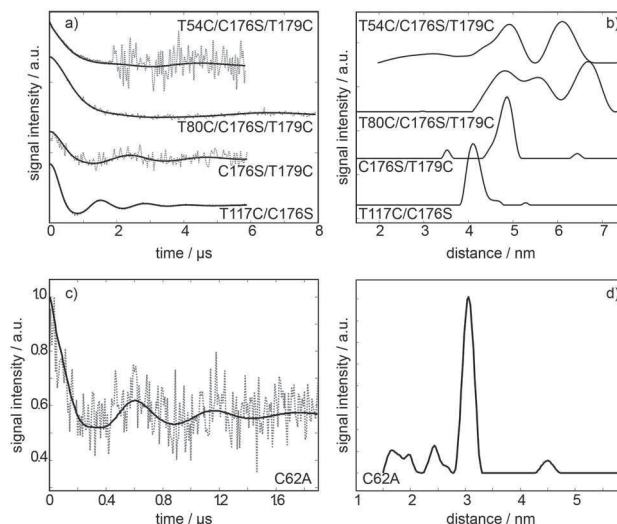


**Fig. 5** (a) Background-corrected DEER spectra of spin-labelled samples recorded at 70 K (dotted lines) and DeerAnalysis fits (solid lines) and (b) inter-spin distance distributions calculated from fit in (a). (c) Background corrected DEER spectrum of the flavin radical in C62A recorded at 160 K (dotted) and fitted time trace (solid), and (d) inter-spin distance distribution calculated from the fit in (c). For YtvA T54C/C176S/T179C a composite time trace derived from measurements with 2  $\mu\text{s}$  and 6  $\mu\text{s}$  is shown. Both the labels at T117C and T179C reveal a clearly defined modulation (a, lower two datasets) corresponding to a very narrow distance distribution (b, lower two distributions).

present in the YtvA dimer, this yields six possible label pairs, each with a corresponding distance distribution.

The distance distribution of YtvA T80C/C176S/T179C shows three different broad distance peaks, centred at  $d = 4.8$  nm, 5.6 nm and 6.7 nm. The shortest distance is identical with the one identified as the T179C–T179C distance; however, since this peak is much broader than the one detected in YtvA C176S/T179C, it is likely that there are other contributions in this distance range as well.

The fast  $T_M$  relaxation of YtvA T54C/C176S/T179C greatly reduces the signal-to-noise ratio that could be achieved in long time traces for this sample. To be able to reliably detect small distances, a combined spectrum consisting of two 4-pulse DEER measurements, one with a 2  $\mu\text{s}$  time trace and one with a 6  $\mu\text{s}$  time trace, was used (Fig. 5). In this combined dataset, the signal-to-noise ratio of the first part of the time trace allowed a clear identification of a short distance at about 3 nm. Despite the use of combined spectra, large regularisation parameters were still necessary to ensure that no artefacts were introduced by the noisy second half of the time trace. Due to the limited length of the time trace, the shape of the largest-distance peak at approximately 6 nm could not reliably be interpreted.

The possibility of ELDOR distance measurements between flavin radicals has been demonstrated previously.<sup>22</sup> Here we successfully used this method on the flavin radical in the radical-forming mutant C62A.<sup>23</sup> While the long  $T_1$  and comparatively short  $T_M$  of this radical species limited the length of the recordable time trace, a clear modulation corresponding to

a narrow distance distribution centred around 3.1 nm could be detected (Fig. 5c and d). The narrow distance distribution again corroborates the very specific dimer structure deduced from the spin-labelled variants above.

## Discussion

While a previous study, using gel filtration chromatography, found that only the isolated YtvA LOV domain forms a dimer, whereas the full-length protein mainly appears in a monomeric form,<sup>12</sup> other studies have indicated that YtvA is mostly dimeric in solution.<sup>6,8,24</sup> By determining spin label distances and measurements of phase relaxation times, we present here evidence that not only supports the latter proposal, but more importantly allows us to provide quantitative information about the dimer conformation.

To better relate our data to the structural information available, domain structures with attached spin labels were created using MMM<sup>25</sup> and mtsslWizard.<sup>26</sup> The results from both programs as well as insights into the label's mobility and surroundings obtained by *cw*- and pulsed EPR allow us to validate the simulation of the label's conformational space with respect to the structure. Results from both simulation methods were mostly compatible, with the exception of the simulations for the label at T179C. Simulations shown here are derived from MMM unless otherwise noted.

### Validation of the YtvA-LOV crystal structure

A LOV-LOV model for YtvA where the domains associate *via* their  $\beta$ -sheets has been previously proposed.<sup>6–8</sup> In a new crystal structure of the hybrid protein YF1, a protein combining the *B. subtilis* YtvA LOV domain with the histidine kinase domain of *Bradyrhizobium japonicum* FixL,<sup>27,28</sup> the two N-terminal helices of the dimer are folded back into the space between the  $\beta$ -sheets, while retaining the overall LOV-LOV orientation, an arrangement that had been previously suggested for a similar YtvA protein from *Bacillus amyloliquefaciens*<sup>29</sup> as well as for a different LOV protein from *Pseudomonas putida*.<sup>30</sup> When using this crystal structure as a basis for our model, calculating the distance distribution for the labels attached to T117C results in excellent agreement with the measured data (Fig. 6).

The distance between the two flavin cofactors in the dimer was calculated using the atoms with the largest spin density, *i.e.* N5 and C4a, in the YF1 structure,<sup>28</sup> resulting in flavin-flavin distances between 2.9 nm and 3.1 nm, which again are in excellent agreement with our measured data (Fig. 5c and d). Interpretation of the distance measurements from YtvA T80C/C176S/T179C and YtvA T54C/C176S/T179C are only possible in light of the structural model for the full-length protein. The fast relaxation and high mobility of the spin label at T54 requires that this spin label is located either in close proximity to another spin label or bound to the protein in such a way that allows for comparatively free movement of the label, while keeping most conformations close to the protein surface to explain the rapid spin relaxation. Looking at the label

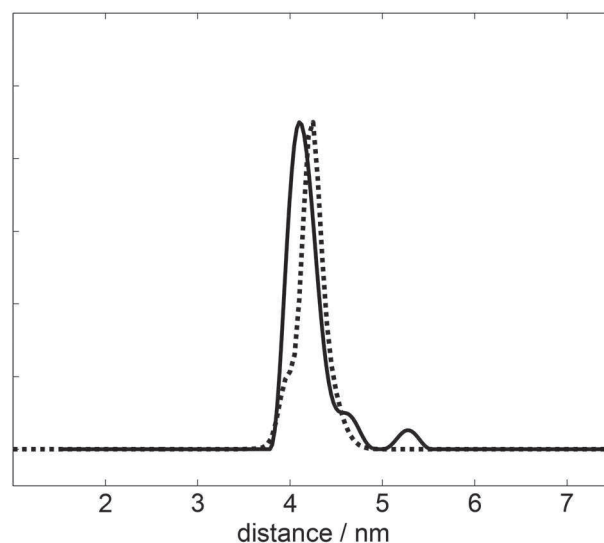


**Fig. 6** MMM distance simulations for the label at T117C based on the YF1 crystal structure (dashed) compared to the experimental result (solid). The very good agreement indicates that, in solution, the LOV domains in YtvA adopt the same conformation.

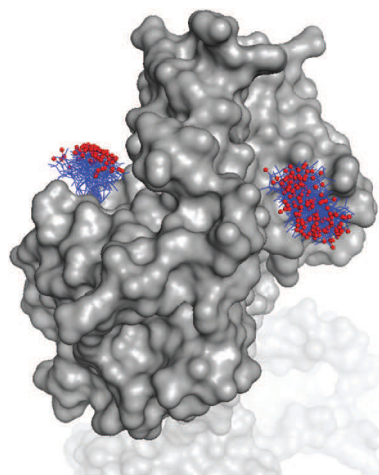


**Fig. 7** Simulated spin label at T54 in the YF1 crystal structure. Shown are the various conformations the spin label can adopt. It can be seen that the label, while mobile, is flanked by the protein, bringing it into close contact with protein protons and thus reducing its relaxation times.

conformations produced by MtsslWizard (Fig. 7), it is obvious that the latter is the case: while the simulation shows a broad, continuous distribution of conformers allowing for a high degree of spin label flexibility, most of the resulting conformations show a close proximity between nitroxide and the protein surface. The alternative, two labels in close proximity, is additionally excluded by the FSE and pELDOR data, neither of which show any indication of small distances between labels.

In summary, neither the distance observed between the spin labels at T117C and between the flavin radicals, nor the observed behaviour of the spin labels attached at T54C is compatible with an LOV-LOV arrangement without the N-terminal



helices folded back between the domains, while all are in excellent agreement with the YF1 crystal structure.<sup>28</sup> This indicates that the LOV domains of YtvA in solution form a dimer as shown for YF1<sup>28</sup> as well as for the LOV domain dimer of *B. amyloliquefaciens* YtvA.<sup>29</sup>

Based on this LOV–LOV conformation we can now derive from our data a model for the STAS–STAS interaction and the structure of the full-length protein.

### The STAS–STAS interface and a model for the full-length structure

MMM simulation of the label at T179C yielded a relatively flexible label with a large conformational space that would result in broad distance distributions (the spin label, when simulated in MtsslWizard, was both far less flexible and more narrowly distributed), while we know from *cw* experiments that this label is in fact highly *immobile*. This discrepancy is most likely due to the fact that the only available structural information for the STAS domain is a homology model. Similar calculations of the spin label conformational space in known STAS domain structures from *B. subtilis* SpoIIAA<sup>31</sup> and *Moor-ella thermoacetica*<sup>32</sup> confirm the susceptibility of the MMM results for this label to small changes in protein structure. Since MtsslWizard and MMM use different methods for calculating allowed conformations (sampling of the conformational space in the case of MtsslWizard and rotamer libraries in the case of MMM; for a detailed discussion see ref. 26), differences in the simulated distance distributions may be expected. In this specific case, our data from *cw* and pulsed EPR experiments showing that the label at T179C is immobilised by the protein are in better agreement with the MtsslWizard simulation, which predicts a less mobile label.

The large measured distance of 4.83 nm between the labels at T179C requires that they are facing outwards from the STAS–STAS dimer. Multiple test structures of bound STAS domains that fulfilled this condition were generated by rigid-body modelling in ZDOCK and then further ranked with respect to the T179C–T179C distance distribution and their compatibility with the structure of the linker. This rigid-body approach, both in simulating possible conformations of the STAS–STAS dimer as well as for the binding of the resulting dimer to the LOV–LOV crystal structure, allows the generation of a model for the full-length protein from relatively few distance constraints (Fig. 8).

The data obtained from ELDOR measurements of YtvA T80C/C176S/T179C and YtvA T54C/C176S/T179C were then used to align the STAS structure in relation to the LOV dimer. These calculations were performed in MMM, since MtsslWizard is less suited for the calculation of multi-spin distance distributions. However, as previously discussed, the MMM simulation overestimates the width of the T179C–T179C distance distribution. This discrepancy results in additional distance features around 4.87 nm appearing in the simulation, not present in the experimental data, which has to be taken into account when interpreting the results, shown in Fig. 9.

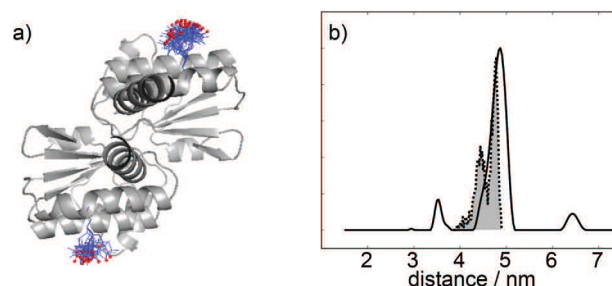


**Fig. 8** (a) Model structure of the STAS–STAS dimer as derived from docking simulations with the allowed conformers of the two labels at T179C as derived from MtsslWizard. The two dark helices in the centre represent the linker peptides; the LOV domains are not shown. (b) Measured T179C–T179C distance distribution (solid) compared to the distance distribution calculated from the structure in (a) (dashed, shaded).

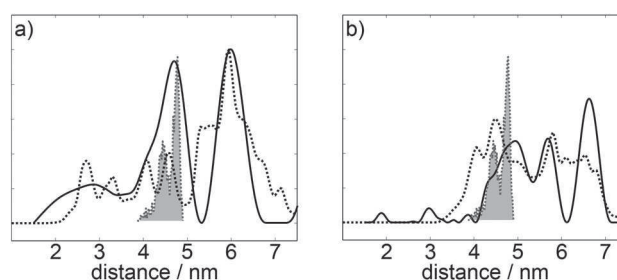


**Fig. 9** Distance distributions for (a) YtvA T54C/C176S/T179C and (b) YtvA T80C/C176S/T179C. Solid: measured distribution, dotted: as calculated from the model using MMM, shaded grey: T179C–T179C distance calculated using mtsslWizard. Comparison of the calculations from MMM and mtsslWizard shows that the discrepancy around 4–5 nm in the simulated distributions can be accounted for by the too broad T179C distribution in MMM calculations.

In the case of YtvA T54C/C176S/T179C the peak at 2.7 nm corresponds to the T54C–T54C distance within the LOV dimer, the peak at 4.7 nm is the signal already previously identified as originating from the T179C–T179C interaction. Thus, the broad peak at 6 nm is the superposition of all four possible T54C–T179C pairs.

The distance distribution of YtvA T80C/C176S/T179C does not split as clearly into identifiable distances. The main discrepancy between the simulation and the measured data relates to the region around 4 nm. This, however, is again due to the overly broad distribution for T179C–T179C in the MMM simulation, as discussed above. While the experimental distance distribution does not agree with the fine structure predicted by MMM calculations, a detail which is beyond the resolution of the present experimental data, the general trimodal shapes of the distance distributions in the simulation and the measured data fit quite well. Thus, the distances observed for the T80C–T80C and T54C–T54C label pairs further strengthen the LOV–LOV binding motif derived from singly labelled variants. The STAS–STAS dimer structure derived from docking simulations in conjunction with the measured T179C–T179C distance constraint correctly reflects the distances observed for the intra-dimer label pairs T80C–T179C and T54C–T179C,

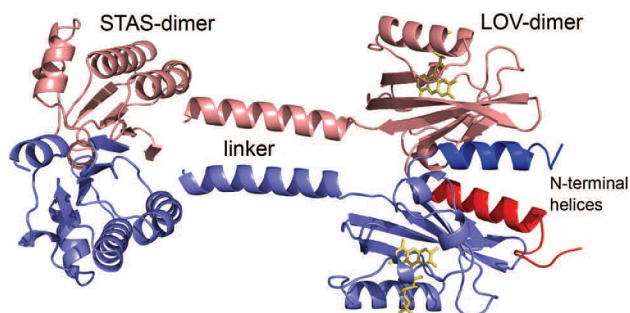


**Fig. 10** Structural model of full-length YtvA, highlighting the N-terminal helices (shown in red and dark blue) between the LOV  $\beta$ -sheets. Five residues between the linker and the STAS-domains are not included in the structure because no data exist on their conformation.

strongly supporting the overall structure of two homo-dimers linked *via* two helices.

## Conclusions

The derived structural model for the full-length protein is shown in Fig. 10. The general motif of two homo-dimers linked by two coiled helices is in very good agreement with SAXS and NMR data;<sup>8</sup> the major and important difference to the earlier models is the inclusion of the N-terminal helices and a different association interface for the STAS-STAS dimer.

This structural model of the full-length protein forms an ideal basis for identifying target residues for further spin labelling studies to elucidate potential conformational changes upon photo-activation.

## Experimental

### Sample preparation

Site-directed mutagenesis was performed as described in ref. 33. Besides the functionally active cysteine (C62), YtvA carries one other cysteine residue (position 176). This, however, was converted into a serine, as labelling studies showed that this residue is only partly accessible ( $\leq 30\%$ ). All five mutants were then based on this *cys*-deletion mutation (C176S). Introduced cysteines were allowed to react with (1-oxyl-2,2,5,5-tetramethylpyrroline-3-methyl)-methanethio-sulfonate (MTSSL) in order to attach the nitric oxide spin label. Yields of label attachment were determined *via* the Ellman test.<sup>34</sup> All samples were measured in a buffer containing 10 mM sodium phosphate and 10 mM NaCl at pH 8.0.

For pulsed EPR measurements, glycerol was added to a concentration of 50% (v/v) in order to slow down electron spin relaxation. To minimise the interaction between the proteins in the solvent and to further increase relaxation times, the samples were reconstituted in fully deuterated buffer/glycerol for relaxation and ELDOR experiments. Deuteration was accomplished by drying and then re-dissolving the buffer in D<sub>2</sub>O in order to maintain the buffer at pH 8. The samples were

then repeatedly exchanged with the deuterated buffer using a *Heracus Primo R* centrifuge with *Millipore UFV5BTK00* 30 kDa membranes. In a final step deuterated glycerol was added to a final concentration of 50% v/v. The final protein concentration was between 75  $\mu$ M and 100  $\mu$ M.

For non-photoinduced samples, all ambient temperature experiments as well as cooling of the samples for low temperature experiments were performed in the dark to avoid photoactivation of the protein. In order to trap the adduct-inhibited mutant C62A in its radical state, the sample was first illuminated for 5 min with a high power LED at 465 nm and then rapidly frozen in liquid nitrogen.

### EPR measurements

X-band EPR-measurements were performed at 9.7 GHz on Bruker BioSpin Elexsys E680 and E580 X-band spectrometers, both using a Bruker SuperX-FT microwave bridge and a Bruker ER 4118X-MD5 dielectric ring resonator. Microwave amplification for pulsed experiments was achieved with Applied Systems Engineering 117X travelling wave tube amplifiers. For ELDOR experiments the internal ELDOR microwave source of the Elexsys E580 spectrometer was used, and the E680 spectrometer was equipped with a Bruker E580-400U microwave source. S-band experiments were performed at 3 GHz on a Bruker BioSpin Elexsys E680 spectrometer with a Bruker Super-S-FTu microwave bridge and a Bruker AmpS solid state amplifier, using an ER 4118S-MS5 split-ring resonator.

*cw*-Spectra were recorded using 20.1  $\mu$ W microwave power, 100 kHz modulation frequency and 1 G modulation amplitude. The sampling time for detection was 81.92 ms.

For field swept echo (FSE) experiments a two pulse echo sequence ( $\pi/2$ - $\tau$ - $\pi$ - $\tau$ -echo) was employed, with pulse lengths of 40 ns and 80 ns for the  $\pi/2$  and  $\pi$  pulses respectively. The same pulse sequence, but with a variable delay  $\tau$ , was used for phase memory time measurements. For ELDOR, the four pulse DEER sequence<sup>21</sup> (probe pulse sequence  $\pi/2$ - $\tau_1$ - $\pi$ - $\tau_2$ - $\pi$ - $\tau_2$ -echo with the microwave pump pulse on the second frequency being swept between the second and third probe pulses) with pulse lengths of 12 ns for the  $\pi/2$  and 32 ns for the  $\pi$  pulses was used.

All *cw*-EPR measurements were performed at room temperature. Low temperatures for pulsed experiments were reached with *Oxford CF-935* cryostats. The temperature was controlled using *Oxford ITC503* temperature controllers for X-band and a *LakeShore 321* temperature controller for S-band measurements. Field swept echoes and relaxation experiments were performed at temperatures between 80 K and 60 K, where a temperature of 70 K was found to yield the best signal-to-noise ratio for ELDOR experiments.

### Analysis

Simulation and fitting of *cw*-spectra and relaxation data was achieved in *MATLAB* using the *EasySpin* toolbox routines '*chili*' and '*exponfit*' respectively.<sup>19</sup> For the evaluation of ELDOR data the *MATLAB* toolbox *DeerAnalysis*<sup>35</sup> was used. The data were phase- and background-corrected before analysis. As a

background model a three dimensional homogeneous spin distribution was fitted to the data. Spin distance distributions were then fitted to the background-corrected spectra using Tikhonov regularisation. The resulting distance distributions were checked against modelled distances for spin label rotamers attached to the protein structure. For this, the *MATLAB* toolbox *MMM*<sup>25</sup> as well as the *PyMol*-plugin *MtsslWizard*<sup>26</sup> were used. The structure for the YtvA-LOV domain was obtained from a high resolution X-ray structure of YF1,<sup>28</sup> an artificial protein that incorporates both the YtvA N-terminus and LOV domain. For the STAS domain a homology model structure was used.<sup>24</sup> Domain docking simulations were performed in *ZDOCK*.<sup>36</sup>

## Notes and references

- 1 W. R. Briggs and C.-T. Lin, Photomorphogenesis-from One Photoreceptor to 14: 40 Years of Progress, *Mol. Plant*, 2012, 5, 531–532.
- 2 J. E. Toettcher, C. A. Voigt, O. D. Weiner and W. A. Lim, The promise of optogenetics in cell biology: interrogating molecular circuits in space and time, *Nat. Methods*, 2011, 8, 35–38.
- 3 A. Losi and W. Gärtner, Old Chromophores, New Photo-activation Paradigms, Trendy Applications: Flavins in Blue Light-Sensing Photoreceptors, *Photochem. Photobiol.*, 2011, 87, 491–510.
- 4 T. A. Gaidenko, T.-J. Kim, A. L. Weigel, M. S. Brody and C. W. Price, The blue-light receptor YtvA acts in the environmental stress signaling pathway of *Bacillus subtilis*, *J. Bacteriol.*, 2006, 188, 6387–6395.
- 5 M. Avila-Perez, K. J. Hellingwerf and R. Kort, Blue light activates the sigma(B)-dependent stress response of *Bacillus subtilis* via YtvA, *J. Bacteriol.*, 2006, 188, 6411–6414.
- 6 M. Avila-Perez, J. Vreede, Y. Tang, O. Bende, A. Losi, W. Gärtner and K. Hellingwerf, In Vivo Mutational Analysis of YtvA from *Bacillus subtilis* MECHANISM OF LIGHT ACTIVATION OF THE GENERAL STRESS RESPONSE, *J. Biol. Chem.*, 2009, 284, 24958–24964.
- 7 A. Möglich and K. Moffat, Structural basis for light-dependent signaling in the dimeric LOV domain of the photo-sensor YtvA, *J. Mol. Biol.*, 2007, 373, 112–126.
- 8 M. Jurk, M. Dorn and P. Schmieder, Blue Flickers of Hope: Secondary Structure, Dynamics, and Putative Dimerization Interface of the Blue-Light Receptor YtvA from *Bacillus subtilis*, *Biochemistry*, 2011, 50, 8163–8171.
- 9 V. Buttani, W. Gärtner and A. Losi, NTP-binding properties of the blue-light receptor YtvA and effects of the E105L mutation, *Eur Biophys. J. Biophys.*, 2007, 36, 831–839.
- 10 Y. Tang, Z. Cao, E. Livoti, U. Krauss, K.-E. Jaeger, W. Gärtner and A. Losi, Interdomain signalling in the blue-light sensing and GTP-binding protein YtvA: a mutagenesis study uncovering the importance of specific protein sites, *Photochem. Photobiol. Sci.*, 2010, 9, 47–56.
- 11 M. Dorn, M. Jurk and P. Schmieder, Blue News Update: BODIPY-GTP Binds to the Blue-Light Receptor YtvA While GTP Does Not, *Plos One*, 2012, 7, E29201.
- 12 V. Buttani, A. Losi, T. Eggert, U. Krauss, K.-E. Jaeger, Z. Cao and W. Gärtner, Conformational analysis of the blue-light sensing protein YtvA reveals a competitive interface for LOV-LOV dimerization and interdomain interactions, *Photochem. Photobiol. Sci.*, 2007, 6, 41–49.
- 13 G. W. Reginsson and O. Schiemann, Studying bimolecular complexes with pulsed electron-electron double resonance spectroscopy, *Biochem. Soc. Trans.*, 2011, 39, 128–129.
- 14 Y. E. Nesmelov and D. D. Thomas, Protein structural dynamics revealed by site-directed spin labeling and multi-frequency EPR, *Biophys. Rev.*, 2010, 2, 91–99.
- 15 G. L. Millhauser, Selective placement of electron-spin-resonance spin labels – new structural methods for peptides and proteins, *Trends Biochem. Sci.*, 1992, 17, 448–452.
- 16 C. Altenbach, S. L. Flitsch, H. G. Khorana and W. Hubbell, Structural studies on transmembrane proteins .2. spin labeling of bacteriorhodopsin mutants at unique cysteines, *Biochemistry*, 1989, 28, 7806–7812.
- 17 W. L. Hubbell, H. S. Mchaourab, C. Altenbach and M. A. Lietzow, Watching proteins move using site-directed spin labeling, *Structure*, 1996, 4, 779–783.
- 18 W. L. Hubbell, C. Altenbach, C. M. Hubbell and H. G. Khorana, Rhodopsin structure, dynamics, and activation: A perspective from crystallography, site-directed spin labeling, sulfhydryl reactivity, and disulfide cross-linking, *Membr. Proteins*, 2003, 63, 243–290.
- 19 S. Stoll and A. Schweiger, EasySpin, a comprehensive software package for spectral simulation and analysis in EPR, *J. Magn. Reson.*, 2006, 178, 42–55.
- 20 M. Lindgren, G. R. Eaton, S. S. Eaton, B. H. Jonsson, P. Hammarstrom, M. Svensson and U. Carlsson, Electron spin echo decay as a probe of aminoxyl environment in spin-labeled mutants of human carbonic anhydrase II, *J. Chem. Soc., Perkin Trans.*, 1997, 12, 2549–2554.
- 21 R. E. Martin, M. Pannier, F. Diederich, V. Gramlich, M. Hubrich and H. W. Spiess, Determination of end-to-end distances in a series of TEMPO diradicals of up to 2.8 nm length with a new four-pulse double electron electron resonance experiment, *Angew. Chem., Int. Ed.*, 1998, 37, 2834–2837.
- 22 C. W. M. Kay, C. Elsässer, R. Bittl, S. R. Farrell and C. Thorpe, Determination of the distance between the two neutral flavin radicals in augments of liver regeneration by pulsed ELDOR, *J. Am. Chem. Soc.*, 2006, 128, 76–77.
- 23 C. W. M. Kay, E. Schleicher, A. Kuppig, H. Hofner, W. Rüdiger, M. Schleicher, M. Fischer, A. Bacher and S. Weber, Blue light perception in plants - Detection and characterization of a light-induced neutral flavin radical in a C450A mutant of phototropin, *J. Biol. Chem.*, 2003, 278, 10973–10982.
- 24 M. Jurk, M. Dorn, A. Kikhney, D. Svergun, W. Gärtner and P. Schmieder, The Switch that Does Not Flip: The Blue-Light Receptor YtvA from *Bacillus subtilis* Adopts an

- Elongated Dimer Conformation Independent of the Activation State as Revealed by a Combined AUC and SAXS Study, *J. Mol. Biol.*, 2010, **403**, 78–87.
- 25 Y. Polyhach, E. Bordignon and G. Jeschke, Rotamer libraries of spin labelled cysteines for protein studies, *Phys. Chem. Chem. Phys.*, 2011, **13**, 2356–2366.
  - 26 G. Hagelueken, R. Ward, J. H. Naismith and O. Schiemann, MtsslWizard: In Silico Spin-Labeling and Generation of Distance Distributions in PyMOL, *Appl. Magn. Reson.*, 2012, **42**, 377–391.
  - 27 A. Möglich, R. A. Ayers and K. Moffat, Structure and Signaling Mechanism of Per-ARNT-Sim Domains, *J. Mol. Biol.*, 2009, **385**, 1433–1444.
  - 28 R. P. Diensthuber, M. Bommer, T. Gleichmann and A. Möglich, Full-Length Structure of a Sensor Histidine Kinase Pinpoints Coaxial Coiled Coils as Signal Transducers and Modulators, *Structure*, 2013, **21**, 1127–1136.
  - 29 H. Ogata, Z. Cao, A. Losi and W. Gärtner, Crystallization and preliminary X-ray analysis of the LOV domain of the blue-light receptor YtvA from *Bacillus amyloliquefaciens* FZB42, *Acta Crystallogr. Section F-Struct. Biol. Crystal. Commun.*, 2009, **65**, 853–855.
  - 30 F. Circolone, J. Granzin, K. Jentzsch, T. Drepper, K. E. Jäger, D. Willbold, U. Kraus and R. Batra-Saffering, Structural Basis for the Slow Dark Recovery of a Full-Length LOV Protein from *Pseudomonas putida*, *J. Mol. Biol.*, 2012, **417**, 362–374.
  - 31 H. Kovacs, D. Comfort, M. Lord, I. D. Campbell and M. D. Yudkin, Solution structure of SpoIIAA, a phosphorylatable component of the system that regulates transcription factor sigma(F) of *Bacillus subtilis*, *Proc. Natl. Acad. Sci. U. S. A.*, 1998, **95**, 5067–5071.
  - 32 M. B. Quin, J. M. Berrisford, J. A. Newman, A. Basle, R. J. Lewis and J. Marles-Wright, The Bacterial Stressosome: A Modular System that has Been Adapted to Control Secondary Messenger Signaling, *Structure*, 2012, **20**, 350.
  - 33 S. Raffelberg, M. Mansurova, W. Gärtner and A. Losi, Modulation of the Photocycle of a LOV Domain Photoreceptor by the Hydrogen-Bonding Network, *J. Am. Chem. Soc.*, 2011, **133**, 5346–5356.
  - 34 G. L. Ellman, Tissue sulfhydryl groups, *Arch. Biochem. Biophys.*, 1959, **82**, 70–77.
  - 35 G. Jeschke, V. Chechik, P. Ionita, A. Godt, H. Zimmermann, J. Banham, C. R. Timmel, D. Hilger and H. Jung, DeerAnalysis2006 – a comprehensive software package for analyzing pulsed ELDOR data, *Appl. Magn. Reson.*, 2006, **30**, 473–498.
  - 36 R. Chen and Z. Weng, Docking unbound proteins using shape complementarity, desolvation, and electrostatics, *Proteins*, 2002, **47**, 281–294.

## **4. Application of the blue light photoreceptor YtvA**

### **4.1 A photochromic bacterial photoreceptor with potential for super-resolution microscopy**

Journal of Photochemical. Photobiological. Science, 2.9, 3. author

Sample generation and preparation: 100 %

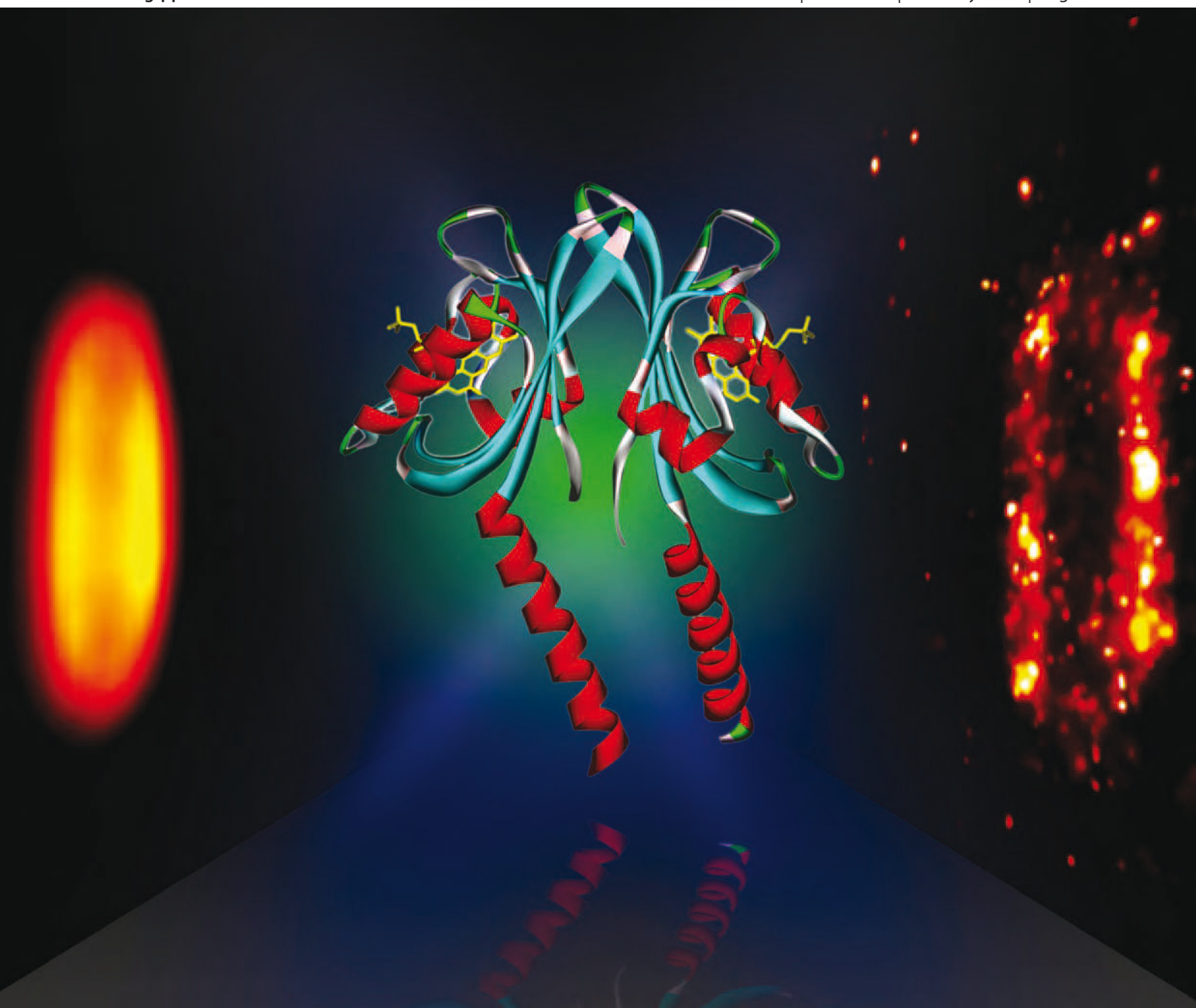


# Photochemical & Photobiological Sciences

An international journal

[www.rsc.org/pps](http://www.rsc.org/pps)

Volume 12 | Number 2 | February 2013 | Pages 221–408



ISSN 1474-905X

RSC Publishing



1474-905X(2013)12:2;1-Z

A photochromic bacterial photoreceptor with potential  
for super-resolution microscopy†Cite this: *Photochem. Photobiol. Sci.*, 2013,  
12, 231Received 13th July 2012,  
Accepted 20th September 2012

DOI: 10.1039/c2pp25254f

www.rsc.org/paps

Aba Losi,<sup>a</sup> Wolfgang Gärtner,<sup>b</sup> Sarah Raffelberg,<sup>b</sup> Francesca Cella Zancacchi,<sup>c</sup>  
Paolo Bianchini,<sup>c</sup> Alberto Diaspro,<sup>c</sup> Carmen Mandalari,<sup>a</sup> Stefania Abbruzzetti<sup>a</sup> and  
Cristiano Viappiani<sup>\*a,d</sup>

**We introduce a novel fluorescent reporter with potential for super-resolution microscopy, based on the bacterial photoreceptor YtvA. YtvA (from *Bacillus subtilis*) comprises a photosensitive flavin-based LOV domain, efficiently photo-switchable between fluorescent and non-fluorescent states. We demonstrate Fluorescence PhotoActivation Localization Microscopy (FPALM) studies of live *Escherichia coli* cells, expressing YtvA molecules.**

The development of genetically encoded photoswitchable fluorescent proteins<sup>1,2</sup> is of greatest interest to expand the toolkit of fluorescent reporters suitable for super-resolution microscopy applications based on random activation of single molecules.<sup>3–5</sup> Application of super-resolution imaging allows studying biological material – including living cells – extending in all three dimensions instead of two-dimensionally spread thin samples,<sup>6–8</sup> and highlights the importance of the development of novel, bright and photoswitchable fluorescent proteins which allow single molecule detection deep within scattering samples.

YtvA is a blue light photoreceptor from *Bacillus subtilis*, composed of a flavin-binding LOV (light, oxygen, voltage) domain, sharing high structural homology with the flavin mononucleotide (FMN)-binding LOV domains of plant phototropins (phot).<sup>9</sup> In *B. subtilis*, YtvA is part of the stress response complex that is activated under threatening environmental conditions.<sup>10</sup>

Illumination of dark-adapted YtvA (YtvAD) with blue-light (~450 nm) triggers a LOV-typical photocycle (Fig. 1a) involving the reversible formation of a blue-shifted FMN-cysteine C(4a)-thiol adduct (YtvAL), which is formed *via* the decay of the red-shifted FMN triplet state. YtvAL is considered the biologically active, signaling state. Upon 450 nm excitation, the yield for this photoreaction is 0.49.<sup>11</sup> This “photoadduct” slowly reverts back to the parent state YtvAD, with a thermally activated dark reaction.<sup>12</sup> Like in the other flavin-binding LOV domains, the dark adapted state, carrying the chromophore in its oxidized state, is characterized by a relatively intense, structured absorption band in the blue ( $\lambda_{\text{max}} = 450 \text{ nm}$ ,  $\epsilon_{\text{max}} 12\,500 \pm 500 \text{ M}^{-1} \text{ cm}^{-1}$ , blue curve in Fig. 1b).<sup>9</sup> YtvA-bound FMN preserves a rather bright fluorescence emission peaked at about 500 nm in the unphotolyzed state (quantum yield  $\Phi_{\text{f}} = 0.22$  at 20 °C, green curve in Fig. 1b).<sup>9</sup> Interestingly, fluorescence excitation and emission cover a spectral range which is very similar to that characteristic for Green Fluorescent Protein (GFP) from *Aequorea victoria*. The fluorescence emission vanishes upon formation of YtvAL (absorption spectrum reported as the black curve in Fig. 1b), in consequence of the photochemical transformation leading to the loss of planarity for FMN and a reduced conjugation. Photoconversion of the parent (YtvAD) to the biologically active (YtvAL) state can thus be followed through disappearance of the fluorescence emission. Thermal recovery to YtvAD is a rather slow process, taking approximately 3 h at 20 °C to be completed. This slow thermal reversion process allows, in contrast to fast cycling LOV domains, steady-state accumulation of the non-fluorescent YtvAL state.<sup>13</sup>

An early report on the LOV2 domain from the phy3 receptor (neochrome) of *Adiantum* indicated that for this protein the light adapted species can be photoconverted in moderate yield to the dark adapted state, by shining near UV-violet light on the photoreceptor.<sup>14</sup> The finding of photoswitching phenomena in LOV domain proteins went largely unnoticed and the potential of this property was almost completely unexplored, although early enough there were good indications for such a process.<sup>15</sup> Besides being an interesting photochemical event in

<sup>a</sup>Dipartimento di Fisica, Università di Parma, viale delle Scienze 7A, 43124 Parma, Italy, Web: <http://www.unipr.it>. E-mail: [aba.losi@fis.unipr.it](mailto:aba.losi@fis.unipr.it), [cristiano.viappiani@fis.unipr.it](mailto:cristiano.viappiani@fis.unipr.it); Fax: +39-0521-905-223;

Tel: +39-0521-905-293/208www.unipr.it

<sup>b</sup>Max-Planck-Institute for Chemical Energy Conversion (CEC), formerly Bioinorganic Chemistry, Stiftstr. 34-36, 45470 Mülheim a.d. Ruhr, Germany.

E-mail: [wolfgang.gaertner@cec.mpg.de](mailto:wolfgang.gaertner@cec.mpg.de); Tel: +49-208-3063693

<sup>c</sup>Fondazione Istituto Italiano di Tecnologia, Via Morego, 30 16163 Genova, Italy

<sup>d</sup>NEST, Istituto Nanoscienze-CNR, Pisa, Italy

†Electronic supplementary information (ESI) available: Experimental methods, kinetic model, bulk and single molecule photoconversion. See DOI: 10.1039/c2pp25254f



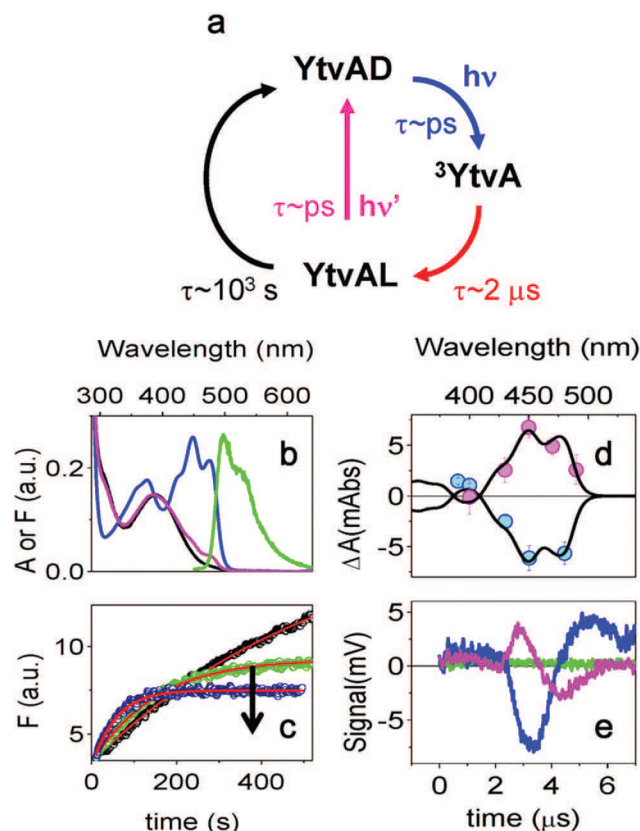


**Fig. 1** (a) Schematic photocycle of YtvA. (b) Absorption spectra of YtvAD (blue) and YtvAL (black). The absorption spectrum of YtvAL was obtained after 5 min of irradiation with LED465 at 0.5 mW. The magenta curve represents the absorption spectrum of the mixture of YtvAD and YtvAL after 5 min irradiation with LED356 at 0.63 mW. Increasing the power of the LED356 above 0.63 mW did not cause any further change in the absorption spectrum. The green solid line shows the fluorescence emission spectrum of YtvAD under excitation at 330 nm. (c) Fluorescence emission recovery of a YtvAL buffered solution under illumination with LED356 at increasing power between 0.05 mW and 0.8 mW. The arrow indicates increasing LED power. The YtvAL solution was prepared by 5 min illumination with LED465.  $T = 20\text{ }^{\circ}\text{C}$ ; excitation was at 330 nm, and detection at 500 nm. Red solid lines result from the fitting with the model described in the text and detailed as ESI†. The non-zero value of the fluorescence emission at time zero is coincident with the background. (d) Comparison between the absorbance changes measured at  $t = 7\text{ }\mu\text{s}$  after 475 nm excitation of a YtvAD solution (blue circles), the absorbance change measured at  $t = 7\text{ }\mu\text{s}$  after excitation at 355 nm of a YtvAL solution (magenta circles), and the steady state absorbance changes between YtvAL and YtvAD (black solid curves). (e) Photoacoustic signal measured at  $T_{\text{ref}} = 3.4\text{ }^{\circ}\text{C}$  for the photocalorimetric reference compound (green, new coccine), and after photoexcitation at 355 nm of YtvAD (blue trace) and of YtvAL (magenta).

itself, this property has potential for applications in a broad context, including super-resolution microscopy based on random activation of single fluorescent molecules,<sup>3–5</sup> and bidirectional control of the functionality of the photoreceptor.

We thus investigated the possibility of reverting to the YtvAD state through excitation of the YtvAL state with near UV light. Illumination of the photoconverted YtvAL solution with near-UV light (LED356) establishes a photoequilibrium with a clearly detectable amount of re-formed YtvAD. The amount of YtvAD present in the mixture increases at increasing light

power, and eventually reaches a saturating value (magenta curve in Fig. 1b). Similar results were obtained when the YtvAL solution was illuminated with violet light (LED405; data not shown). The amount of YtvAD, present at the photoequilibrium established under saturating light, is independent of the fact that the illumination is performed on a previously fully photoconverted YtvAL solution, or on a dark adapted YtvAD solution, demonstrating that the 356 (405) nm illumination triggers both forward and reverse photoreactions, although to a different extent. The latter process is quite straightforward when considering that the steady state photoequilibrium is attained also under 405 nm excitation, a wavelength at which both species, YtvAL and YtvAD, have almost the same extinction coefficient.

The photoconversion yield can be easily calculated under saturating conditions. The concentrations of both species are readily determined from a simple balance between rates for forward and reverse photoreactions induced by photons of energy  $h\nu$  ( $h$  = Planck's constant,  $\nu$  = frequency of the photons):<sup>16</sup>



To a first approximation, the back reaction rate of the thermal (dark) relaxation of YtvAL to YtvAD can be neglected in view of its very small value ( $k_{\text{LD}}^d \sim 3 \times 10^{-4}\text{ s}^{-1}$  at  $20\text{ }^{\circ}\text{C}$ ), compared to light induced reactions at high photon density.  $\Phi_{\text{DL}}$  and  $\Phi_{\text{LD}}$  represent the forward and reverse reaction yields, respectively. Under this approximation, the reverse yield  $\Phi_{\text{LD}}$  can be estimated as

$$\Phi_{\text{LD}} = \frac{\text{SO}(\text{YtvAD})}{\text{SO}(\text{YtvAL})} \frac{[\text{YtvAD}]_{\text{eq}}}{[\text{YtvAL}]_{\text{eq}}} \Phi_{\text{DL}} \quad (2)$$

where  $\text{SO}(\text{YtvAD})$  and  $\text{SO}(\text{YtvAL})$  represent the spectral overlaps between the LED emission and the absorption spectra of YtvAL and YtvAD, respectively (ESI Fig. S2†).  $[\text{YtvAL}]_{\text{eq}}$  and  $[\text{YtvAD}]_{\text{eq}}$  are the concentrations of the two molecular species under photostationary conditions. These concentrations are readily determined from the absorption spectrum of the mixture, which can be described as a linear combination of the pure YtvAL (90%) and YtvAD (10%) spectra under LED356 excitation. Similarly, 9.7% YtvAD and 90.3% YtvAL are obtained under LED405 excitation. Taking into account the forward yields at 465 nm ( $\Phi_{\text{DL}} = 0.49^9$ ) and at 356 nm ( $\Phi_{\text{DL}} = 0.3 \pm 0.1$ , from photoacoustic data, this work), one obtains  $\Phi_{\text{LD}} = 0.049$  from the photoequilibrium with LED405. A similar value results for the photoequilibrium with LED356,  $\Phi_{\text{LD}} = 0.046$ . The retrieved value for  $\Phi_{\text{LD}}$  is about tenfold lower than the yield for the forward reaction, and is also substantially lower than the figure reported for the LOV2 domain of phototropin,<sup>14</sup> the latter likely arising from an overestimate of the fraction of the dark state which is accumulated at photoequilibrium under near UV excitation. Reverse reaction yields can be estimated also by following the kinetics of establishment of the photoequilibrium, under steady state illumination.<sup>16,17</sup> In

these experiments, we monitored fluorescence emission at 500 nm under 330 nm excitation, a wavelength at which photo-conversion of YtvAD to YtvAL is negligible.<sup>18</sup> Starting from a YtvAL solution, LED405 (or LED356) was switched on and the recovery of the fluorescence emission was followed (Fig. 1c). The global fitting of the kinetics recorded at several illumination powers (ESI†) afforded  $\Phi_{LD} = 0.06 \pm 0.01$  (LED356) and  $\Phi_{LD} = 0.05 \pm 0.01$  (LED405), perfectly consistent with the determination from the photoequilibrium data. Data collected at high LED power demonstrate the remarkably high stability of YtvA in the saturating level reached by fluorescence emission in different illumination cycles (ESI Fig. S3†).

Reverse photoconversion from YtvAD to YtvAL is further confirmed by nanosecond laser flash photolysis. Photoexcitation of YtvAL with 355 nm laser pulses leads to absorbance changes consistent with formation of the YtvAD state (Fig. 1c), with a kinetics falling below the resolution of the experimental setup, suggesting this reaction proceeds from the singlet state, as proposed for the LOV2 domain of phototropin.<sup>14</sup> This photochemistry contrasts that of YtvAD which upon excitation with a 475 nm nanosecond laser pulse forms a reactive triplet state within the resolution of the experimental setup, with 0.6 quantum yield, which then through its decay (*vide supra*) leads with high efficiency to formation of the covalent adduct between FMN and Cys62 (Fig. 1d).<sup>9</sup> Additional evidence that 355 nm illumination leads to back conversion to YtvAD is provided by time resolved photoacoustic data. We showed previously that 475 nm excitation of YtvAD is accompanied by a fast (lifetime below ~20 ns) contraction corresponding to triplet formation, followed by a slower (~1.6  $\mu$ s) and larger ongoing contraction.<sup>19</sup>

The latter was interpreted as the formation of the adduct in YtvAL. A similar pattern of structural volume changes is observed, starting from YtvAD, with 355 nm excitation (blue curve in Fig. 1e). The L-to-D photoconversion instead leads to a photoacoustic signal (magenta curve in Fig. 1e) characterized by a fast (lifetime below ~20 ns) and small expansion,  $\Delta V_{LD} = 0.55$  ml einstein<sup>-1</sup>. Taking into account that the molar volume contraction for adduct formation (*i.e.* for the D-to-L conversion) is  $\Delta V_{R,DL} = -6.2$  ml einstein<sup>-1</sup>,<sup>19</sup>  $\Phi_{LD}$  is readily calculated as the ratio  $\Phi_{LD} = \Delta V_{LD}/\Delta V_{R,DL} = 0.04$ , in good agreement with the above estimates.

The photoswitching between YtvAD and YtvAL is observed also for molecules deposited on a coverslip (ESI†), or expressed within *Escherichia coli* colonies. We have exploited this property to perform sub-diffraction localization of individual molecules deposited on a coverslip (ESI Fig. S4†) or in *Escherichia coli* colonies over-expressing wild-type YtvA. The switching between the fluorescent and the dark state is obtained using a low-level 405 nm activation laser and a 488 nm readout laser continuously running. Super-resolution experiments are carried out by collecting and analyzing individual fluorescent molecules of YtvA, following the procedure previously reported for Fluorescence PhotoActivation Localization Microscopy (FPALM).<sup>4</sup> Localization of YtvA molecules deposited on a coverslip can be performed with an average precision of 18 nm

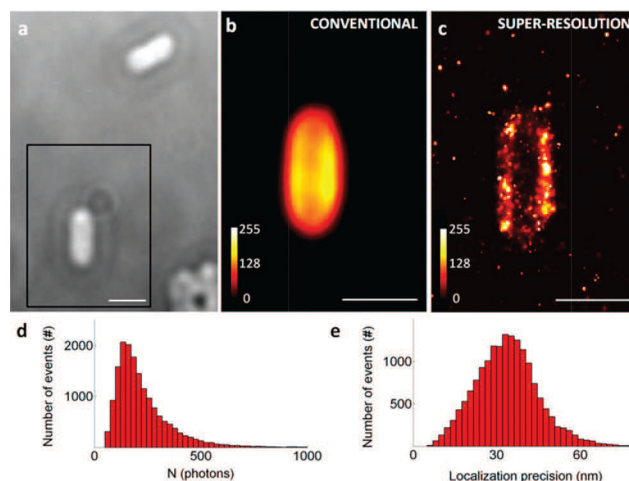


**Fig. 2** Super-resolution imaging of *Escherichia coli* over-expressing wild-type YtvA. Transmitted image (a), conventional fluorescence image obtained by adding the total signal from all the frames (b) and super-resolution (FPALM) image (c) of an *E. coli* cell. Photoactivation localization microscopy experiments have been carried out with a 405 nm activation laser and a 488 nm readout laser continuously running. Number of photons collected for each molecule (d) and localization precision in (e). The activation and excitation laser intensities were at 0.025 kW cm<sup>-2</sup> and 1 kW cm<sup>-2</sup>, respectively. Total acquisition time for (c) was 3 min. Images were acquired with a frame rate of 25 frames s<sup>-1</sup>. The final image was reconstructed after collection and localization of approximately 12 000 events. Roll ball background subtraction and filtering (on the basis of width and number of photons per molecule) allowed the rejection of the misleading events due to the high background levels measured within the *E. coli* cells (a mean value of 6.4 photons per pixel due to the background was measured). Scale bars, 1  $\mu$ m (a, b, c).

(Fig. S4†). FPALM images of live *Escherichia coli* (Fig. 2) show the intracellular distribution of expressed YtvA molecules, with an average localization precision (35 nm) similar to the one observed for the molecules deposited on a coverslip.

A comparison between the conventional wide-field fluorescence image (Fig. 2a, b) and the FPALM image (Fig. 2c) shows the remarkable resolution improvement and clearly demonstrates the suitability of YtvA for super-resolution applications in cells.

In the present experiments, FPALM allows us to achieve an average localization precision of 35 nm (Fig. 2e). It appears in these experiments as if YtvA preferentially allocates in the membrane regions of the *E. coli* cells. It remains to be proven in future experiments whether this is due to its natural function, *i.e.*, integration into a complex like the stressosome in *B. subtilis*, or whether it might be caused by the recording conditions in these experiments, where over-expression may lead to artifactual accumulation within inclusion bodies.

Also Fluorescence Lifetime Imaging Microscopy (FLIM) images under two-photon excitation (TPE) of live *Escherichia coli* were acquired, showing fluorescent molecules with a lifetime around 2.2 ns (the lifetime observed for bulk YtvAD solutions) clustering around a few spots (Fig. 3c). The spatial distribution is similar to the one observed in some of the FPALM images (Fig. 3a, b).

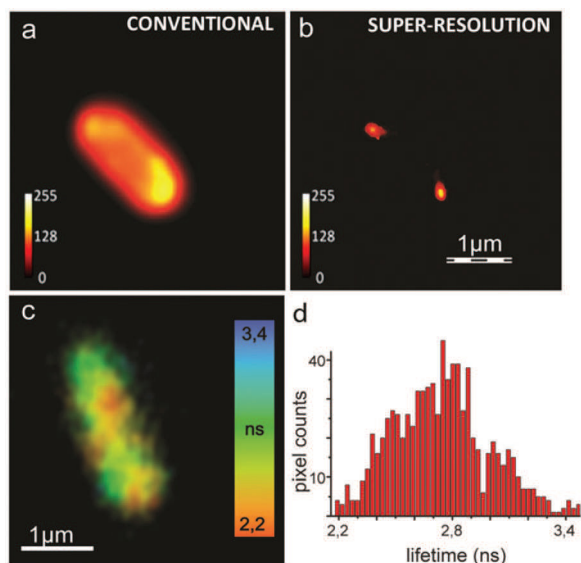


**Fig. 3** Fluorescence lifetime imaging (FLIM) with two-photon excitation of *Escherichia coli* over-expressing YtvA. Conventional fluorescence image obtained by adding the total signal from all the frames (a), super-resolution (FPALM) image (b) and FLIM image (c) of an *E. coli* cell. The lifetimes distribution of the image (c) is depicted by the histogram in (d).

These FPALM/FLIM results clearly demonstrate the usefulness of YtvA, and potentially other flavin-based phototropins for microscopical studies in cell biology. The already reported broad variety of LOV domains with respect to the quantum yield of photoadduct formation and fluorescence, the here demonstrated photoswitchable fluorescence, and the wide range of thermal recovery kinetics<sup>20</sup> make this class of photoreceptors promising tools for the above demonstrated applications. This is especially advantageous when taking their small size and their high thermal and photochemical stability into account. As a final advantage (even over the widely employed GFP derivatives), their readiness and immediate maturation even under anaerobic conditions<sup>21</sup> should be mentioned that outperform those of GFPs.<sup>22</sup> FMN binding LOV domains are ideally suited as fluorescent reporters of bacterial location or gene expression in obligate anaerobes, for example the opportunistic pathogens *Porphyromonas gingivalis*<sup>23</sup> and *Bacteroides fragilis*,<sup>24</sup> and the facultative anaerobe *Rhodobacter capsulatus*.<sup>21</sup> They have also been proposed as fluorescent tools to study fungine colonization of hypoxic niches during infections, based on model studies on gene expression in *Candida albicans* and *Saccharomyces cerevisiae*.<sup>25</sup> Finally, the small fluorescent protein iLOV was engineered for studying the dynamics of viral infections in plants.<sup>26</sup>

Although the present super-resolution experiments exploited just the wild type photoreceptor expressed in *Escherichia coli*, the localization precision obtained with YtvA is at least comparable to those reported for a photoconvertible YFP fusion to target bacterial actin protein MreB in live *Caulobacter crescentus* cells.<sup>27</sup> The development of chimeric structures with suitable peptides will allow labelling specific cellular structures in eukaryotic cells.

The photochromic properties of YtvA make this photoreceptor and, more generally, LOV domain proteins convenient genetically encodable fluorescent reporters for super-resolution microscopy. In addition, these biological photoreceptors exhibit double application potential. Besides allowing applications in super-resolution microscopies, the photo-switching, if connected to an on/off-regulation of fused enzyme activities (as found naturally occurring in many photoreceptors), opens perspectives for new paradigms in optogenetics, as recently demonstrated for a bacterial photoactivated adenylyl cyclase, bPAC, of the soil bacterium *Beggiatoa*, through which modulation of cellular cAMP by light was attained.<sup>28</sup>

Photoinduced switching between the YtvAD and YtvAL states allows controlling the activity of the photoreceptor and it is foreseen that tuning of photochemical and fluorescence-emission yields by engineered mutations will improve control of the functional states of coupled enzymatic units.

## Acknowledgements

This work has been partially supported by the Vigoni programme (to A.L. and W.G.), the University of Parma (fellowship to C.M.), and MiUR (PRIN 2008JZ4MLB). We thank S.T. Hess for software and training.

## Notes and references

- G. Patterson, M. Davidson, S. Manley and J. Lippincott-Schwartz, *Annu. Rev. Phys. Chem.*, 2010, **61**, 345–367.
- K. A. Lukyanov, D. M. Chudakov, S. Lukyanov and V. V. Verkhusha, *Nat. Rev. Mol. Cell Biol.*, 2005, **6**, 885–891.
- E. Betzig, G. H. Patterson, R. Sougrat, W. Lindwasser, S. Olenych, J. S. Bonifacino, M. W. Davidson, J. Lippincott-Schwartz and H. F. Hess, *Science*, 2006, **313**, 1642–1645.
- S. T. Hess, T. P. K. Girirajan and M. D. Mason, *Biophys. J.*, 2006, **91**, 4258–4272.
- M. J. Rust, M. Bates and X. Zhuang, *Nat. Methods*, 2006, **3**, 793–795.
- F. Cella Zanacchi, Z. Lavagnino, M. P. Donnorso, A. D. Bue, L. Furia, M. Faretta and A. Diaspro, *Nat. Methods*, 2011, **8**, 1047–1049.
- A. G. York, A. Ghitani, A. Vaziri, M. W. Davidson and H. Shroff, *Nat. Methods*, 2011, **8**, 327–333.
- S. A. Jones, S. H. Shim, J. He and X. Zhuang, *Nat. Methods*, 2011, **8**, 499–505.
- A. Losi, E. Polverini, B. Quest and W. Gärtner, *Biophys. J.*, 2002, **82**, 2627–2634.
- T. Gaidenko, T. Kim, A. Weigel, M. Brody and C. Price, *J. Bacteriol.*, 2006, **188**, 6387–6395.
- M. Salomon, J. M. Christie, E. Knieb, U. Lempert and W. R. Briggs, *Biochemistry*, 2000, **39**, 9401–9410.
- A. Losi, *Photochem. Photobiol.*, 2007, **83**, 1–18.
- S. Raffelberg, M. Mansurova, W. Gärtner and A. Losi, *J. Am. Chem. Soc.*, 2011, **133**, 5346–5356.

- 14 J. T. M. Kennis, I. H. M. van Stokkum, S. Crosson, M. Gauden, K. Moffat and R. van Grondelle, *J. Am. Chem. Soc.*, 2004, **126**, 4512–4513.
- 15 T. Kottke, J. Heberle, D. Hehn, B. Dick and P. Hegemann, *Biophys. J.*, 2003, **84**, 1192–1201.
- 16 V. Voliani, R. Bizzarri, R. Nifosi, S. Abbruzzetti, E. Grandi, C. Viappiani and F. Beltram, *J. Phys. Chem. B*, 2008, **112**, 10714–10722.
- 17 R. Bizzarri, M. Serresi, F. Cardarelli, S. Abbruzzetti, B. Campanini, C. Viappiani and F. Beltram, *J. Am. Chem. Soc.*, 2010, **132**, 85–95.
- 18 Y. Tang, Z. Cao, E. Livoti, U. Krauss, K.-E. Jaeger, W. Gärtner and A. Losi, *Photochem. Photobiol. Sci.*, 2010, **9**, 47–56.
- 19 A. Losi, B. Quest and W. Gärtner, *Photochem. Photobiol. Sci.*, 2003, **2**, 759–766.
- 20 A. Losi and W. Gärtner, *Photochem. Photobiol.*, 2011, **87**, 491–510.
- 21 T. Drepper, T. Eggert, F. Circolone, A. Heck, U. Krauss, J. K. Guterl, M. Wendorff, A. Losi, W. Gärtner and K.-E. Jaeger, *Nat. Biotechnol.*, 2007, **25**, 443–445.
- 22 T. Drepper, R. Huber, A. Heck, F. Circolone, A. K. Hillmer, J. Büchs and K. E. Jäger, *Appl. Environ. Microbiol.*, 2010, **76**, 5990–5994.
- 23 C. H. Choi, J. V. DeGuzman, R. J. Lamont and Ö. Yilmaz, *PLoS One*, 2011, **6**, e18499.
- 24 L. A. Lobo, C. J. Smith and E. R. Rocha, *FEMS Microbiol. Lett.*, 2011, **317**, 67–74.
- 25 D. Tielker, I. Eichhof, K. E. Jaeger and J. F. Ernst, *Eukaryotic Cell*, 2009, **8**, 913–915.
- 26 S. Chapman, C. Faulkner, E. Kaiserli, C. Garcia-Mata, E. I. Savenkov, A. G. Roberts, K. Oparka and J. M. Christie, *Proc. Natl. Acad. Sci. U. S. A.*, 2008, **105**, 20038–20043.
- 27 J. S. Biteen, M. A. Thompson, N. K. Tselentis, G. R. Bowman, L. Shapiro and W. E. Moerner, *Nat. Methods*, 2008, **5**, 947–949.
- 28 M. Stierl, P. Stumpf, D. Udvari, R. Gueta, R. Hagedorn, A. Losi, W. Gärtner, L. Petereit, M. Efetova, M. Schwarzel, T. G. Oertner, G. Nagel and P. Hegemann, *J. Biol. Chem.*, 2011, **286**, 1181–1188.

## **5. Characterization of the novel PAC protein mPAC**

### **5.1 A LOV domain-mediated, blue light-activated Adenylyl Cyclase from the cyanobacterium *Microcoleus chthonoplastes* PCC 7420**

Accepted. Proof version. Biochem. Journal, 4.8, 1. author

Sample generation and preparation: 100 %

Measurements: 50 %



# A LOV-domain-mediated blue-light-activated adenylate cyclase from the cyanobacterium *Microcoleus chthonoplastes* PCC 7420

Sarah RAFFELBERG<sup>\*1</sup>, Linzhu WANG<sup>†1</sup>, Shiqiang GAO<sup>†</sup>, Aba LOSI<sup>‡</sup>, Wolfgang GÄRTNER<sup>\*2</sup> and Georg NAGEL<sup>†2</sup>

<sup>\*</sup>Max-Planck Institute for Chemical Energy Conversion, Stiftstrasse 34-36, D-45470 Mülheim, Germany, <sup>†</sup>Botanik I, University of Würzburg, Julius-von-Sachs-Platz 2, D-97082

Würzburg, Germany, and <sup>‡</sup>Department of Physics and Earth Sciences, University of Parma, Parma, Italy

Genome screening of the cyanobacterium *Microcoleus chthonoplastes* PCC 7420 identified a gene encoding for a protein (483 amino acids, 54.2 kDa in size), characteristic for a BL (blue light)-regulated adenylate cyclase function. The photoreceptive part showed signatures of a LOV (light, oxygen, voltage) domain. The gene product, mPAC (*Microcoleus* photoactivated adenylate cyclase), exhibited the LOV-specific three-peaked absorption band ( $\lambda_{\text{max}} = 450$  nm) and underwent conversion into the photoadduct form ( $\lambda_{\text{max}} = 390$  nm) upon BL-irradiation. The lifetime for thermal recovery into the parent state was determined as 16 s at 20 °C (25 s at 11 °C). The adenylate cyclase function showed a constitutive activity (in the dark) that was *in-vitro*-amplified by a factor of 30 under BL-irradiation. Turnover of the purified protein at saturating light and pH 8 is estimated to 1

cAMP/mPAC per s at 25 °C (2 cAMP/mPAC per s at 35 °C). The lifetime of light-activated cAMP production after a BL flash was ~14 s at 20 °C. The temperature optimum was determined to 35 °C and the pH optimum to 8.0. The value for half-maximal activating light intensity is 6 W/m<sup>2</sup> (at 35 °C). A comparison of mPAC and the BLUF (BL using FAD) protein bPAC (*Beggiatoa* PAC), as purified proteins and expressed in *Xenopus laevis* oocytes, yielded higher constitutive activity for mPAC in the dark, but also when illuminated with BL.

**Key words:** adenylate cyclase, cAMP, cyclic nucleotide-gated channel, flavin photoreceptor, LOV (light, oxygen, voltage) domain, photoactivation.

## INTRODUCTION

Organisms adjust their lifestyle through the activity of various receptors that respond selectively to signals from the environment. Of particular importance are photoreceptors that, for many micro-organisms, turn out to be major players in modulation of physiological processes. This became evident from a recent survey of deposited genomes and metagenomes which revealed a particularly wide distribution of BL (blue light)-sensitive photoreceptors, being present in nearly one quarter of all screened genomes [1,2]. Sensing of BL is essential as this light quality can be harmful, as many photosensitizing compounds generating singlet oxygen and other ROS (reactive oxygen species) exhibit a strong absorption in the range between 400 and 450 nm. On the other hand, BL can drive photosynthesis and is used by DNA-repair enzymes (photolyases) [3].

Sensing of UV-A and BL is accomplished by three types of flavin-binding photoreceptors, each of which shows a different light-driven flavin photochemistry: cryptochromes (cry) with strong sequential and structural similarity to photolyases, incorporating non-covalently FAD [4], BLUF (BL-sensing using FAD) domain receptors [5] and the LOV (light, oxygen, voltage) domain proteins [6]. This latter class of BL-sensing receptors incorporates an FMN chromophore that, upon light absorption, becomes covalently bound to the protein via the thiol side chain of a cysteine residue. The lifetime of this 'photoadduct', being considered the signalling state of these photoreceptors, can vary from an outstandingly long period ( $t > 10\,000$  s, see e.g. [7] and

references cited therein) down to several seconds, after which time the covalent bond re-opens and the parent state is regenerated [8].

Light detection, signal generation and signal propagation is a multi-step process. In many cases the signalling property is performed through the light-induced initiation of an enzyme activity, fused to the light-sensing domain and thus making photoreceptors multidomain proteins. Bacterial photoreceptors exhibit quite a variety of signalling domains, among which (histidine) kinases, phosphodiesterases, adenylate cyclases and di-GMP cyclases, and DNA-binding domains are the most prominent ones [9]. In particular this type of activation by light, i.e. in a non-invasive manner, has brought photoreceptors into the focus of many scientists aiming at the regulation and detection of physiological processes in living cells or even in living animals [10,11]. Especially one class of signalling domains, the adenylate cyclases, has gained attention in cell biology, as their product molecule, cAMP, is an important second messenger also in cells of higher organisms. The usefulness of light-activated adenylate cyclases has been demonstrated for PAC (photoactivated adenylate cyclase) from the protist *Euglena gracilis*. This photoreceptor exhibits an  $\alpha\beta$ -dimeric arrangement with each of the monomers carrying in a tandem array two units of a BLUF domain fused to an adenylate cyclase function [12]. Light-regulated cAMP formation could be demonstrated in *Xenopus* oocytes and even in living animals [13]. However, the protein could so far only be purified from its natural source [12,14], and expression in *Escherichia coli* was only achieved for the BLUF domains, whereas full-length protein so far could not be purified

Abbreviations used: BL, blue light; BLUF, BL using FAD; bPAC, *Beggiatoa* photoactivated adenylate cyclase; CNG, cyclic nucleotide-gated; EuPAC, *E. gracilis* photoactivated adenylate cyclase; LOV, light, oxygen, voltage; mPAC, *Microcoleus* photoactivated adenylate cyclase; nPAC, *Naegleria gruberi* photoactivated adenylate cyclase; PAC, photoactivated adenylate cyclase; ST, streptavidin tag.

<sup>1</sup> These authors contributed equally to this work.

<sup>2</sup> Correspondence may be addressed to either of these authors (email wolfgang.gaertner@cec.mpg.de or nagel@uni-wuerzburg.de).

MNPSCEENEPNLFHGEASLQAFFDLSEALLCIRDSNGYFREINSVWEKTLGWTLDLRL  
SRPWLEFVHPDDVAFTFDMENQCHTLQDNKTPICLKNRFRCDGSYRWLSWRLGAY  
QNSVSHGIAHDVTESNWRGSQAYRKGVQETVKLRDQAIASSVGIVADARLPDMPLIY  
VNPAFEITGYSDAEVLGYNCRFLQGKDTSQPAVDQLRAAIKAGENCVTLLNRYKDGIT  
PFWNELTISPIYDDHNNLTHFVGIQSDISDRIKAEQALRLEQEKSERLLLNLKPKIVDQLK  
QFEGSLAQQFTEATILFADIVGFTQLSAQMSPLELLNLLNNIFSVFDKLAEKHGIEKIKTIG  
DAYMAVAGLPVANDHHAIAIANMALDMQQAIQQFKTPQGEFPQIRIGINTGLVVAGVIGI  
KKFSYDLWGDVAVNASRMESGLPGKIQVTAATKERLQDKYVFKEKRAIVVKKGKGEI  
NYWLVGKQE

PAS domain (1-127)

LOV domain (157-260)

Adenylyl Cyclase (AC) domain (302-483)

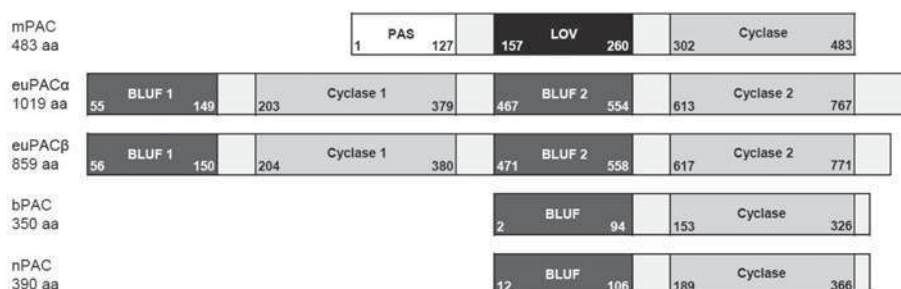


**Figure 1** Amino acid sequence and domain structure of mPAC

Top panel: amino acid sequence of mPAC. PAS domain, white background; LOV domain, black background; and cyclase domain, grey background. Bottom panel: schematic domain presentation of mPAC in comparison with established PACs, EuPAC $\alpha/\beta$  from *E. gracilis* [12] and bPAC from *Beggiatoa* [17], as well as nPAC from *N. gruberi* [20] for which PAC activity, so far, was not demonstrated.

from heterologous expression systems. When purified from *E. coli*, only the second BLUF domain (F2) binds FAD and seems functional as it shows a photocycle [15]. In addition, the active state of the full-length protein exhibits a short lifetime of less than 1 s, resulting in a need of high-light intensity for maximal activation [13,14]. A bacterial orthologue protein from the large sulfur bacterium *Beggiatoa* sp. could recently be presented as an alternative, as this bacterial protein (bPAC) exhibits only one BLUF domain per monomer and has a slow photocycle resulting in a low-light intensity requirement [16,17]. As bPAC is also smaller in size, it seems a more favourable tool for light-modulated (cAMP) control [17].

Ongoing research in this field yielded a novel combination of a BL-sensing receptor domain fused to an adenylate cyclase motif: the genome of the cyanobacterium *Microcoleus chthonoplastes* PCC 7420 (several listings use *Coleofasciculus chthonoplastes* instead of *M. chthonoplastes*) carries a gene encoding for two PAS domains (where the second PAS is an LOV domain) fused to an adenylate cyclase domain. The putative gene product (mPAC, locus ZP\_05024462.1) of 483 amino acids in size would add the LOV domains with their potentially favourable photochemical properties to the family of light-modulated adenylate cyclases (Figure 1). In the present paper we report on the generation and the photochemical and enzymatic characterization of this novel photoreceptor, demonstrating its light-induced enzymatic function *in vitro* upon bacterial expression, and also after expression in oocytes from *Xenopus laevis*.

## MATERIALS AND METHODS

### Cloning

*M. chthonoplastes* PCC 7420 (Taxonomy ID 118168) was grown under moderate stirring in ASN-III media [18] at 28 °C. Filtered air was supplied to the culture.

Genomic DNA was extracted using the mi-Bacterial Genomic DNA Isolation kit (Metabion), following the Gram-positive protocol according to the manufacturer's protocol. The gene (ZP\_05024462.1) was blunt-end cloned into the vector pJET1.2 using the CloneJET™ PCR Cloning kit (Fermentas); an NdeI restriction site was inserted at the 5'-end (GCCAGTG-CATATGAATCCTTCTTGTGAGGAGAATGAGCC, NdeI site underlined), and a SacI site was inserted at the 3'-end (GTTGGGAAGCAGGAGTAGCTCGAGCTC, SacI site underlined). These restriction sites were then used for cloning the gene into the expression vector pET28a (Novagen/Merck).

### Protein expression and purification

N-terminally His<sub>6</sub>-tagged mPAC was expressed in *E. coli* BL21 cells from the pET28a vector (Novagen/Merck). After IPTG induction (final concentration 0.5 mM) cells were grown for 48 h at 18 °C, gently stirred and supplied with filtered artificial air. The protein was purified via affinity chromatography on a Ni<sup>2+</sup> resin by imidazole elution (Clontech), and finally concentrated in Tris buffer [50 mM Tris, 200 mM NaCl and 5 % glycerol (pH = 8)].

### Spectroscopy

Steady-state absorbance was measured using a Shimadzu UV-2401PC UV–visible spectrophotometer; steady-state fluorescence measurements were performed with a Cary eclipse fluorescence spectrometer (Varian). Time-resolved fluorescence lifetime measurements were performed with a Fluorescence Lifetime Spectrometer FL920 (Edinburgh Instruments) using the F900 software provided by the manufacturer.

Steady-state irradiation in order to generate the photoadduct state and monitoring its thermal recovery was done with an LED ( $\lambda_{em} = 460 \pm 10$  nm, Zweibrüder) placed directly above the



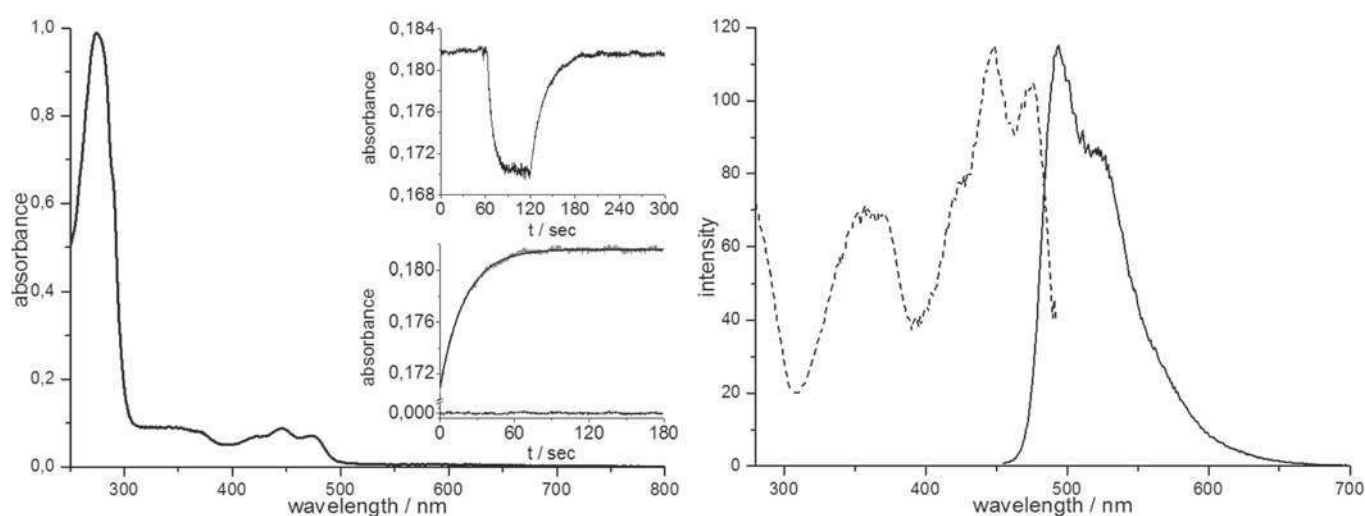


**Figure 2** Photochemical properties of mPAC

Left-hand panel: absorption spectrum of mPAC. Inset, top panel: photobleaching. Dark-state protein was illuminated for 60 s with BL (470 nm), leading to reduced absorbance of mPAC at 450 nm. Inset, bottom panel: recovery of absorbance at 450 nm after photobleaching is fitted by monoexponential function with  $t = 24$  s at  $14^\circ\text{C}$ . Right-hand panel: fluorescence spectra. Excitation (broken line) and emission (solid line) spectrum of mPAC.

cuvette within the spectrophotometer. Recovery to the parent state was then observed at 450 nm immediately after removing the light source at various temperatures (see the inset in Figure 2).

### cAMP immunoassay

The quantitative determination of cAMP in *Xenopus* oocytes and in the enzyme assay with purified recombinant protein was performed with a competitive immunoassay (Biotrend Total cAMP Enzyme Immunoassay kit). The mPAC-expressing oocytes were homogenized in 0.1 M HCl. Some oocytes were illuminated with intense BL (2 min, 455 nm,  $1\text{ mW/mm}^2$ ) before homogenization. For the calculation of the cAMP concentration, an oocyte volume of  $1\text{ }\mu\text{l}$  was assumed. The enzyme activity was assayed by incubation of  $5\text{ }\mu\text{l}$  (40 ng) of mPAC (purified from *E. coli*) in  $20\text{ }\mu\text{l}$  of an assay buffer [300 mM KCl, 50 mM Hepes-Tris (pH 8.0), 1 mM  $\text{MgCl}_2$  and 1% BSA] containing  $100\text{ }\mu\text{M}$  Mg-ATP. Experiments were performed at different well-controlled temperatures. The reaction mixture was either kept in darkness or irradiated for 2 min with BL (455 nm,  $1\text{ mW/mm}^2$ ) and was finally stopped by the addition of  $225\text{ }\mu\text{l}$  of 0.1 M HCl.

### Electrical measurements of adenylate cyclase activity

In TEVC (two-electrode voltage-clamp) experiments, mPAC was co-expressed with a CNG (cyclic nucleotide-gated) mutant channel (CNGA2-T537S, *Bos taurus* CNGA2) [19]. The oocytes were incubated for 3 days at  $17^\circ\text{C}$  in Ringer's (ORI) solution containing 100 mg/ml gentamycin. Irradiation of the oocytes was performed with a high power LED (LUXEON Emitter 1 W; royal blue, 455 nm) or a DPSS (diode-pumped solid-state) laser (473 nm). The light output near the oocyte was determined to  $3\text{ mW/mm}^2$ . Measurements were taken in oocyte Ringer's solution in which  $\text{CaCl}_2$  was substituted with  $2\text{ mM}$   $\text{BaCl}_2$ . Oocytes were clamped to a membrane potential of  $-20$  or  $-40\text{ mV}$ , with  $+10\text{ mV}$  pulses for conductance measurements. Currents were recorded for 60 s with the software CellWorks (NPI Electronic).

## RESULTS

### Photochemical properties of mPAC

The genome of the cyanobacterium *Microcoleus chthonoplastes* PCC 7420 carries a gene encoding a protein (54.2 kDa, 483 amino acids, genome locus ZP\_05024462), composed of three domains, a PAS, a LOV and a predicted adenylate cyclase function (Figure 1).

The putative LOV-domain-encoding part showed all signatures typical for bacterial LOV domains. The full-length gene was cloned and expressed with an N-terminal His<sub>6</sub>-tag in *E. coli* BL21 cells. The gene product, mPAC, displayed the LOV-domain-specific three-peaked absorption band ( $\lambda_{\text{max}} = 450\text{ nm}$ , Figure 2). The absorbance ratio  $A_{450/280}$  in Figure 2 indicated a 74.4% loading of chromophore in mPAC, based on a 450/280 ratio of 1:7.6 for a fully chromophore-assembled protein ( $\epsilon_{450} = 12500\text{ M}^{-1}\cdot\text{cm}^{-1}$ ,  $\epsilon_{280} = 95445\text{ M}^{-1}\cdot\text{cm}^{-1}$ ; calculation of the molar absorption coefficient was performed by the protparam tool of ExPASy; <http://web.expasy.org/protparam/>; the contribution of the flavin absorbance around 280 nm was taken into account). BL-irradiation caused conversion into the photoadduct form ( $\lambda_{\text{max}} = 390\text{ nm}$ ), which showed a lifetime for thermal recovery into the parent state of 16 s at  $20^\circ\text{C}$  (24 s at  $14^\circ\text{C}$ , inset in Figure 2). Also the fluorescence excitation and emission maxima ( $\lambda_{\text{exc}} = 445\text{ nm}$ ,  $\lambda_{\text{em}} = 500\text{ nm}$ ) are in full accordance with protein-bound FMN (Figure 2, right-hand panel).

### Enzymatic activity of mPAC, expressed in *Xenopus laevis* oocytes

The sequence of mPAC suggested light-regulated adenylate cyclase activity and the photochemical data confirmed a light response of the protein. All four previously described PACs are BLUF proteins; however, for only three of them (PAC $\alpha$  and PAC $\beta$  from *Euglena* [12,13] and bPAC from *Beggiatoa* [16,17]) photoactivated adenylate cyclase activity was shown, whereas it was only reported (results not shown) that nPAC (*Naegleria gruberi* PAC) "shows cAMP activity in oocytes and *in vitro*" [20]. To check for cyclase activity and to learn whether

**Table 1** PAC-mediated cAMP concentration in oocytes

D, cAMP was measured after 1 day of expression in the dark, following injection of 5 ng of RNA, coding for bPAC or mPAC. L, illumination with BL (455 nm) for 2 min increases cAMP dramatically.  $n = 2$  different batches, each with average value of four oocytes.

Treatment	bPAC ( $\mu$ M cAMP)	mPAC ( $\mu$ M cAMP)
D	$1.5 \pm 1.0$	$9 \pm 8$
L	$42 \pm 10$	$330 \pm 200$

light inhibits or activates the suspected activity, we expressed mPAC first in oocytes of *Xenopus laevis* and measured cAMP with an immunoassay. When RNA encoding mPAC (without any tag) was prepared *in vitro* and injected into oocytes, an increased cAMP concentration was detected already after 1 day of incubation in the dark. A further strong increase in cellular cAMP concentration was induced by illumination for 2 min with BL (Table 1). For comparison of mPAC with the light-activated adenylate cyclase bPAC [16,17], we expressed bPAC in the same batches of oocytes under the same conditions as mPAC (Table 1). For this comparison we injected 5 ng of RNA in each case which corresponded to  $\sim 30\%$  less mPAC than bPAC RNA molecules because of the longer amino acid chain of mPAC. Although we do not know the translation efficiency and stability against degradation of these two proteins we noted a strong difference in the cAMP concentrations obtained (see Table 1), which was partially reflected in the measured turnover of the purified enzymes (see below; Table 2b). The concentration of PAC-induced cAMP after 1 day of PAC expression in these oocytes was nearly 10-fold higher in mPAC-expressing than in bPAC-expressing oocytes, either without any illumination (D) or measured after 2 min of intense BL (L) (see Table 1). The L/D (light-to-dark activity) ratio for bPAC and mPAC therefore seemed similar in these *in vivo* experiments; however, in Table 1, D reflects activity during 24 h expression and cyclase activity in the dark, whereas L reflects activity after 24 h expression and cyclase activity during 2 min of illumination. Therefore an exact number for the light-to-dark activity ratio cannot be extracted from these data, also because *in vivo* cAMP assays are influenced by cellular phosphodiesterase activity.

We then tested the light-induced cAMP increase in oocytes by co-expression with a cAMP-sensitive cation channel (OLF/T537S from bovine olfactory organ), as was previously shown for PAC $\alpha$  and PAC $\beta$  from *Euglena gracilis* [18] and for bPAC [17]. A pronounced increase in inward current, maximal after 1 min, was observed upon a light flash in mPAC- and OLF/T537S-co-expressing oocytes (Figure 3). This light-induced channel activation was completely reversible, with a return to the basal level within 10 min.

#### Enzymatic activity of purified mPAC expressed in *E. coli*

Recombinant mPAC, purified from *E. coli* as described above, was measured for cAMP production in the dark and with 2 min of BL illumination at controlled temperature, light intensity and pH. The purified enzyme showed a strong pH-dependence with maximal activity at around pH 8.0 (Figure 4A). The activation by more alkaline pH is similar to the BLUF protein BlrP1, a bacterial light-regulated cyclic nucleotide phosphodiesterase, which is maximally active above pH 8 and at pH 9.3 no additional light activation is observed [6]. The temperature-dependence of light-activated adenylate cyclase activity exhibited a sharp peak

**Table 2** *In vitro* PAC assays

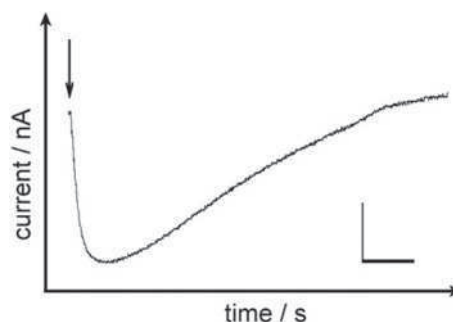
(a) Adenylate cyclase activities of two differently purified mPAC proteins, at 25 °C and at 35 °C, pH 8 and saturating light. His-mPAC, mPAC with N-terminal His<sub>6</sub> tag. ST-mPAC-ST, mPAC with N-terminal and C-terminal ST. D, activity in the dark; L, activity during 2 min of saturating BL. Both purified from *E. coli*. (b) Turnover comparison of purified bPAC and mPAC. Turnover of cAMP molecules per PAC molecule and time. bPAC-ST, bPAC with C-terminal ST, purified from *X. laevis* oocytes; ST-mPAC-ST = mPAC with N-terminal and C-terminal ST, purified from *E. coli*.

#### (a) Adenylate cyclase activity

Temperature Treatment	His-mPAC (nmol of cAMP/mg of protein per min)		ST-mPAC-ST (nmol of cAMP/mg of protein per min)	
	25 °C	35 °C	25 °C	35 °C
D	$20 \pm 15$	$40 \pm 20$	$30 \pm 20$	$60 \pm 30$
L	$0.6 \pm 0.4$	$1.2 \pm 0.6$	$1.0 \pm 0.6$	$1.8 \pm 0.8$

#### (b) Turnover

Treatment	bPAC-ST (40 kDa) (cAMP/s)	ST-mPAC-ST (55 kDa) (cAMP/s)
D	$0.0004 \pm 0.0002$	$0.03 \pm 0.02$
L	$0.13 \pm 0.07$	$0.9 \pm 0.6$

**Figure 3** CNG cation channels are activated by light-activation of mPAC

Time course of light-induced inward current by activation of a cAMP-sensitive cation channel, co-expressed with mPAC, in oocytes. A total of 1 ng of mPAC-RNA and 10 ng of OLF/T537S-RNA (for cGMP/cAMP-gated cation channel) were injected into *Xenopus* oocytes and expression was allowed for 3 days at 17 °C. Experimental conditions:  $-20$  mV holding potential and 1 s BL flash (indicated by arrow). Scale: 200 nA and 120 s.

for thermal stability with maximal activity at 35 °C (Figure 4B). Adenylate cyclase activity was dependent on light intensity with half-maximal activity at  $6 \mu\text{W}/\text{mm}^2$  ( $6 \text{ W}/\text{m}^2$ ) at 35 °C and pH 8 (Figure 4C).

The relatively high light sensitivity of mPAC most probably results from a light-activated mPAC intermediate with high cyclase activity which slowly relaxes to the less active 'dark state'. We therefore measured cAMP concentrations at different time points after a short light flash. Following a BL flash of 0.5 s, the concentration of cAMP rose in the dark with a time constant of  $\sim 14$  s at 20 °C (Figure 4D) and  $\sim 7$  s at 30 °C (results not shown). The slope of the fitted curve in Figure 4(D) is, of course, decaying with the same time constant of  $\sim 14$  s (broken line in Figure 4D), reflecting the decaying activity of the light-induced mPAC intermediate. This time constant is in good agreement with the determined photoadduct lifetime of 16 s at 20 °C (see above and Figure 2).

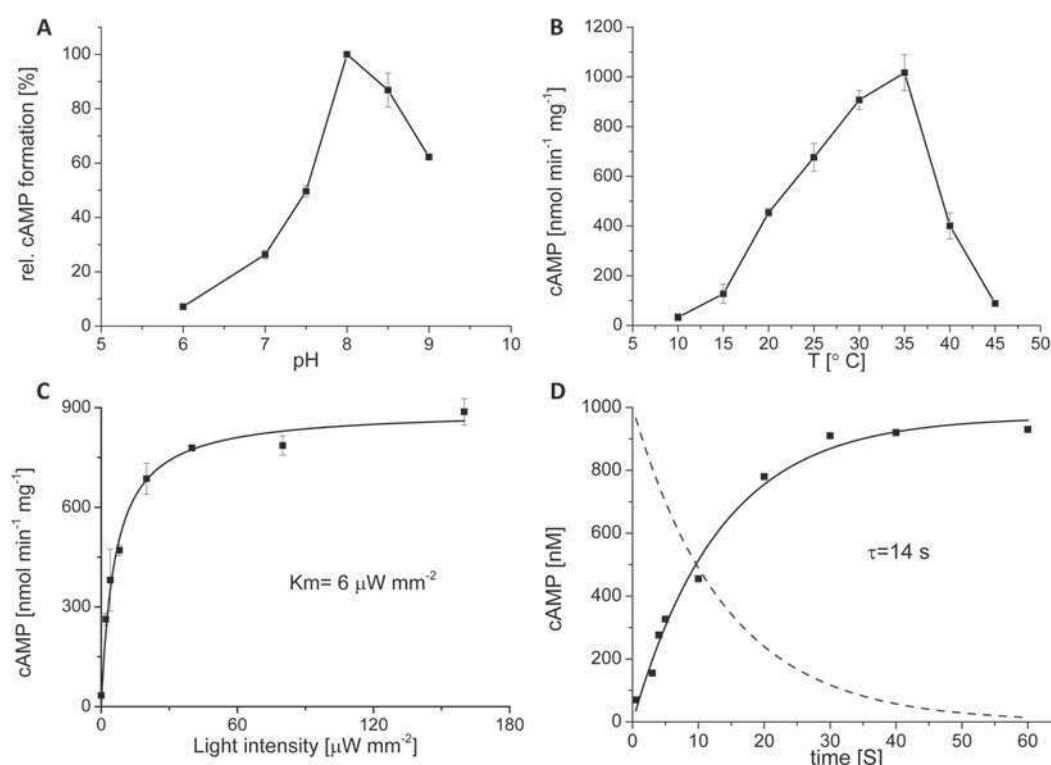


**Figure 4** Adenylate cyclase activity of His<sub>6</sub>-mPAC, purified from transgene *E. coli*

(A) pH-dependence of mPAC. Light-induced cAMP production (as a percentage, with 100 % for pH 8) at different pH values ( $n = 3$ ). (B) Temperature-dependence. Light-induced cAMP production of recombinant purified mPAC at different temperatures, saturating light and pH 8 ( $n = 2$ ). (C) Light-intensity-dependence. Light-induced cAMP production at different BL (455nm) intensities, applied for 2 min at pH 8 at 35 °C ( $n = 2$ ). (D) Life-time of active intermediate of PAC. Time course of cAMP production in the dark after a 0.5 s light flash. Fit (solid curve) to data at a temperature of 20 °C yielded a time constant of 14 s. The broken line shows the slope of the fit curve, obtained by differentiation, and represents the time course of the intermediate with increased cyclase activity.

The ratio of cAMP production in saturating light to cAMP production in the dark was determined to 30 at 20 °C (at pH 7 and pH 8). This rather low ratio is surprising considering the strong light-activated cAMP increase, measured in living cells (Table 1 and Figure 3).

The maximal specific activity of bPAC was previously reported as 10 nmol of cAMP/mg of protein per min at pH 7.4, 100 μM ATP and room temperature (??°C) [17] or as 57 nmol of cAMP/mg of protein per min at pH 8, saturating ATP (2 mM) and room temperature [16]. These values are much lower than the 600 nmol of cAMP/mg of protein per min that we found for His<sub>6</sub>-mPAC at pH 8, 80 μM ATP and 25 °C (Table 2a). An even higher activity of 1 μmol of cAMP/mg of protein per min was obtained with a ST-mPAC-ST (ST is streptavidin tag; N- and C-terminal ST tag on mPAC) construct (see Table 2b). The protein purified from *E. coli* in Stierl et al. [17] was actually a bPAC SUMO (small ubiquitin-related modifier) fusion construct whereas in Q6 Ryu et al. [16] a bPAC MBP-His<sub>6</sub> tag fusion construct was assayed.

For a better comparison, we also labelled bPAC with a C-terminal ST (bPAC-ST), expressed and purified it from oocytes which yielded now a much higher specific activity of 190 nmol of cAMP/mg of protein per min at pH 8, 25 °C and 80 μM ATP. With the ST-purified proteins, the two enzymes (bPAC-ST and ST-mPAC-ST) are more similar in their light-activated turnover; however, mPAC (~1 cAMP/mPAC per s at 25 °C) shows an approximately 7-fold higher turnover in the light than bPAC (Table 3).

## DISCUSSION

The BL-driven adenylate cyclase from the cyanobacterium *M. chthonoplastes* (mPAC) is the first member in this class of light-regulated cyclases carrying a LOV domain as a sensing/modulating unit. Formerly described PACs from the protist *E. gracilis* (EuPAC [12,13]), from *N. gruberi* (nPAC [20]) and from the large sulfur bacterium *Beggiatoa* sp. (bPAC [16,17]) all carry BLUF domains as regulatory units. Common to all of these enzymes is their regulatory sensing domain which in general makes such proteins suitable candidates for biotechnological applications, as BLUF and also LOV domains use ubiquitous flavin derivatives as chromophores. The LOV domain, as shown by many examples found in Nature, is more versatile with respect to fused signalling domains as, for example, LOV-coupled histidine kinases, di-GMP cyclases and helix-turn-helix motifs (enabled to bind to DNA in a light-dependent manner) have been described and functionally characterized. The larger overall number of identified LOV-domain-regulated photoreceptors and the greater variability of signalling domains found for LOV domains (in comparison with the BLUF manifold) might provide another advantage for mPAC, whereas a preliminary study of site-directed mutagenesis (S. Raffelberg, unpublished work) does not significantly alter the recovery lifetime, one might consider a complete swap of one LOV domain for another one with a long-lived photoadduct state. This might be even more favourable (again in comparison with BLUF domains), as a similar activation mechanism has been identified for several LOV domains, based



on a torque-generating movement of coiled-coil structures [21]. Alternatively, one might also consider an on- and off-reactivity initiated by light in long-lived LOV domains, as had just been demonstrated for YtvA from *B. subtilis* [22].

A comparison between the adenylate cyclases described so far reveals that mPAC is more similar to bPAC than to EuPAC as its photocycle is similarly slow ( $t = 10\text{--}20\text{ s}$ ) and therefore the light intensity for half-maximal activation can be kept low ( $\sim 6\text{ }\mu\text{W}/\text{mm}^2$ , for mPAC;  $\sim 4\text{ }\mu\text{W}/\text{mm}^2$  for bPAC [17]). EuPAC, however, shows a fast photocycle and therefore requires higher half-saturating light intensities [18]. Similar data are not yet available for the remaining PAC from *N. gruberi* (nPAC [20]).

In the present study we used the cloned DNA from the cyanobacterium *M. chthonoplastes* and expressed it for *in vivo* assays in oocytes of *X. laevis* or for *in vitro* assays, with His<sub>6</sub> or a ST attached, in *E. coli*. This approach is in contrast with the codon usage-optimized DNA, different for oocyte and *E. coli* expression in two previous studies on the BLUF protein bPAC [16,18]. When we compared the cyclase activity of purified mPAC and bPAC we found a pronouncedly increased activity of mPAC, both in the dark and in saturating BL (Table 3) which was also apparent from cAMP concentrations in mPAC- and bPAC-expressing oocytes (Table 1).

An interesting, yet not understood, difference in the cAMP synthesis of bPAC and mPAC appears when both enzymes are compared for their *in vitro* and *in vivo* activity: purified bPAC yields a strong light-activation in *in vitro* assays with an L/D ratio of 300 [17]. Under the same conditions, a value of 30 was determined for purified mPAC. However, this lower L/D activity was not obvious when cAMP concentrations were assayed in PAC-expressing oocytes. Under these conditions, mPAC reveals a stronger light-induced increase of cAMP concentration than bPAC, together with a similarly higher dark activity compared with bPAC (Table 1). Although no L/D ratio can be obtained from these *in vivo* data due to an inherent intracellular phosphodiesterase activity, the values in Table 1 suggest very similar L/D ratios for bPAC and mPAC. As most *in vitro* assays were performed at the optimum of pH 8, whereas oocyte cytoplasm is closer to pH 7, we determined the L/D ratio also at pH 7, again yielding a value of 30. Further tests will have to show whether substrate or product concentrations, redox potential, or binding of FMN or other cofactors are responsible for this enigma. We cannot exclude that purified mPAC molecules without bound FMN have higher activity in the dark than FMN-bound mPAC and/or are more abundant (than the estimated 25 %, see above) in our *in vitro* assay with purified protein than in the cytoplasm of oocytes. Both possibilities would decrease the apparent L/D ratio of purified mPAC protein.

Another difference between oocyte measurements and *in vitro* assays with recombinant protein from *E. coli* is the tag used for affinity purification of protein. In order to test for an effect of the routinely used His-tag, we repeated the *in vitro* activity assays with an ST-purified mPAC (ST-mPAC-ST) which showed a slightly increased activity, both in light and in the dark, but yielded again the same L/D ratio of 30. In the course of the present study we also re-evaluated the specific light-induced activity of purified bPAC protein (now purified with a C-terminal ST from oocytes) and found it to be approximately 20-fold more active than originally reported by us [17] and others [16]. But even this activity, with one molecule of cAMP produced by one molecule of light-activated bPAC every 8 s (at 25°C), seems low, as is the nearly 10-fold higher, but still low light-induced, turnover of mPAC (1 cAMP/mPAC per s at 25°C and 2 at 35°C). Further careful analysis of functional protein might lead to another re-evaluation of turnover numbers and possibly also of the L/D ratio of mPAC.

## AUTHOR CONTRIBUTION

Sarah Raffelberg, Linzhu Wang, Shiqiang Gao, Aba Losi, Wolfgang Gärtner, and Georg Nagel designed and performed the research and analysed the data. Wolfgang Gärtner and Georg Nagel wrote the first draft of the paper and all of the authors revised the paper and approved the final version to be published.

## ACKNOWLEDGEMENTS

We thank Elfriede Reisberg (University of Würzburg) for expert technical assistance.

## FUNDING

This work was supported by the Deutsche Forschungsgemeinschaft (DFG) [grant number FOR1279 (to G.N.)]. S.R. is a recipient of a Ph.D. grant from the Biostruct initiative of University of Düsseldorf, Germany.

## REFERENCES

- Krauss, U., Minh, B. Q., Losi, A., Gärtner, W., Eggert, T., von Haeseler, A. and Jaeger, K. E. (2009) Distribution and phylogeny of light-oxygen-voltage-blue-light-signaling proteins in the three kingdoms of life. *J. Bacteriol.* **191**, 7234–7242
- Losi, A. and Gärtner, W. (2012) The evolution of flavin-binding photoreceptors: an ancient chromophore serving trendy blue-light sensors. *Annu. Rev. Plant Biol.* **63**, 49–72
- Weber, S. (2005) Light-driven enzymatic catalysis of DNA repair: a review of recent biophysical studies on photolyase. *Biochim. Biophys. Acta* **1707**, 1–23
- Lin, C., Robertson, D. E., Ahmad, M., Raibekas, A. A., Jorns, M. S., Dutton, P. L. and Cashmore, A. R. (1995) Association of flavin adenine dinucleotide with the *Arabidopsis* blue light receptor CRY1. *Science* **269**, 968–970
- Gomelsky, M. and Klug, G. (2002) BLUF: a novel FAD-binding domain involved in sensory transduction in microorganisms. *Trends Biochem. Sci.* **27**, 497–500
- Christie, J. M., Salomon, M., Nozue, K., Wada, M. and Briggs, W. R. (1999) LOV (light, oxygen, or voltage) domains of the blue-light photoreceptor phototropin (nph1): binding sites for the chromophore flavin mononucleotide. *Proc. Natl. Acad. Sci. U.S.A.* **96**, 8779–8783
- Zoltowski, B. D. and Crane, B. R. (2008) Light activation of the LOV protein Vivid generates a rapidly exchanging dimer. *Biochemistry* **47**, 7012–7019
- Herrou, J. and Crosson, S. (2011) Function, structure, and mechanism of bacterial photosensory LOV proteins. *Nat. Rev. Microbiol.* **9**, 713–723
- Losi, A. and Gärtner, W. (2008) Bacterial bilin- and flavin-binding photoreceptors. *Photochem. Photobiol. Sci.* **7**, 1168–1178
- Deisseroth, K. (2011) Optogenetics. *Nat. Methods* **8**, 26–29
- Wu, Y. I., Frey, D., Lungu, O. I., Jaehrig, A., Schlichting, I., Kuhlman, B. and Hahn, K. M. (2009) A genetically encoded photoactivatable Rac controls the motility of living cells. *Nature* **461**, 104–108
- Iseki, M., Matsunaga, S., Murakami, A., Ohno, K., Shiga, K., Yoshida, K., Sugai, M., Takahashi, T., Hori, T. and Watanabe, M. (2002) A blue-light-activated adenylyl cyclase mediates photoavoidance in *Euglena gracilis*. *Nature* **415**, 1047–1051
- Schröder-Lang, S., Schwärzel, M., Seifert, R., Strücker, T., Kateriya, S., Looser, J., Watanabe, M., Kaupp, B., Hegemann, P. and Nagel, G. (2007) Fast manipulation of cellular cAMP level by light *in vivo*. *Nat. Methods* **4**, 39–42
- Yoshikawa, S., Suzuki, T., Watanabe, M. and Iseki, M. (2005) Kinetic analysis of the activation of photoactivated adenylyl cyclase (PAC), a blue light receptor for photomovements of *Euglena gracilis*. *Photochem. Photobiol. Sci.* **4**, 727–731
- Ito, S., Murakami, A., Sato, K., Nishina, Y., Shiga, K., Takahashi, T., Higashi, S., Iseki, M. and Watanabe, M. (2005) Photocycle features of heterologously expressed and assembled eukaryotic flavin-binding BLUF domains of photoactivated adenylyl cyclase (PAC), a blue-light receptor in *Euglena gracilis*. *Photochem. Photobiol. Sci.* **4**, 762–769
- Ryu, M. H., Moskvina, O. V., Siltberg-Liberles, J. and Gomelsky, M. (2010) Natural and engineered photoactivated nucleotidyl cyclases for optogenetic applications. *J. Biol. Chem.* **285**, 41501–41508
- Stierl, M., Stumpf, P., Udvari, D., Gueta, R., Hagedorn, R., Losi, A., Gärtner, W., Petereit, L., Efetova, M., Schwarzel, M. et al. (2011) Light-modulation of cellular cAMP by a small bacterial photoactivated adenylyl cyclase, bPAC, of the soil bacterium *Beggiatoa*. *J. Biol. Chem.* **286**, 1181–1188
- Rippka, R., Deruelles, J., Waterbury, J. B., Herdman, M. and Stanier, R. Y. (1979) Generic assignments, strain histories and properties of pure cultures of cyanobacteria. *J. Gen. Microbiol.* **111**, 1–61

- 
- 19 Altenhofen, W., Ludwig, J., Eismann, E., Kraus, W., Bönigk, W. and Kaupp, U. B. (1991) Control of ligand specificity in cyclic nucleotide-gated channels from rod photoreceptors and olfactory epithelium. *Proc. Natl. Acad. Sci. U.S.A.* **88**, 9868–9872
- 20 Penzkofer, A., Stierl, M., Hegemann, P. and Kateriya, S. (2011) Photodynamics of the BLUF domain containing soluble adenylyl cyclase (nPAC) from the amoeboid flagellate *Naegleria gruberi* NEG-M strain. *Chem. Phys.* **387**, 25–38
- 21 Möglich, A., Ayers, R. A. and Moffat, K. (2009) Design and signaling mechanism of light-regulated histidine kinases. *J. Mol. Biol.* **385**, 1433–1444
- 22 Losi, A., Gärtner, W., Raffelberg, S., Cella Zanacchi, F., Bianchini, P., Diaspro, A., Mandalari, C., Abbruzzetti, S. and Viappiani, C. (2013) A photochromic bacterial photoreceptor with potential for super-resolution microscopy. *Photochem. Photobiol. Sci.* **12**, 231–235
- 

Received 13 May 2013/19 August 2013; accepted 28 August 2013  
Published on the Internet 10 October 2013, doi:10.1042/BJ20130637

## 6. General Discussion

Photoreceptors have been studied for a long time. Starting from very basic observations, more and more photoreceptors could be identified and characterized in great detail. New techniques and methods were developed, yielding - in recent years - an exploding amount of information. Nowadays, in each photoreceptor family one or more proteins have emerged as well-characterized „model proteins“. Nevertheless, there are still several questions unanswered and new paradigms emerge, calling for an ongoing research in order to gain more information about chromophores, photocycles, and signal transduction. Photoreceptors combine ultrafast photophysics and photochemistry and extend their physiological activity into the ms-to-s time range. Therefore, photoreceptors are perfect proteins to investigate signal perception and transduction activity, as they can be easily and instantaneously triggered with short light pulses, the resulting signal activity can be observed by a many spectroscopic techniques, and their physiological function can be followed in living organisms <sup>141</sup>. Furthermore, the functional induction by light as a non-invasive technique gains more and more attention, as sophisticated applications based on photoreceptors are emerging.

Biomedical or biotechnological applications of photoreceptors, though fascinating, are still in their early stages. There is strong need to understand in detail these small proteins and present them as useful, manageable tools in biophysics, systems biology or medicine. Blue light photoreceptors are hereby of particular interest, as they host an endogenous flavin molecule as a chromophore. Moreover, the family of LOV photoreceptors contains small proteins that show a robust three-dimensional structure and a very broad variety of naturally occurring effector domains. These findings make them desirable tools to apply them for sophisticated experiments, e.g., in living cells <sup>142, 143, 144</sup>.

However, the premise of the way from mechanism to application is to provide detailed knowledge about how the photochemistry of a selected photoreceptor works and how it can be tuned in a way that it is applicable for further development of applications.

## 6.1 Influencing the mechanism

The publications “Modulation of the Photocycle of a LOV Domain Photoreceptor by the Hydrogen-Bonding Network” and “The amino acids surrounding the flavin 7a-methyl group determine the UVA spectral features of a LOV protein” (chapter 2) deal with the topic of the photocycle mechanism and how it can be influenced and altered. These investigations have been performed with the small blue light photoreceptor YtvA from *Bacillus subtilis*. The presented results prove that there are strong interactions and contacts between the chromophore and the protein and between various amino acids of the binding pocket.

Although the LOV paradigm is highly conserved, the photocycle itself is not a fixed process, as it is dictated by three facts. (i) The inherent photochemical and photophysical properties of the bound FMN <sup>70</sup>. Photochemical properties were extensively studied with inserted artificial chromophores <sup>145, 33, 146, 147, 148, 149</sup>. (ii) The influence of chemical parameters like pH or bases (e.g., imidazole <sup>72, 150</sup>). These latter factors accelerate the thermal dark recovery by several orders of magnitude; however, the interpretation of these reactivities is not clear. It is assumed that they work via steric stabilization of the ground state, direct base effects on position N5, changes in solvation of the active site, or interruption of the hydrogen bonding network around the chromophore <sup>72, 150</sup>. (iii) The third strongly modulating effect is accomplished via the protein microenvironment <sup>52, 76</sup>. Here, two mechanisms have been identified: on the one hand, several amino acids have been identified as “hot spots” influencing the protein stability, signal transduction and inter- and intra- protein interactions, and on the other hand, the entire surrounding protein microenvironment that is in direct contact to the chromophore, has been found to have a strong impact on the photocycle by effects of protein – chromophore interactions. Spectral and photochemical properties of the surrounding protein environment have been studied within the last years. Recently, phot1-LOV2 from *Avena sativa* has been investigated through a series of mutations, designed to alter steric restrictions in the vicinity of the 8 $\alpha$ -methyl group at the xylene side of the FMN cofactor <sup>76</sup>. The asparagine at position 425 is part of the A $\beta$ -B $\beta$  loop and stabilizes by interactions with the 8 $\alpha$ -methyl group the isoalloxazine ring into a precise conformation, thus stabilizing the cysteinyl-C(4a) adduct. The mutant N425C accelerates the recovery lifetime of the photoadduct from



48 s in the Asphot1-LOV2 wild type to 7.5 s. Another residue of Asphot1-LOV2 was investigated by Christie and co-workers<sup>52</sup>: they mutated I427 on strand B $\beta$  into a valine, resulting in a 2-fold slower formation and 10-fold faster decay of the photoadduct by removing the  $\delta$ -carbon of the isoleucine chain. This effect on the kinetics is not due to direct contact of Ile427 with FMN but is based on a van der Waals contact between a CH<sub>2</sub> group and the closeby located sulfur of the reactive cysteine. The mutations in *Arabidopsis thaliana* (At) phot1-LOV2 I403V and Asphot1-LOV2 I16V have been recently used to attain a very fast photocycle. These mutations accelerate the adduct decay rate by one order of magnitude, without altering the UV/Vis spectrum<sup>151, 52</sup>. Besides the faster recovery, these two mutations show a twofold decrease of the adduct formation rate. Both effects were assigned to a loss of steric support because of the absence of one CH<sub>2</sub> group in the amino acid side chain in the vicinity of the chromophore<sup>151</sup>.

Moreover, the LOV domain of YtvA from *B. subtilis* was studied by generating a double mutant I39V/F46H. Although both mutation sides are not in direct contact with the chromophore, the recovery time of the adduct is accelerated 75-fold (52 sec) compared to the wild type (3900 sec). Position F46 undergoes a light-induced flipping in its side chain, proposing that the protein is especially flexible in this region<sup>59</sup>.

### 6.1.1 The hydrogen bonding network

The directly surrounding protein microenvironment is built up by hydrogen bonds (HB) between side chains of the residues of the chromophore pocket and the chromophore itself. It has been demonstrated that the HB connecting the isoalloxazine ring to the protein is an important protein – chromophore interface that undergoes conformational changes upon illumination<sup>152, 153, 154, 31</sup>.

Moreover, these HB were identified to affect the photocycle regarding the kinetics, energetics and the efficiency of the individual photoreceptor steps<sup>61</sup>. Several studies performing mutations in the chromophore binding pocket have clearly demonstrated that the kinetics of the protein conversion are affected or structural changes can be induced<sup>155, 156, 157</sup>.

#### Direct influence of the HB network on the photochemistry

The effects of seven mutations are presented in the publication “Modulation of the Photocycle of a LOV Domain Photoreceptor by the Hydrogen-Bonding Network” in chapter 2 aiming to characterize the energetic properties of an altered YtvA. The paper “The amino acids surrounding the flavin 7a-methyl group determine the UVA spectral features of a LOV protein” completes this approach to modify the hydrogen bonding network by extending the investigation onto two mutations at position Q66. The focus of this work is directed to the HB network between N(5), C(4)=O, N(3)H and C(2)=O and the isoalloxazine ring of the FMN chromophore of YtvA, involving the polar, uncharged residues Q66, N94, N104 and Q123, as shown in fig. 6-1.

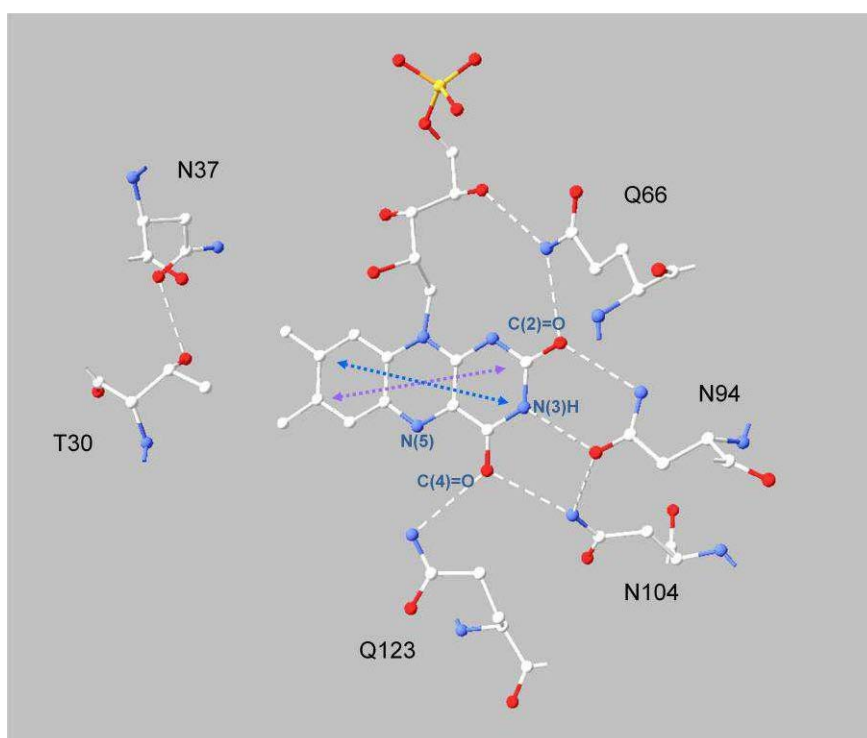


**Figure 6-1: HB network stabilizing the FMN chromophore in YtvA.** Residues taken part at the HB network, Q66, N94, N104 and Q123, are shown, as well as the neighbored residues T30 and N37. T30 and N94 are in direction of the dipole moment (represented by arrows) of the FMN.

Advanced infrared spectroscopic techniques have revealed that the hydrogen bonds at these positions undergo band shifts during blue light exposure<sup>158, 154, 151</sup>, and upon adduct formation the hydrogen bonds to both carbonyl groups of the chromophore are weakened<sup>159, 158, 160</sup>. Following these spectroscopic evidences, the network of hydrogen bonds was probed by mutagenesis to be a major player in chromophore stability and energetics of the photochemistry. For this, the four amino acids that mostly contribute to the HB network were mutated.

The glutamine nearby the chromophore (Q123 in YtvA) was investigated on Asphot1-LOV2 (Q513N) before, showing a strong effect to the thermal recovery kinetics (37 sec instead of 68 sec of the wt)<sup>156</sup>. This is in agreement to the corresponding mutation in YtvA that accelerated 85-times the dark state recovery (compared to YtvA WT). As furthermore a high energy content of the photoadduct (224 kJ/mol) and a lower activation energy for the thermal recovery (62 kJ/mol) was determined, these findings are clear proof that a mutation of the glutamine into an asparagine destabilizes the covalent photoadduct. Not only the recovery reaction is influenced by this mutation, flash photolysis measurements revealed that also the forward

photochemistry is affected to some extent as the triplet lifetime is shortened (1.6  $\mu$ s) and the quantum yield is lowered (0.22). However, wt-YtvA has a triplet lifetime of 2  $\mu$ s and a photocycle quantum yield of 0.49.

The positions N94 and N104 are the main components of the HB network by forming three HB to the isoalloxazine ring of FMN and thereby stabilizing the chromophore. Whereas alanine and serine mutations at residue N94 strongly accelerate the recovery kinetics at 20 °C, the same insertions at position N104 reduce the activation enthalpy and entropy drastically, e.g., the enthalpy from 101 kJ/mol for wt-YtvA to 65 kJ/mol for N104A. However, the effect on the kinetics (3-fold decrease of recovery time) is not that strong like in N94A/S with a 44-fold and 20-fold acceleration, respectively. Position Q66, described in the publication “The amino acids surrounding the flavin 7a-methyl group determine the UVA spectral features of a LOV protein”, was mutated into four different variants, but only in Q66K and Q66H were sufficiently chromophore-loaded to perform further measurements. Both mutants show a longer triplet life time compared to wt-YtvA and are in accordance with alanine and serine mutations at positions N94 and N104.

Whereas the mutation Q66K does not yield any further outstanding data, Q66H showed a remarkably low fluorescence yield (0.08 compared to 0.16 of wt-YtvA) and a very fast fluorescence lifetime (1.3 ns compared to 2.1 ns of wt-YtvA), leading to the assumption that the histidine causes a quenching of the flavin triplet state, potentially via transient electron transfer.

Regarding the thermal recovery, several mutants, shown in table 5-1, significantly accelerate the photocycle. Taking the energetics data from LIOAS measurements into account (table 5-1), a connection between a faster dark recovery and more favourable energetics, i.e., a smaller activation enthalpy or higher activation entropy can easily be drawn.

**Table 6-1: recovery kinetics (20 °C) and energetic data of wt-YtvA and mutants.**

Highlighted in blue: wt-YtvA; highlighted in yellow: mutants with higher activation energy, entropy and enthalpy values than wt-YtvA.

	$t_{\text{rec},20^\circ/\text{s}}$	$E_a/\text{kJ mol}^{-1}$	$\Delta H^\#/\text{kJ mol}^{-1}$	$\Delta S^\#/\text{kJ mol}^{-1}\text{K}^{-1}$
YtvA-N104D	6890	115	112	+0.066
YtvA-WT	6240	104	101	+0.031
YtvA-T30V/N37C	5260	62	60	-0.110
YtvA-T30V	4280	75	72	-0.067
YtvA-N37C	3300	63	60	-0.10
YtvA-Q66K	2510	95	92	+0.006
YtvA-N104A	2250	67	65	-0.09
YtvA-T30A	1690	82	80	-0.034
YtvA-Q66H	1650	86	83	-0.022
YtvA-T30S	1625	68	65	-0.082
YtvA-N37F	1470	90	87	-0.008
YtvA-N94D	1250	151	148	+0.20
YtvA-N104S	1120	78	76	-0.043
YtvA-N37V	930	49	76	-0.033
YtvA-R63K	485	70	68	-0.065
YtvA-N94S	300	103	100	+0.05
YtvA-N94A	140	117	115	+0.10
YtvA-Q123N	72	65	62	-0.067

Nearly all mutants have lower activation entropies and enthalpies combined with a faster recovery kinetics compared to the wild type of YtvA (highlighted in blue). Four mutants, highlighted in yellow, show higher activation energy, entropy and enthalpy values, only the mutation N104D decelerates the  $\tau_{\text{rec}}$ . Interestingly, the other three mutants are all at position N94 and significantly accelerate the recovery kinetics. It can thus be assumed that position 94 has the greatest impact on the protein and its photocycle.

## Signal transduction

Besides investigations on the light-induced reactivities of the chromophore, the link between chromophore – protein interactions and signal transduction was studied in greater detail. Thus, an extension into the study of inter-domain interactions was performed.

For such an approach, one has to keep in mind that several amino acid residues were already identified as being involved in the HB network to contribute to inter-domain signal transduction in YtvA. One important residue, E105 was studied in detail<sup>161, 162</sup>. E105 is a direct neighbour of N104 (discussed above), being located within the central  $\beta$ -sheet of the LOV core. In this thesis, the position N104 is mutated into alanine and serine. These mutations cause a disruption of the HB towards the C(4)=O carbonyl group of FMN, and thereby a lower activation energy results. The same effect was observed for the “switching glutamine”, when converted into Q123N. As the rotation (“switching”) of the amide group in Q123 was identified during the dark- to lit state conversion<sup>153</sup>, it is assumed that this rotation might be impaired by the mutation.

Results of the investigated N94 mutants, such as a faster photocycle and a higher entropy value, lead to the proposal that the HB-rearrangement is one of the major rate-limiting steps during thermal recovery as well as a major determinant for triplet formation and decay, and in addition, being paramount for the signal transduction process. Interestingly, N94 is on the G $\beta$  strand that was until now not suggested for being important for signal transduction. The salt bridge between E56 and K97, both residues in close vicinity to Q66 and N94, is localized at the surface of the LOV core, in the D $\alpha$  and G $\beta$  strand, respectively. Recently, it could be demonstrated that the salt bridge stabilizes the chromophore binding pocket and regulates the kinetics of the photocycle, but it has a minor role in stabilizing the overall protein structure and transmitting conformational changes<sup>162</sup>.

### 6.1.2 Shifts of absorption bands

As outlined above, many aspects of LOV-based photoreceptors have been intensively investigated. A property that only recently came into closer focus is the UVA spectral region. Evidences were reported that irradiation with ultraviolet light (exciting this UVA  $S_2$  state) instead of blue light ( $S_1$  transition) results in a lower quantum yield of photoadduct formation<sup>58, 163</sup>. As, in relation to this, detailed characterization of the spectral UVA region is necessary for further nanoscopy applications based on the photochromicity of LOV domains, a better understanding of this phenomenon was intended, also aiming at a way to modify the spectral properties of LOV domains. The data set of the HB variants identified some mutants with shifted absorption spectra. Spectroscopic analysis of inserting an aspartic acid at position N94 yielded two effects: first, a red-shift in the UVA absorption band in N94D (6 nm, fig. 6-2), giving experimental proof to the assumption of Climent and co-workers that the transition dipole is oriented toward the C(2)=O bond<sup>164</sup>. A similar red-shift was already published by Salomon et al. for the wild type protein Asphot1-LOV2 when compared to the LOV1 domain of the same protein<sup>53</sup>. These authors assumed a weaker HB at this position. Second, the transition I band is slightly blue shifted in N94D. This blue shift was also observed in mutant N104D.

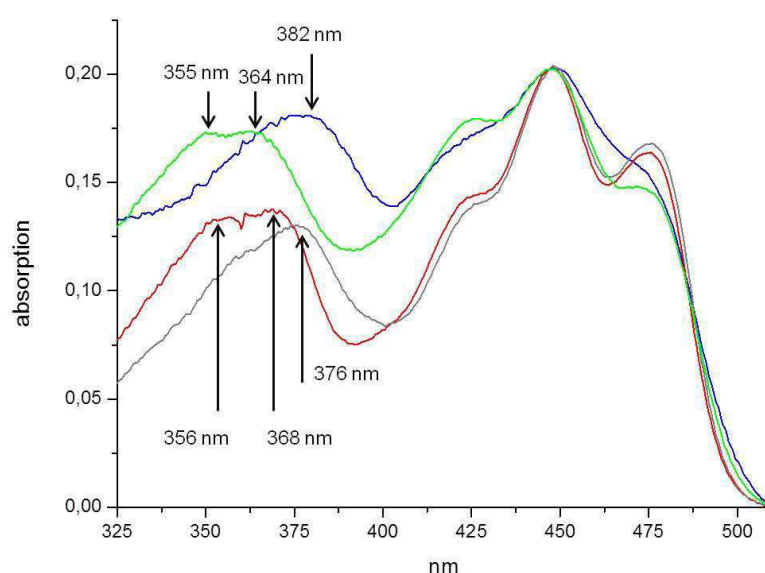


**Figure 6-2: shifts in the transition II region of YtvA mutants.** grey: wt-YtvA, red: YtvA-T30A, green: YtvA-N94A, blue: YtvA-N94D. Maxima are indicated by arrows.



Insertion of an alanine at position N94 leads to a remarkable blue shift of 12 nm compared to the wt-YtvA absorption in the UVA region (transition II, fig. 6-2), in contrast to the 6 nm red shift in N94D compared to the wild type. In total, there is a gap of 18 nm between the maxima of these two mutants, offering the possibility of exciting these mutants with different wavelengths in future applications.

The publication “The amino acids surrounding the flavin 7a-methyl group determine the UVA spectral features of a LOV protein” presents mutations of the possible tuner positions T30 and N37 (both positions being in close vicinity to the hydrophobic phenyl ring site of FMN), which do not affect transition I bands but have significant influence on the transition II region. Surprisingly, the largest alterations (~ 5 nm) are caused by substituting T30 with an apolar residue (A, V), whereas mutations of N37 yield only minor effects of the UVA region. The blue shift of T30A/V is similar to that of N94A, changing the wild type UVA peak carrying a small shoulder (WT- $\lambda_{\text{max}}$ = 375/359 nm) into two separated peaks ( $\lambda_{\text{max}}$ = 368 and 356 nm; fig 6-2). The strong effects that these mutations generate can be well understood, as both residues are directly in line with the transition dipole moment (fig. 6-1).

The effects obtained from mutating asparagine 37 have been reported for other LOV domains before. This position is equivalent to position N425 from AsLOV2 studied by Brosi et al. in 2010 <sup>76</sup>. These investigations revealed that the N425C variant showed a 7-fold longer thermal recovery reaction time compared to the wild type. This finding is in contrast to the here presented YtvA N37C mutant with a 50 % shorter recovery time. Not to speak of N37F/V, which are even faster in their recovery. Zoltowski et al. had reported on mutations on position T83 in VIVID from *Neurospora crassa*, which is at the equivalent position to YtvA-N37 <sup>72</sup>. VIVID T83V has some effect on  $\tau_{\text{rec}}$ , but it was not been further inspected by these authors.

## 6.2 Structure of YtvA

The elucidation of protein structures contributes a large step forward to the understanding of photoreceptors providing the basis for investigations of three issues, namely intra-protein arrangement, inter-protein arrangement and conformational changes upon light activation. These three issues are strongly connected.

### Inter-protein arrangement

The field of inter-protein arrangement refers to the relative orientation of the protein molecules. The question whether LOV proteins are monomeric or dimeric is discussed since several years as well as the question about which residues take part in inter-protein signal transduction. LOV domains behave different in their dimerization states, e.g. phototropin LOV2. Phot2-LOV2 was postulated being monomeric, as well as Phot1-LOV2. However, recent SAXS measurements give evidence that the latter one is dimeric <sup>165</sup>.

Buttani et al. <sup>62</sup> studied the dimerization states of YtvA by size-exclusion chromatography. In solution, YtvA-LOV mostly occurs as a dimer, including the N-terminal cap in front of the LOV domain. *In vitro* investigations of the full-length protein showed a larger heterogeneity between the three dimerization states: dimeric, elongated monomeric and spherical monomeric. The authors assumed that the C-terminal domain, in YtvA a STAS domain, reduces the dimerization tendency, as the same surface or amino acid residues are involved in homodimerization and interdomain interactions between the STAS and LOV domain. In 2008 Marles-Wright and co-workers assumed that the functionally active form of YtvA *in vivo* is dimeric, as they had investigated the RsbR paralogs, to which YtvA belongs, forming the  $\sigma^B$  stressosome <sup>166</sup>. Avila Perez confirmed this assumption by mutagenesis experiments <sup>63</sup>. In this study the acidic residues E105 and D109 of YtvA, both located in the H $\beta$  strand of the LOV domain, build intermolecular contacts in YtvA's dimeric state and are involved in signal transduction <sup>63, 65</sup>.

How come that one protein can be found in different oligomeric states? A hint is given by the phototropins Asphot1 and the fungal VVD protein. Dimer formation in solution,

where the molecules can move freely, seems to be a very dynamic process, as Asphot1 and VVD undergo reversible, light-dependent dimerization *in vivo*<sup>167, 55</sup>.

### Intra-protein arrangement

Within the YtvA dimer, the relative orientation of the LOV and STAS domain to each other remains unclear, as only a full-length structure can safely answer this question. The two domains of YtvA, the LOV and the STAS domain, functionally interact through hydrogen bonds but also the helical linker seems to play a major role in folding the full-length YtvA<sup>63</sup>. Within the LOV-LOV dimer, a coiled coil structure with an involved  $\beta$ -scaffold surface has been proposed<sup>168</sup>. However, as Buttani et al. found out that in YtvA the same  $\beta$ -scaffold surface is used for homodimerization and for interdomain interactions, the coiled coil assumption for the full-length protein is probably not valid anymore, but still for the LOV-LOV dimer.

### Conformational changes

High-resolution crystal structures offer molecular insights into the photoprocess upon illumination. One of the first LOV domain structures could be obtained from *Chlamydomonas reinhardtii* and *Adiantum capillus-veneris*<sup>22, 153, 152</sup>. Small conformational changes during light exposure were detected but only in the direct protein microenvironment of the chromophore. From these data it could not be derived how the light signal is transmitted from the sensor towards the effector domain<sup>31</sup>.

The group of Kevin Gardner worked on AsLOV2 and identified a small  $\alpha$ -helix, J $\alpha$ , that is involved in the photoprocess. In this LOV protein class, the linker J $\alpha$  unfolds from the LOV core upon blue light exposure and was presumed to be an essential part in signal transduction<sup>51, 169</sup>. On the other hand, the importance of the linker during the signal transduction could not be confirmed so far for the LOV kinases<sup>170</sup>.

Up to now, several three-dimensional structures of LOV proteins have been published, like *Adiantum capillus-veneris* phy3<sup>22</sup>, *Avena sativa* phot1<sup>196</sup>, *Chlamydomonas reinhardtii* phot1-LOV1<sup>152</sup> and *Neurospora crassa* Vivid<sup>197</sup>. YtvA was also a desired object for 3D-structures, but up to now, only a truncated YtvA-LOV protein could be crystallized and X-ray diffracted<sup>31, 80</sup>. Möglich et al. provided

structures of both the dark and the lit state. A comparison of both states yielded no change of the global folding pattern and no gross structural changes.

A problem of isolated domains is the loss of the full-length character of the protein, giving single modules the opportunity to behave different, by, e.g., adapting a different folding. This aspect is essential for all the three issues discussed above. Therefore, it is important to identify a full-length structure of the blue light sensitive YtvA, either by classical crystallization, NMR studies or Electron Paramagnetic Resonance (EPR) studies with site directed spin labels. The most recent information of a YtvA LOV-LOV model in a full-length protein is published by Diensthuber et al. (2013) who studied the crystal structure of the hybrid protein YF1 (fig. 6-3), which carries the LOV domain of YtvA as a sensor domain <sup>79</sup>.

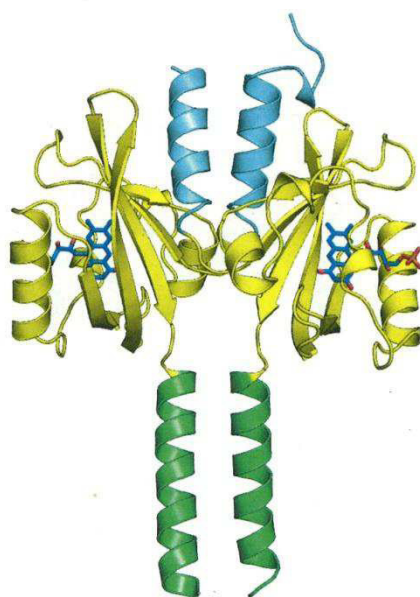


**Figure 6-3: structure of C-terminally truncated LOV domain dimers from YF1 <sup>79</sup>.** Blue: N-terminal helices; yellow: LOV cores with blue-coloured FMN chromophore; green: C-terminal linkers.

In this thesis, a three-dimensional structure prediction of YtvA is presented, including the N-terminal cap and the C-terminal STAS domain. These data were obtained by site directed spin labelling EPR, as this method yields inter-protein distances over a wide spatial range and offers information on a protein's flexibility and dynamics <sup>171</sup>. The procedure of introducing site directed spin labels is widely accepted and proven for many protein systems <sup>172, 173</sup>. The spin label was inserted into the protein by using MTSSL (fig. 6-4), which binds covalently to the SH-groups of inserted cysteines.

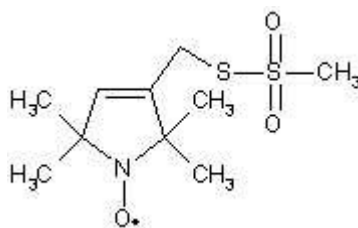


**Figure 6-4: chemical structure of MTSSL (C<sub>10</sub>H<sub>18</sub>NO<sub>3</sub>S<sub>2</sub>)**

This procedure allows insertion of single labels (probing potential dimeric structures), or double/multiple labels that would then yield distances within a monomeric unit. The yield of labelling in this work was > 95 % with only a small amount of free spin labels. The five investigated mutants are listed in table 6-2 and revealed, based on modelling, a full-length protein model of YtvA.

**Table 6-2: mutants generated and labelled for ENDOR-EPR**

mutant	mutation	label
1	T117C	single
2	T179C	single
3	T80C/T179C	double
4	T54C/T179C	double
5	C62A	none

The results of ELDOR-EPR measurements support the idea of a full-length dimer of YtvA as it was published recently<sup>63, 174</sup>. Within this dimer, the mono-labelled positions 117 and 179 are at a distance of 4.13 nm and 4.87 nm, respectively.

Combining all spin-label results, a structural model of the dimer can be presented. The LOV-LOV structure of YtvA was investigated already in several other investigations<sup>79</sup>. These authors showed an LOV-LOV arrangement, similar to that of YtvA from *Bacillus amyloliqueformens*<sup>80</sup>, with the two N-terminal helices of the dimer folded into in the space between the  $\beta$ -scaffold. Their results are in very good agreement with the data presented in this thesis.

A model of the STAS-STAS interface was obtained by measurements of the label mobility and relaxation rates. Both doubly labelled mutants 3 and 4 (tab. 6-2) revealed the basic data for aligning the STAS structure in relation to the LOV dimer. Data can be seen in chapter 3.

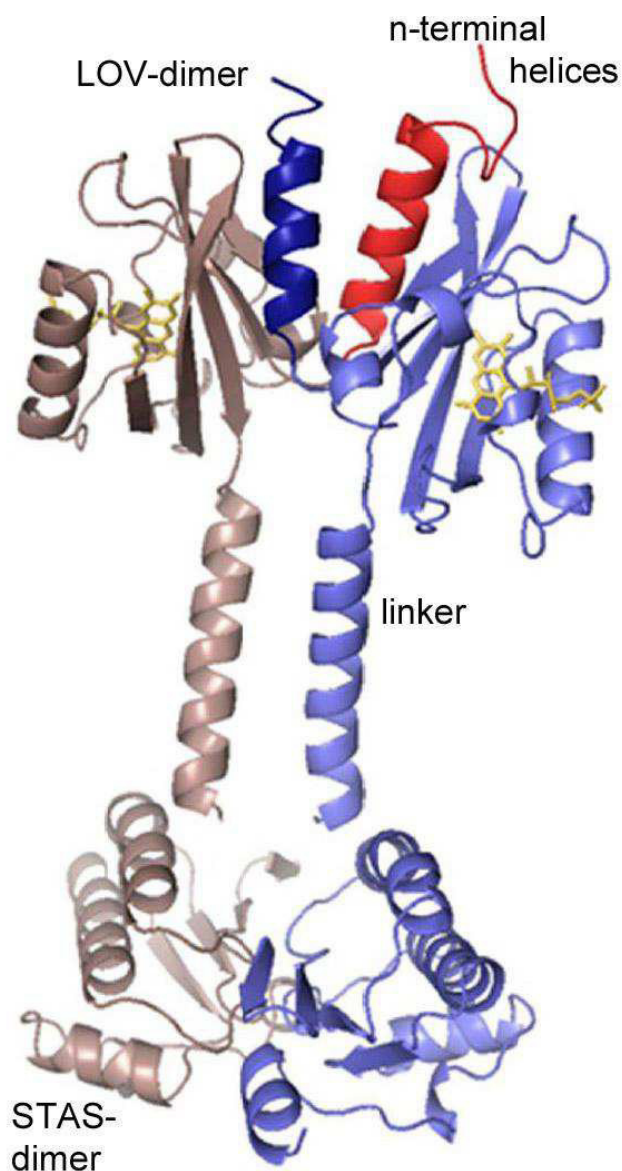


**Figure 6-5: structural model of full-length YtvA based on ENDOR-EPR data.** Model was calculated based on site-directed spin labelling mutants, measured with ENDOR-EPR. N-terminal helices are highlighted in red and dark blue, the FMN chromophore is coloured in yellow. Five residues between the linker and the STAS domain are not included as no data exists on their conformation.

The large distance between the two mono-labels at position 179 (mutant 2) within the dimer leads to the assumption that this position is pointing outwards from the STAS-STAS dimer. Cw and pulsed EPR data present a highly immobile label at position T179C in contrast to MMM simulations. This difference is based on the fact that the only available structural information can be derived from a homology model. Immobile label data together with relaxation times result in the STAS-STAS dimer model, shown in fig. 6-6.



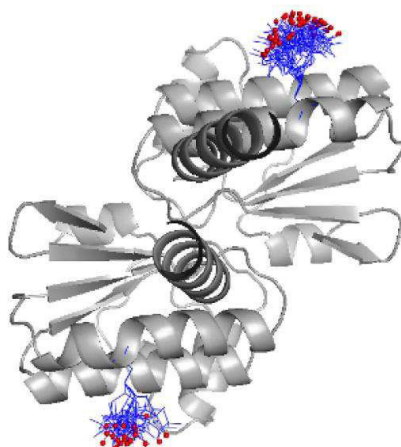


**Figure 6-6: STAS-STAS dimer of YtvA.** Model structure derived from docking simulations with the allowed conformers of the two labels at T179C as derived from MtsslWizard. Highlighted in blue: the two mono-labels at position 179. The two dark helices in the middle represent the linker peptides.

The resulting full-length structure of two homodimers linked by two coiled J $\alpha$  helices are in good agreement with recently published SAXS and NMR data <sup>174</sup>. This full-length structure of YtvA represents another step towards the understanding of LOV photoreceptors, as it brings together conformational changes upon irradiation with functional aspects.

As ongoing research, crystallization attempts of the dark state of YtvA wild type and different mutants were performed, all as full-length proteins. As an intermediary result small microcrystals could be obtained from the mutants T30V-N37C, T30V and T30S (fig. 6-7), while growing with 0.1 M HEPES pH 7.5, 0.15 M Na-acetate, 26 % PEG 3000 and 0.1 M Tris pH 8.5, 0.2 M Li<sub>2</sub>SO<sub>4</sub>, 25 % PEG 400, respectively. Crystals will be used for x-ray diffraction of the structure (Raffelberg et al., unpublished data).

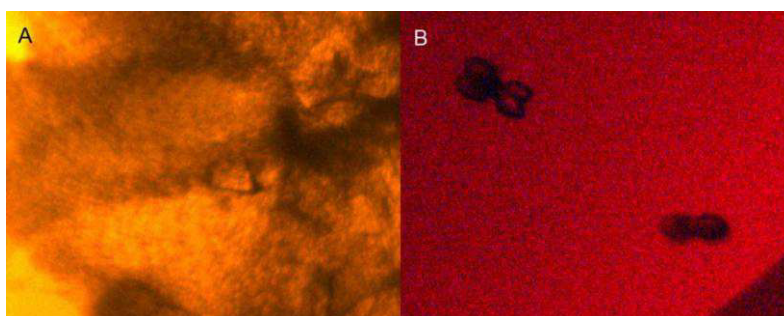


**Figure 6-7: microcrystals of (A) T30V and (B) T30S.** Red color occurs from dark state protection light and microscope filters. Crystallizing conditions for A) T30V: 0.1 M HEPES pH 7.5, 0.15 M Na-acetate, 26 % PEG 3000; B) T30S: 0.1 M Tris pH 8.5, 0.2 M Li<sub>2</sub>SO<sub>4</sub>, 25 % PEG 400

### 6.3 Nanoscopy

In recent years, photoreceptors turned from being the main target of fundamental research to a novel, but still small part in advanced applications. Research of applications include engineering suitable proteins and, in addition, expressing them selectively in desired cell organelles <sup>175</sup>. Up to now two major directions of application have been developed: first, light-dependent control of biological processes, called optogenetics and second physical applications like high-resolution fluorescence microscopy, called nanoscopy. The majority of optogenetics applications is based on the various channelrhodopsins; the here discussed examples, however, are directed to, e.g., light regulated gene expression <sup>176</sup> or second messenger production within cells via light. This kind of application has been discussed in detail in chapter 5.4 in this thesis.

Physical applications like fluorescence tagging (using photoreceptors as the counterparts to the various GFP derivatives) and nanoscopy are currently the most promising applications. Nanoscopy is based on stochastic activation of single fluorescent molecules resulting in a high resolution picture of a cell <sup>177, 178</sup>. With this method it is now possible to study biological material like living cells in a three-dimensional manner with much higher spatial resolution than obtainable with the “classical” fluorescence microscope that is limited by roughly half the wavelength of the excitation light (Abbe’s law) <sup>179, 180</sup>. To push this method forward, generation of a toolkit of novel, bright and photoswitchable fluorescent proteins for single molecule detection deep within scattering biological samples is absolutely urgent.

Within the large world of photoreceptors blue light sensitive flavoproteins containing a LOV or BLUF domain are favourable as they offer a very small size of less than approximately 140 amino acids and they utilize flavin chromophores that are ubiquitous in cells. Another advantage of LOV domains is their bright green fluorescence from their dark state (LOV<sub>447</sub>) that vanishes when the photoreceptor is turned into the lit state (LOV<sub>390</sub>) upon illumination. As the LOV<sub>390</sub> state is the biologically active state with no fluorescence and the LOV<sub>447</sub> state shows fluorescence but no biological activity, one can use this principle for designing a fluorescence reporter protein. A fluorescence reporter protein works under the

premise  $\text{LOV}_{447} = \text{Fluo}_{\text{ON}}\text{Bio}_{\text{OFF}}$  and vice versa  $\text{LOV}_{390} = \text{Fluo}_{\text{OFF}}\text{Bio}_{\text{ON}}$ <sup>181</sup>. First studies in cells have been made with mutated LOV proteins with an interrupted photocycle by an alanine or serine insertion at its conserved, reactive cysteine position<sup>44</sup>. This construct, however, shows a constitutive fluorescence and no biological activity.

The publication “A photochromic bacterial photoreceptor with potential for super-resolution microscopy” in chapter 4 is based on the small, blue light sensitive photoreceptor YtvA from *Bacillus subtilis* that was tested for the first time with nanoscopy. The protein was expressed in *E. coli* cells, which were tested with Fluorescence Lifetime Imaging Microscopy (FLIM) and Fluorescence PhotoActivation Localization Microscopy (FPALM) (fig. 6-8). The most important result of the investigations done in the framework of this study is the proof-of-principle which demonstrates that the blue light-detecting YtvA is suitable for nanoscopy applications. Fluorescence of the  $\text{LOV}_{447}$  state of the proteins could be detected and, compared with conventional fluorescence microscopy, this method offers high resolution imaging of single fluorescent molecules; compared to classical fluorescence microscopy, the resolution could be improved by nearly one order of magnitude.

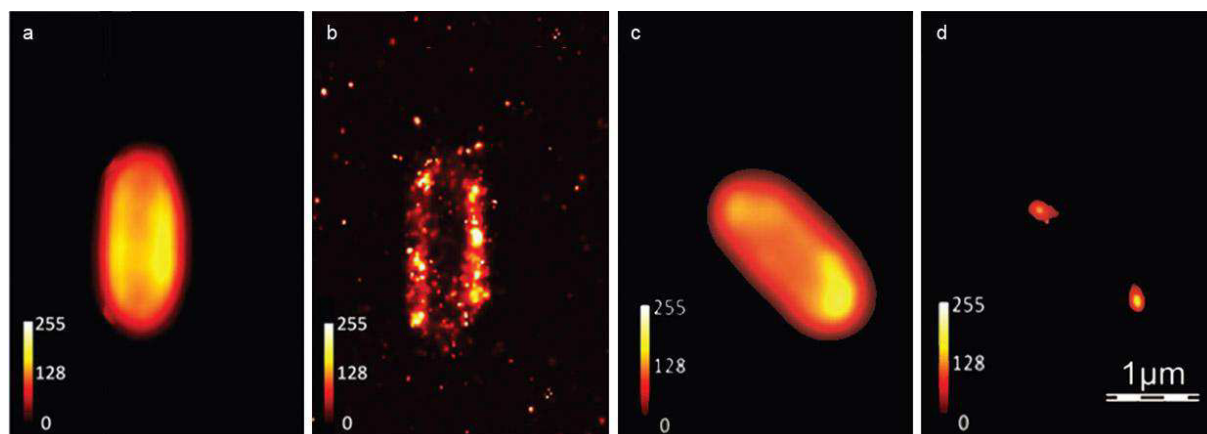


**Figure 6-8: comparison between conventional fluorescence and super-resolution imaging.** Super-resolution imaging of *E. coli* over-expressing wild-type YtvA, a) conventional image obtained by adding the total signal from all the frames and (b) super-resolution (FPALM) image of an *E. coli* cell. Photoactivation localization microscopy experiments have been carried out with a 405 nm activation laser and a 488 nm readout laser continuously running; c) conventional image; d) Fluorescence lifetime imaging (FLIM) with two-photon excitation of *E. coli* cell.

With this specific glow of a single Fluo<sub>ON</sub>Bio<sub>OFF</sub> molecule a precise localisation of the photoreceptors or fluorescence reporter proteins within a cell is possible. By using this principle, it is possible to capture the complete set of fluorescent molecules within a cell by an overlay of distinct pictures (fig. 6-9). In each picture several distinct molecules blink. This effect is a great advantage over the traditional fluorescence microscopy, which can just detect if a cell is fluorescent but not where in this cell the fluorescent molecule is located.

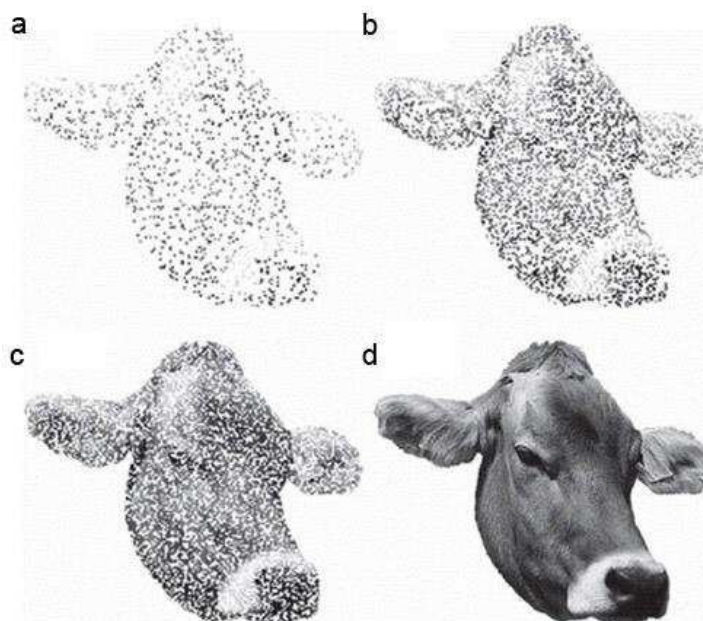


**Figure 6-9: principle of blinking effect.** a) some, distinct molecules blink by first laser shot illumination; b) and c) more laser shot illuminated images are accumulated; d) full picture is created by an overlay of the single snapshots.

The effect is based on the proof-of-principle of photoswitchability for the photoreceptor YtvA. The process of photoswitchability describes photoconversion of excited light sensitive domains, like LOV<sub>390</sub>, back into their dark state, LOV<sub>447</sub>, by illumination with specific light qualities. Hints for photoconversion of a LOV domain by UV light were reported several years ago<sup>182, 71</sup>, but remained relatively unnoticed, and this phenomenon was not further investigated. This photochemical effect can move forward a broad range of applications by making them to some extent independent from the thermal recovery time of the used photoreceptors. By this, it would offer a bidirectional control of the functionality of photoreceptors<sup>69</sup>. In this thesis two wavelengths could be identified, the UV light 356 nm and violet 405 nm, to convert back and forth the excited blue light photoreceptor YtvA, YtvA<sub>390</sub>, back into its ground state, YtvA<sub>447</sub>. Thereby, a photoequilibrium could be established with a clearly

identifiable amount of YtvA molecules in their dark state formed by the photoconversion. This amount is independent from the initial solution, dark or light stated molecules, it just depends on the illumination with 356 nm or 405 nm light that triggers both, a forward and a reverse photoreaction but to different extend.

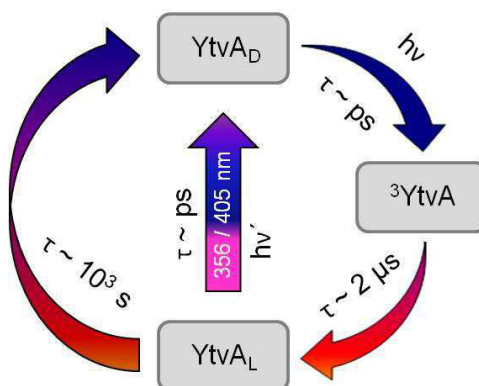


**Figure 6-10: schematic photocycle of YtvA.** Arrows are shown in the colour of the photocycle step (blue light for illumination, red excited triplet state, UV / near UV light for back conversion). Lifetimes are given for each step.

As figure 6-10 demonstrates, the 356 nm / 405 nm photoconversion takes place within picoseconds, making YtvA a fluorescence reporter with properties comparable to GFP. GFP from the jellyfish *Aequorea victoria* have become the most popular fluorescence *in vivo* reporters in biology<sup>183, 184, 185</sup>. However, due to the slow maturation of GFPs (min – hours) and their significant environmental drawbacks (e.g., dependence on oxygen for chromophore maturation), new alternatives were wanted<sup>186</sup>. In contrast, fluorescent LOV proteins (FMN-binding fluorescent proteins; FbFP) offer, due to their fast folding kinetics and immediately cofactor loading, a rapid fluorescence-active conformation. Their lack of a high fluorescence yield can be overcome by mutating the conserved cysteine (like in YtvA) into a constitutive alanine mutant<sup>44</sup>.

Compared to GFP derivatives, YtvA is beneficial as a fluorescence reporter as the protein is clearly more stable in mechanical and photochemical terms. This feature is quite important as for an accumulated blinking picture of a biological sample more than 10000 cycles of excitation and re-photoconversion are required.

This study demonstrated that LOV proteins, here YtvA, are suitable candidates to broaden the toolkit of photoreceptor applications with focus on super-resolution

microscopy. Moreover, the photoswitchability will make the LOV domains an outstanding, favourable group of photoreceptors, offering many various ways for advanced applications in nanoscopy and optogenetics.

## 6.4 mPAC

One of the currently most wanted methods in research is optogenetics. The identification of channelrhodopsins and their first applications in neuronal cells for a non-invasive manipulation of cellular processes by regulating ion channels were a milestone in photoreceptor research and the rising of optogenetics and were honoured as the method of the year 2010.

Besides neurobiological applications of photoreceptors, scientific community was aiming for further light-sensitive proteins catalyzing second messengers like cAMP, cGMP,  $\text{Ca}^{2+}$  or inositol triphosphate, that are small enough to be used in classical experimental systems and make use of ubiquitous chromophores <sup>24</sup>. The field of optogenetics deals with optical control of cellular parameters like cAMP generated by light sensitive proteins and thereby brings the “old” field of photoreceptor research to the next generation.

cAMP (3',5'-cyclic AMP) is one of the most important ubiquitous second messengers in cells and is therefore an allosteric part of the signal cascade within cells. It can be found in nearly every organism in all kingdoms of life. Depending on the organism, cAMP controls a variety of physiological functions like displaying the stress caused by outer environmental signals. This second messenger thereby regulates the carbon metabolism, virulence, biofilm formation <sup>187</sup>, but also the movement of flagella. Besides being important for intracellular processes, cAMP is for some organisms also important for intercellular processes like communication between the amoeba *Dictyostelium* with other conspecifics. Similar as in lower organisms, cAMP plays a central role also in cells of higher organisms.

The synthesis of cAMP is performed by adenylyl cyclases (AC). Their function is the catalysis of converting ATP into cAMP and pyrophosphate under the involvement of



divalent cations like  $Mg^{2+}$  within this enzymatic process. These ACs consist of a cyclase homology domain (CHD, app. 150 residues long) with several conserved residues in their active sides that provide functional and structural features of an AC. Based on these structural properties, six distinct classes of ACs could be identified so far. The best known is the class AC-III, which is wide spread in eukaryotes and prokaryotes.

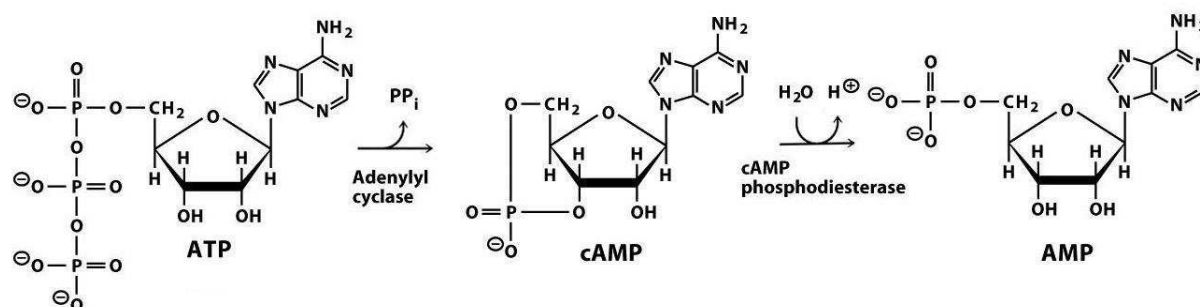


**Figure 6-11: cAMP synthesis from ATP and hydrolysis to AMP** <sup>188</sup>.

Formed by ACs, cAMP has a characteristically short life time as cytosolic cAMP phosphodiesterases hydrolyse the second messenger to adenosine monophosphate (AMP). This short half life time ensures a relatively low basal cAMP level in cells, an aspect being important for an adequate increase of cAMP during concentration dependent enzymatic regulation within cells.

In 2002, Iseki et al. isolated the first photoactivated adenylyl cyclase (PAC) out of the photosynthetic protist *Euglena gracilis*. The gene product euPAC is heterotetrameric with an  $\alpha\beta$ -dimeric arrangement, consisting of four soluble homolog subunits: two euPAC $\alpha$  (105 kDa) and two smaller euPAC $\beta$  (90 kDa) <sup>104</sup>. Each euPAC subunit contains two blue light sensitive BLUF domains that alternate with two AC as effector domains. The protein has a low basal cAMP level, which is increased 80-fold by light. As a physiological function of euPAC a positive and negative phototaxis could be identified and it is assumed that this protein regulates the flagella movement in *Euglena gracilis* <sup>189</sup>.

The first bacterial PAC was identified in the sulfide-oxidizing soil bacterium *Beggiatoa* <sup>24</sup> that can switch between aerobic and anaerobic sulphur oxidation by utilizing oxygen or nitrate, respectively, as electron acceptors. This photosensitive AC was denoted bPAC, a protein consisting of an N-terminal BLUF domain connected to a C-

terminal cyclase domain by a linker sequence that is approximately 50 residues long. The entire length of the protein is about 350 amino acids.

A recently discovered PAC is nPAC (390 aa) from the widespread free-living soil and freshwater amoeba-flagellate *Naegleria gruberi*, an organisms that runs through three life cycle stages, ranging from cyst to flagellate and amoeba<sup>190, 191</sup>. The genome of this organism contains more than 100 potentially cyclase-encoding genes, four of them being fused to BLUF domains and only one of them has been characterized and published so far<sup>192</sup>. Enzymatic data of nPAC are not yet published (Stierl, M. unpublished data). Photochemical and enzymatic properties of these so far known PACs are discussed below together with the new protein mPAC.

The blue light sensitive protein mPAC studied in this thesis is from the cosmopolitan cyanobacterium *Microcoleus chthonoplastes* PCC 7420. This protein (483 residues in length) is characterized for the first time in the publication “A LOV domain-mediated, blue light-activated Adenylyl Cyclase from the cyanobacterium *Microcoleus chthonoplastes* PCC 7420”. The data set comprises spectroscopical measurements as well as activity measurements of the cyclase domain within *Xenopus* oocytes. The first remarkable property of mPAC is its LOV domain in its sensory N-terminal part. The other three PACs that were known so far (listed above) all carry a BLUF domain as a sensor domain. Spectroscopic investigations of mPAC revealed absorbance ( $\lambda_{\text{max}} = 450 \text{ nm}$ ) and fluorescence spectra ( $\lambda_{\text{exc}} = 445 \text{ nm}$ ,  $\lambda_{\text{em}} = 500 \text{ nm}$ ) typical for LOV domains.

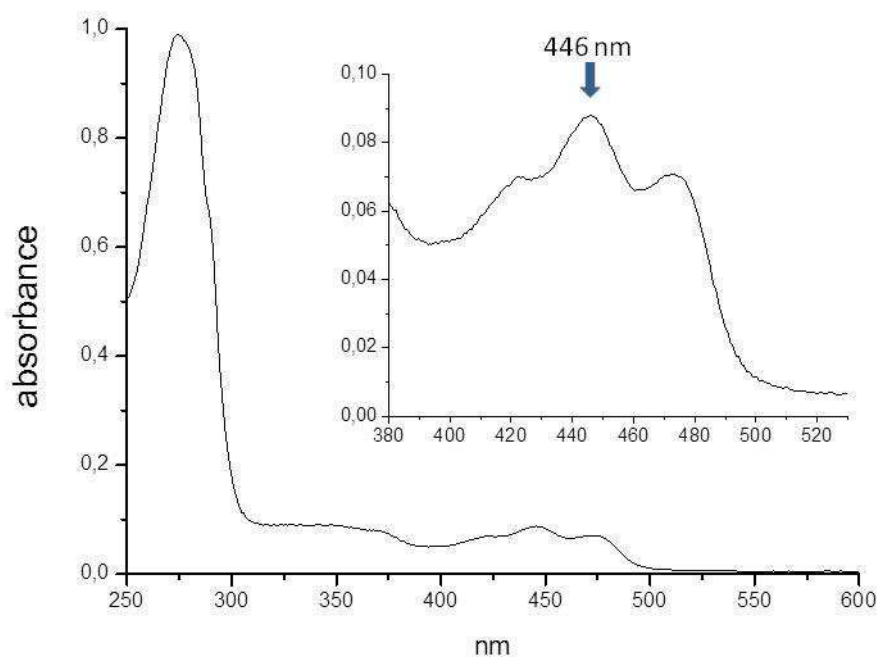


**Figure 6-12: absorption spectra of dark state mPAC.** The region of the FMN chromophore is zoomed in to show the maxima at 446 nm.

Observing the thermal recovery of mPAC reveals an unexpected short lifetime of 16 s at 20 °C and accordingly 25 s at 11 °C. The photocycle is reproducible over many times without any chromophore loss.

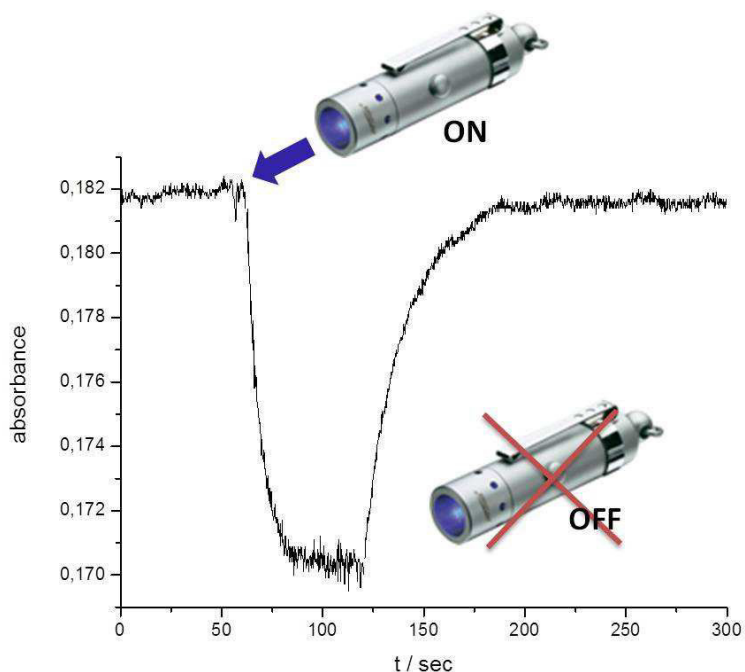


**Figure 6-13: kinetics of mPAC.** Dark state mPAC was illuminated for 60 sec with a 460 nm LED lenser; after bleaching the protein the light was turned off and thermal recovery at 20 °C could be observed with a lifetime of 16 sec.

Searching for reasons for this very fast recovery kinetics within the sequence of mPAC, one finds two specifics. i) The neighbored residues A162 and M169 (T30 and N37 in YtvA) are in close vicinity to the chromophore (fig. 6-14) and can therefore be expected to influence the kinetics and energetics of the photocycle. An alanine at this position can also be found in other LOV domains like in *Chlamydomonas reinhardtii* (Cr) phot-LOV1 (fig. 6-14). The methionine at the position 169 is outstanding in LOV domains and might induce a steric hinderance of the FMN binding. Initial, unpublished data of an mPAC-M169C mutant, comparable to Crphot-LOV1, revealed slower recovery kinetics but still it remains a fast process.

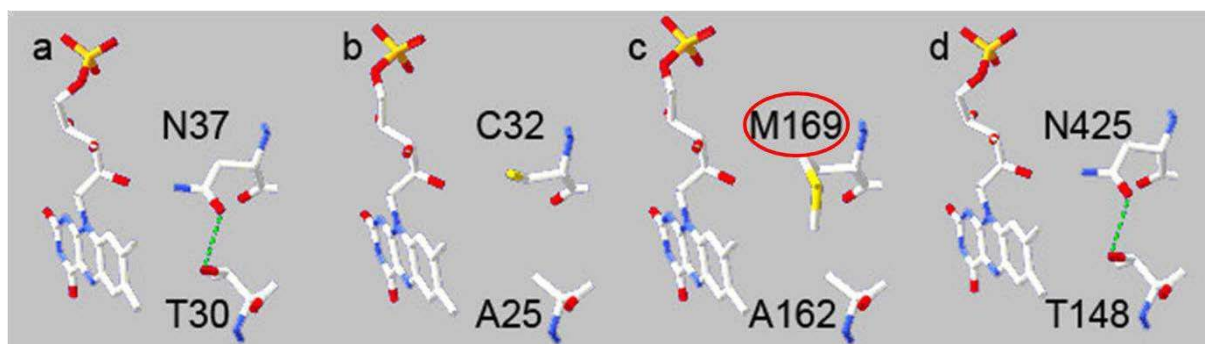


**Figure 6-14: comparison of mPAC residues A162 and M169 to other LOV domains.** a) *Bacillus subtilis* YtvA-LOV, b) *Chlamydomonas reinhardtii* phot-LOV1, c) *Microcoleus chthonoplastes* mPAC LOV, d) *Avena sativa* phot1-LOV2. Highlighted in red is the outstanding M169 of mPAC.

ii) In front of the light sensing LOV domain, mPAC carries an additional PAS domain (fig. 6-15) showing no typical signature for light sensing features. PAS domain are known to be responsible for dimer formation, so it can be assumed that this additional PAS domain stabilizes the protein, maybe by dimer formation, and accelerates the photocycle. The domain architecture of mPAC and the other four light sensing AC proteins can be seen in figure 6-15.

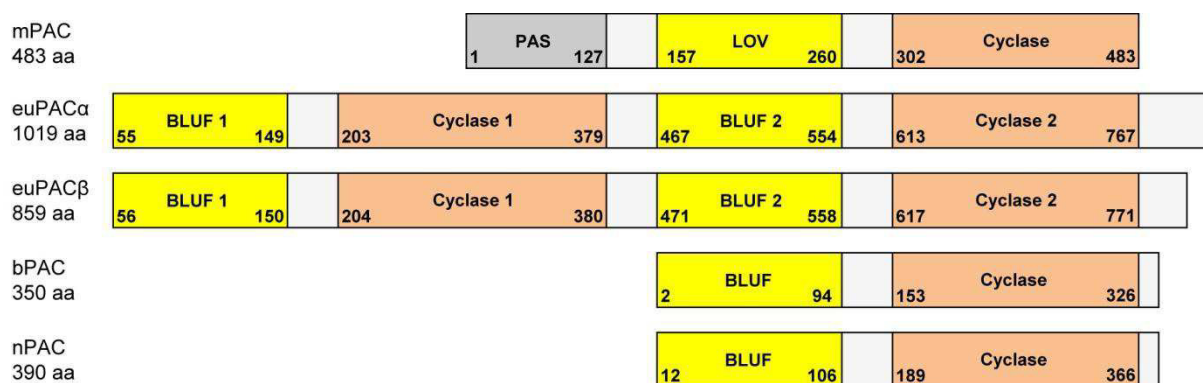


**Figure 6-15: domain alignment of known PAC proteins.** mPAC from *Microcoleus chthonoplastes*, euPAC $\alpha$  and euPAC $\beta$  from *Euglena gracilis*, bPAC from *Beggiatoa* and nPAC from *Naegleria gruberi*. Light sensing domains (LOV and BLUF) are marked in yellow, cyclase domains in orange and the additional PAS domain of mPAC in grey. Small numbers within the domains identify first and last residues of the domains.

A preliminary activity test of the enzymatic function of the cyclase was done by incubation of two isolated and purified mPAC protein samples with 150  $\mu$ M ATP and AMP at 25 °C illuminated with blue light and in the dark, respectively. After 0, 30 and 60 min aliquots were taken, heat inactivated and purified from the degraded protein

by centrifugation with an AMICON 10 kDa device. The amount of ATP and cAMP were detected by HPLC measurements.

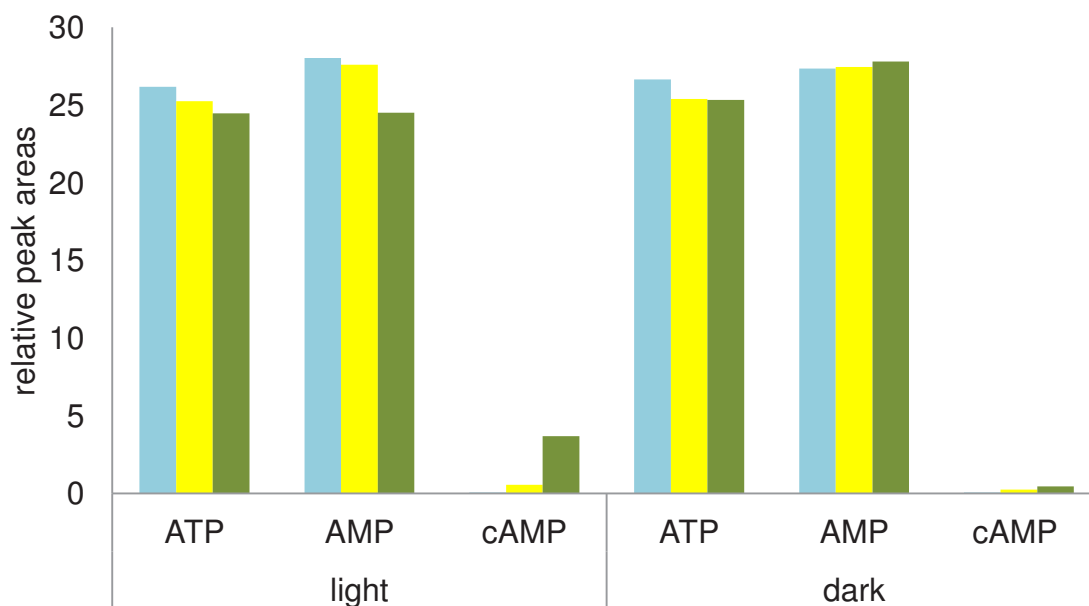


**Figure 6-16: activity assay of mPAC with ATP to cAMP conversion.** Bars represent the calculated relative peak areas measured with HPLC, blue: sample taken at  $t = 0$  min, yellow:  $t = 30$  min, green:  $t = 60$  min. Experiments were done in parallel in light and dark at 25 °C.

Formation of cAMP could be clearly detected in light conditions and gave hints on the activity of the cyclase. Therefore, the purified protein was measured for cAMP production in the dark and with two minutes of blue light illumination at controlled parameters. With these measurements the pH optimum (pH 8.0), light intensity (6 W/m<sup>2</sup>) and temperature maxima (35 °C) of mPAC could be determined. After a short (0.5 s) light flash, cAMP production lasts for about 14 s at 20 °C before the protein relaxes back into the ground state. These data are in good accordance to the determined photoproduct lifetime (fig. 6-13).

Further activation tests were made in cooperation with Georg Nagel, University of Würzburg, Germany. The enzymatic activity of mPAC, expressed in *Xenopus laevis* oocytes, was measured with an immuno assay. For this method, the RNA encoding mPAC (without any tag) was prepared *in-vitro* and injected into oocytes, causing an increased cAMP level after one day of incubation in the dark. A two-minute-exposure with blue light further increased significantly the cAMP level. These measurements together with other tests published in the paper “A LOV domain-mediated, blue light-activated Adenylyl Cyclase from the cyanobacterium *Microcoleus chthonoplastes* PCC 7420” demonstrate a relatively high basal activity of mPAC that is further



increased by blue light illumination. A comparison between the four kinds of PACs (euPAC, bPAC, nPAC and the here identified, most recent mPAC, Table 6-3) highlights the most relevant functional parameters.

**Table 6-3: comparison of four PAC proteins.** mPAC from *Microcoleus chthonoplastes*, euPAC $\alpha$  and euPAC $\beta$  from *Euglena gracilis*, bPAC from *Beggiatoa* and nPAC from *Naegleria gruberi*. n.g.: not given.

	euPAC	bPAC	nPAC	mPAC	
light saturation of AC activity	> 2.8 $\mu$ W/mm	3.7 $\mu$ W/mm	n.g.	6 $\mu$ W/mm	
light / dark ratio of cAMP production	80	> 100	80	30	
period of activity after light flash	< 0.1 s	23 s	n.g.	14 s	
maximal specific activity	3.5 pmol/min/mg	10 nmol/min/mg	313 nmol/min/mg	600 nmol/min/mg	1 $\mu$ M/min/mg
assay conditions	100 $\mu$ M ATP, [PAC] n.g., pH 7.5, 2.8 $\mu$ W/mm	100 $\mu$ M ATP, SUMO-bPAC, pH 7.4, 2.8 $\mu$ W/mm	n.g.	100 $\mu$ M ATP, pH 8.0, His6-mPAC	100 $\mu$ M ATP, pH 8.0, Strep-mPAC-Strep
light induced CNG currents in <i>Xenopus</i> oocysts					
activation	< 0.2 s	< 0.5 s	10 s	60 sec	
deactivation	4 s	300 s	50 s	600 sec	

The here discussed mPAC is not the smallest of the four proteins, but with a total length of ~ 480 aa it offers a convenient handling in most of the common cell systems. mPAC carries, preceding the LOV domain, an additional PAS domain (1 - 127 residues), which is proposed to be non-involved in photochemistry and cyclase activity of the protein, also shown by preliminary results (Raffelberg et al., unpublished data). By abandoning this domain, the mPAC protein would be ~ 320 residues in length and therefore the smallest PAC known so far.

Prokaryotic type III cyclases often form homodimers. Stierl et al. already suggested, that this oligomeric state of bPAC, and here mPAC, respectively, would make the protein to a favourable small, folded complex compared to the tetrameric euPAC<sup>24</sup>. Its LOV domain as a blue light sensor makes it outstanding among the four PACs

identified so far, as all these carry a BLUF domain. LOV domains have recently been shown to be photoswitchable by UV (356 nm) and near-UV light (405 nm) <sup>69</sup>, making them a more favourable tool in optogenetics than BLUF domains. Photoswitchable means in optogenetics to be more flexible in application as one has not to wait for thermal recovery to get the protein back into the mostly inactive ground state. Switching the protein back by light offers the opportunity to re-stimulate it in shorter time intervals to yield a higher efficiency.

The three proteins mPAC, bPAC and nPAC offer another advantage over euPAC: whereas the latter one carries a tandem arrangement of two BLUF domains and two cyclases in each monomer, the former ones show only one light activatable function, facilitating any changes with respect to optimizing their function. The mPAC protein in particular offers a further advantages over all others such that changes at its N-terminal LOV domain will be much more easily tolerated than in case of the BLUF domains.

Ongoing experiments are currently performed with the single- and multi-cellular eukaryotic amoeba *Dictyostelium* (collaboration with research group Pauline Schaap, University of Dundee, UK). *Dictyostelium* passes during its life cycle (ca. 24 hours) through several stages, starting from spores, which develop under warm and moist conditions to single, haploid and independent amoeba cells (fig. 6-17). In their vegetative life stage these cells, attracted by folic acid, feed on bacteria by phagocytosis. After feeding, cells enter the aggregation state and fuse, thus forming a real multicellular organism. This process is initiated by cAMP as a chemotactic signal. Secreted cAMP binds to cAMP receptors of neighboured conspecifics and a concentration-dependent cell movement begins towards the aggregation centre. After 6 – 10 hours the aggregate consists of up to 100.000 cells and forms an elongated mound, also called finger that can either move around on the surface or form a fruiting body via the stage of the “Mexican hat” <sup>193</sup>. This fruiting body then generates new spores as the origin of a new life cycle <sup>194</sup>.

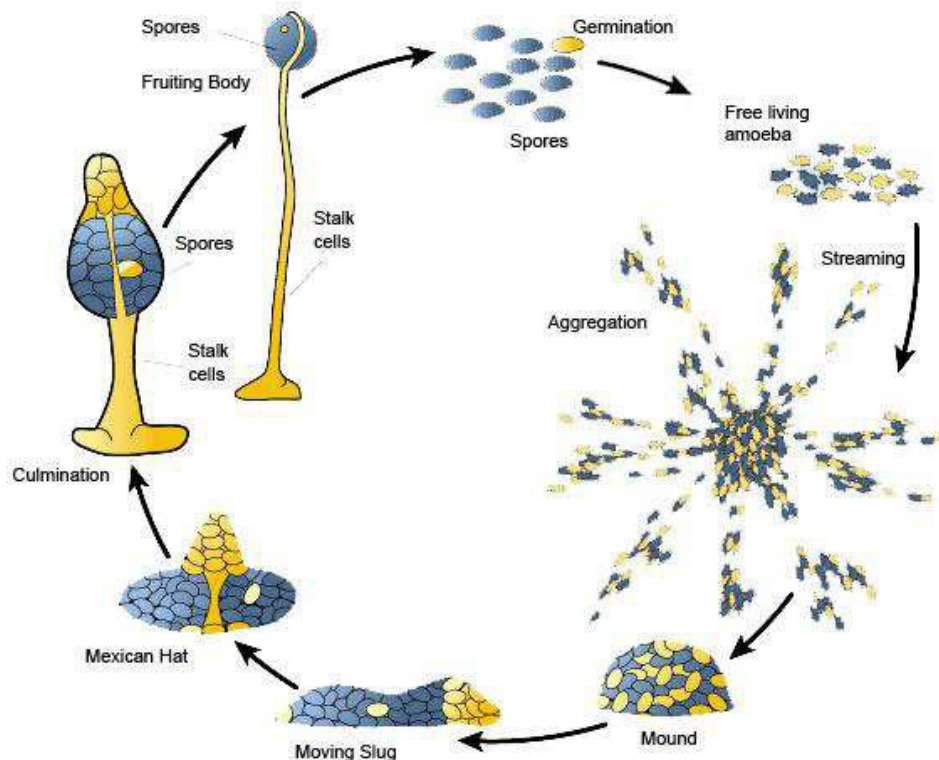


**Figure 6-17: life cycle of *Dictyostelium*.** Figure modified from <sup>194</sup>. Spores germinate to free living spores, living off soil bacteria. Aggregation is induced by chemotactic cAMP signals from centrally located amoeba. Motile slugs are then formed from aggregates, which can contain up to 100,000 cells. Finally, fruiting bodies are formed, producing new spores.

*Dictyostelium discoideum* contains three adenylyl cyclases: ACA, ACB and ACG. ACA is a seven transmembrane ubiquitous adenylyl cyclase and is a key player in *Dictyostelium* development for producing cAMP as a chemotactic signal for aggregation of single amoeba. The cAMP-dependent differentiation of *Dictyostelium* would make this organism an ideal test system to investigate the light-induced cAMP generation by a light-regulated AMP cyclase. A mutant was thus used that was void of the ACA cyclase. This so-called “null” mutant had been generated in the research group of Pauline Schaap, making it an ideal test case for functional studies for mPAC.

For experiments with mPAC, *aca* – null mutant cells were transformed with mPAC inserted into the pB17S-EYFP vector as a *Ddnull-mutant:mPAC* construct. The pB17S-EYFP is an expression vector that carries an eYFP (elongated yellow fluorescent protein) tag. The transformed cells were selected for growth in presence

of 50 µg/ml G418 (Geneticin). Selected cells were cultured in HL5 liquid medium, harvested and resuspended in 10 mM sodium/phosphate buffer, pH 6.5 at  $2 \times 10^7$  cells / ml cell density<sup>195</sup>. Following, the cells were developed on a nonnutrient-agar plate (1.5 % agar in 10 mM sodium/phosphate buffer, pH 6.5) under white light, and pictures were taken at different time points of their development (fig. 6-18). It is clearly seen that the mPAC transformed cells form fruiting bodies upon white light irradiation at  $t = 20$  hrs. However, figure 6-18 demonstrates that, in comparison to *Dictyostelium discoideum* ACA the fruiting bodies in the rescue mutant are somewhat smaller, indicating that the function of mPAC cannot fully restore the deleted cyclase function.

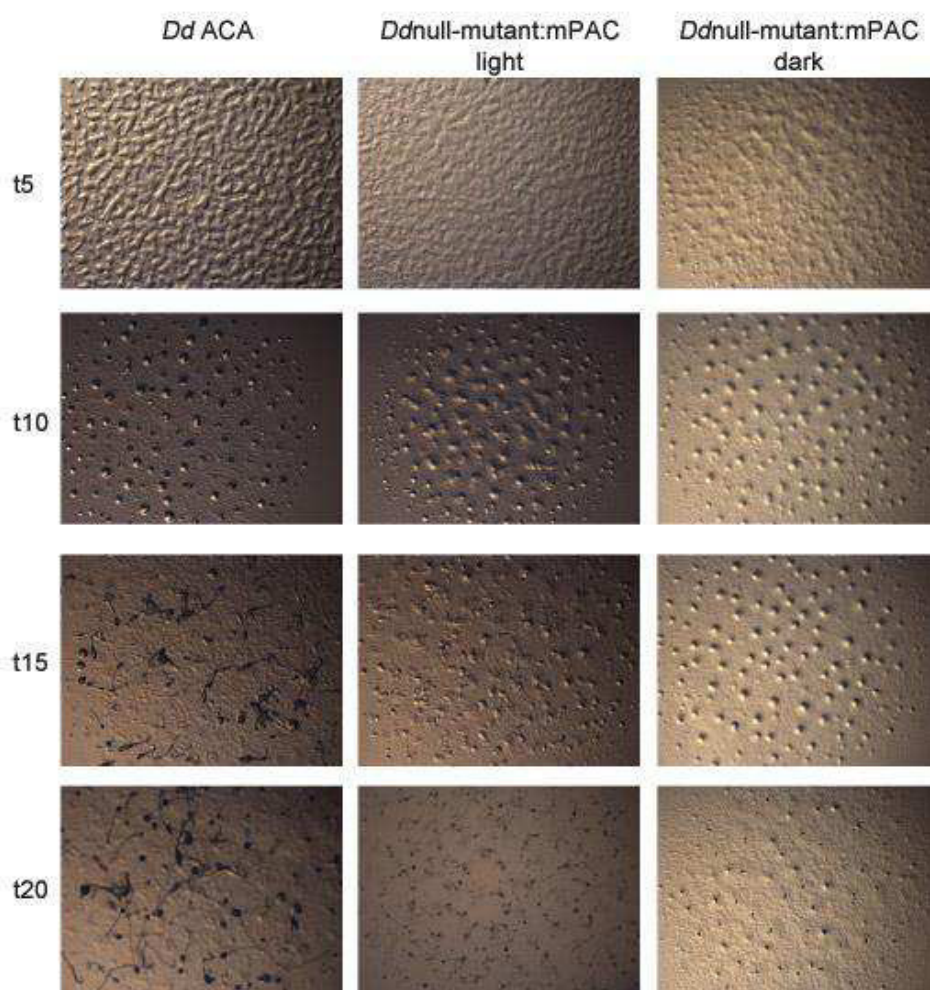


**Figure 6-18: life cycles of (left) *Dictyostelium discoideum* ACA (WT), (middle) *Dictyostelium discoideum* null mutant, transformed with mPAC in light and (right) *Dictyostelium discoideum* null mutant, transformed with mPAC in dark, followed over 20 h.** Experiments were performed as described elsewhere<sup>195</sup>. Light experiments were done under white light. At time step t20 generated fruiting bodies of *DdACA* and somewhat smaller fruiting bodies of *Ddnull-mutant:mPAC* in light are clearly identified. *Ddnull-mutant:mPAC* in dark (left) still developed cells but failed to form fruiting bodies at t20.

In the control experiment in the dark, *Ddhull*-mutant:mPAC cells could still develop but failed to form fruiting bodies. This is in accordance with the formerly described low constitutive activity of mPAC in dark yielding very low levels of cAMP, apparently sufficient to partly rescue and aggregate *aca*-null mutant cells, but not being sufficient to reach the further multicellular steps of culmination including the formation of the fruiting bodies. This absence of fruiting body formation due to a lack of cAMP proves mPAC a good candidate to control cell processes in living organisms.

Ongoing experiments under blue irradiation will reveal whether the spectrally selective irradiation of *Ddhull*-mutant:mPAC can increase the cAMP production to fully restore the fruiting body formation. Preliminary tests under white light irradiation led only to smaller fruiting bodies compared to the *DdACA* wild type (fig. 6-18). It has to be kept in mind that white light is a combination of all wavelengths, including near-UV in the range of 400 nm. As we know from the photoswitch experiments in chapter 6.3, this light quality can convert an illuminated LOV domain back into its dark state and reduce the lifetime of the active protein. Experiments under selective blue light would ensure that the mPAC protein is constantly active.

Taking together, mPAC shows the potential for a further milestone in optogenetics by connecting the huge field of LOV photoreceptors with PAC proteins. For future applications, a slowed-down mPAC photocycle might be favourable, as a longer-lived active state of the protein will generate more cAMP per photocycle. Deceleration might be accomplished either by mutagenesis or by a complete exchange/fusion of the cycling domain with another LOV domain, e.g., the LOV domain of the photoreceptor VIVID. VIVIDs might be interesting candidates, as in these proteins the LOV domain does not recover thermally to its dark state and remains active once photoexcited. If such a construct could be shown to be photoswitchable by UV- or near UV light (as was demonstrated in this thesis for the LOV domain of *YtvA*), this would add a novel and most promising tool to optogenetic applications.



## 6.5 Conclusion and further perspectives

This Ph.D. thesis dealing with blue light photoreceptors has moved forward from fundamental studies of light perception mechanism to photoreceptor application. It has broadened our knowledge about molecular and structural basics of bacterial and cyanobacterial photoreceptors like YtvA and mPAC. The initial characterization of mPAC has shown that there are still exciting photoreceptors to discover and to identify in order to extend the world of photosensitive proteins and the toolkit for application.

Though YtvA is one of the best characterized blue light photoreceptors and this work has gained a more detailed knowledge about its properties, there are still some open questions left. The full-length protein structure provided in this thesis relies on proven data, in good accordance to so far published results. However, crystal structures would gain a more detailed insight into the protein folding and its possible conformational changes during blue light exposure. The next step would thus be to optimize the conditions for crystallization and to investigate them by x-ray diffraction. Furthermore, with respect to biotechnological applications of YtvA as an FbFP, ongoing studies with original wt-YtvA in *Bacillus subtilis* cells and YtvA fusion proteins will refine this part of the work.

Besides YtvA, the novel LOV-PAC protein mPAC also implies open questions. The molecular basis of this protein is not yet fully understood. Unanswered issues are the function of the PAS domain in front of the LOV domain, showing no typical signature of light perception, remaining unclear in function. It can be suggested that the PAS domain might be responsible for protein stabilization or dimer formation.

Moreover, the neighbored residues T30 and N37 (YtvA counting) within the LOV core are in mPAC replaced by an alanine (A162) and methionine (M169). Unpublished data of a M169C mutant revealed slower recovery kinetics but it remains a fast process. By focussing on molecular cloning work, one could generate a “slow” mPAC variant that then would be a highly promising tool for application in optogenetics.



## References

1. solar radiation spectrum. photobiology.info . 2010.  
Ref Type: Online Source
2. Jablonski, A. About the mechanism of photo-luminescence of dye phosphors. *Zeitschrift fur Physik* **1935**, 94 (1-2), 38-46.
3. Jablonski diagram. photobiology.info . 2010.  
Ref Type: Online Source
4. Poggioli, S. Della influenza che ha il raggio magnetico sulla vegetazione delle piante. *Bologna-Coi Tipi di Annesio nobili Opusc Scientif Fasc* **1817**, 19-23.
5. Schaefer, E.; Nagy, F. Historical Overview. In *Photomorphogenesis in Plants and Bacteria. 3rd Edition*, Schaefer, E., Nagy, F., Eds.; Springer: 2006; pp 1-12.
6. Darwin, C. R. A. b. F. D. *The power of movement in plants*; John Murray: London, 1880.
7. Butler, W. L.; Norris, K. H.; Siegelman, H. W.; Hendricks, S. B. Detection, Assay, and Preliminary Purification of the Pigment Controlling Photoresponsive Development of Plants. *Proceedings of the National Academy of Sciences of the United States of America* **1959**, 45 (12), 1703-1708.
8. Hughes, J.; Lamparter, T.; Mittmann, F.; Hartmann, E.; Gartner, W.; Wilde, A.; Borner, T. A prokaryotic phytochrome. *Nature* **1997**, 386 (6626), 663.
9. Briggs, W. R. Blue/UV-A Receptors: Historical Overview. In *Photomorphogenesis in Plants and Bacteria. 3rd Edition*, Schaefer, E., Nagy, F., Eds.; Springer: 2006; pp 171-197.
10. Ahmad, M.; Cashmore, A. R. Hy4 Gene of A-Thaliana Encodes A Protein with Characteristics of A Blue-Light Photoreceptor. *Nature* **1993**, 366 (6451), 162-166.
11. Losi, A.; Polverini, E.; Quest, B.; Gartner, W. First evidence for phototropin-related blue-light receptors in prokaryotes. *Biophysical Journal* **2002**, 82 (5), 2627-2634.
12. Krauss, U.; Minh, B. Q.; Losi, A.; Gartner, W.; Eggert, T.; von Haeseler, A.; Jaeger, K. E. Distribution and Phylogeny of Light-Oxygen-Voltage-Blue-Light-Signaling Proteins in the Three Kingdoms of Life. *Journal of Bacteriology* **2009**, 191 (23), 7234-7242.
13. O'Hara, A.; Jenkins, G. I. In Vivo Function of Tryptophans in the Arabidopsis UV-B Photoreceptor UVR8. *Plant Cell* **2012**, 24 (9), 3755-3766.
14. Kliebenstein, D. J.; Lim, J. E.; Landry, L. G.; Last, R. L. Arabidopsis UVR8 regulates ultraviolet-B signal transduction and tolerance and contains sequence similarity to human Regulator of Chromatin Condensation 1. *Plant Physiology* **2002**, 130 (1), 234-243.

15. Christie, J. M.; Arvai, A. S.; Baxter, K. J.; Heilmann, M.; Pratt, A. J.; O'Hara, A.; Kelly, S. M.; Hothorn, M.; Smith, B. O.; Hitomi, K.; Jenkins, G. I.; Getzoff, E. D. Plant UVR8 Photoreceptor Senses UV-B by Tryptophan-Mediated Disruption of Cross-Dimer Salt Bridges. *Science* **2012**, 335 (6075), 1492-1496.
16. O'Hara, A.; Jenkins, G. I. In Vivo Function of Tryptophans in the Arabidopsis UV-B Photoreceptor UVR8. *Plant Cell* **2012**, 24 (9), 3755-3766.
17. Rizzini, L.; Favory, J. J.; Cloix, C.; Faggionato, D.; O'Hara, A.; Kaiserli, E.; Baumeister, R.; Schafer, E.; Nagy, F.; Jenkins, G. I.; Ulm, R. Perception of UV-B by the Arabidopsis UVR8 Protein. *Science* **2011**, 332 (6025), 103-106.
18. Heijde, M.; Ulm, R. UV-B photoreceptor-mediated signalling in plants. *Trends in Plant Science* **2012**, 17 (4), 230-237.
19. Schmidt, W. Bluelight Physiology. *Bioscience* **1984**, 34 (11), 698-704.
20. Ghetti, F.; Checcucci, G.; Lenci, F. Photosensitized Reactions As Primary Molecular Events in Photomovements of Microorganisms. *Journal of Photochemistry and Photobiology B-Biology* **1992**, 15 (3), 185-198.
21. Zeiger, E.; Zhu, J. X. Role of zeaxanthin in blue light photoreception and the modulation of light-CO<sub>2</sub> interactions in guard cells. *Journal of Experimental Botany* **1998**, 49, 433-442.
22. Crosson, S.; Moffat, K. Structure of a flavin-binding plant photoreceptor domain: Insights into light-mediated signal transduction. *Proceedings of the National Academy of Sciences of the United States of America* **2001**, 98 (6), 2995-3000.
23. Ito, S.; Murakami, A.; Sato, K.; Nishina, Y.; Shiga, K.; Takahashi, T.; Higashi, S.; Iseki, M.; Watanabe, M. Photocycle features of heterologously expressed and assembled eukaryotic flavin-binding BLUF domains of photoactivated adenylyl cyclase (PAC), a blue-light receptor in *Euglena gracilis*. *Photochemical & Photobiological Sciences* **2005**, 4 (9), 762-769.
24. Stierl, M.; Stumpf, P.; Udvari, D.; Gueta, R.; Hagedorn, R.; Losi, A.; Gartner, W.; Petereit, L.; Efetova, M.; Schwarzel, M.; Oertner, T. G.; Nagel, G.; Hegemann, P. Light Modulation of Cellular cAMP by a Small Bacterial Photoactivated Adenylyl Cyclase, bPAC, of the Soil Bacterium *Beggiatoa*. *Journal of Biological Chemistry* **2011**, 286 (2), 1181-1188.
25. Taylor, B. L.; Zhulin, I. B. PAS domains: Internal sensors of oxygen, redox potential, and light. *Microbiology and Molecular Biology Reviews* **1999**, 63 (2), 479-+.
26. Gong, W. M.; Hao, B.; Mansy, S. S.; Gonzalez, G.; Gilles-Gonzalez, M. A.; Chan, M. K. Structure of a biological oxygen sensor: A new mechanism for heme-driven signal transduction. *Proceedings of the National Academy of Sciences of the United States of America* **1998**, 95 (26), 15177-15182.
27. Miyatake, H.; Mukai, M.; Park, S. Y.; Adachi, S.; Tamura, K.; Nakamura, H.; Nakamura, K.; Tsuchiya, T.; Iizuka, T.; Shiro, Y. Sensory mechanism of oxygen sensor FixL from *Rhizobium meliloti*: Crystallographic, mutagenesis and resonance Raman spectroscopic studies. *Journal of Molecular Biology* **2000**, 301 (2), 415-431.

28. Herrou, J.; Crosson, S. Function, structure and mechanism of bacterial photosensory LOV proteins. *Nature Reviews Microbiology* **2011**, *9* (10), 713-723.
29. Losi, A.; Gartner, W. Old Chromophores, New Photoactivation Paradigms, Trendy Applications: Flavins in Blue Light-Sensing Photoreceptors. *Photochemistry and Photobiology* **2011**, *87* (3), 491-510.
30. Christie, J. M.; Gawthorne, J.; Young, G.; Fraser, N. J.; Roe, A. J. LOV to BLUF: Flavoprotein Contributions to the Optogenetic Toolkit. *Molecular Plant* **2012**, *5* (3), 533-544.
31. Moglich, A.; Moffat, K. Structural basis for light-dependent signaling in the dimeric LOV domain of the photosensor YtvA. *Journal of Molecular Biology* **2007**, *373* (1), 112-126.
32. Zoltowski, B. D.; Gardner, K. H. Tripping the Light Fantastic: Blue-Light Photoreceptors as Examples of Environmentally Modulated Protein-Protein Interactions. *Biochemistry* **2011**, *50* (1), 4-16.
33. Losi, A.; Gartner, W. Bacterial bilin- and flavin-binding photoreceptors. *Photochemical & Photobiological Sciences* **2008**, *7* (10), 1168-1178.
34. Purcell, E. B.; Siegal-Gaskins, D.; Rawling, D. C.; Fiebig, A.; Crosson, S. A photosensory two-component system regulates bacterial cell attachment. *Proceedings of the National Academy of Sciences of the United States of America* **2007**, *104* (46), 18241-18246.
35. Swartz, T. E.; Tseng, T. S.; Frederickson, M. A.; Paris, G.; Comerchi, D. J.; Rajashekara, G.; Kim, J. G.; Mudgett, M. B.; Splitter, G. A.; Ugalde, R. A.; Goldbaum, F. A.; Briggs, W. R.; Bogomolni, R. A. Blue-light-activated histidine kinases: Two-component sensors in bacteria. *Science* **2007**, *317* (5841), 1090-1093.
36. Cao, Z.; Buttani, V.; Losi, A.; Gartner, W. A blue light inducible two-component signal transduction system in the plant pathogen *Pseudomonas syringae* pv. tomato. *Biophysical Journal* **2008**, *94* (3), 897-905.
37. Djouani-Tahri, E. B.; Christie, J. M.; Sanchez-Ferandin, S.; Sanchez, F.; Bouget, F. Y.; Corellou, F. A eukaryotic LOV-histidine kinase with circadian clock function in the picoalga *Ostreococcus*. *Plant Journal* **2011**, *65* (4), 578-588.
38. Cao, Z.; Livoti, E.; Losi, A.; Gartner, W. A Blue Light-inducible Phosphodiesterase Activity in the Cyanobacterium *Synechococcus elongatus*. *Photochemistry and Photobiology* **2010**, *86* (3), 606-611.
39. Buttani, V.; Losi, A.; Poverini, E.; Gartner, W. Blue news: NTP binding properties of the blue-light sensitive YtvA protein from *Bacillus subtilis*. *Febs Letters* **2006**, *580* (16), 3818-3822.
40. Nash, A. I.; McNulty, R.; Shillito, M. E.; Swartz, T. E.; Bogomolni, R. A.; Luecke, H.; Gardner, K. H. Structural basis of photosensitivity in a bacterial light-oxygen-voltage/helix-turn-helix (LOV-HTH) DNA-binding protein. *Proceedings of the National Academy of Sciences of the United States of America* **2011**, *108* (23), 9449-9454.

41. Galperin, M. Y.; Nikolskaya, A. N.; Koonin, E. V. Novel domains of the prokaryotic two-component signal transduction systems. *Fems Microbiology Letters* **2001**, *203* (1), 11-21.
42. Christie, J. M.; Briggs, W. R. Blue Light Sensing and Signaling by the Phototropins. In *Handbook of Photosensory Receptors*, Briggs, W. R., Spudich, J. L., Eds.; Wiley-VCH: Weinheim, 2005; pp 277-303.
43. Chapman, S.; Faulkner, C.; Kaiserli, E.; Garcia-Mata, C.; Savenkov, E. I.; Roberts, A. G.; Oparka, K. J.; Christie, J. M. The photoreversible fluorescent protein iLOV outperforms GFP as a reporter of plant virus infection. *Proceedings of the National Academy of Sciences of the United States of America* **2008**, *105* (50), 20038-20043.
44. Drepper, T.; Eggert, T.; Circolone, F.; Heck, A.; Krauss, U.; Guterl, J. K.; Wendorff, M.; Losi, A.; Gartner, W.; Jaeger, K. E. Reporter proteins for in vivo fluorescence without oxygen. *Nature Biotechnology* **2007**, *25* (4), 443-445.
45. Huala, E.; Oeller, P. W.; Liscum, E.; Han, I. S.; Larsen, E.; Briggs, W. R. Arabidopsis NPH1: A protein kinase with a putative redox-sensing domain. *Science* **1997**, *278* (5346), 2120-2123.
46. Christie, J. M.; Reymond, P.; Powell, G. K.; Bernasconi, P.; Raibekas, A. A.; Liscum, E.; Briggs, W. R. Arabidopsis NPH1: A flavoprotein with the properties of a photoreceptor for phototropism. *Science* **1998**, *282* (5394), 1698-1701.
47. Sakai, T.; Kagawa, T.; Kasahara, M.; Swartz, T. E.; Christie, J. M.; Briggs, W. R.; Wada, M.; Okada, K. Arabidopsis nph1 and npl1: Blue light receptors that mediate both phototropism and chloroplast relocation. *Proceedings of the National Academy of Sciences of the United States of America* **2001**, *98* (12), 6969-6974.
48. Kagawa, T.; Sakai, T.; Suetsugu, N.; Oikawa, K.; Ishiguro, S.; Kato, T.; Tabata, S.; Okada, K.; Wada, M. Arabidopsis NPL1: A phototropin homolog controlling the chloroplast high-light avoidance response. *Science* **2001**, *291* (5511), 2138-2141.
49. Sakamoto, K.; Briggs, W. R. Cellular and subcellular localization of phototropin 1. *Plant Cell* **2002**, *14* (8), 1723-1735.
50. Kinoshita, T.; Doi, M.; Suetsugu, N.; Kagawa, T.; Wada, M.; Shimazaki, K. phot1 and phot2 mediate blue light regulation of stomatal opening. *Nature* **2001**, *414* (6864), 656-660.
51. Harper, S. M.; Neil, L. C.; Gardner, K. H. Structural basis of a phototropin light switch. *Science* **2003**, *301* (5639), 1541-1544.
52. Christie, J. M.; Corchnoy, S. B.; Swartz, T. E.; Hokenson, M.; Han, I. S.; Briggs, W. R.; Bogomolni, R. A. Steric interactions stabilize the signaling state of the LOV2 domain of phototropin 1. *Biochemistry* **2007**, *46* (32), 9310-9319.
53. Salomon, M.; Christie, J. M.; Knieb, E.; Lempert, U.; Briggs, W. R. Photochemical and mutational analysis of the FMN-binding domains of the plant blue light receptor, phototropin. *Biochemistry* **2000**, *39* (31), 9401-9410.

54. Nakasako, M.; Zikihara, K.; Matsuoka, D.; Katsura, H.; Tokutomi, S. Structural basis of the LOV1 dimerization of Arabidopsis phototropins 1 and 2. *Journal of Molecular Biology* **2008**, *381* (3), 718-733.
55. Kaiserli, E.; Sullivan, S.; Jones, M. A.; Feeney, K. A.; Christie, J. M. Domain Swapping to Assess the Mechanistic Basis of Arabidopsis Phototropin 1 Receptor Kinase Activation and Endocytosis by Blue Light. *Plant Cell* **2009**, *21* (10), 3226-3244.
56. Christie, J. M.; Swartz, T. E.; Bogomolni, R. A.; Briggs, W. R. Phototropin LOV domains exhibit distinct roles in regulating photoreceptor function. *Plant Journal* **2002**, *32* (2), 205-219.
57. Sullivan, S.; Thomson, C. E.; Lamont, D. J.; Jones, M. A.; Christie, J. M. In vivo phosphorylation site mapping and functional characterization of Arabidopsis phototropin 1. *Molecular Plant* **2008**, *1* (1), 178-194.
58. Losi, A. The bacterial counterparts of plant phototropins. *Photochemical & Photobiological Sciences* **2004**, *3* (6), 566-574.
59. Moglich, A.; Moffat, K. Engineered photoreceptors as novel optogenetic tools. *Photochemical & Photobiological Sciences* **2010**, *9* (10), 1286-1300.
60. Propsticciuti, C.; Lubin, L. B. Light-Induced Inhibition of Sporulation in *Bacillus-Licheniformis*. *Journal of Bacteriology* **1976**, *128* (1), 506-509.
61. Raffelberg, S.; Mansurova, M.; Gartner, W.; Losi, A. Modulation of the Photocycle of a LOV Domain Photoreceptor by the Hydrogen-Bonding Network. *Journal of the American Chemical Society* **2011**, *133* (14), 5346-5356.
62. Buttani, V.; Losi, A.; Eggert, T.; Krauss, U.; Jaeger, K. E.; Cao, Z.; Gartner, W. Conformational analysis of the blue-light sensing protein YtvA reveals a competitive interface for LOV-LOV dimerization and interdomain interactions. *Photochemical & Photobiological Sciences* **2007**, *6* (1), 41-49.
63. Avila-Perez, M.; Vreede, J.; Tang, Y. F.; Bende, O.; Losi, A.; Gartner, W.; Hellingwerf, K. In Vivo Mutational Analysis of YtvA from *Bacillus subtilis* mechanism of light activation of the general stress response. *Journal of Biological Chemistry* **2009**, *284* (37), 24958-24964.
64. Moglich, A.; Ayers, R. A.; Moffat, K. Design and Signaling Mechanism of Light-Regulated Histidine Kinases. *Journal of Molecular Biology* **2009**, *385* (5), 1433-1444.
65. Tang, Y. F.; Cao, Z.; Livoti, E.; Krauss, U.; Jaeger, K. E.; Gartner, W.; Losi, A. Interdomain signalling in the blue-light sensing and GTP-binding protein YtvA: A mutagenesis study uncovering the importance of specific protein sites. *Photochemical & Photobiological Sciences* **2010**, *9* (1), 47-56.
66. Aravind, L.; Koonin, E. V. The STAS domain - a link between anion transporters and antisigma-factor antagonists. *Current Biology* **2000**, *10* (2), R53-R55.
67. Nakasone, Y.; Hellingwerf, K. J. On the Binding of BODIPY-GTP by the Photosensory Protein YtvA from the Common Soil Bacterium *Bacillus subtilis*. *Photochemistry and Photobiology* **2011**, *87* (3), 542-547.



68. Dorn, M.; Jurk, M.; Schmieder, P. Blue News Update: BODIPY-GTP Binds to the Blue-Light Receptor YtvA While GTP Does Not. *Plos One* **2012**, *7* (1).
69. Losi, A.; Gartner, W.; Raffelberg, S.; Zancacchi, F. C.; Bianchini, P.; Diaspro, A.; Mandalari, C.; Abbruzzetti, S.; Viappiani, C. A photochromic bacterial photoreceptor with potential for super-resolution microscopy. *Photochemical & Photobiological Sciences* **2013**, *12* (2), 231-235.
70. Losi, A. Flavin-based blue-light photosensors: A photobiophysics update. *Photochemistry and Photobiology* **2007**, *83* (6), 1283-1300.
71. Kottke, T.; Heberle, J.; Hehn, D.; Dick, B.; Hegemann, P. Phot-LOV1: Photocycle of a blue-light receptor domain from the green alga *Chlamydomonas reinhardtii*. *Biophysical Journal* **2003**, *84* (2), 1192-1201.
72. Zoltowski, B. D.; Vaccaro, B.; Crane, B. R. Mechanism-based tuning of a LOV domain photoreceptor. *Nature Chemical Biology* **2009**, *5* (11), 827-834.
73. Akbar, S.; Gaidenko, T. A.; Kang, C. M.; O'Reilly, M.; Devine, K. M.; Price, C. W. New family of regulators in the environmental signaling pathway which activates the general stress transcription factor sigma(B) of *Bacillus subtilis*. *Journal of Bacteriology* **2001**, *183* (4), 1329-1338.
74. Gaidenko, T. A.; Kim, T. J.; Weigel, A. L.; Brody, M. S.; Price, C. W. The blue-light receptor YtvA acts in the environmental stress signaling pathway of *Bacillus subtilis*. *Journal of Bacteriology* **2006**, *188* (17), 6387-6395.
75. Jurk, M.; Schramm, P.; Schmieder, P. The blue-light receptor YtvA from *Bacillus subtilis* is permanently incorporated into the stressosome independent of the illumination state. *Biochemical and Biophysical Research Communications* **2013**, *432* (3), 499-503.
76. Brosi, R.; Illarionov, B.; Mathes, T.; Fischer, M.; Joshi, M.; Bacher, A.; Hegemann, P.; Bittl, R.; Weber, S.; Schleicher, E. Hindered Rotation of a Cofactor Methyl Group as a Probe for Protein-Cofactor Interaction. *Journal of the American Chemical Society* **2010**, *132* (26), 8935-8944.
77. Zoltowski, B. D.; Nash, A. I.; Gardner, K. H. Variations in Protein-Flavin Hydrogen Bonding in a Light, Oxygen, Voltage Domain Produce Non-Arrhenius Kinetics of Adduct Decay. *Biochemistry* **2011**, *50* (41), 8771-8779.
78. Raffelberg, S.; Gutt, A.; Gartner, W.; Mandalari, C.; Abbruzzetti, S.; Viappiani, C.; Losi, A. The amino acids surrounding the flavin 7a-methyl group determine the UVA spectral features of a LOV protein. *Journal of Biological Chemistry*, in press.
79. Diensthuber, R.P.; Bommer, M.; Gleichmann, T.; Moglich, A. Full-length structure of a sensor histidine kinase pinpoints coaxial coiled coils as signal transducers and modulators. *Structure*, in press.
80. Ogata, H.; Cao, Z.; Losi, A.; Gartner, W. Crystallization and preliminary X-ray analysis of the LOV domain of the blue-light receptor YtvA from *Bacillus amyloliquefaciens* FZB42. *Acta Crystallographica Section F-Structural Biology and Crystallization Communications* **2009**, *65*, 853-855.



81. Engelhard, C.; Raffelberg, S.; Tang, Y.; Diensthuber, R.P.; Moglich, A.; Losi, A.; Gartner, W.; Bittl, R. A structural model for the full-length blue light-sensing protein YtvA from *Bacillus subtilis*, based on EPR spectroscopy. *Photochemical & Photobiological Sciences*, in press.
82. Bolhuis, H.; Severin, I.; Confurius-Guns, V.; Wollenzien, U. I. A.; Stal, L. J. Horizontal transfer of the nitrogen fixation gene cluster in the cyanobacterium *Microcoleus chthonoplastes*. *Isme Journal* **2010**, 4 (1), 121-130.
83. Banerjee, R.; Batschauer, A. Plant blue-light receptors. *Planta* **2005**, 220 (3), 498-502.
84. Takase, T.; Nishiyama, Y.; Tanihigashi, H.; Ogura, Y.; Miyazaki, Y.; Yamada, Y.; Kiyosue, T. Lov Kelch Protein2 and Zeitlupe Repress Arabidopsis Photoperiodic Flowering Under Non-Inductive Conditions, Dependent on Flavin-Binding Kelch Repeat F-Box1. *Plant Journal* **2011**, 67 (4), 608-621.
85. Baudry, A.; Ito, S.; Song, Y. H.; Strait, A. A.; Kiba, T.; Lu, S.; Henriques, R.; Pruneda-Paz, J. L.; Chua, N. H.; Tobin, E. M.; Kay, S. A.; Imaizumi, T. F-Box Proteins FKF1 and LKP2 Act in Concert with ZEITLUPE to Control Arabidopsis Clock Progression. *Plant Cell* **2010**, 22 (3), 606-622.
86. Fujiwara, S. Novel blue light receptors with an F-box: their direct control of the circadian clock and the flowering timing in Arabidopsis. *Plant Biotechnology* **2008**, 25 (2), 123-129.
87. Lechner, E.; Achard, P.; Vansiri, A.; Potuschak, T.; Genschik, P. F-box proteins everywhere. *Current Opinion in Plant Biology* **2006**, 9 (6), 631-638.
88. Demarsy, E.; Fankhauser, C. Higher plants use LOV to perceive blue light. *Current Opinion in Plant Biology* **2009**, 12 (1), 69-74.
89. Imaizumi, T.; Tran, H. G.; Swartz, T. E.; Briggs, W. R.; Kay, S. A. FKF1 is essential for photoperiodic-specific light signalling in Arabidopsis. *Nature* **2003**, 426 (6964), 302-306.
90. Zikihara, K.; Iwata, T.; Matsuoka, D.; Kandori, H.; Todo, T.; Tokutomi, S. Photoreaction cycle of the light, oxygen, and voltage domain in FKF1 determined by low-temperature absorption spectroscopy. *Biochemistry* **2006**, 45 (36), 10828-10837.
91. Deisenhofer, J. DNA photolyases and cryptochromes. *Mutation Research-Dna Repair* **2000**, 460 (3-4), 143-149.
92. Sancar, A. Photolyase and cryptochrome blue-light photoreceptors. *Dna Repair and Replication* **2004**, 69, 73-100.
93. Brudler, R.; Hitomi, K.; Daiyasu, H.; Toh, H.; Kucho, K.; Ishiura, M.; Kanehisa, M.; Roberts, V. A.; Todo, T.; Tainer, J. A.; Getzoff, E. D. Identification of a new cryptochrome class: Structure, function, and evolution. *Molecular Cell* **2003**, 11 (1), 59-67.
94. Liu, H. T.; Liu, B.; Zhao, C. X.; Pepper, M.; Lin, C. T. The action mechanisms of plant cryptochromes. *Trends in Plant Science* **2011**, 16 (12), 684-691.

95. Chaves, I.; Pokorny, R.; Byrdin, M.; Hoang, N.; Ritz, T.; Brettel, K.; Essen, L. O.; van der Horst, G. T. J.; Batschauer, A.; Ahmad, M. The Cryptochromes: Blue Light Photoreceptors in Plants and Animals. *Annual Review of Plant Biology*, Vol 62 **2011**, 62, 335-364.
96. Solov'yov, I. A.; Domratcheva, T.; Shahi, A. R. M.; Schulten, K. Decrypting Cryptochrome: Revealing the Molecular Identity of the Photoactivation Reaction. *Journal of the American Chemical Society* **2012**, 134 (43), 18046-18052.
97. Gomelsky, M.; Klug, G. BLUF: a novel FAD-binding domain involved in sensory transduction in microorganisms. *Trends in Biochemical Sciences* **2002**, 27 (10), 497-500.
98. Gotze, J. P.; Greco, C.; Mitric, R.; Bonacic-Koutecky, V.; Saalfrank, P. BLUF Hydrogen network dynamics and UV/Vis spectra: A combined molecular dynamics and quantum chemical study. *Journal of Computational Chemistry* **2012**, 33 (28), 2233-2242.
99. Jung, A.; Domratcheva, T.; Tarutina, M.; Wu, Q.; Ko, W. H.; Shoeman, R. L.; Gomelsky, M.; Gardner, K. H.; Schlichting, L. Structure of a bacterial BLUF photoreceptor: Insights into blue light-mediated signal transduction. *Proceedings of the National Academy of Sciences of the United States of America* **2005**, 102 (35), 12350-12355.
100. van der Horst, M. A.; Hellingwerf, K. J. Photoreceptor Proteins, "Star Actors of Modern Times": A Review of the Functional Dynamics in the Structure of Representative Members of Six Different Photoreceptor Families. *Accounts of Chemical Research* **2004**, 37 (1), 13-20.
101. Zirak, P.; Penzkofer, A.; Schiereis, T.; Hegemann, P.; Jung, A.; Schlichting, I. Photodynamics of the small BLUF protein BlrB from *Rhodobacter sphaeroides*. *Journal of Photochemistry and Photobiology B-Biology* **2006**, 83 (3), 180-194.
102. Kennis, J. T. M.; Groot, M. L. Ultrafast spectroscopy of biological photoreceptors. *Current Opinion in Structural Biology* **2007**, 17 (5), 623-630.
103. Gomelsky, M.; Kaplan, S. Appa, A Novel Gene Encoding A Trans-Acting Factor Involved in the Regulation of Photosynthesis Gene-Expression in *Rhodobacter-Sphaeroides*-2.4.1. *Journal of Bacteriology* **1995**, 177 (16), 4609-4618.
104. Iseki, M.; Matsunaga, S.; Murakami, A.; Ohno, K.; Shiga, K.; Yoshida, K.; Sugai, M.; Takahashi, T.; Hori, T.; Watanabe, M. A blue-light-activated adenylyl cyclase mediates photoavoidance in *Euglena gracilis*. *Nature* **2002**, 415 (6875), 1047-1051.
105. Ntefidou, M.; Iseki, M.; Watanabe, M.; Lebert, M.; Hader, D. P. Photoactivated adenylyl cyclase controls phototaxis in the flagellate *Euglena gracilis*. *Plant Physiology* **2003**, 133 (4), 1517-1521.
106. Ryu, M. H.; Moskvina, O. V.; Siltberg-Liberles, J.; Gomelsky, M. Natural and Engineered Photoactivated Nucleotidyl Cyclases for Optogenetic Applications. *Journal of Biological Chemistry* **2010**, 285 (53), 41501-41508.

107. Meyer, T. E. Isolation and Characterization of Soluble Cytochromes, Ferredoxins and Other Chromophoric Proteins from the Halophilic Phototrophic Bacterium *Ectothiorhodospira-Halophila*. *Biochimica et Biophysica Acta* **1985**, 806 (1), 175-183.
108. Imamoto, Y.; Kataoka, M. Structure and photoreaction of photoactive yellow protein, a structural prototype of the PAS domain superfamily. *Photochemistry and Photobiology* **2007**, 83 (1), 40-49.
109. Pellequer, J. L.; Wager-Smith, K. A.; Kay, S. A.; Getzoff, E. D. Photoactive yellow protein: A structural prototype for the three-dimensional fold of the PAS domain superfamily. *Proceedings of the National Academy of Sciences of the United States of America* **1998**, 95 (11), 5884-5890.
110. Jiang, Z. Y.; Swem, L. R.; Rushing, B. G.; Devanathan, S.; Tollin, G.; Bauer, C. E. Bacterial photoreceptor with similarity to photoactive yellow protein and plant phytochromes. *Science* **1999**, 285 (5426), 406-409.
111. van der Horst, M. A.; Hendriks, J.; Vreede, J.; Yermenko, S.; Crielard, W.; Hellingwerf, K. J. Photoactive Yellow Protein, the Xanthopsin. In *Handbook of Photosensory Receptors*, Briggs, W. R., Spudich, J. L., Eds.; Wiley-VCH Verlag GmbH & Co: Weinheim, 2005; pp 391-415.
112. Meyer, T. E.; Kyndt, J. A.; Memmi, S.; Moser, T.; Colon-Acevedo, B.; Devreese, B.; Van Beeumen, J. J. The growing family of photoactive yellow proteins and their presumed functional roles. *Photochemical & Photobiological Sciences* **2012**, 11 (10), 1495-1514.
113. Rockwell, N. C.; Martin, S. S.; Lagarias, J. C. Red/Green Cyanobacteriochromes: Sensors of Color and Power. *Biochemistry* **2012**, 51 (48), 9667-9677.
114. Enomoto, G.; Hirose, Y.; Narikawa, R.; Ikeuchi, M. Thiol-Based Photocycle of the Blue and Teal Light-Sensing Cyanobacteriochrome Tlr1999. *Biochemistry* **2012**, 51 (14), 3050-3058.
115. Rockwell, N. C.; Lagarias, J. C. A Brief History of Phytochromes. *Chemphyschem* **2010**, 11 (6), 1172-1180.
116. Vierstra, R. D.; Quail, P. H. Proteolysis Alters the Spectral Properties of 124 K Dalton Phytochrome from Avena. *Planta* **1982**, 156 (2), 158-165.
117. Hershey, H. P.; Barker, R. F.; Idler, K. B.; Lissemore, J. L.; Quail, P. H. Analysis of Cloned Cdna and Genomic Sequences for Phytochrome - Complete Amino-Acid-Sequences for 2 Gene-Products Expressed in Etiolated Avena. *Nucleic Acids Research* **1985**, 13 (23), 8543-8559.
118. Davis, S. J.; Vener, A. V.; Vierstra, R. D. Bacteriophytochromes: Phytochrome-like photoreceptors from nonphotosynthetic eubacteria. *Science* **1999**, 286 (5449), 2517-2520.
119. Yeh, K. C.; Wu, S. H.; Murphy, J. T.; Lagarias, J. C. A cyanobacterial phytochrome two-component light sensory system. *Science* **1997**, 277 (5331), 1505-1508.
120. Karniol, B.; Wagner, J. R.; Walker, J. M.; Vierstra, R. D. Phylogenetic analysis of the phytochrome superfamily reveals distinct microbial subfamilies of photoreceptors. *Biochemical Journal* **2005**, 392, 103-116.

121. Hughes, J. Phytochrome three-dimensional structures and functions. *Biochemical Society Transactions* **2010**, *38*, 710-716.
122. Quail, P. H.; Boylan, M. T.; Parks, B. M.; Short, T. W.; Xu, Y.; Wagner, D. Phytochromes - Photosensory Perception and Signal-Transduction. *Science* **1995**, *268* (5211), 675-680.
123. Wagner, J. R.; Brunzelle, J. S.; Forest, K. T.; Vierstra, R. D. A light-sensing knot revealed by the structure of the chromophore-binding domain of phytochrome. *Nature* **2005**, *438* (7066), 325-331.
124. Wagner, J. R.; Zhang, J. R.; Brunzelle, J. S.; Vierstra, R. D.; Forest, K. T. High resolution structure of Deinococcus bacteriophytochrome yields new insights into phytochrome architecture and evolution. *Journal of Biological Chemistry* **2007**, *282* (16), 12298-12309.
125. Essen, L. O.; Mailliet, J.; Hughes, J. The structure of a complete phytochrome sensory module in the Pr ground state. *Proceedings of the National Academy of Sciences of the United States of America* **2008**, *105* (38), 14709-14714.
126. Franklin, K. A.; Quail, P. H. Phytochrome functions in Arabidopsis development. *Journal of Experimental Botany* **2010**, *61* (1), 11-24.
127. Kehoe, D. M.; Grossman, A. R. Similarity of a chromatic adaptation sensor to phytochrome and ethylene receptors. *Science* **1996**, *273* (5280), 1409-1412.
128. Schmitz, O.; Katayama, M.; Williams, S. B.; Kondo, T.; Golden, S. S. CikA, a bacteriophytochrome that resets the cyanobacterial circadian clock. *Science* **2000**, *289* (5480), 765-768.
129. Ikeuchi, M.; Ishizuka, T. Cyanobacteriochromes: a new superfamily of tetrapyrrole-binding photoreceptors in cyanobacteria. *Photochemical & Photobiological Sciences* **2008**, *7* (10), 1159-1167.
130. Auldrige, M. E.; Forest, K. T. Bacterial phytochromes: More than meets the light. *Critical Reviews in Biochemistry and Molecular Biology* **2011**, *46* (1), 67-88.
131. Chen, Y.; Zhang, J.; Luo, J.; Tu, J.-M.; Zeng, X.-L.; Xie, J.; Zhou, M.; Zhao, J.-Q.; Scheer, H.; Zhao, K. H. Photophysical diversity of two novel cyanobacteriochromes with phycocyanobilin chromophores: photochemistry and dark reversion kinetics. *Febs Journal* **2012**, *279*, 40-54.
132. Ma, Q.; Hua, H. H.; Chen, Y.; Liu, B. B.; Kramer, A. L.; Scheer, H.; Zhao, K. H.; Zhou, M. A rising tide of blue-absorbing biliprotein photoreceptors - characterization of seven such bilin-binding GAF domains in Nostoc sp PCC7120. *Febs Journal* **2012**, *279* (21), 4095-4108.
133. Rockwell, N. C.; Ohlendorf, R.; Moglich, A. Cyanobacteriochromes in full color and three dimensions. *Proceedings of the National Academy of Sciences of the United States of America* **2013**, *110* (3), 806-807.
134. Song, J. Y.; Cho, H. S.; Cho, J. I.; Jeon, J. S.; Lagarias, J. C.; Park, Y. I. Near-UV cyanobacteriochrome signaling system elicits negative phototaxis in the cyanobacterium Synechocystis sp PCC 6803. *Proceedings of the National Academy of Sciences of the United States of America* **2011**, *108* (26), 10780-10785.

135. Bhaya, D.; Takahashi, A.; Shahi, P.; Grossman, A. R. Novel motility mutants of *Synechocystis* strain PCC 6803 generated by in vitro transposon mutagenesis. *Journal of Bacteriology* **2001**, *183* (20), 6140-6143.
136. Zhang, J. A.; Wu, X. J.; Wang, Z. B.; Chen, Y.; Wang, X.; Zhou, M.; Scheer, H.; Zhao, K. H. Fused-Gene Approach to Photoswitchable and Fluorescent Biliproteins. *Angewandte Chemie-International Edition* **2010**, *49* (32), 5456-5458.
137. Kato, H. E.; Zhang, F.; Yizhar, O.; Ramakrishnan, C.; Nishizawa, T.; Hirata, K.; Ito, J.; Aita, Y.; Tsukazaki, T.; Hayashi, S.; Hegemann, P.; Maturana, A. D.; Ishitani, R.; Deisseroth, K.; Nureki, O. Crystal structure of the channelrhodopsin light-gated cation channel. *Nature* **2012**, *482* (7385), 369-U115.
138. Kandori, H. Rhodopsins - Intermembrane Signaling by Hydrogen Bonding. 2013; pp 2243-2247.
139. Dutta, A.; Klein-Seetharaman, J. Rhodopsin - Stability and Characterization of Unfolded Structures. 2013; pp 2247-2252.
140. Pathak, G. P.; Vrana, J. D.; Tucker, C. L. Optogenetic control of cell function using engineered photoreceptors. *Biology of the Cell* **2013**, *105* (2), 59-72.
141. Song, S. H.; Freddolino, P. L.; Nash, A. I.; Carroll, E. C.; Schulten, K.; Gardner, K. H.; Larsen, D. S. Modulating LOV Domain Photodynamics with a Residue Alteration outside the Chromophore Binding Site. *Biochemistry* **2011**, *50* (13), 2411-2423.
142. Nagel, G.; Brauner, M.; Liewald, J. F.; Adeishvili, N.; Bamberg, E.; Gottschalk, A. Light activation of channelrhodopsin-2 in excitable cells of *Caenorhabditis elegans* triggers rapid Behavioral responses. *Current Biology* **2005**, *15* (24), 2279-2284.
143. Tsai, H. C.; Zhang, F.; Adamantidis, A.; Stuber, G. D.; Bonci, A.; de Lecea, L.; Deisseroth, K. Phasic Firing in Dopaminergic Neurons Is Sufficient for Behavioral Conditioning. *Science* **2009**, *324* (5930), 1080-1084.
144. Jazayeri, M.; Lindbloom-Brown, Z.; Horwitz, G. D. Saccadic eye movements evoked by optogenetic activation of primate V1. *Nature Neuroscience* **2012**, *15* (10), 1368-1370.
145. Mansurova, M.; Scheercousse, P.; Simon, J.; Kluth, M.; Gartner, W. Chromophore Exchange in the Blue Light-Sensitive Photoreceptor YtvA from *Bacillus subtilis*. *Chembiochem* **2011**, *12* (4), 641-646.
146. Mansurova, M.; Koay, M. S.; Gartner, W. Synthesis and Electrochemical Properties of Structurally Modified Flavin Compounds. *European Journal of Organic Chemistry* **2008**, (32), 5401-5406.
147. Salzmann, S.; Martinez-Junza, V.; Zorn, B.; Braslavsky, S. E.; Mansurova, M.; Marian, C. M.; Gartner, W. Photophysical Properties of Structurally and Electronically Modified Flavin Derivatives Determined by Spectroscopy and Theoretical Calculations. *Journal of Physical Chemistry A* **2009**, *113* (33), 9365-9375.
148. Mathes, T.; Vogl, C.; Stolz, J.; Hegemann, P. In Vivo Generation of Flavoproteins with Modified Cofactors. *Journal of Molecular Biology* **2009**, *385* (5), 1511-1518.



149. Zirak, P.; Penzkofer, A.; Mathes, T.; Hegemann, P. Absorption and emission spectroscopic characterization of BLUF protein Slr1694 from *Synechocystis* sp PCC6803 with roseoflavin cofactor. *Journal of Photochemistry and Photobiology B-Biology* **2009**, 97 (2), 61-70.
150. Alexandre, M. T. A.; Arents, J. C.; van Grondelle, R.; Hellingwerf, K. J.; Kennis, J. T. M. A base-catalyzed mechanism for dark state recovery in the *Avena sativa* phototropin-1 LOV2 domain. *Biochemistry* **2007**, 46 (11), 3129-3137.
151. Pfeifer, A.; Majerus, T.; Zikihara, K.; Matsuoka, D.; Tokutomi, S.; Heberle, J.; Kottke, T. Time-Resolved Fourier Transform Infrared Study on Photoadduct Formation and Secondary Structural Changes within the Phototropin LOV Domain. *Biophysical Journal* **2009**, 96 (4), 1462-1470.
152. Fedorov, R.; Schlichting, I.; Hartmann, E.; Domratcheva, T.; Fuhrmann, M.; Hegemann, P. Crystal structures and molecular mechanism of a light-induced signaling switch: The Phot-LOV1 domain from *Chlamydomonas reinhardtii*. *Biophysical Journal* **2003**, 84 (4), 2474-2482.
153. Crosson, S.; Moffat, K. Photoexcited structure of a plant photoreceptor domain reveals a light-driven molecular switch. *Plant Cell* **2002**, 14 (5), 1067-1075.
154. Alexandre, M. T. A.; Domratcheva, T.; Bonetti, C.; van Wilderen, L. J. G. W.; van Grondelle, R.; Groot, M. L.; Hellingwerf, K. J.; Kennis, J. T. M. Primary Reactions of the LOV2 Domain of Phototropin Studied with Ultrafast Mid-infrared Spectroscopy and Quantum Chemistry. *Biophysical Journal* **2009**, 97 (1), 227-237.
155. Yamamoto, A.; Iwata, T.; Sato, Y.; Matsuoka, D.; Tokutomi, S.; Kandori, H. Light Signal Transduction Pathway from Flavin Chromophore to the J alpha Helix of Arabidopsis Phototropin1. *Biophysical Journal* **2009**, 96 (7), 2771-2778.
156. Nash, A. I.; Ko, W. H.; Harper, S. M.; Gardner, K. H. A Conserved Glutamine Plays a Central Role in LOV Domain Signal Transmission and Its Duration. *Biochemistry* **2008**, 47 (52), 13842-13849.
157. Nozaki, D.; Iwata, T.; Ishikawa, T.; Todo, T.; Tokutomi, S.; Kandori, H. Role of Gln1029 in the photoactivation processes of the LOV2 domain in *Adiantum phytochrome3*. *Plant and Cell Physiology* **2004**, 45, S87.
158. Alexandre, M. T. A.; van Grondelle, R.; Hellingwerf, K. J.; Kennis, J. T. M. Conformational Heterogeneity and Propagation of Structural Changes in the LOV2/J alpha Domain from *Avena sativa* Phototropin 1 as Recorded by Temperature-Dependent FTIR Spectroscopy. *Biophysical Journal* **2009**, 97 (1), 238-247.
159. Alexandre, M. T. A.; Purcell, E. B.; van Grondelle, R.; Robert, B.; Kennis, J. T. M.; Crosson, S. Electronic and Protein Structural Dynamics of a Photosensory Histidine Kinase. *Biochemistry* **2010**, 49 (23), 4752-4759.
160. Eisenreich, W.; Joshi, M.; Illarionov, B.; Richter, G.; Romisch-Margl, W.; Muller, F.; Bacher, A.; Fischer, M. C-13 Isotopologue editing of FMN bound to phototropin domains. *Febs Journal* **2007**, 274 (22), 5876-5890.



161. Buttani, V.; Gartner, W.; Losi, A. NTP-binding properties of the blue-light receptor YtvA and effects of the E105L mutation. *European Biophysics Journal with Biophysics Letters* **2007**, *36* (7), 831-839.
162. Losi, A.; Ghiraldelli, E.; Jansen, S.; Gartner, W. Mutational effects on protein structural changes and interdomain interactions in the blue-light sensing LOV protein YtvA. *Photochemistry and Photobiology* **2005**, *81* (5), 1145-1152.
163. Penzkofer, A.; Endres, L.; Schiereis, T.; Hegemann, P. Yield of photo-adduct formation of LOV domains from *Chlamydomonas reinhardtii* by picosecond laser excitation. *Chemical Physics* **2005**, *316* (1-3), 185-194.
164. Climent, T.; Gonzalez-Luque, R.; Merchan, M.; Serrano-Andres, L. Theoretical insight into the spectroscopy and photochemistry of isoalloxazine, the flavin core ring. *Journal of Physical Chemistry A* **2006**, *110* (50), 13584-13590.
165. Nakasako, M.; Iwata, T.; Matsuoka, D.; Tokutomi, S. Light-induced structural changes of LOV domain-containing polypeptides from *Arabidopsis* phototropin 1 and 2 studied by small-angle X-ray scattering. *Biochemistry* **2004**, *43* (47), 14881-14890.
166. Marles-Wright, J.; Grant, T.; Delumeau, O.; van Duinen, G.; Firbank, S. J.; Lewis, P. J.; Murray, J. W.; Newman, J. A.; Quin, M. B.; Race, P. R.; Rohou, A.; Tichelaar, W.; van Heel, M.; Lewis, R. J. Molecular architecture of the "stressosome," a signal integration and transduction hub. *Science* **2008**, *322* (5898), 92-96.
167. Zoltowski, B. D.; Crane, B. R. Light activation of the LOV protein Vivid generates a rapidly exchanging dimer. *Biochemistry* **2008**, *47* (27), 7012-7019.
168. Moglich, A.; Yang, X. J.; Ayers, R. A.; Moffat, K. Structure and Function of Plant Photoreceptors. *Annual Review of Plant Biology, Vol 61* **2010**, *61*, 21-47.
169. Harper, S. M.; Christie, J. M.; Gardner, K. H. Disruption of the LOV-J alpha helix interaction activates phototropin kinase activity. *Biochemistry* **2004**, *43* (51), 16184-16192.
170. Matsuoka, D.; Tokutomi, S. Blue light-regulated molecular switch of Ser/Thr kinase in phototropin. *Proceedings of the National Academy of Sciences of the United States of America* **2005**, *102* (37), 13337-13342.
171. Reginsson, G. W.; Schiemann, O. Studying bimolecular complexes with pulsed electron-electron double resonance spectroscopy. *Biochemical Society Transactions* **2011**, *39*, 128-139.
172. Hubbell, W. L.; Mchaourab, H. S.; Altenbach, C.; Lietzow, M. A. Watching proteins move using site-directed spin labeling. *Structure* **1996**, *4* (7), 779-783.
173. Altenbach, C.; Kusnetzow, A. K.; Ernst, O. P.; Hofmann, K. P.; Hubbell, W. L. High-resolution distance mapping in rhodopsin reveals the pattern of helix movement due to activation. *Proceedings of the National Academy of Sciences of the United States of America* **2008**, *105* (21), 7439-7444.
174. Jurk, M.; Dorn, M.; Schmieder, P. Blue Flickers of Hope: Secondary Structure, Dynamics, and Putative Dimerization Interface of the Blue-Light Receptor YtvA from *Bacillus subtilis*. *Biochemistry* **2011**, *50* (38), 8163-8171.

175. Losi, A.; Viappiani, C.; Nonell, S. Photofunctional proteins: from understanding to engineering. *Photochemical & Photobiological Sciences* **2010**, 9 (10), 1285.
176. Drepper, T.; Krauss, U.; Berstenhorst, S. M. Z.; Pietruszka, J.; Jaeger, K. E. Lights on and action! Controlling microbial gene expression by light. *Applied Microbiology and Biotechnology* **2011**, 90 (1), 23-40.
177. Hess, S. T.; Girirajan, T. P. K.; Mason, M. D. Ultra-high resolution imaging by fluorescence photoactivation localization microscopy. *Biophysical Journal* **2006**, 91 (11), 4258-4272.
178. Rust, M. J.; Bates, M.; Zhuang, X. W. Sub-diffraction-limit imaging by stochastic optical reconstruction microscopy (STORM). *Nature Methods* **2006**, 3 (10), 793-795.
179. Zanicchi, F. C.; Lavagnino, Z.; Donnorso, M. P.; Del Bue, A.; Furia, L.; Faretta, M.; Diaspro, A. Live-cell 3D super-resolution imaging in thick biological samples. *Nature Methods* **2011**, 8 (12), 1047-+.
180. Jones, S. A.; Shim, S. H.; He, J.; Zhuang, X. W. Fast, three-dimensional super-resolution imaging of live cells. *Nature Methods* **2011**, 8 (6), 499-U96.
181. Losi, A.; Gartner, W. *Fine-tuning of the photobiophysics of photoreceptor proteins for applications in high resolution fluorescence microscopy and optogenetics*; 12.
182. Kennis, J. T. M.; van Stokkum, I. H. M.; Crosson, S.; Gauden, M.; Moffat, K.; van Grondelle, R. The LOV2 domain of phototropin: A reversible photochromic switch. *Journal of the American Chemical Society* **2004**, 126 (14), 4512-4513.
183. Niedz, R. P.; Sussman, M. R.; Satterlee, J. S. Green Fluorescent Protein - An In-Vivo Reporter of Plant Gene-Expression. *Plant Cell Reports* **1995**, 14 (7), 403-406.
184. Marshall, J.; Molloy, R.; Moss, G. W. J.; Howe, J. R.; Hughes, T. E. The Jellyfish Green Fluorescent Protein - A New Tool for Studying Ion-Channel Expression and Function. *Neuron* **1995**, 14 (2), 211-215.
185. Lei, Y.; Chen, W.; Mulchandani, A. Microbial biosensors. *Analytica Chimica Acta* **2006**, 568 (1-2), 200-210.
186. Drepper, T.; Gensch, T.; Pohl, M. Advanced in vivo applications of blue light photoreceptors as alternative fluorescent proteins. *Photochemical & Photobiological Sciences*, in press.
187. Gomelsky, M.; Hoff, W. D. Light helps bacteria make important lifestyle decisions. *Trends in Microbiology* **2011**, 19 (9), 441-448.
188. cAMP synthesis. Pearsons Prentice Hall, Inc. 2006.  
Ref Type: Online Source
189. Ntefidou, M.; Iseki, M.; Watanabe, M.; Lebert, M.; Hader, D. P. Photoactivated adenylyl cyclase controls phototaxis in the flagellate *Euglena gracilis*. *Plant Physiology* **2003**, 133 (4), 1517-1521.
190. Fulton, C. Macromolecular Syntheses During the Quick-Change Act of *Naegleria*. *Journal of Protozoology* **1983**, 30 (2), 192-198.

191. Fulton, C.; Kowit, J. D. Programmed Synthesis of Flagellar Tubulin During Cell-Differentiation in *Naegleria*. *Transactions of the New York Academy of Sciences* **1974**, *36* (6), 601.
192. Penzkofer, A.; Stierl, M.; Hegemann, P.; Kateriya, S. Photo-dynamics of the BLUF domain containing soluble adenylate cyclase (nPAC) from the amoeboflagellate *Naegleria gruberi* NEG-M strain. *Chemical Physics* **2011**, *387* (1-3), 25-38.
193. Mutzel, R. Molecular biology, growth and development of the cellular slime mold *Dictyostelium discoideum* - Introduction. *Experientia* **1995**, *51* (12), 1103-1109.
194. Kessin, R. H. Evolutionary biology - Cooperation can be dangerous. *Nature* **2000**, *408* (6815), 917-919.
195. Kawabe, Y.; Weening, K. E.; Marquay-Markiewicz, J.; Schaap, P. Evolution of self-organisation in *Dictyostelia* by adaptation of a non-selective phosphodiesterase and a matrix component for regulated cAMP degradation. *Development* **2012**, *139* (7), 1336-1345.
196. Halavaty, A. S.; Moffat, K. N- and C-terminal flanking regions modulate light-induced signal transduction in the LOV2 domain of the blue light sensor phototropin 1 from *Avena sativa*. *Biochemistry* **2007**, *46* (49), 14001-14009.
197. Zoltowski, B. D.; Schwerdtfeger, C.; Widom, J.; Loros, J. J.; Bilwes, A. M.; Dunlap, J. C.; Crane, B. R. Conformational switching in the fungal light sensor *vivid*. *Science* **2007**, *316* (5827), 1054-1057.

## Curriculum vitae

### Personal Information

Name: Sarah Raffelberg  
 Date of Birth: Nov. 1, 1984  
 Place of Birth: Duisburg, Germany

### Education

2009 – present	Max-Planck-Institute for Chemical Energy Conversion, formerly Max-Planck-Institute for Bioinorganic Chemistry, Mülheim, Germany. PhD thesis: Blue light photoreceptors – From Mechanism To Application
2009	Alfred – Wegener – Institute for Polar and Marine Research, Biological Institute Helgoland. Master thesis: characterisation of potentially pathogenic <i>Vibrio</i> spp. in the German Bight.
2007 – 2009	University of Duisburg-Essen, Germany Master of Science “Water Science”
2007	Institute for Water Research GmbH, Dortmund, Germany Bachelor thesis: Evaluation of fluorescent dyes for the quantitative proof of total cell count in different waters.
2004 – 2007	University of Duisburg-Essen, Germany Bachelor of Science “Water Science”
1995 – 2004	secondary school Mülheim-Broich, Germany
1991 – 1995	Basic Primary School, Mülheim, Germany

Die hier vorgelegte Dissertation habe ich eigenständig und ohne unerlaubte Hilfe angefertigt. Die Dissertation wurde in der vorgelegten oder in ähnlicher Form noch bei keiner anderen Institution eingereicht. Ich habe bisher keine erfolglosen Promotionsversuche unternommen.

Mülheim an der Ruhr, den 01.05.2013

Sarah Raffelberg